Dissertation zur Erlangung des Doktorgrades

an der Fakultät für Chemie und Pharmazie

der Ludwig-Maximilians-Universität München

The potential of phyllobilins, the breakdown products of the green plant pigment chlorophyll, as bioactive natural compounds

Cornelia Andrea Karg

aus München, Deutschland

2021

Erklärung

Diese Dissertation wurde im Sinne von §7 der Promotionsordnung vom 28. November 2011 von Frau Prof. Dr. Angelika M. Vollmar betreut.

Eidesstattliche Versicherung

Diese Dissertation wurde eigenständig und ohne fremde Hilfe erarbeitet.

München, den 16.06.2021

_____

(Cornelia Andrea Karg)

Dissertation eingereicht am: 17.06.2021

1. Gutachter: Prof. Dr. Angelika M. Vollmar

2. Gutachter: Prof. Dr. Stefan Zahler

Mündliche Prüfung am: 20.07.2021

Meiner Familie

Table of contents

Table of contents

1 List of manuscripts

I. **Karg, C. A.,** Wang, P., Vollmar, A. M., & Moser, S. (2019). Re-opening the stage for *Echinacea* research - Characterization of phylloxanthobilins as a novel anti-oxidative compound class in *Echinacea purpurea*. *Phytomedicine, 60*, 152969.

II. **Karg, C. A.,** Schilling, C. M., Allmendinger, L., & Moser, S. (2019). Isolation, characterization, and antioxidative activity of a dioxobilin-type phylloxanthobilin from savoy cabbage. *Journal of Porphyrins and Phthalocyanines, 23*, 881-888.

III. **Karg, C. A.**, Doppler, C., Schilling, C., Jakobs, F., Dal Colle, M. C. S., Frey, N., Bernhard, D., Vollmar, A. M., & Moser, S. (2021). A yellow chlorophyll catabolite in leaves of *Urtica dioica* L.: An overlooked phytochemical that contributes to health benefits of stinging nettle. *Food Chemistry, 359*, 129906.

IV. **Karg, C. A.,** Neubig, C. M., Roosen, J., & Moser, S. (2021). Rising levels of antioxidative phyllobilins in stored agricultural produce and their impact on consumer acceptance. A*ccepted for publication in npj Science of Food*

V. **Karg, C. A.,** Wang, P., Kluibenschedl, F., Müller, T., Allmendinger, L., Vollmar, A. M., & Moser, S. (2020). Phylloxanthobilins are Abundant Linear Tetrapyrroles from Chlorophyll Breakdown with Activities Against Cancer Cells. *European Journal of Organic Chemistry, 2020*, 4499-4509.

VI. **Karg, C. A.,** Wang, S., Danaf, N., Pemberton, R., Bernard, D., Kretschmer, M., Schneider, S., Zisis, T., Vollmar, A. M., Lamb, D. C., Zahler, S., & Moser, S.. Tetrapyrrolic pigments are actin targeting compounds.
Submitted for publication in Angewandte Chemie International Edition

Reprints of all manuscripts can be found in the Appendix.

SUMMARY

2 Summary

The breakdown of the green plant pigment chlorophyll in colorful fall foliage is a spectacular natural phenomenon and one of the most visible signs of life on earth. The resulting products of chlorophyll degradation are the phyllobilins, linear tetrapyrrolic bilin-type catabolites. Over the last three decades, research on the degradation of chlorophyll has revealed the formation of non-colored phyllobilins, the phylloleucobilins, as major breakdown products that accumulate in the vacuoles of senescent chloroplasts. Since chlorophyll breakdown has been and still is regarded as a detoxification process, the formation of the water-soluble, non-phototoxic phylloleucobilins apparently fulfills the major goal of chlorophyll catabolism. However, the discovery of colored oxidation products, the phylloxanthobilins and the phylloroseobilins, which are more lipophilic and again photoactive, indicates a clear contradiction of this achievement. Albeit especially these colored phyllobilins have emerged as potential candidates in the quest for bioactive natural compounds, apart from an *in vitro* antioxidative activity of a phylloleucobilin, no report of any physiologically relevant activity existed. This is of particular relevance, since chlorophyll breakdown occurs not only in senescent leaves of deciduous trees; the same biochemical process takes place in all higher plants, including herbaceous plants, fruits, and vegetables. In theory, every plant based produce that has once been green contains phyllobilins.

Within the scope of this thesis, phyllobilins could be identified and structurally characterized in leaves of the medicinal plant *Echinacea purpurea* (manuscript I), in senescent leaves of savoy cabbage (manuscript II), in fresh nettle leaves and in nettle tea (manuscript III), in iceberg lettuce and cucumber peels (manuscript IV) as well as in senescent leaves of the plane tree (manuscript V).

In the first projects, we addressed two medicinal plants, *Echinacea purpurea* and *Urtica dioica* L., as well as savoy cabbage, and investigated the occurrence of phyllobilins and their potential bioactivities. Phylloxanthobilins were detected in an unprecedented amount and diversity in leaves of *Echinacea purpurea*, a medicinal plant of high pharmaceutical importance. We were able to demonstrate strong antioxidative properties for phylloxanthobilins such as intracellular radical scavenging activities and preservation of redox homeostasis upon oxidative stress, providing the first evidence of a relevant bioactivity in cells (manuscript I).

Moreover, we isolated a dioxobilin-type phylloxanthobilin from senescent leaves of savoy cabbage, which turned out to resemble the structure of the bile pigment bilirubin in a

_____

remarkable manner. This plant derived 'bilirubin-mimic' was shown to possess an even higher antioxidative potential than bilirubin itself (manuscript II).

Following these findings, we identified a phylloxanthobilin in fresh nettle leaves and nettle tea, providing first evidence for chlorophyll catabolites in a processed plant product. Beside strong antioxidative activities, anti-inflammatory properties were observed. We demonstrated inhibitory activities on the pro-inflammatory enzymes COX-1 and COX-2 *in vitro* and on COX-2 expression and prostaglandin E2 production in cells to a similar or even higher extent than known bioactive phytochemicals in nettle extracts. These data indicate that the phylloxanthobilin contributes to the health benefits of nettle tea, which is commonly used to treat inflammatory urinary tract diseases (manuscript III).

Considering the high amounts of phyllobilins ingested in vegetables, fruits, and herbal remedies, we unveiled initial insights into the bioaccessibility and metabolism of phylloxanthobilins by demonstrating cellular uptake into human cells, their stability in simulated gastric and intestinal digestion, as well as their metabolic stability using human liver microsomes (manuscript I and III).

Thus, we have uncovered an important role of phyllobilins as bioactive ingredients of herbal remedies and human nutrition, which underlines the importance of taking these tetrapyrroles into account in phytochemical profiling of medicinal plants and plant based food in future.

Phyllobilins do not only arise in senescent plant tissue but also in fresh leaves without visible signs of chlorophyll breakdown, as evidenced in fresh *Echinacea* and nettle leaves in manuscript I and III. However, with progressing chlorophyll degradation and corresponding fading of the green color, phyllobilins are expected to appear in high amounts especially in aged greens. Indeed, by a comprehensive time-series experiment, we found that phyllobilin contents in iceberg lettuce and cucumber peels increased significantly with storage time, while the microbial load did not increase. Remarkably, the extracts of the stored cucumber peels and lettuce exhibited a higher antioxidant potential than extracts obtained from fresh produce. If consumers were aware of the fact that the vegetables they ingest might be better with age than expected, our results could possibly initiate a shift of thinking towards a more sustainable consumer behavior. Indeed, using an online survey with more than one thousand participants, we demonstrated that consumers, who received information about rising levels of phyllobilins in stored iceberg lettuce, were willing to eat the lettuce significantly longer. Furthermore, consumers assessed the stored lettuce as more edible and healthy in comparison to a control group. Overall, the results of this project indicate that aged agricultural produce, containing high

_____

amounts of antioxidant phyllobilins, is more than just waste and even beneficial for human health, which bears a high potential to reduce consumer produced food waste (manuscript IV).

As promising anti-cancer activities have been reported for structurally related tetrapyrroles such as bilirubin and phycocyanobilin, we went one step further in unravelling potential bioactivities of phyllobilins and examined possible anti-cancer effects. A phylloxanthobilin turned out to possess anti-proliferative activities on human bladder and breast cancer cells, and to induce apoptosis as well as a G2/M cell cycle arrest. Although the corresponding phylloleucobilin did not inhibit proliferation in cancer cells, modifying the structure by esterification of the free propionic acid side chain led to an increase in anti-proliferative activity. Nevertheless, the phylloxanthobilin was shown to be the most potent candidate, which gained in importance as paper spray mass spectrometry measurements demonstrated that this structure is more abundant in plants than previously assumed (manuscript V).

Since manuscript V unveiled effects of phyllobilins on cancer cells, we tested the influence of two late stage phyllobilins, a phylloxanthobilin and a phylloroseobilin, on cell migration in bladder and cervical cancer cells in comparison to their structural counterparts from heme breakdown, bilirubin and biliverdin. While all tetrapyrroles inhibited cancer cell migration, the phyllobilins turned out to be more potent, with the phylloroseobilin as the most active compound. Since actin is a key player in cell migration and cell motility, influences on the actin cytoskeleton were elucidated upon treatment with phyllobilins and their heme derived bilin analogues, and revealed an inhibition of actin polymerization and nucleation by all tested compounds, as well as induction of depolymerization. These observations suggested a direct interaction of the linear tetrapyrroles with G-actin, which could be confirmed by affinity chromatography using G-actin beads. Moreover, we were able to predict a common binding site of phyllobilins and bilins on G-actin by a molecular docking study, which was verified by a competition pull down assay. Characterization of the binding using different biophysical techniques disclosed affinities in the low micromolar range for the phylloroseobilin, the phylloxanthobilin, and biliverdin. With these findings we were able to introduce G-actin as the first human biological target for phyllobilins and a novel target for bilins (manuscript VI).

Taken together, we have identified novel phyllobilin structures in medicinal plants and vegetables and are able to establish phyllobilins as bioactive natural products contributing to the health benefits of a plant based diet and to the efficacies of phytotherapies. In addition, we provided first evidence for effects of phyllobilin structures on cancer cells.

_____

Moreover, we identified and verified the cytoskeletal protein actin as a target for phyllobilins and thus discovered a human biologically relevant target for this class of natural products for the first time.

This thesis summarizes the first approaches on investigating the bioactivities and physiological roles of phyllobilins and provides results on physiologically relevant effects and underlying molecular mechanisms in a cancer context. This work opens up a new chapter of chlorophyll catabolites and exciting fields of possible therapeutic applications.
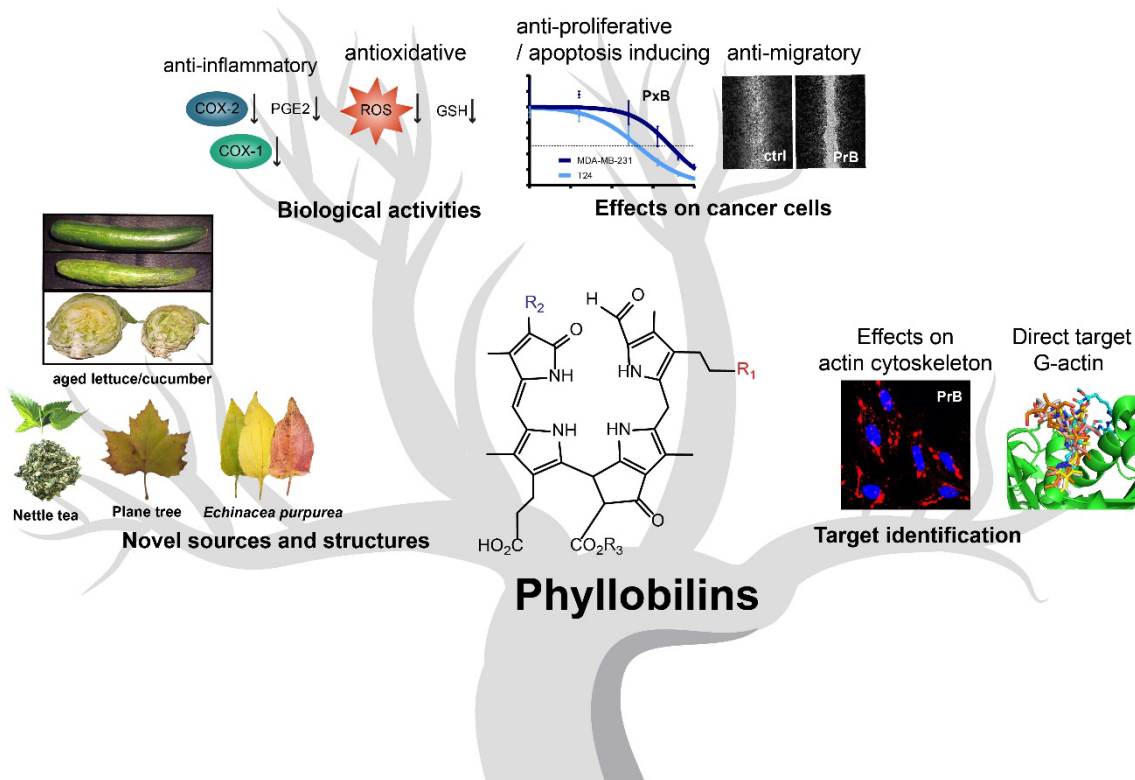

Figure 1. Graphical summary of the results obtained on an underexplored class of natural products throughout this thesis.

INTRODUCTION

3   Introduction

3.1   Chlorophyll – a pigment of life

Tetrapyrrolic structures occur in almost every living organism, since they play essential roles in a wide variety of critical biological processes and without tetrapyrrolic pigments, life on earth would not be possible[1]. Chlorophyll (Chl) is one of these 'pigments of life', is found in all higher plants, algae, and cyanobacteria, and is crucial for sustaining most light dependent life forms[2]. During photosynthesis, Chl is responsible for light harvesting and energy transduction acting as photocatalyst[3].

Several types of Chl exist in nature, with Chl a and b representing the most abundant forms in higher plants[4]. Their structure consists of a chlorin macrocycle with an extended conjugated π-system, which not only accounts for the intensive color of the so-called leaf green, but also for the extraordinary photo- and electrochemical activity[2]. Generally, macrocyclic tetrapyrroles are able to serve as tetradentate ligands forming chelate complexes with many (transition) metal ions[5]. Magnesium is the chelating metal found in most of the Chls[2]. Additionally, Chl a and b carry an apolar phytyl chain at ring D, which enables the metal complex to anchor to the thylakoid membranes of the chloroplasts (Figure 2)[6].

Chl a: R=CH$_3$ **Chl b:** R= HC=O
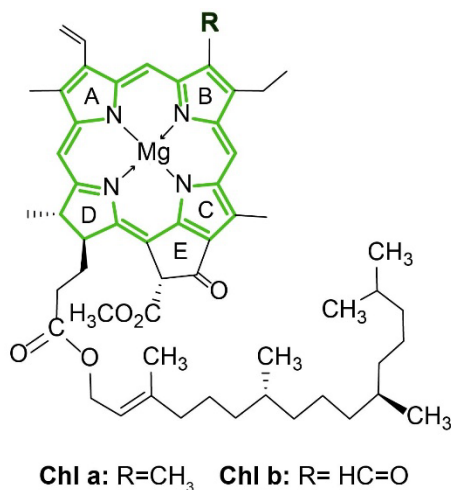
Figure 2: Chemical structure of chlorophyll a and chlorophyll b. The chlorin core (highlighted in green) is substituted with a propionic acid side chain at ring D esterified with a lipophilic phytol tail, and co-ordinated to a central magnesium ion. Chl a and b differ in the modification at ring B with Chl a carrying a methyl group and Chl b featuring a formyl moiety[2].

With the onset of shorter photoperiods and lower light intensities, deciduous plants begin to prepare for the winter season[7]. Accompanied by decreased photosynthesis rates, the

plant starts to senesce reaching the final stage of leaf development[8,9]. Senescence is an organized and highly regulated process, which is crucial for sustaining plant fitness as it involves the remobilization and recovery of nutrients, metal ions, and nitrogen. Cellular components such as proteins and nucleic acids are transformed into transportable units, which are then relocated from decaying plant organs to juvenile and reproductive tissues[9]. Since chloroplasts contain up to 70 % of the total leaf protein and 75 % of the total leaf nitrogen[9-11], leaf senescence at the early stage implies the disassembly of chloroplast components such as thylakoid membranes and Chl binding proteins[9]. This causes the release of free Chl, which is known for its photosensitizing potential. By generating highly reactive singlet oxygen, photoactivated unbound Chl can lead to serious cellular damage[12].

In order to protect the cell from photo-damage and to ensure the complete disintegration of intracellular components and recycling of nutrients during senescence, plant cells urgently need to detoxify free Chl[9].

3.2　The fate of chlorophyll and the formation of phyllobilins

With the fascinating spectacle of the seasonal fall coloration with estimated 10^9 tons of Chl broken down every year, nature reveals one of the most conspicuous signs of life[13,14]. Strikingly, the degradation of the green plant pigment remained mysterious for many decades and Chl seemed to vanish without leaving a trace. It was only about 30 years ago that the mystery was uncovered and the first Chl catabolites, now generally named phyllobilins, were finally discovered[15]. Inspired by the colored degradation products of the structurally similar tetrapyrrole heme, researchers first suspected the breakdown products of Chl to be colored as well. Against all expectations, the first identified Chl catabolites turned out to be colorless. Matile, Thomas, and co-workers succeeded in identifying colorless compounds that only appeared in senescent leaves of wild-type *Festuca pratensis* in contrast to a 'stay-green' mutant[15,16]. In 1991, the structure of the first breakdown product of Chl, a non-fluorescent Chl catabolite (NCC), could be characterized in senescent leaves of barley by Kräutler and co-workers and revealed a linear tetrapyrrole with unconjugated pyrrole units and a Chl-characteristic additional cyclopentanone unit featuring a methoxycarbonyl moiety (Figure 3)[17]. The structural elucidation of this first PleB unveiled interesting insights into the pathway of Chl degradation as it indicated the Chl breakdown to involve the removal of the magnesium ion and the phytol chain as well as an oxygenolytic opening of the Chl macrocycle.

Hv-**PleB**-1

Figure 3: Chemical formula of the first characterized phyllobilin structure. *Hv*-PleB-1 was isolated from senescent leaves of barley (*Hordeum vulgare*)[17].

Since 2014, chlorophyll catabolites have been named as 'phyllobilins' referring to the Chl-origin and the remarkable structural relation to the heme-derived bilins[18,19]. Accordingly, non-fluorescent chlorophyll catabolites are now called phylloleucobilins (PleBs), with respect to their physical properties. Phyllobilins identified from different plant species are named after the initials of the Latin name of the plant, the type of the phyllobilin structure, and a number accounting for the polarity in reversed-phase chromatography, i.e., the first non-fluorescent Chl catabolite identified in senescent leaves of barley (*Hordeum vulgare*) was named *Hv*-NCC-1, or corresponding to the new nomenclature *Hv*-PleB-1.

3.3 The biochemical program of chlorophyll breakdown – The PaO/phyllobilin pathway

The discovery of the first catabolite paved the way for the identification of a number of phyllobilins and a large structural variety with more than 40 different structures identified from more than 20 different species until today[20]. All explored phyllobilins furnish the basic linear tetrapyrrolic core structure and only differ in characteristic side chain patterns and stereoisomeric features.

Research of more than a quarter of a century revealed the elucidation of important key enzymes and a non-enzymatic reaction of the mechanism behind Chl breakdown. Chl catabolism turned out to be a strictly controlled biochemical program taking place in three departments of the plant cell: the chloroplast, the cytosol, and the vacuole[21].

Since almost all phyllobilin structures carry a methyl group at C2 (with one exception in *Arabidopsis thaliana* with a hydroxymethyl moiety instead[22]), they all seem to be derived from the degradation of Chl a. Along that line, two of the downstream enzymes of the

catabolism pathway were found to be Chl a specific[23,24], but also Chl b occurs in plants in substantial amounts. That is why plant cells regulate levels of both types via the so-called 'Chl cycle', in which Chl b is converted to Chl a in a two-step reaction catalyzed by Chl b reductases[25].

The first steps of Chl breakdown involve the conversion of Chl a to pheophorbide a (Pheo a) by removal of the magnesium ion and the phytol side chain[20].

The following reaction is considered as the key step of Chl degradation, since it is responsible for the loss of green color and the generation of the characteristic linear tetrapyrrolic core. Hence, the pheophorbide a oxygenase (PaO), the responsible enzyme, became the eponym for the biochemical program of Chl to phyllobilins, the PaO/phyllobilin pathway[18].

PaO is a monooxygenase with two transmembrane domains within the thylakoid membrane[26] and catalyzes the oxygenolytic opening of the chlorin macrocycle to obtain the red chlorophyll catabolite (RCC). The specific incorporation of an oxygen atom generates the formyl moiety[27] and therefore, the RCC comprises the first 1-formyl-oxobilin-type phyllobilin, the precursor of all catabolites that are subsequently produced (Figure 4)[21]. Detection of RCC turned out to be challenging, as it is usually enzyme bound and as it rapidly metabolizes further to the primary fluorescent chlorophyll catabolite (*p*FCC), or later named primary phyllolumibilin (*p*PluB) (Figure 4)[19]. The enzyme responsible for the corresponding reduction of the double bond at C15/16 is the RCC reductase (RCCR)[28]. RCCR, which has two isoforms, introduces the new stereocenter in *p*PluB either in the 'n' or 'epi' configuration, depending on the plant species[29]. *p*PluBs are transported into the vacuoles by transporters that remain to be identified, where different modifications are assumed to proceed yielding modified *m*PluBs.
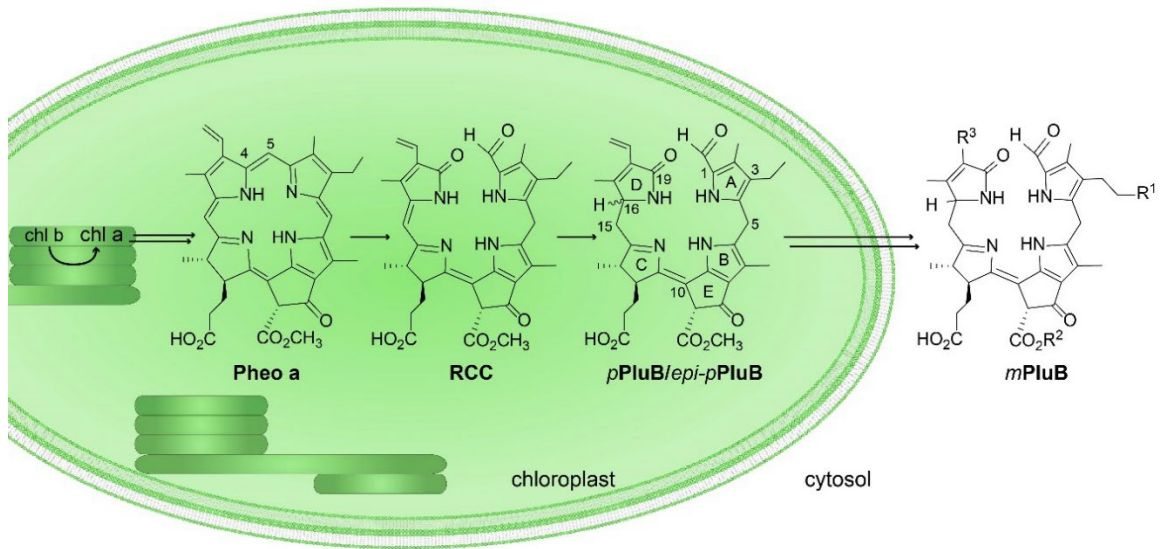
Figure 4: Early steps of Chl breakdown. First steps of Chl breakdown take place in the chloroplasts: Chl b is transformed to Chl a in the membranes of the thylakoids[25]. Chl a is exported from the thylakoids and dephytylation and dechelation furnish pheophorbide a (Pheo a), which is then converted to the RCC by an oxygenolytic opening of the macrocycle[27]. This reaction is catalyzed by pheophorbide a oxygenase and is the key step of the so called PaO/phyllobilin pathway. The RCC is further reduced to the primary PluB (*p*PluB) or its epimeric form (*epi-p*PluB) in dependence of the source of the responsible enzyme[29]. The *p*PluB is then transported into the cytosol of the plant cell, where further modifications take place resulting in modified PluBs (*m*PluBs).

3.4 Two branches of chlorophyll breakdown – type-I and type-II phyllobilins

At the stage of the *p*PluB, the biochemical program of Chl breakdown is split into two main branches: the type-I phyllobilins (1-formyl-19-oxobilin) and the type-II phyllobilins lacking the formyl moiety and carrying a carbonyl instead (1,19-dioxobilin) (Figure 5)[19]. The corresponding oxidative deformylation of PluBs to dioxobilin-type PluBs (DPluBs) was found to be catalyzed by a cytochrome P450 monooxygenase (CYP89A9 in *A. thaliana*), which is localized to the ER[30].

PluBs and DPluBs are transported into the vacuoles, where they rapidly isomerize due to the acidic pH to type-I PleBs and type-II DPleBs, respectively (Figure 5)[31,32]. Interestingly, this acid induced tautomerization is the only non-enzymatic reaction of the PaO/phyllobilin pathway that has been elucidated so far. PleBs and DPleBs represent a stable storage form accumulating in the vacuoles, which explains why these phyllobilins are the best-characterized representatives to date. On the one hand, a high number of structures with different modification motifs has been identified for PleBs[20]. On the other hand, also

DPleBs could be shown to be abundant in a variety of plants, e.g., making up more than 90% of all found phyllobilins in *A. thaliana*[33,34].
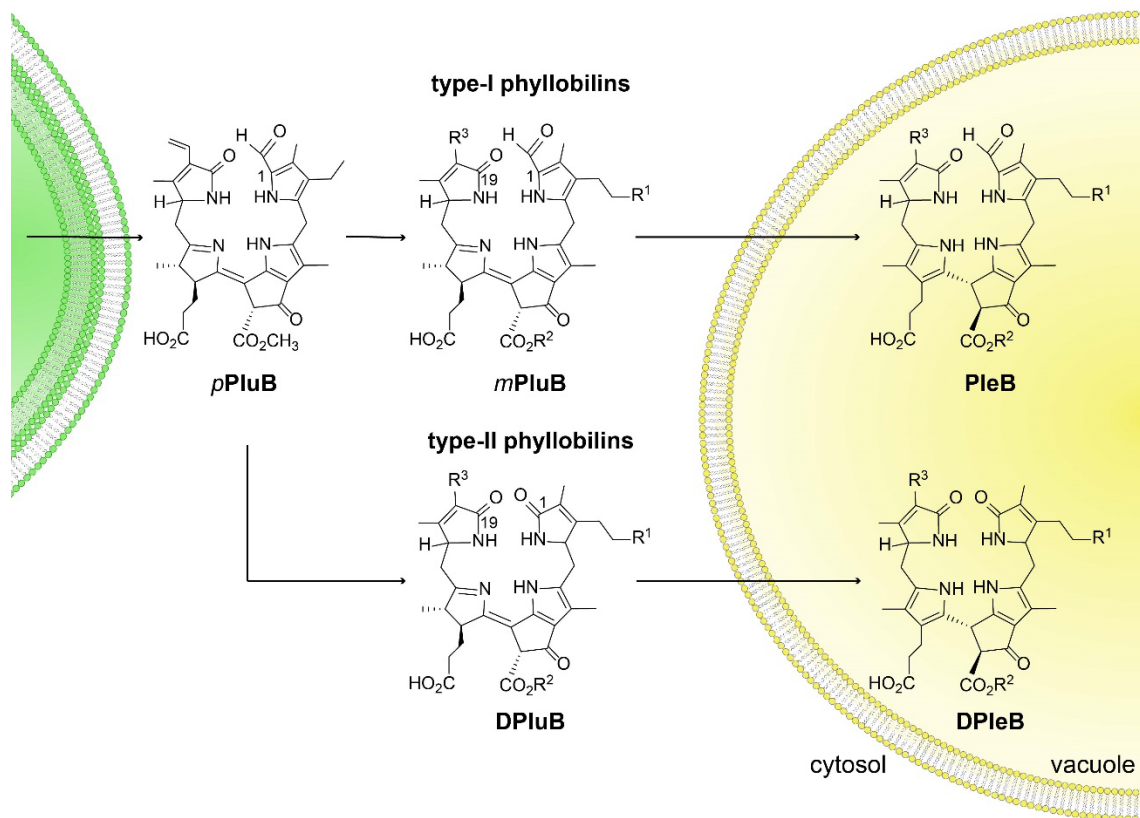

Figure 5: Branching of PaO/phyllobilin pathway. *p*PluBs are exported from the chloroplasts into the cytosol. A second branch of Chl breakdown is introduced by generating dioxobilin-type PluBs (DPluBs)[19]. Modifications at the peripheral side chains yield modified PluBs (*m*PluBs) or corresponding DPluBs, which are then imported into the vacuoles where the prevailing low pH leads to a non-enzymatic isomerization to PleBs and DPleBs[31].

The most abundant of all investigated PleBs up to now appears to be the relatively 'simple' catabolite being modified by a hydroxyethyl group at ring A. This 3^2-OH PleB is formed by the acid-induced isomerization of the corresponding 3^2-OH PluB[35] and has been identified, among others, in *Cercidiphyllum japonicum*[36]*, Spinacia oleracea*[37]*,* and *Spathiphyllum wallisii*[38].

3.5 Phyllochromobilins – colored late stage phyllobilins

Type-I and type-II PleBs were long thought to be the 'final' degradation products of Chl breakdown, until in 2008 the first colored Chl catabolite was discovered[39]. Moser *et al* identified a yellow chlorophyll catabolite, later called phylloxanthobilin (PxB), in senescent leaves of the Katsura tree (*Cercidiphyllum japonicum*). The same structure could be also prepared via partial synthesis by oxidation of the PleB, the main catabolite of the plant.

Structural elucidation revealed the PxB to feature a double bond between C15 and C16, resulting in a conjugated π-electron system extended over ring C and D, which is responsible for the intense yellow color (Figure 6). Strikingly, this color was found to contribute significantly to the fall color in senescent leaves[39]. Although the underlying mechanism responsible for the formation of PxBs still needs to be elucidated in detail, it is assumed that an enzymatic 'oxidative activity' in leaf extracts efficiently accounts for the stereo- and regio-selective formation of PleBs to PxBs via a hydroxylated intermediate[40]. Hence, PxBs seem to be formed actively in plants. However, only few examples of PxBs could be identified, e.g., in *Egeria densa*[41], wych elm[42], or lime tree[43], and in only minor amounts in contrast to PleBs.

In senescent leaves of grapevine, a yellow chlorophyll catabolite of the type-II class of phyllobilins was detected that lacks the formyl moiety, and therefore represents the oxidation product of the corresponding DPleB (Figure 6)[44]. Similar to the formation of PleBs to PxBs, also the formation of dioxobilin-type phylloxanthobilins (DPxBs) is assumed to result from the endogenous oxidative activity present in specific plant species[45].

In correspondence to their PleB-precursors, also PxBs tend to oxidize further furnishing pink Chl breakdown products (PiCCs), the phylloroseobilins (PrBs) (Figure 6). To date, the only naturally occurring PrB has been detected in senescent leaves of *Cercidiphyllum japonicum*[46]. However, synthetic approaches succeeded in generating the PrB by complexation and oxidation of the corresponding PxB with an excess of Zn[II]-ions, and subsequent de-complexation of the PrB[47]. Following this reaction, also a type-II DPrB could be synthesized[48]; though, the structure of a DPrB has not been identified in plants yet.

Colored phyllobilins, the so-called phyllochromobilins, represent a class of fascinating late stage phyllobilins not only because of their intensive colors but also as they were shown to possess interesting chemical properties. Photoactivation of PxBs and DPxBs leads to a reversible Z/E- isomerization rendering these types of phyllobilins potent photoswitches[45,49]. In addition, irradiation of a PxB in apolar solvents was found to result in a dimerization following a [2+2] cycloaddition[49].

As mentioned above, the porphyrin core structure of the 'pigment of life' Chl serves as excellent tetradentate ligand to bind Mg[II]. The breakdown of Chl furnishes linear tetrapyrroles, mainly phylloleucobilins that are not expected to be able to coordinate metal ions[50]. However, the more unsaturated oxidation products PxBs and PrBs, featuring two or three conjugated pyrrole units, respectively, serve as multi-dentate ligands for

physiologically relevant divalent metal ions. A PrB was shown to effectively coordinate in tridentate complexes with Zn^{II}-, Cd^{II}-, Cu^{II}-, Ni^{II}- and Pd^{II}-ions, in case of the Zn^{II}- and Cd^{II} resulting in deep blue complexes that strongly luminesce[47]. Very recently, the blue complex of a DPrB with Zn^{II} ions was characterized and similar to the PrB-Zn^{II}-complex reported to exhibit a bright red fluorescence[51]. Furthermore, also the PxB was demonstrated to build orange-yellowish 2:1 Zn^{II}-complexes emitting in the green spectral range[52].
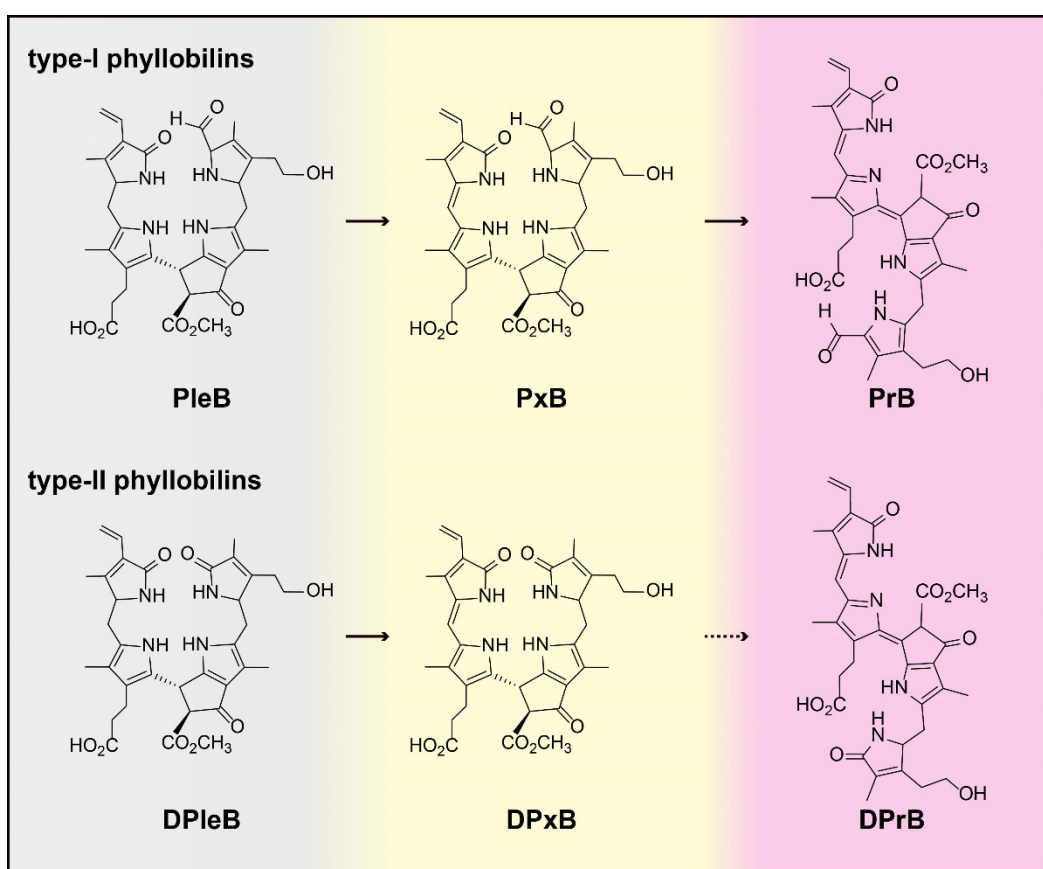
Figure 6: Chemical structures of late stage type-I and type-II phyllobilins. Colorless PleBs and DPleBs have been considered as the 'final' stage of Chl breakdown for a long time. However, they were found to easily oxidize to colored phyllobilins (phyllochromobilins). Oxidation of PleBs/DPleBs results in yellow structures, PxBs and DPxBs[39,44], and further oxidation yields the pink phylloroseobilins (PrB/DPrB)[46,48]. Although the PleBs/DPleBs appear to be the most abundant phyllobilins to date, PxBs could be detected in some plant species. Structures of DPxBs and a PrB were found to occur naturally, too. Up to now, the DPrB has been generated by synthetic approaches only (indicated by the dashed arrow)[48].

3.6   Structural elucidation and characterization

The structural characterization of phyllobilins is usually carried out in three steps. Since phyllobilins possess characteristic absorbance properties, the analysis of crude plant extracts by HPLC/UV-Vis detection allows not only for the identification of phyllobilins, but also for the characterization of the specific type of Chl catabolite. A typical absorption maximum near λ=315 nm of the α-formylpyrrole unit can be observed for type-I phyllobilins, which in contrast is missing for the type-II phyllobilins carrying a lactam group at ring A. Phyllochromobilins feature additional UV-Vis maxima due to their extended π-systems; PxBs and DPxBs can be identified by their additional maximum near λ=430 nm, and PrBs and DPrBs are characterized by the maximum near λ=520 nm (Figure 7)[21].
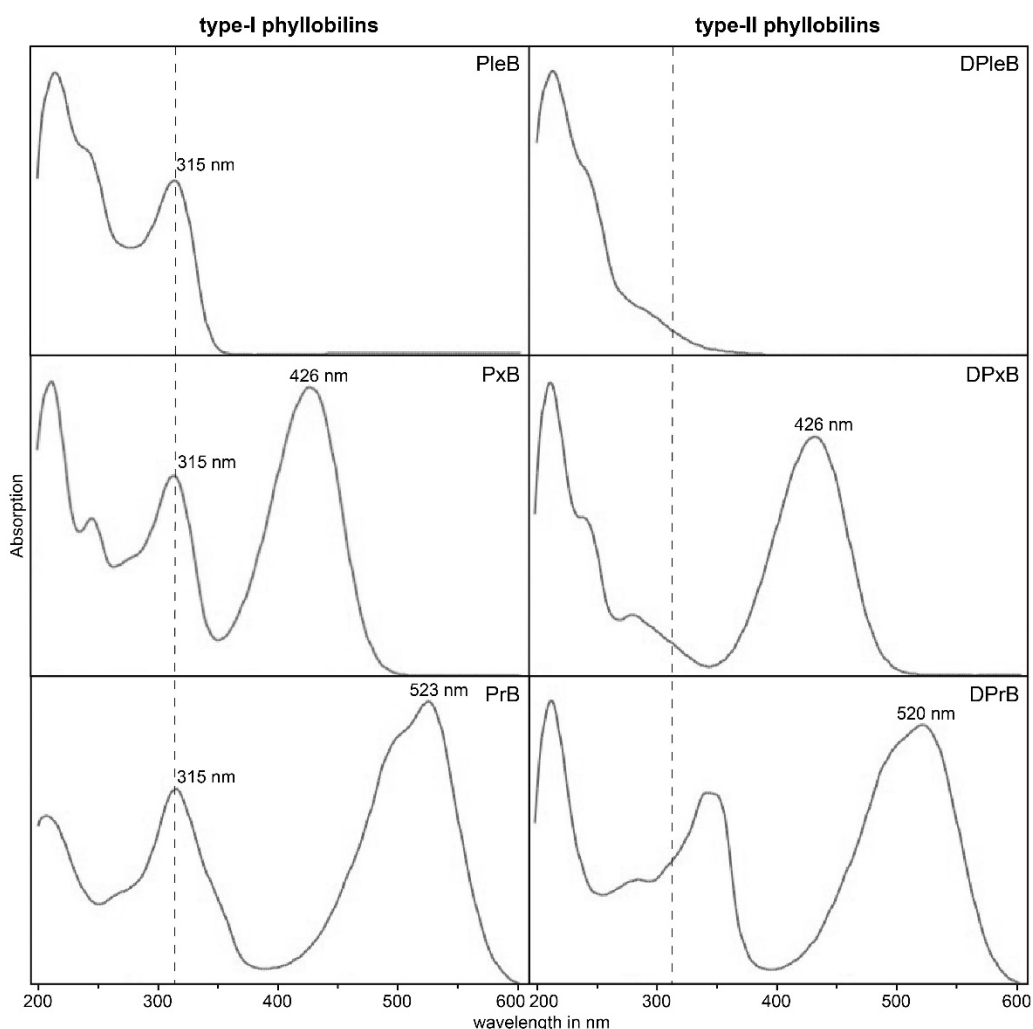
Figure 7: Characteristic UV-Vis spectra of type-I and type-II phyllobilins. Generally, type-II phyllobilins lack the characteristic absorption maximum of the 1-formylpyrrole moiety at around 315 nm of type-I phyllobilins. Phyllochromobilins feature extended π-systems resulting in a bathochromic shift of their absorption maxima[21].

Following the identification of phyllobilins, different mass spectrometry techniques are used to deduce the structural formulae as well as specific modification patterns of the basic phyllobilin core. Mass spectrometry (MS) has already contributed to the identification of the first Chl catabolite and the technology has been developed to a fundamental tool for the structural analysis of phyllobilins until today. Phyllobilin databases have been established by extensive analysis of different phyllobilin structures during the last years, which can be utilized nowadays to identify known modification patterns of the tetrapyrrole core structure[33,53,54]. Especially specific fragmentation patterns of MS^n-based reactions, which are well characterized for these tetrapyrroles, facilitate the structural characterization. Finally, nuclear magnetic resonance spectroscopy (NMR) experiments involving both homonuclear 1D and heteronuclear 2D spectra are employed for detailed characterization, especially of novel phyllobilin structures that have not been identified in other plant species yet.

3.7 Phyllobilins as ingredients of human nutrition

Chl breakdown is mainly associated with the discoloration of senescent leaves in fall, but de-greening and the appearance of yellowish and reddish colors are also signs of ripening processes. In 2007, phylloleucobilins could be detected in the peels of ripe apples and pears in amounts of up to 0.6 µg/cm^2 [55], and in the last years, a number of fruits and vegetables have been investigated for the occurrence of phyllobilins detecting PluBs, PleBs, and PxBs in broccoli[56], spinach[37], plums[57], and olives[58], among others.

Furthermore, the biochemical program of Chl degradation is now known to be induced not only during senescence or ripening but also to be triggered by environmental factors such as droughts or reduced temperature and light conditions. Accordingly, phyllobilins are also expected to occur in de-greening, stored or aged plant based food. Indeed, high levels of phyllobilins were detected in stored broccoli and banana peels[56,59], which provides first indications that the process of Chl catabolism is still proceeding post-harvest.

3.8 Indications for potential bioactivities of phyllobilins

The extensive work of researchers in the field of phyllobilins in the last three decades opened up a class of natural products with an unexpected and striking structural diversity. Therefore, the question arises on whether the breakdown of Chl only serves as a detoxification process, protecting cells from the phototoxicity of free Chl.

Phyllobilins feature a remarkable structural similarity to the heme-derived bile pigments bilirubin (BR) and biliverdin (BV)[21]. The red blood pigment heme is also one of the

pigments of life and, similar to Chl, toxic when released from its binding proteins[60]. The bile pigments, which are formed during heme degradation, where long considered as useless detoxification products. Interestingly, beneficial effects have been elucidated for BR and BV, e.g., highly potent antioxidant properties and cytoprotective roles against a variety of diseases[61-64]. In addition, phyllobilins are structurally related to phycocyanobilin derived from the blue-green algae *Spirulina platensis*, for which health promoting effects have been reported, too[65,66]. Thus, the structural similarity to already validated bioactive natural products indicates the high potential of phyllobilins being more than just waste products. Indeed, first investigations by Müller *et al* revealed *in vitro* antioxidative activity of a PleB isolated from apple and pear[55].

Furthermore, phyllobilins were associated with pathogen infections in plants. Pathogen-induced chlorosis was found to yield the same Chl breakdown products as senescence induced degradation, indicating that the PaO/phyllobilin pathway is of relevance upon biotic stress to the plant[67]. Additional research showed that phyllobilin contents increased upon herbivore and fungi infestation in basil, thereby particular localizing in the infected areas of the leaf[68]. Hence, induction of Chl degradation seems to be triggered due to pathogen attack, which initiates considerations regarding the roles of phyllobilins in plant defense or signaling mechanisms.

Overall, these facts give reason to assume that phyllobilins possess physiologically relevant bioactivities and important roles in plants and in humans. Phylloxanthobilins, for which interesting chemical properties where demonstrated by recent investigations as described above, are of particular interest in that context.

4 Aims of the study

Phyllobilins have emerged as an intriguing class of ubiquitous natural products. Although there are several indications for physiological roles of phyllobilins in plants and in humans, detailed reports on bioactive properties of the compound class remain scarce to date. Thus, there is an urgent need for analyzing these tetrapyrroles in depth.

The aims of this study can be summarized as follows:

1. Identification and structural characterization of phyllobilins in novel plant sources focusing on medicinal plants and plant based food
2. Elucidating potential bioactivities of phyllobilins focusing on activities responsible for the health benefits of the corresponding plant
3. Investigating the impact of informing consumers about phyllobilins in stored plant based food
4. Exploring anti-cancer activities of phyllobilins
5. Target identification and verification

5   Summary of manuscripts

5.1   Re-opening the stage for *Echinacea* research – Characterization of phylloxanthobilins as novel anti-oxidative compound class in *Echinacea purpurea*

Cornelia A. Karg, Pengyu Wang, Angelika M. Vollmar & Simone Moser (2019). *Phytomedicine, 60*, 152969.

Chlorophyll degradation is mainly associated with a detoxification process and the derived phyllobilins have been regarded as mere waste products without any additional function. Especially with the discovery of the phylloxanthobilins (PxBs), a type of phyllobilins was introduced with a suspected high potential of bioactivities possibly contributing to the health benefits of the plant of origin. However, their physiological roles still remain largely unexplored. *Echinacea purpurea* is a medicinal plant of high pharmaceutical importance in the treatment of the common cold. Phytochemical analyses identified different bioactive constituents, which, however, cannot account for all of the pharmacological effects. We therefore examined *Echinacea* leaf extracts for the occurrence of phyllobilins and identified six different PxBs in senescent as well as in fresh green leaves without visible signs of chlorophyll degradation. Isolation and structural elucidation by HPLC/UV-Vis analysis and mass spectrometry demonstrated PxBs to occur in an unprecedented abundance and diversity. The PxB core structure was found to be modified at two different positions, being attached at ring A either by a simple hydroxyl group or by different glycosylated modification motifs. Strikingly, *Echinacea* PxBs were shown to possess a high *in vitro* antioxidant potential and to be taken up by human cells indicating that these PxBs are stable in cell growth medium for several hours. Furthermore, measuring intracellular GSH levels as well as H_2DCF-DA fluorescence revealed that PxBs scavenge intracellular ROS to a higher or similar extent as caffeic acid, a known active phytochemical in *Echinacea purpurea.* In summary, this study unveils PxBs in *Echinacea* extracts to emerge as overlooked antioxidative phytochemicals and provides the basis for further exploring potential bioactivities of phyllobilins in medicinal plants.

5.2 Isolation, characterization, and antioxidative activity of a dioxobilin-type phylloxanthobilin from savoy cabbage

Cornelia A. Karg, Charlotte M. Schilling, Lars Allmendinger & Simone Moser (2019). *Journal of Porphyrins and Phthalocyanines*, *23*, 881-888.

The breakdown of the green plant pigment chlorophyll yields two branches of chlorophyll catabolites, the formyloxobilin-type (type-I) and dioxobilin-type (type-II) phyllobilins. While for type-I phyllobilins, first bioactivities were uncovered as demonstrated for phylloxanthobilins (PxBs) from *Echinacea purpurea* in manuscript I, biological effects of dioxobilin-type phyllobilins were still elusive. We identified and isolated a type-II PxB in de-greening savoy cabbage, which is appreciated for its antioxidant-related health benefits. Structure elucidation by comprehensive spectroscopic and spectrometric analysis revealed the PxB to feature two propionic acid side chains at the southern hemisphere of the phyllobilin core structure, a rather rare structural characteristic for phyllobilins. Thus, the phylloxanthobilin in savoy cabbage closely resembles the structure of the endogenous antioxidant bilirubin, the degradation product of the red blood pigment heme, thereby representing a plant-derived 'bilirubin-mimic'. Interestingly, by conducting two different *in vitro* approaches, the type-II PxB could be shown to possess even higher antioxidative activity than bilirubin and the vitamin-E derivative Trolox. This study identified a novel dioxobilin-type phyllobilin structure and provided first evidence for bioactivities of the type-II branch of phyllobilins, which further strengthens the presumption of an important role of phyllobilins as antioxidant ingredients in human nutrition.

5.3 A yellow chlorophyll catabolite in leaves of *Urtica dioica* L.: An overlooked phytochemical that contributes to health benefits of stinging nettle

Cornelia A. Karg, Christian Doppler, Charlotte Schilling, Franziska Jakobs, Marlene C. S. Dal Colle, Nadine Frey, David Bernhard, Angelika M. Vollmar & Simone Moser (2021). *Food Chemistry*, 359, 129906.

Manuscript I has provided evidence for the appearance of phyllobilins in a medicinal plant with high pharmaceutical importance. With the identification of a phylloxanthobilin (PxB) in fresh nettle leaves as well as in nettle tea, we prove the occurrence of phyllobilins also in a processed plant product and in tea in general for the first time. Using mass spectrometry and NMR spectroscopy, we elucidated the structure, which turned out to feature a glycosylated modification motif attached to ring A of the phyllobilin core structure. Quantification of the PxB in different brands of nettle tea disclosed an amount of up to 100 µg in one cup of tea, depending on the supplier. Since nettle tea is used against a variety of inflammatory diseases such as arthritis or urinary tract infections, we examined the antioxidative and anti-inflammatory effects of the phyllobilin. The PxB exhibited similar or even stronger antioxidative activities *in vitro* as well as in a cellular approach than selected bioactive phytochemicals known to occur in nettle extracts. Moreover, it inhibited the pro-inflammatory enzymes COX-1 and COX-2 *in vitro*, and COX-2 expression and prostaglandin E2 production in murine macrophages. In order to gain first insights into the bioaccessibility of a phylloxanthobilin being part of human nutrition, we performed stability studies in simulated digestion fluids and demonstrated the chlorophyll catabolite to be stable in gastric and intestinal digestive milieus. Furthermore, we tested the metabolic stability using human liver microsomes, which revealed the PxB to be stable against hepatic enzymes that catalyze, e.g., the glucuronidation of the structural relative bilirubin. As already shown for PxBs in *Echinacea purpurea*, also the PxB in nettle tea appeared to be a completely overlooked phytochemical, for which bioactivities were observed that contribute to the health benefits of stinging nettle and nettle tea.

5.4 Rising levels of antioxidative phyllobilins in stored agricultural produce and their impact on consumer acceptance

Cornelia A. Karg, Christina M. Neubig, Jutta Roosen & Simone Moser (2021).
Accepted for publication in npj Science of Food

Phyllobilins are a class of natural products with high abundance in plants. Since they occur not only in deciduous trees and shrubs, but also in fruits and vegetables, they are included in a daily diet. Manuscript II and III showed that stored vegetables and even processed plant products contain high levels of phyllobilins, indicating the chlorophyll degradation program also to be active post-harvest. However, a detailed analysis of phyllobilin contents in edible greens over a time course of several days after harvesting has not been performed yet. By a comprehensive time-series experiment, we showed that phyllobilin contents significantly increase in iceberg lettuce and cucumber peels with storage time of seven and twelve days, respectively. At the last day of storage when the vegetables appeared de-greened and wrinkly but still edible, both were tested for microbial load and were proven to be still safe to eat. We isolated abundant phyllobilins from the aged produce and conducted targeted bioactivity assays, which confirmed the results from manuscript I-III, revealing phyllobilins as potent antioxidants. Furthermore, these phyllobilins were shown not to be cytotoxic or genotoxic in cells. In accordance with higher phyllobilin levels, extracts of stored lettuce and cucumbers exhibited a significantly higher antioxidative activity than extracts of fresh produce. Thus, we could show, that the amount of phyllobilins we ingest as a substantial part of a regular human diet depends on storage time. In general, green and fresh looking vegetables are preferred by consumers and perceived as healthy. Therefore, we utilized an online study to answer the question whether informing consumers about antioxidative phyllobilins that occur in higher amounts in aged greens can initiate a shift of thinking from consuming fresh and green to valuing de-greened 'old' lettuce. Indeed, we were able to show that consumers, who received information about phyllobilins, were willing to eat stored lettuce significantly longer than consumers who received a general information about chlorophyll. Furthermore, consumers perceived stored lettuce significantly more safe and healthy. As nowadays 1.3 billion tons of food is lost or wasted every year worldwide, our study has a great potential to reduce consumer food waste at home. Moreover, the results presented here unveil that aged plant produce might be more valuable than just waste and lay the groundwork for future studies aiming at establishing aged greens as beneficial for human health.

5.5 Phylloxanthobilins are abundant linear tetrapyrroles from chlorophyll breakdown with activities against cancer cells

Cornelia A. Karg, Pengyu Wang, Florian Kluibenschedl, Thomas Müller, Lars Allmendinger, Angelika M. Vollmar & Simone Moser (2020). *European Journal of Organic Chemistry, 2020*, 4499-4509.

Colorless phylloleucobilins have been thought to represent the end of the chlorophyll degradation pathway. However, oxidation products, the yellow phylloxanthobilins (PxBs), were discovered and could be established as bioactive constituents of herbal remedies and de-greening stored vegetables as demonstrated in manuscript I-IV. In order to gain further insights into the spectrum of phyllobilin bioactivities, we investigated anti-cancer effects of the chlorophyll derived linear tetrapyrroles. We thereby focused on a simple 3^2-OH-PxB and its phylloleucobilin (PleB) precursor. We identified plane tree as novel plant source for this PxB, and by using paper spray mass spectrometry, we could additionally show that yellow chlorophyll catabolites are more prevalent in plants than assumed previously. In contrast to its colorless PleB precursor, we identified a potent anti-proliferative activity for the PxB at low micromolar concentrations in human bladder and breast cancer cell lines. Moreover, the PxB inhibited colony formation and induced apoptotic cell death and a G2/M cell cycle arrest. Interestingly, esterification of the PleB resulted in an anti-proliferative activity, which correlated with increasing chain lengths of the alkyl esters. To unveil the influence of polarity on the observed effects, uptake studies were performed in bladder cancer cells and revealed all compounds to be taken up. More specifically, cellular uptake of esterified PleBs was found to increase with apolarity. Although the PxB was detected in smaller amounts in contrast to the esterified PleBs, it exhibited a higher or similar anti-proliferative activity. Therefore, PxB reactivity could not be explained by polarity or uptake, but indicated small structural variations to likely play a role with regards to anti-tumor potency. These findings provide first evidence for the anti-cancer potential of phyllobilins and point towards promising activities of these tetrapyrrolic natural products against cancer cells.

5.6 Tetrapyrroles are actin-targeting compounds

Cornelia A. Karg, Shuaijun Wang, Nader Danaf, Ryan Pemberton, Denzil Bernard, Maibritt Kretschmer, Sabine Schneider, Themistoklis Zisis, Angelika M. Vollmar, Don C. Lamb, Stefan Zahler, Simone Moser.

Phyllobilins are structurally closely related to the heme-derived bilins, which could also be verified in manuscript II. In particular, the phylloxanthobilins and phylloroseobilins resemble the structure of bilirubin and biliverdin. In addition, they share the same story of long considered useless waste products of their precursors. Extensive literature exists now concerning important physiological roles for bilins and we could establish phyllobilins in manuscript I-V as important bioactive natural products, too. However, the knowledge about direct biological targets of these tetrapyrroles is sparse, in case of the phyllobilins no human target could be elucidated yet. We observed anti-migratory effects on cancer cells using a wound healing assay for a phylloxanthobilin and a phylloroseobilin as well as for bilirubin and biliverdin. As the actin cytoskeleton plays an important role in cell migration, we set out to investigate the influence on actin dynamics. The four compounds were shown to inhibit actin polymerization and actin nucleation, as well as to facilitate actin depolymerization. The phylloroseobilin appeared to act as the most potent candidate in all of the different approaches. Direct binding of phyllobilins and bilins was determined using affinity chromatography with G-actin beads and confirmed an interaction with G-actin of each compound. A computational study showed the potential of the tetrapyrroles to interact with the same binding site as the known actin targeting compound kabiramide C. Using a competitive pull down approach with the actin binding protein profilin, phyllobilins were found to significantly prevent profilin binding, whereas bilins exerted a small effect. Moreover, the interaction of the linear tetrapyrroles with G-actin was studied by different biophysical techniques: fluorescence quenching measurements, microscale thermophoresis, and isothermal titration calorimetry. The binding affinity could be characterized by K_d values in the low micromolar range for BV, PxB, and PrB; the latter was, in accordance with the observed effects on actin functions, demonstrated to possess the strongest interaction. With this study, we could introduce a human biological target for phyllobilins for the first time and a novel human target for bilins, which holds large promise for therapeutic applications of phyllobilins and opens up an interesting field for further investigations.

6   References

1   Battersby, A. R. Tetrapyrroles: The Pigments of Life. *Natural product reports* **17**, 507-526 (2000).

2   Scheer, H. in *Chlorophylls and Bacteriochlorophylls: Biochemistry, Biophysics, Functions and Applications*   (eds Bernhard Grimm, Robert J. Porra, Wolfhart Rüdiger, & Hugo Scheer)   1-26 (Springer Netherlands, 2006).

3   Rabinowitch, E. I. & Govindjee. The Role of Chlorophyll in Photosynthesis. *Scientific American* **213**, 74-83 (1965).

4   Allen, M. B. in *The Chlorophylls*   (eds Leo P. Vernon & Gilbert R. Seely)   511-519 (Academic Press, 1966).

5   Williams, R. J. P. The Properties Of Metalloporphyrins. *Chemical Reviews* **56**, 299-328 (1956).

6   Durrett, T. P. & Welti, R. The tail of chlorophyll: Fates for phytol. *Journal of Biological Chemistry* **296**, 100802 (2021).

7   Fracheboud, Y. *et al.* The Control of Autumn Senescence in European Aspen. *Plant Physiology* **149**, 1982-1991 (2009).

8   Keskitalo, J., Bergquist, G., Gardeström, P. & Jansson, S. A Cellular Timetable of Autumn Senescence. *Plant Physiology* **139**, 1635-1648 (2005).

9   Lim, P. O., Kim, H. J. & Nam, H. G. Leaf Senescence. *Annual Review of Plant Biology* **58**, 115-136 (2007).

10   Peoples, M. B. & Dalling, M. J. in *Senescence and Aging in Plants*   (eds L. D. Noodén & A. C. Leopold)   181-217 (Academic Press, 1988).

11   Stocking, C. R. & Ongun, A. The Intracellular Distribution of Some Metallic Elements in Leaves. *American Journal of Botany* **49**, 284-289 (1962).

12   Wang, P., Richter, A. S., Kleeberg, J. R. W., Geimer, S. & Grimm, B. Post-translational coordination of chlorophyll biosynthesis and breakdown by BCMs maintains chlorophyll homeostasis during leaf development. *Nature Communications* **11**, 1254 (2020).

13   Hendry, G. A. F., Houghton, J. D. & Brown, S. B. The Degradation of Chlorophyll - a Biological Enigma. *New Phytologyst* **107**, 255-302 (1987).

14   Kräutler, B. & Matile, P. Solving the riddle of chlorophyll breakdown. *Accounts of Chemical Research* **32**, 35-43 (1999).

15   Matile, P., Ginsburg, S., Schellenberg, M. & Thomas, H. Catabolites of Chlorophyll in Senescent Leaves. *Journal of Plant Physiology* **129**, 219-228 (1987).

16   Thomas, H., Bortlik, K., Rentsch, D., Schellenberg, M. & Matile, P. Catabolism of chlorophyll in vivo: significance of polar chlorophyll catabolites in a non-yellowing senescence mutant of Festuca pratensis Huds. *New Phytologist* **111**, 3-8 (1989).

17   Kräutler, B., Jaun, B., Bortlik, K., Schellenberg, M. & Matile, P. On the Enigma of Chlorophyll Degradation - the Constitution of a Secoporphinoid Catabolite. *Angewandte Chemie International Edition* **30**, 1315-1318 (1991).

18   Kräutler, B. & Hörtensteiner, S. in *Handbook of Porphyrin Science* Vol. 28 *Handbook of Porphyrin Science*   117-185 (World Scientific Publishing Company, 2014).

19   Kräutler, B. Phyllobilins – the Abundant Tetrapyrrolic Catabolites of the Green Plant Pigment Chlorophyll. *Chemical Society Reviews* **43**, 6227-6238 (2014).

20   Hörtensteiner, S., Hauenstein, M. & Kräutler, B. in *Advances in Botanical Research* Vol. 90 (ed Bernhard Grimm) 213-271 (Academic Press, 2019).

21   Kräutler, B. Breakdown of Chlorophyll in Higher Plants - Phyllobilins as Abundant, Yet Hardly Visible Signs of Ripening, Senescence and Cell Death. *Angewandte Chemie International Edition* **55**, 4882-4907 (2016).

22   Müller, T. *et al.* A Divergent Path of Chlorophyll Breakdown in the Model Plant Arabidopsis thaliana. *ChemBioChem* **7**, 40-42 (2006).

23   Hörtensteiner, S., Vicentini, F. & Matile, P. Chlorophyll Breakdown in Senescent Cotyledons of Rape, Brassica napus L.: Enzymatic Cleavage of Phaeophorbide a In vitro. *New Phytologist* **129**, 237-246 (1995).

24   Shimoda, Y., Ito, H. & Tanaka, A. Conversion of chlorophyll b to chlorophyll a precedes magnesium dechelation for protection against necrosis in Arabidopsis. *The Plant Journal* **72**, 501-511 (2012).

25   Tanaka, R. & Tanaka, A. Chlorophyll cycle regulates the construction and destruction of the light-harvesting complexes. *Biochimica et Biophysica Acta (BBA) - Bioenergetics* **1807**, 968-976 (2011).

26   Pružinska, A., Tanner, G., Anders, I., Roca, M. & Hörtensteiner, S. Chlorophyll breakdown: Pheophorbide *a* oxygenase is a Rieske-type iron-sulfur protein, encoded by the *accelerated cell death 1* gene. *Proceedings of the National Academy of Sciences of the United States of America* **100**, 15259-15264 (2003).

27   Hörtensteiner, S., Wüthrich, K. L., Matile, P., Ongania, K. H. & Kräutler, B. The key step in chlorophyll breakdown in higher plants. Cleavage of pheophorbide a macrocycle by a monooxygenase. *The Journal of biological chemistry* **273**, 15335-15339 (1998).

28   Wüthrich, K. L., Bovet, L., Hunziker, P. E., Donnison, I. S. & Hörtensteiner, S. Molecular cloning, functional expression and characterisation of RCC reductase involved in chlorophyll catabolism. *The Plant Journal* **21**, 189-198 (2000).

29   Pruzinská, A. *et al.* In vivo participation of red chlorophyll catabolite reductase in chlorophyll breakdown. *The Plant cell* **19**, 369-387 (2007).

30   Christ, B. *et al.* Cytochrome P450 CYP89A9 is involved in the formation of major chlorophyll catabolites during leaf senescence in *Arabidopsis thaliana*. *The Plant cell* **25**, 1868-1880 (2013).

31   Oberhuber, M., Berghold, J., Breuker, K., Hörtensteiner, S. & Kräutler, B. Breakdown of chlorophyll: A nonenzymatic reaction accounts for the formation of the colorless "nonfluorescent" chlorophyll catabolites. *Proceedings of the National Academy of Sciences of the United States of America* **100**, 6910-6915 (2003).

32   Tommasini, R. *et al.* An ABC-transporter of Arabidopsis thaliana has both glutathione-conjugate and chlorophyll catabolite transport activity. *The Plant Journal* **13**, 773-780 (1998).

33 Christ, B., Hauenstein, M. & Hörtensteiner, S. A liquid chromatography-mass spectrometry platform for the analysis of phyllobilins, the major degradation products of chlorophyll in Arabidopsis thaliana. *The Plant Journal* **88**, 505-518 (2016).

34 Süssenbacher, I., Christ, B., Hörtensteiner, S. & Kräutler, B. Hydroxymethylated Phyllobilins: A Puzzling New Feature of the Dioxobilin Branch of Chlorophyll Breakdown. *Chemistry – A European Journal* **20**, 87-92 (2014).

35 Hauenstein, M., Christ, B., Das, A., Aubry, S. & Hörtensteiner, S. A Role for TIC55 as a Hydroxylase of Phyllobilins, the Products of Chlorophyll Breakdown during Plant Senescence. *The Plant cell* **28**, 2510-2527 (2016).

36 Curty, C. & Engel, N. Detection, isolation and structure elucidation of a chlorophyll a catabolite from autumnal senescent leaves of Cercidiphyllum japonicum. *Phytochemistry* **42**, 1531-1536 (1996).

37 Berghold, J., Breuker, K., Oberhuber, M., Hörtensteiner, S. & Kräutler, B. Chlorophyll breakdown in spinach: on the structure of five nonfluorescent chlorophyll catabolites. *Photosynthesis research* **74**, 109-119 (2002).

38 Kräutler, B. *et al.* A novel blue fluorescent chlorophyll catabolite accumulates in senescent leaves of the peace lily and indicates a split path of chlorophyll breakdown. *FEBS letters* **584**, 4215-4221 (2010).

39 Moser, S., Ulrich, M., Müller, T. & Kräutler, B. A yellow chlorophyll catabolite is a pigment of the fall colours. *Photochemical & photobiological sciences* **7**, 1577-1581 (2008).

40 Vergeiner, C. *et al.* Stereo- and Regioselective Phyllobilane Oxidation in Leaf Homogenates of the Peace Lily (Spathiphyllum wallisii): Hypothetical Endogenous Path to Yellow Chlorophyll Catabolites. *Chemistry – A European Journal* **21**, 136-149 (2015).

41 Wakana, D. *et al.* NMR-based characterization of a novel yellow chlorophyll catabolite, Ed-YCC, isolated from Egeria densa. *Tetrahydron Letters* **55**, 2982-2985 (2014).

42 Scherl, M. *et al.* Chlorophyll Catabolites in Fall Leaves of the Wych Elm Tree Present a Novel Glycosylation Motif. *Chemistry – A European Journal* **22**, 9498-9503 (2016).

43 Scherl, M., Müller, T. & Kräutler, B. Chlorophyll Catabolites in Senescent Leaves of the Lime Tree (Tilia cordata). *Chemistry & biodiversity* **9**, 2605-2617 (2012).

44 Erhart, T. *et al.* Novel Types of Hypermodified Fluorescent Phyllobilins from Breakdown of Chlorophyll in Senescent Leaves of Grapevine (Vitis vinifera). *Chemistry – A European Journal* **24**, 17268-17279 (2018).

45 Li, C., Erhart, T., Liu, X. & Kräutler, B. Yellow Dioxobilin-Type Tetrapyrroles from Chlorophyll Breakdown in Higher Plants—A New Class of Colored Phyllobilins. *Chemistry – A European Journal* **25**, 4052-4057 (2019).

46 Ulrich, M., Moser, S., Müller, T. & Kräutler, B. How the Colourless "Nonfluorescent" Chlorophyll Catabolites Rust. *Chemistry – A European Journal* **17**, 2330-2334 (2011).

47 Li, C. *et al.* Blue Transition Metal Complexes of a Natural Bilin-Type Chlorophyll Catabolite. *Chemical Science* **5**, 3388-3395 (2014).

48   Li, C. & Kräutler, B. A pink colored dioxobilin-type phyllobilin from breakdown of chlorophyll. *Monatshefte für Chemie - Chemical Monthly* **150**, 813-820 (2019).

49   Li, C. *et al.* Chlorophyll-Derived Yellow Phyllobilins of Higher Plants as Medium-Responsive Chiral Photoswitches. *Angewandte Chemie International Edition* **55**, 15760-15765 (2016).

50   Li, C. & Kräutler, B. Transition metal complexes of phyllobilins – a new realm of bioinorganic chemistry. *Dalton Transactions* **44**, 10116-10127 (2015).

51   Li, C., Podewitz, M. & Kräutler, B. A Blue Zinc Complex of a Dioxobilin-Type Pink Chlorophyll Catabolite Exhibiting Bright Chelation-Enhanced Red Fluorescence. *European Journal of Inorganic Chemistry* **2021**, 1903-1903 (2021).

52   Li, C. & Kräutler, B. Zn-complex of a natural yellow chlorophyll catabolite. *Journal of Porphyrins and Phthalocyanines* **20**, 388-396 (2016).

53   Müller, T., Vergeiner, S. & Kräutler, B. Structure elucidation of chlorophyll catabolites (phyllobilins) by ESI-mass spectrometry—Pseudo-molecular ions and fragmentation analysis of a nonfluorescent chlorophyll catabolite (NCC). *International Journal of Mass Spectrometry* **365-366**, 48-55 (2014).

54   Rios, J., Roca, M. & Pérez-Gálvez, A. Systematic HPLC/ESI-High Resolution-qTOF-MS Methodology for Metabolomic Studies in Nonfluorescent Chlorophyll Catabolites Pathway. *Journal of Analytical Methods in Chemistry* **2015**, 1-10 (2015).

55   Müller, T., Ulrich, M., Ongania, K.-H. & Kräutler, B. Colourless tetrapyrrolic chlorophyll catabolites found in ripening fruit are effective antioxidants. *Angewandte Chemie International Edition* **46**, 8699-8702 (2007).

56   Roiser, M. H., Müller, T. & Kräutler, B. Colorless Chlorophyll Catabolites in Senescent Florets of Broccoli (Brassica oleracea var. italica). *Journal of Agricultural and Food Chemistry* **63**, 1385-1392 (2015).

57   Roca, M., Rios, J. J., Chahuaris, A. & Perez-Galvez, A. Non-fluorescent and yellow chlorophyll catabolites in Japanese plum fruits (Prunus salicina, Lindl.). *Food Research International* **100**, 332-338 (2017).

58   Vergara-Domínguez, H., Ríos, J. J., Gandul-Rojas, B. & Roca, M. Chlorophyll catabolism in olive fruits (var. Arbequina and Hojiblanca) during maturation. *Food Chemistry* **212**, 604-611 (2016).

59   Moser, S. *et al.* Blue luminescence of ripening bananas. *Angewandte Chemie International Edition* **47**, 8954-8957 (2008).

60   Kumar, S. & Bandyopadhyay, U. Free heme toxicity and its detoxification systems in human. *Toxicology letters* **157**, 175-188 (2005).

61   Gazzin, S., Vitek, L., Watchko, J., Shapiro, S. M. & Tiribelli, C. A Novel Perspective on the Biology of Bilirubin in Health and Disease. *Trends in molecular medicine* **22**, 758-768 (2016).

62   Stocker, R., Yamamoto, Y., McDonagh, A. F., Glazer, A. N. & Ames, B. N. Bilirubin is an antioxidant of possible physiological importance. *Science* **235**, 1043-1046 (1987).

63   Zahir, F. *et al.* The pharmacological features of bilirubin: the question of the century. *Cellular & molecular biology letters* **20**, 418-447 (2015).

64   Zheng, J. *et al.* Biliverdin's regulation of reactive oxygen species signalling leads to potent inhibition of proliferative and angiogenic pathways in head and neck cancer. *British journal of cancer* **110**, 2116-2122 (2014).

65   Hirata, T., Tanaka, M., Ooike, M., Tsunomura, T. & Sakaguchi, M. Antioxidant activities of phycocyanobilin prepared from Spirulina platensis. *Journal of Applied Phycology* **12**, 435-439 (2000).

66   McCarty, M. F. Clinical potential of Spirulina as a source of phycocyanobilin. *Journal of medicinal food* **10**, 566-570 (2007).

67   Mittelberger, C. *et al.* Pathogen-Induced Leaf Chlorosis: Products of Chlorophyll Breakdown Found in Degreened Leaves of Phytoplasma-Infected Apple (Malus × domestica Borkh.) and Apricot (Prunus armeniaca L.) Trees Relate to the Pheophorbide a Oxygenase/Phyllobilin Pathway. *Journal of Agricultural and Food Chemistry* **65**, 2651-2660 (2017).

68   Moser, S., Erhart, T., Neuhauser, S. & Kräutler, B. Phyllobilins from Senescence-Associated Chlorophyll Breakdown in the Leaves of Basil (Ocimum basilicum) Show Increased Abundance upon Herbivore Attack. *Journal of Agricultural and Food Chemistry* **68**, 7132-7142 (2020).

7   Abbreviations

ACN/MeCN	Acetonitrile
AcOH	Acetic acid
AnnV	Annexin V
ANOVA	Analysis of variance
APS	Ammonium persulfate
ATP	Adenosine triphosphate
BOP	Benzotriazol-1-yloxytris(dimethylamino)phosphonium hexafluorophosphate
Bos	*Brassica oleracea var. sabauda*
BR	Bilirubin
BSA	Bovine serum albumin
BV	Biliverdin
BVRA	Biliverdin reductase A
CA	Caffeic acid
$CaCl_2$	Calcium chloride
$CaCl_2(H_2O)_6$	Calcium chloride hexahydrate
Caco	Colon carcinoma
CD_3OD	Deuterated methanol
CFU	Colony forming units
CGA	Chlorogenic acid
CH_2Cl_2/DCM	Dichloromethane
Chl	Chlorophyll
CI	Confidence interval
CID	Collision-induced dissociation
Cj	*Cercidiphyllum japonicum*
Co	*Cydonia oblonga*
CO	Carbon monooxide
CO_2	Carbon dioxide
COSY	Correlation spectroscopy
COX	Cyclooxygenase
CTB	CellTiter-Blue®
ctrl	Control
CYP	Cytochrome P450
DCF	2′,7′-Dichlorofluorescein
DMEM	Dulbecco´s modified eagle´s medium
DMSO	Dimethylsulfoxide
DNA	Deoxyribonucleic acid
DPleB	Dioxobilin-type phylloleucobilin
DPluB	Dioxobilin-type phyllolumibilin
DPPH	2,2-diphenyl-1-picrylhydrazyl
DPrB	Dioxobilin-type phylloroseobilin
DPxB	Dioxobilin-type phylloxanthobilin
DSMZ	Deutsche Sammlung für Mikroorganismen und Zellkulturen
DTT	Dithiothreitol
EDTA	Ethylenediaminetetraacetic acid

EGTA	Ethylene glycol-bis(2-aminoethylether)-N,N,N′,N′-tetraacetic acid
Ej	*Eribotrya japonica*
ELISA	Enzyme-linked immunosorbent assay
Em	Emission
EMA	European medicines agency
Ep	*Echinacea purpurea*
ER	Endoplasmic reticulum
ESI-MS	Electrospray ionisation-mass spectrometry
Et_3N	Triethylamine
EtOH	Ethanol
Ex	Excitation
FCC	Fluorescent chlorophyll catabolite
FCS	Fetal calf serum
$FeCl_3$	Iron(III) chloride
FITC	Fluoresceinisothiocyanat
FRAP	Ferric reducing antioxidant power
GSH	Glutathion
$H_2DCF-DA$	2′,7′-Dichlorofluorescein-diacetate
H_2O_2	Hydrogen peroxide
HCl	Hydrochloric acid
HEK	Human embryonic kidney
HEPES	Hydroxyethyl-piperazineethane-sulfonic acid buffer
HMBC	Heteronuclear multiple bond correlation
HMQC	Heteronuclear multiple quantum correlation
HPLC	High performance liquid chromatography
HR-MS	High resolution-mass spectrometry
HRP	Horseradish peroxidase
HSD	Honestly significant difference
HSQC	Heteronuclear single quantum correlation
Hv	*Hordeum vulgare*
IC_{50}	Half maximal inhibitory concentration
ITC	Isothermal titration calorimetry
K_2HPO_4	Potassium phosphate dibasic
KabC	Kabiramide C
KCl	Potassium chloride
K_d	Dissociation constant
KH_2PO_4	Potassium phosphate monobasic
KOH	Potassium hydroxide
LatB	Latrunculin B
LB	Lysogeny broth
LC	Liquid chromatography
LF	Lettuce fraction
LPS	Lipopolysaccharide
m/z	Mass/charge
Mc	*Musa cavendish*

MD	Mean differences
MEM	Minimum essential medium
MeOH	Methanol
MgCl$_2$	Magnesium chloride
MgCl$_2$(H$_2$O)$_6$	Magnesium chloride hexahydrate
*m*PluB	Modified phyllolumibilin
MS	Mass spectrometry
MST	Microscale thermophoresis
MTT	3-(4,5-dimethylthiazol-2-yl)-2,5-diphenyl tetrazolium bromide
n. a.	Not applicable
NaCl	Sodium chloride
NADPH	Nicotinamide adenine dinucleotide phosphate
NaHCO$_3$	Sodium bicarbonate
NaOH	Sodium hydroxide
NCC	Non-fluorescent chlorophyll catabolite
NEAA	Non-essential amino acids
NEM	N-ethylmaleimide
NH$_4$AcO	Ammonium acetate
(NH$_4$)$_2$CO$_3$	Ammonium carbonate
NMR	Nuclear magnetic resonance
NOESY	Nuclear overhauser effect spectroscopy
ns	Not significant
P/S	Penicillin/streptomycin
PaO	Pheophorbide a oxygenase
PB	Phyllobilin
PBS	Phosphate buffered saline
Pd	*Prunus x domestica*
PDB	Protein data bank
PFA	Paraformaldehyde
*p*FCC	Primary fluorescent chlorophyll catabolite
PGE2	Prostaglandin E2
PGG2	Prostaglandin G2
PGH2	Prostaglandin H2
Pheo a	Pheophorbide a
PI	Propidium iodide
PiCC	Pink chlorophyll catabolite
PleB	Phylloleucobilin
PluB	Phyllolumibilin
Po	*Platanus occidentalis*
pPluB	Primary phyllolumibilin
PrB	Phylloroseobilin
PVDF	Polyvinylidene difluoride
PxB	Phylloxanthobilin
PyBoP	Benzotriazol-1-yloxytripyrrolidinophosphonium hexafluorophosphate
RCC	Red chlorophyll catabolite
RCCR	Red chlorophyll catabolite reductase

RH	Relative humidity
ROS	Reactive oxygen species
RPMI	Roswell park memorial institute medium
SD	Standard deviation
SDS-PAGE	Sodium dodecyl sulfate-polyacrylamide gel electrophoresis
SEM/s.e.m.	Standard error of the mean
SGF	Simulated gastric fluid
SIF	Simulated intestinal fluid
sn	Supernatant
So	*Spinacia oleracea*
Sw	*Spathiphyllum wallisii*
T/E	Trypsin/ethylenediaminetetraacetic acid
TBS-T	Tris-buffered saline - Tween20
Tc	*Tilia cordata*
TCE	Trichloroethylene
TEA	Triethanolamine
TEMED	Tetramethylethylendiamin
TFA	Trifluoroacetic acid
TIRF	Total Internal Reflection Fluorescence
TPTZ	2,4,6-Tri(2-pyridyl)-s-triazine
t_R	Retention time
Tris	Tris(hydroxymethyl)aminomethane
Ud	*Urtica dioica L.*
UDPGA	Uridine 5′-diphosphoglucuronic acid trisodium salt
Ug	*Ulmus glabra*
UGT1A1	UDP-glucuronosyltransferases 1A1
UV-Vis	Ultraviolet/visible
vh-ctrl	Vehicle control
YCC	Yellow chlorophyll catabolite
YPD	Yeast extract-peptone-dextrose
Zm	*Zea mays*
$Zn(AcO)_2$	Zink acetate

8 Acknowledgements

An allererster Stelle geht mein herzlichster Dank an meine Doktormutter, Frau Prof. Dr. Angelika Vollmar. Frau Prof. Vollmar, ich danke Ihnen, dass Sie mir die Möglichkeit gegeben haben, an Ihrem Lehrstuhl zu promovieren. Die zahlreichen produktiven Diskussionen mit Ihnen und Ihr wertvoller fachlicher Input waren für mich von außerordentlichem Wert. Ihr Engagement und Ihre ansteckende Begeisterung für die Forschung und Lehre bewundere ich sehr, außerdem habe ich Ihre freundliche und offene Art stets als sehr motivierend empfunden.

Mein besonderer Dank geht an Frau Dr. Simone Moser für die hervorragende Betreuung. Liebe Simone, ich danke Dir, dass Du mich mit deinem enormen fachlichen Wissen in jeder Phase meiner Promotion unterstützt hast. Ich konnte zu jeder Zeit mit Fragen und Anliegen zu Dir kommen und habe durch Dich das wissenschaftliche Arbeiten erlernen und vertiefen dürfen. Ich hätte mir keine bessere Betreuerin wünschen können und freue mich sehr auf unsere weitere Zusammenarbeit.

Ein weiteres Dankeschön geht an Herrn Prof. Dr. Stefan Zahler für die fachliche Unterstützung und die wertvollen Ratschläge und für die Bereitschaft, meine Arbeit als Zweitprüfer zu bewerten.

Meiner weiteren Prüfungskommission, bestehend aus Frau Prof. Dr. Olivia Merkel, Herrn Prof. Dr. David Bernhard, Herrn Prof. Dr. Franz Bracher und Herrn Prof. Dr. Franz Paintner, danke ich für das Interesse an meiner Arbeit und für die Bewertung.

Außerdem möchte ich mich bei meinen Kooperationspartnern Prof. Dr. Thomas Müller (UIBK Innsbruck), Dr. Lars Allmendinger (Department Pharmazie, LMU München), Dr. Christian Doppler und Prof. Dr. David Bernhard (JKU Linz), Christina Neubig und Prof. Dr. Jutta Roosen (TU München), und Nader Danaf und Prof. Dr. Don Lamb (Department Chemie, LMU München) für die produktive Zusammenarbeit im Rahmen unserer gemeinsamen Projekte bedanken.

Ein herzliches Dankeschön geht an meine StudentInnen Julian, Charlotte, Nadine, Marlene und Franziska für ihre großartige Arbeit und die motivierte Teilnahme an meinen Projekten.

Acknowledgements

9 List of publications and conference contributions

9.1 Research articles

i. **Karg, C. A.,** Wang, P., Vollmar, A. M., & Moser, S. (2019). Re-opening the stage for *Echinacea* research - Characterization of phylloxanthobilins as a novel anti-oxidative compound class in *Echinacea purpurea*. *Phytomedicine, 60*, 152969.

ii. **Karg, C. A.,** Schilling, C. M., Allmendinger, L., & Moser, S. (2019). Isolation, characterization, and antioxidative activity of a dioxobilin-type phylloxanthobilin from savoy cabbage. *Journal of Porphyrins and Phthalocyanines, 23*, 881-888.

iii. **Karg, C. A.,** Wang, P., Kluibenschedl, F., Müller, T., Allmendinger, L., Vollmar, A. M., & Moser, S. (2020). Phylloxanthobilins are Abundant Linear Tetrapyrroles from Chlorophyll Breakdown with Activities Against Cancer Cells. *European Journal of Organic Chemistry, 2020*, 4499-4509.

iv. **Karg, C. A.**, Doppler, C., Schilling, C., Jakobs, F., Dal Colle, M. C. S., Frey, N., Bernhard, D., Vollmar, A. M. & Moser, S. (2021). A yellow chlorophyll catabolite in leaves of *Urtica dioica* L.: An overlooked phytochemical that contributes to health benefits of stinging nettle. *Food Chemistry, 359*, 129906.

v. **Karg, C. A.,** Neubig, C., Roosen, J. & Moser, S. (2021). Rising levels of antioxidative phyllobilins in stored agricultural produce and their impact on consumer acceptance. A*ccepted for publication in npj Science of Food*

vi. **Karg, C. A.,** Wang, S., Danaf, N., Pemberton, R., Bernard, D., Kretschmer, M., Schneider, S., Zisis, T., Vollmar, A. M., Lamb, D. C., Zahler, S. & Moser, S.. Tetrapyrrolic pigments are actin targeting compounds.
Submitted for publication in Angewandte Chemie International Edition

vii. Wang, P., **Karg, C. A.,** Frey, N., Frädrich, J., Vollmar A. M. & Moser, S. (2021). Phyllobilins as challenging diverse natural product class – exploration of pharmacological activities. *Archiv der Pharmazie*. *In Press*

9.2 Conference contributions

i. **Karg, C. A.,** Zahler, S., Vollmar, A.M., and Moser, S., **10th International Conference on Porphyrins and Phytalocyanines (ICPP-10) in Munich, Germany (July 2018)**. Probing the Effects of Tetrapyrroles Derived from Chlorophyll Breakdown on Cancer Cells. Final Programme and Book of Abstracts.

ii. **Karg, C. A.,** Wang, P., Fuchs, D., Vollmar, A.M., Gostner, J.M., Moser, S., **39th International Winter-Workshop Clinical, Chemical and Biochemical Aspects of Pteridines and Related Topics in Innsbruck, Austria (February 2020).** Phylloxanthobilins as overlooked components of medicinal plants - investigations on bioactivities. *Pteridines*, Vol. 31, 2020.

10 Appendix

In the following, manuscripts I-VI are reprinted:

I. **Karg, C. A.,** Wang, P., Vollmar, A. M., & Moser, S. (2019). Re-opening the stage for Echinacea research - Characterization of phylloxanthobilins as a novel anti-oxidative compound class in *Echinacea purpurea. Phytomedicine, 60*, 152969.

II. **Karg, C. A.,** Schilling, C. M., Allmendinger, L., & Moser, S. (2019). Isolation, characterization, and antioxidative activity of a dioxobilin-type phylloxanthobilin from savoy cabbage. *Journal of Porphyrins and Phthalocyanines, 23*, 881-888.

III. **Karg, C. A.**, Doppler, C., Schilling, C., Jakobs, F., Dal Colle, M. C. S., Frey, N., Bernhard, D., Vollmar, A. M., & Moser, S. (2021). A yellow chlorophyll catabolite in leaves of *Urtica dioica* L.: An overlooked phytochemical that contributes to health benefits of stinging nettle. *Food Chemistry, 359*, 129906.

IV. **Karg, C. A.,** Neubig, C. M., Roosen, J., & Moser, S. (2021). Rising levels of antioxidative phyllobilins in stored agricultural produce and their impact on consumer acceptance. A*ccepted for publication in npj Science of Food*

V. **Karg, C. A.,** Wang, P., Kluibenschedl, F., Müller, T., Allmendinger, L., Vollmar, A. M., & Moser, S. (2020). Phylloxanthobilins are Abundant Linear Tetrapyrroles from Chlorophyll Breakdown with Activities Against Cancer Cells. *European Journal of Organic Chemistry, 2020*, 4499-4509.

VI. **Karg, C. A.,** Wang, S., Danaf, N., Pemberton, R., Bernard, D., Kretschmer, M., Schneider, S., Zisis, T., Vollmar, A. M., Lamb, D. C., Zahler, S., & Moser, S.. Tetrapyrrolic pigments are actin targeting compounds.
Submitted for publication in Angewandte Chemie International Edition

Original Article

Re-opening the stage for *Echinacea* research - Characterization of phylloxanthobilins as a novel anti-oxidative compound class in *Echinacea purpurea*

Cornelia A. Karg, Pengyu Wang, Angelika M. Vollmar, Simone Moser*

Pharmaceutical Biology, Department Pharmacy, Ludwig-Maximilians University of Munich, Butenandtstraße 5-13, Munich 81377, Germany

ABSTRACT

Background: Phylloxanthobilins are tetrapyrrolic natural products that arise from the degradation of chlorophyll. Phylloxanthobilins have been discovered roughly 10 years ago in the leaves of deciduous trees, and are now considered a compound class with high and still unexplored potential of bioactivities. To date, however, there are no reports on the occurrence of phylloxanthobilins in parts of a medicinal plant used for pharmaceutical preparations.

Purpose: The relevance of *Echinacea purpurea* as medicinal plant is undoubtedly high, and a large variety of pharmaceutical preparations is available on the market, mostly for the treatment of the common cold. Nevertheless, its phytochemical profiling has been limited to analysis for previously characterized substances, and this has not explained all its pharmacological efficacies. We therefore set out to investigate the occurrence of phylloxanthobilins in *Echinacea purpurea*.

Methods: Phylloxanthobilins in leaf extracts of *Echinacea purpurea* were detected using analytical HPLC. Identified phyllobilins were purified from plant material and characterized by UV/Vis, mass spectrometry, MS/MS, and confirmed by co-injections with previously published phyllobilins from different sources. The antioxidant activity of selected isolated phylloxanthobilins was assessed by an *in vitro* ferric reducing antioxidant power (FRAP) assay; in addition, the ability to scavenge ROS in cells caused by hydrogen peroxide stimulation was determined by measuring H$_2$DCF-DA fluorescence and by assessing cellular GSH levels.

Results: In extracts of *Echinacea purpurea* leaves, an unprecedented diversity of phylloxanthobilins was detected; surprisingly, not only in senescent yellow leaves, but also in green leaves with no visible chlorophyll degradation. Six phylloxanthobilins were identified and structurally characterized. The uptake of phylloxanthobilins by human endothelial kidney cells was demonstrated. When investigating the anti-oxidative activity of these natural products, a potent *in vitro* activity was demonstrated; in addition, phylloxanthobilins possess intracellular ROS scavenging ability and can prevent oxidative stress as assessed by total cellular GSH levels.

Conclusion: Phylloxanthobilins are important constituents of *Echinacea purpurea* extracts, and our first exploratory studies hint towards promising bioactivities of these natural products, which may be relevant for understanding *Echinacea* efficacies.

Introduction

Roughly 1000 million tons of chlorophyll (Chl) are broken down each year on Earth (Hendry et al., 1987). Leaf senescence and fruit ripening are visual signs of Chl degradation. In spite of its everyday presence, the chemical and biological basis of Chl degradation remained a mystery for a long time until the first Chl catabolite from a higher plant was identified and characterized (Kräutler et al., 1991).
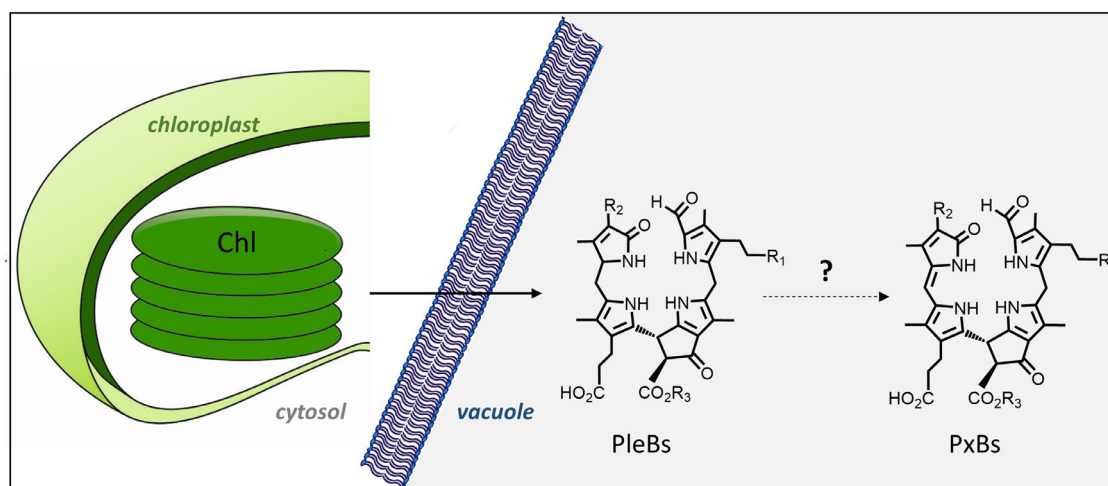

Fig. 1. Topological outline of the Chl degradation pathway leading to colorless PleBs in the vacuoles. PxBs are oxidation products of PleBs.

The structure of this catabolite gave the first clues as to the fate of the green plant pigment. Unlike Chl, the identified catabolite was a colorless, non-phototoxic, and more water-soluble tetrapyrrole. After its discovery, many more catabolites from different plant species followed, each showing the same linear tetrapyrrolic core structure; differences arose from modifications of the periphery. Linear Chl catabolites are now termed 'phyllobilins' (PBs) due to their structural relation to the tetrapyrrolic 'bilin' degradation products of heme (Kräutler, 2016). Once released from its binding proteins, Chl is phototoxic for the cell and has to be destroyed. The pathway to accomplish the detoxification has been studied extensively and has been shown to be strictly controlled and regulated in all higher plants, yielding colorless phylloleucobilins (PleBs) (Kuai et al., 2018). For a long time, PleBs were considered the 'final' products of Chl breakdown, and were regarded as stable storage form of degraded Chl in the vacuoles – until the discovery of the yellow phyllobilins, termed phylloxanthobilins (PxBs, Fig. 1). PxBs are oxidation products of PleBs and were found to occur naturally, thereby contributing significantly to the autumn colors (Moser et al., 2008).

How PxBs are formed from PleBs is still elusive; an uncharacterized, possibly enzymatic 'oxidative activity', however, has been recently discovered in leaf extracts that can efficiently transform PleBs to PxBs via a hydroxylated intermediate (Vergeiner et al., 2015). Although this appears to indicate that plants actively form PxBs from PleB precursors, which occur in a vast structural variety of modifications, reports on naturally occurring PxBs have been few. To date, only one or two PxBs have so far been identified in extracts of *Egeria densa* (Wakana et al., 2014), *Cercidiphyllum japonicum* (Moser et al., 2008), *Tilia cordata* (Scherl et al., 2012), and were detected as minor fractions in extracts of the leaves of the plum tree (Erhart et al., 2016) and wych elm (Scherl et al., 2016).

For a long time, PBs have been regarded as 'mere' detoxification products of Chl. In recent years, however, the structural characterization of highly modified PBs and the identification of PxBs has changed the view on these natural products: PBs, especially PxBs, bear a strong resemblance to bilirubin, for which more and more data accumulate indicating a protective function in diseases linked to oxidative stress (Gazzin et al., 2016). PBs, too, are suspected to be of significant pharmaceutical interest (Erhart et al., 2018; Scherl et al., 2016), although so far, no direct evidence for a pharmacological activity - safe for the *in vitro* anti-oxidative activity of PleBs (Müller et al., 2007) - has been identified. In addition, there is no published report about any investigation of relevant medicinal plant extracts in terms of PB contents.

Echinacea purpurea is a plant of high pharmaceutical importance: herbal preparations are approved by the European Medicines Agency

(EMA) from traditional use for the treatment of small superficial wounds, and approved from well-established use for the short-term prevention and treatment of the common cold (EMA/HMPC/48704/2014). In the USA, it is estimated that dietary supplements to treat the common cold based on *Echinacea* are among the most used natural products (Clarke et al., 2015).

Despite its broad application as cold remedy, clinical data to support the therapeutic benefit of *Echinacea* preparations are inconclusive. The outcomes of the numerous studies vary greatly, from a significant beneficial effect lessening cold symptoms and shortening their duration, to no effect at all (Barrett et al., 2010). Systematic reviews on existing controlled clinical trials, however, indicate that immunomodulatory effects from preparations containing extracts of *Echinacea* can indeed be translated into the clinics. Still, there is no clear guideline for posology and which preparation to use, calling for further clinical trials (Melchart et al., 1994).

In contrast, non-clinical assays evaluating the immunomodulatory effects of *Echinacea* extracts or isolated constituents certainly prove immunomodulatory effects in plentiful pharmacological studies. Extensive studies by Wagner and co-workers demonstrated stimulation of phagocytosis *in vitro* and in mice (Bauer et al., 1989; Bauer and Wagner, 1991, 1988b), as well as of macrophages and as a consequence, cytokines (Bauer, 2002; Roesler et al., 1991; Stimpel et al., 1984). Still, no single chemical entity or class of compounds can be held responsible for all immunomodulatory effects reported for *Echinacea* (Ardjomand-Woelkart and Bauer, 2014; Barrett, 2003), and finding a consensus about the efficacies of *Echinacea* has proven difficult (Kreft and Razinger, 2014). Furthermore, recent studies attribute the immunostimulating effects of *Echinacea* extracts to the bacterial load of *Echinacea purpurea* herb samples (Pugh et al., 2013).

Phytochemical profiling of extracts of different *Echinacea* species and plant parts has revealed a complex chemical composition as well as high variability among the different extracts, rendering a generalization of occurrence and quantification of constituents difficult (Bruni et al., 2018). Compound classes in *Echinacea purpurea* that appear to contribute to health promoting effects are caffeic acid derivatives such as cichoric acid, echinacoside, chlorogenic acid, cynarin, and caftaric acid, the high molecular weight compounds polysaccharides and glycoproteins, and alkylamides, the latter being apolar constituents mostly of root extracts (Barrett, 2003).

Since no chemical entity alone can account for all health promoting effects, caffeic acid derivatives are commonly used of markers of medicinal quality (caftaric acid and cichoric acid contents) (Kreft and Razinger, 2014). Caffeic acid derivatives were shown to possess many bioactivities, including high free-radical scavenging activity

(Pellati et al., 2004). Phytochemical profiling and new analytical techniques mostly focus on the compound classes listed above (Konar et al., 2014; Lepojević et al., 2017), still, the pharmacological efficacies of *Echinacea* cannot be tied to a single constituent or compound class and cannot be completely explained by those already identified (Barrett, 2003).

On one hand, further research is clearly needed in regards to bioactivity related principles in *Echinacea purpurea*. On the other hand, PxBs represent underexplored natural products in terms of their potential bioactivities. We therefore set out to study the bioactivities of PxBs in the context of *Echinacea* efficacies. We reasoned that PBs might be a yet unidentified bioactive constituent of this important medicinal plant, which could help fill the gap between the vast repertoire of *Echinacea* bioactivities and the still incomplete phytochemical profiling.

Material and methods

Reagents and chemicals

HPLC grade acetonitrile (MeCN), methanol (MeOH), ethanol (EtOH), dimethylsulfoxide (DMSO) and hydrochloric acid (HCl) were obtained from VWR International GmbH (Ismaning, Germany) and ultra-pure water (18 MΩ.cm^{-1}) from a Millipore S.A.S. Milli-Q Academic system (18,2 MΩ cm^{-1}, Molsheim, France). 2,4,6-Tri(2-pyridyl)-s-triazine (TPTZ), potassium phosphate monobasic (KH$_2$PO$_4$), potassium phosphate dibasic (K$_2$HPO$_4$), ammonium acetate (NH$_4$AcO), iron(III) chloride (FeCl$_3$), N-ethylmaleimide (NEM), trifluoroacetic acid (TFA), hydrogen peroxide (30%), and glass beads (acid-washed, diameter 0.5 mm) were from Merck (Darmstadt, Germany). Trolox was from Enzo Life Sciences GmbH (Lörrach, Germany), SepPak Plus C18 cartridges from Waters Associates (Milford, USA) and 2′,7′-dichlorodihydrofluorescein diacetate (H$_2$DCF-DA) were from Thermo Fisher (Waltham, MA, USA). DMEM medium, penicillin, and streptomycin were from PAN-Biotech (Aidenbach, Germany); Fetal calf serum (FCS) was from PAA Laboratories GmbH (Pasching, Austria).

Plant material

Fresh senescent and green leaves of *Echinacea purpurea* (L.) Moench were collected in the medicinal plant garden at the department of pharmacy of the Ludwig-Maximilians University of Munich and either used immediately or stored at −80 °C until further use. The identity of the plant was determined by Prof. Susanne S. Renner (Department of Systematic Botany and Mycology, Faculty of Biology, University of Munich), and a voucher specimen has been deposited in the Munich herbarium (acronym M; Moser & Karg 1). Tobacco (*Nicotiana rustica)* seeds were purchased from Van der Wal (Hoogeveen, Netherlands), germinated, senescent leaves harvested and stored at −80 °C. Spinach (*Spinacia oleracea*) was bought in a local supermarket and Chl breakdown was induced by incubation in the dark at RT for 3 days. Katsura tree (*Cercidiphyllum japonicum*) and lime tree (*Tilia cordata*) leaves were collected in the botanical garden of Munich.

Chromatography

i) Analytical HPLC: Agilent 1260 Infinity II LC system with a 1260 Infinity Degasser, a 1100 Series quaternary pump and 1100 Series diode array detector; Agilent Poroshell column 120EC−C18 4 μm 46 × 150 mm at 15 °C protected by Phenomenex ODS 4 × 3 mm i.d. pre-column; injection volume: 100 μl. Solvent system: mobile phase A = ammonium acetate buffer 10 mM pH 7, B = MeOH, flow 0,5 ml/min; Solvent composition: 0–5 min 20% B, 5–55 min 20% to 70% B, 55–57 min 70% to 100% B. Solvent system for GSH measurements: mobile phase A = 0,1% TFA, B = MeOH, flow 1 ml/min; Solvent composition: 0–5 min 1% B, 5–17 min 1.2% B, 17–20 min 1.2% to 100% B, 20–24 min 100% B, 24–28 min 100 to 1% B. Data

were processed with OpenLab CDS 2.3.
ii) Semi-preparative HPLC: Gynkotek LC-System with manual sampler, M480 pump, Phenomenex DG-301 online degasser, Gynkotek UVD 640 diode array detector and a Rheodyne injection valve with 5 ml loop; column Phenomenex Luna 5μ C18, 100 Å, with Phenomenex pre-column ODS 9 × 16 mm; mobile phase A = ammonium acetate buffer 10 mM pH 7, B = MeCN, flow 2.5 ml/min; solvent composition: 0–2 min 12% B, 2–12 min 12% to 20% B, 12–30 min 20% to 80% B, 30–40 min 80% to 100% B. Data were processed with Gynkosoft 5.50.

Spectroscopy

UV/Vis: λ$_{max}$ [nm] (ε$_{rel}$), Thermo Spectronic Genesys 5 (336001) UV-Visible spectrophotometer. Concentrations of *Ep*-PxBs were calculated using log ε $_{(426\,nm)}$ = 4.51 (Moser et al., 2008).

ESI-MS and MS/MS: Thermo Finnigan LCQ Deca XP Plus mass spectrometer, ESI source, positive ion mode, spray voltage 4.7 kV; ions of selected m/z were isolated in the ion trap prior to fragmentation by CID (collision induced dissociation, 9%). High Resolution-Mass Spectra were measured in the LMU Department of Chemistry MS facility; data were processed with Xcalibur.

Chemoprofiling of Echinacea purpurea leaves

Selected *Echinacea purpurea* leaves of different colors (one leaf each) were each ground with 2 ml of MeOH/potassium phosphate buffer 100 mM pH 7 (20/80) in a mortar. After centrifugation, the extract was subjected to analytical HPLC (injection volume 100 μl). PxBs were identified by their UV/Vis characteristics. To estimate the relative PxB contents from HPLC peak areas (one run each), sums of the peak areas of all six PxBs at 420 nm were calculated, corrected for the differences in weight of the extracted leaf material, and normalized to the sum of peak areas of all six PxBs in the yellow leaf.

Chl contents determination in Echinacea purpurea leaves

Chl a, Chl b, and total Chl contents in green, yellow and red leaves were determined as follows: Three leaves of each color were used for three independent experiments. 1 cm^2 of leaf material was extracted four times with 1 ml of 80% acetone containing 1 mM KOH each (Pružinská et al., 2005); extracts were combined and Chl contents was determined spectrophotometrically as described (Strain et al., 1971).

Isolation and structure elucidation of Ep-PxBs from fresh senescent leaves

200 g of fresh senescent leaves were ground with 500 ml of solvent mixture by a Braun hand blender Model MR 5000 in a 5 l stainless steel beaker. The solvent consisted of 60% MeOH and 40% potassium phosphate buffer 50 mM pH 5.2. The mixture was incubated at RT for 1 h, then filtered through a cotton cloth and the solid residue was washed with 400 ml solvent, and filtered again. The clear solution was acidified to pH 3.5 by addition of 50% AcOH and was stirred at RT in the dark overnight. Afterwards, the mixture was concentrated to 50 ml, centrifuged and filtered prior to purification by semi-preparative HPLC. Fractions were dried on a rotary evaporator, re-dissolved in 20/80 MeOH/potassium phosphate buffer 100 mM pH 7 and re-purified by semi-preparative HPLC. The purity of the six isolated PxBs was controlled by analytical HPLC prior to concentrating on a rotary evaporator at 35 °C and lyophilization. The lyophilized samples were dissolved in DMSO and stored at −20 °C. Yields were 0.63 μmoles *Ep*-PxB-1, 0.67 μmoles *Ep*-PxB-2, 0.92 μmoles *Ep*-PxB-3, 0.14 μmoles *Ep*-PxB-4, 1.1 μmoles *Ep*-PxB-5 and 0.27 μmoles *Ep*-PxB-6. A peak purity test was performed using Agilent OpenLab CDS software (UV-Peak purity (p) in parts per million): *Ep*-PxB-1 *p* = 785; *Ep*-PxB-2 *p* = 823; *Ep*-PxB-3 *p* = 877; *Ep*-PxB-4 *p* = 814; *Ep*-PxB-5 *p* = 904; *Ep*-PxB-6 *p* = 701. The

peak purity variability is due to the known 8^2-epimerization, which is a natural feature of all phyllobilins and results in non-baseline separated signals (Moser et al., 2017).

Spectroscopic data

Retention time (r.t.) from analytical HPLC

Ep-PxB-1 (1). r.t. = 24.6 min. UV/Vis (HPLC trace, 100 mM aq. ammonium acetate buffer pH 7/MeOH 80/20): 244 (0.52), 314 (0.67), 414 (1.00) nm. HR-ESI-MS: $m/z_{calculated}$ ($C_{44}H_{53}O_{18}N_4$) = 925.3277 $[M + H]^+$; m/z_{found} = 925.3365 (Δ = 1.7 ppm). ESI-MS (MS/MS of isolated $[M + H]^+$ (CID 9%); positive mode): m/z (%) = 925.07 (33) $[M + H]^+$; 906.07 (12) $[M-H_2O +H]^+$; 891.87 (100) $[M-MeOH+H]^+$; 838.67 (19) $[M-O-malonyl+H]^+$; 807.07 (5) $[M-ring D + K]^+$, 528.27 (1) $[M-H_2O-ring A+Na]^+$.

Ep-PxB-2 (2). r.t. = 28.9 min. UV/Vis (HPLC trace, 100 mM aq. ammonium acetate buffer pH 7/MeOH 80/20): 244 (0.52), 314 (0.70), 414 (1.00) nm. HR-ESI-MS: $m/z_{calculated}$ ($C_{41}H_{51}O_{15}N_4$) = 839.3273 $[M + H]^+$; m/z_{found} = 839.3354 (Δ = 1.0 ppm). LC/ESI-MS: m/z (%) = 861.3 (4) $[M+Na]^+$; 839.3 (100) $[M + H]^+$; 821.3 (25) $[M + H-H_2O]^+$; 789.3 (2) $[M + H-H_2O-MeOH]^+$; 659.3 (6) $[M + H-H_2O-C_6H_{10}O_5]^+$.

Ep-PxB-3 (3) r.t. = 33.3 min. UV/Vis (HPLC trace, 100 mM aq. ammonium acetate buffer pH 7/MeOH 80/20): 244 (0.52), 314 (0.69), 414 (1.00) nm. HR-ESI-MS: $m/z_{calculated}$ ($C_{35}H_{41}O_{10}N_4$) = 677.2744 $[M + H]^+$; m/z_{found} = 677.2821 (Δ = 0.6 ppm).

Ep-PxB-4 (4). r.t. = 41.8 min. UV/Vis (HPLC trace, 100 mM aq. ammonium acetate buffer pH 7/MeOH 80/20): 244 (0.61), 314 (0.75), 428 (1.00) nm. HR-ESI-MS: $m/z_{calculated}$ ($C_{44}H_{51}O_{16}N_4$) = 891.3222 $[M + H]^+$; m/z_{found} = 891.3308 (Δ = 1.5 ppm).

Ep-PxB-5 (5). r.t. = 45.5 min. UV/Vis (HPLC trace, 100 mM aq. ammonium acetate buffer pH 7/MeOH 80/20): 244 (0.56), 314 (0.76), 428 (1.00) nm. HR-ESI-MS: $m/z_{calculated}$ ($C_{41}H_{49}O_{13}N_4$) = 805.3218 $[M + H]^+$; m/z_{found} = 805.3210 (Δ = 1.1 ppm).

Ep-PxB-6 (6). r.t. = 51.7 min. UV/Vis (HPLC trace, 100 mM aq. ammonium acetate buffer pH 7/MeOH 80/20): 244 (0.58), 314 (0.75), 428 (1.00) nm. HR-ESI-MS: $m/z_{calculated}$ ($C_{35}H_{39}O_8N_4$) = 643.2690 $[M + H]^+$; m/z_{found} = 643.2764 (Δ = 0.3 ppm).

Tentative structure assignment of Ep-PxB-1

Ep-PxB-1 represents a PxB with a previously unpublished combination of modifications; therefore, an MS/MS experiment was performed that allows for deducing structural patterns in PBs due to characteristic fragmentations (Müller et al., 2014; Ríos et al., 2015). Furthermore, a ^{1}H-NMR spectrum (500 MHz, solvent d^4-MeOH, measurement at room temperature) was recorded, confirming the lack of the vinyl group at ring D by the absence of the typical signals from an ABX spin system typically observed at 5.3–6.4 ppm (Moser et al., 2017) (Supplementary Information).

Identification of (2–6) by co-injection with previously characterized phyllobilins

The spectroscopic data indicated that the molecular constitution of Ep-PxB-2 and Ep-PxB-6 were identical to the PxBs in *Tilia cordata* (*Tc*-PxB) (Scherl et al., 2012) and *Cercidiphyllum japonicum* (*Cj*-PxB-2) (Moser et al., 2008). The structures were further confirmed by HPLC co-injection. The purified samples of Ep-PxB-2, Tc-PxB, and a mixture thereof, as well as Ep-PxB-6, Cj-PxB-2, and a mixture thereof showed

identical chromatographic characteristics (Supplementary Information).

Based on the MS spectra the structural pattern of Ep-PxB-4 an Ep-PxB-5 were deduced to be the same like the oxidation products of already identified PleBs in tobacco, *Nr*-PleB-1 and *Nr*-PleB-2 (Berghold et al., 2004). *Nr*-PleBs were oxidized to the corresponding PxBs, provisionally named *Nr*-PxB-1 and *Nr*-PxB-2, according to the protocol of Vergeiner et al. (2015), isolated and characterized by MS (Supplementary Information). HPLC co-injection experiments of isolated compounds Ep-PxB-4, Nr-PxB-1 and Ep-PxB-5, Nr-PxB-2 and corresponding mixtures, respectively, showed identical peaks. The same oxidation and co-injection experiment was performed with *So*-PleB-2 from *Spinacia oleracea* (Berghold et al., 2002), as the structure of the resulting PxB, temporary named *So*-PxB-2, was indicated to be consistent to the structure of Ep-PxB-3. HPLC chromatograms of Ep-PxB-3, So-PxB-2 and the mixture showed an identical retention time for the two compounds.

Ferric reducing antioxidant power (FRAP) assay

The FRAP assay was performed according to the protocol of Benzie et al. (Benzie and Strain, 1996) with minor adaptations. Briefly, 50 μM of the different compounds and several concentrations of Trolox were incubated with the freshly prepared FRAP reagent for 5 min at 37 °C. The reagent included 10 vol 300 mM acetate buffer pH 3.5, 1 vol 10 mM TPTZ (2,4,6-Tri(2-pyridyl)-s-triazine) in 40 mM HCl and 1 vol 20 mM iron(III)chloride. The antioxidant reduces the Fe^{3+}-(TPTZ)$_2$-complex to Fe^{2+}-(TPTZ)$_2$, which absorbs light at 620 nm. Absorbance of Trolox concentrations were used to create a calibration curve and antioxidant power of the compounds was expressed as Trolox equivalents.

Cell culture

Human embryonic kidney derived HEK 293 cells (HEK) and HeLa cells were obtained from the *Deutsche Sammlung von Mikrorgansimen und Zellkulturen* (DSMZ; Braunschweig, Germany) and cultured in DMEM medium supplemented with 10% fetal calf serum (FCS) and 1% penicillin/streptomycin. Cells were cultivated at 37 °C under 5% CO$_2$ atmosphere and split in a 1:10 ratio every 3 to 4 days.

Uptake of Ep-PxBs by HEK cells

2×10^6 cells were seeded in 60 mm dishes and incubated for 24 h. Cells were treated with Ep-PxB-3 (150 μM), Ep-PxB-5 (150 μM) and Ep-PxB-6 (60 μM) or DMSO control. Three PxBs with different polarities were chosen as representative compounds; a lower concentration of Ep-PxB-6 was used to compensate for a possible better uptake due to its higher lipophilicity compared to the other two tested PxBs. After 4 h, cells were washed with phosphate buffered saline (PBS) twice and scraped off in 5 ml medium. The cell suspension was centrifuged and again washed with PBS. Cells were lysed and proteins were precipitated with MeCN for 1 h on ice. Lysates were cleared by centrifugation and purified by solid phase extraction (Waters SepPak C18) prior to analytical HPLC.

Detection of intracellular ROS

Intracellular ROS levels in HeLa cells were measured following a published protocol (Yokomizo and Moriwaki, 2006) with minor modifications: In brief, 1×10^5 cells/ml in 96 well plates were treated with Ep-PxB-1, Ep-PxB-3, Ep-PxB-5, caffeic acid (10 μM), and a DMSO control for 24 h. After removal of the medium, H$_2$DCF-DA (10 μM) was added and the mixture was incubated for 30 min. Cells were washed with PBS and treated with hydrogen peroxide (1 mM) for 30 min. The conversion of H$_2$DCF-DA into highly fluorescent 2′,7′-dichlorofluorescein (DCF) was measured with a Tecan SpectraFluor plus microplate reader (excitation wavelength 485 nm; emission wavelength 530 nm) and data

were normalized to the hydrogen peroxide treated DMSO control. The cell viability was determined by a crystal violet staining. The amount of dye taken up by living cells was measured with a spectrophotometer at 590 nm. The number of viable cells was normalized to a DMSO control.

Detection of intracellular GSH

GSH levels were measured following a published protocol (Zahler et al., 2000). In brief, 0.5×10^6 HeLa cells were seeded in 24 well plates and treated with *Ep*-PxB-1, *Ep*-PxB-3, *Ep*-PxB-5, caffeic acid (10 μM), and a DMSO control for 24 h. After this incubation time, the medium was removed and hydrogen peroxide was added to a final concentration of 1 mM, followed by incubation for 30 min. Cells were washed with PBS, scraped off in 200 μl PBS pH 7.4 containing 70 mM NEM, and lysed by bead beating (3 cycles of 30 s vortexing with glass beads, 30 s on ice). The lysate was centrifuged at 13000 rpm for 5 min and 100 μl of the supernatant were subjected to analytical HPLC. The peak of the GSH-NEM conjugate was confirmed by ESI-MS, and the peak area was used for quantitation.

Statistical analysis

Unless stated otherwise, results represent the mean of at least three independent experiments (means ± standard deviation), which were each carried out in at least three replicates. Statistical significance was determined by one-way analysis of variance with post hoc analysis using Dunnett's multiple comparison test. All statistical analyses were performed with GraphPad Prism 7.

Results

High abundance of phylloxanthobilins in leaf extracts of Echinacea purpurea

When analyzing extracts of *Echinacea purpurea* leaves by analytical HPLC, 6 PxBs were identified due to their UV/Vis absorbance properties, and were named *Ep*-PxB-(1–6) numbered with decreasing polarity; the UV/Vis spectra of the PxB HPLC signals showed characteristic maxima at 244 and 312 nm (*Supplementary Information*); the absorbance maximum at 426 nm which is characteristic for an extended π-system in the ring segments A to D (ring D carrying a vinyl group) (Moser et al., 2008), was only observed for *Ep*-PxB-(4–6). Interestingly, in the UV/Vis spectra of *Ep*-PxB-(1–3), this maximum was shifted to 414 nm, as was reported for the PxB from *Egeria densa*, which carries a dihydroxyethyl motive instead of the vinyl group at ring D (Wakana et al., 2014).

Not only is the wide polarity range and the overall abundance of the identified PxBs striking; when analyzing leaves of different colors (green - red - orange/yellowish - yellow) PxBs can be detected in all 4 extracts (Fig. 2).

The individual composition of *Ep*-PxBs was found to vary among tested leaves. *Ep*-PxB-2 and *Ep*-PxB-5 were present in all leaves in relatively high amounts, while *Ep*-PxB-4 and *Ep*-PxB-6 occurred only in minute amounts. The relative abundance of all six PxBs in the differently colored leaves was estimated by comparing the sum of all six peak areas (normalized to the leaf area from which the extract was produced). The amount of PxBs was found to be highest in the yellow leaf (set to 100%), and 12% and 13% in the yellow/red and red leaf, respectively. Surprisingly, 23% of PxBs were estimated to have already been formed in the green leaf showing no visible signs of Chl degradation (*Supplementary Information*). So far, signs for Chl degradation as evidenced by the occurrence of PBs in green leaves is sparse, and is limited to a report on the presence of PBs in green florets of broccoli (Roiser et al., 2015). Determining the Chl contents in green, red, and yellow leaves showed that chl contents was highest in the green leaves, lower in red leaves, and only low amounts of Chl were detected in the yellow leaves. In the same samples, the relative total amount of PxBs was again determined by HPLC analysis to correlate the degradation of

Chl with the appearance of PxBs; it turned out that the amount of PxBs increased as Chl decreased (*Supplementary Information*).

For structure determination, PxBs were isolated from 200 g of fresh yellow *Echinacea purpurea* leaves as described in the experimental section, giving yields of *Ep*-PxB-1 (**1**) of 0.63 μmol, *Ep*-PxB-2 (**2**) of 0.67 μmol, *Ep*-PxB-3 (**3**) of 0.92 μmol, *Ep*-PxB-4 (**4**) of 0.14 μmol, *Ep*-PxB-5 (**5**) of 1.1 μmol, and *Ep*-PxB-6 (**6**) of 0.27 μmol. Comparison of spectroanalytical data of the isolated PxBs from *Echinacea purpurea* with literature data of the thoroughly characterized common PxB core structure allowed for the identification of all tentatively identified PxBs (**1–6**) as $8^2S,10R,15Z$-3^2-hydroxy-1-formyl-19-oxo-19,N24-dihydrophyllobilenes. The modifications of the PxB core resulting in different polarities were unambiguously identified for (**2–6**), and tentatively identified for the novel modification pattern found in (**1**). For phyllobilins, extensive MS measurements have been performed and a database has been established, allowing for the identification of known modification patterns of the tetrapyrrolic core structure by mass spectrometry (Christ et al., 2016; Müller et al., 2014; Ríos et al., 2015).

The molecular formula of *Ep*-PxB-1 was deduced as $C_{44}H_{52}N_4O_{18}$ by HR-MS analysis. Further ESI-MS analysis confirmed the pseudo-molecular ion at m/z 925.2 $[M + H]^+$ and MS/MS measurements allowed for the detection of fragment ions at m/z 906.1 and m/z 891.87 from the loss of water and methanol, respectively, originating from the free propionic acid side chain at C12 and the methoxycarbonyl function at $C8^2$ (Müller et al., 2014). In addition, fragment-ions at m/z 838.67, m/z 807.1, and m/z 528.3 were detected, corresponding to the loss of the malonic acid group $[M - O\text{-malonyl} + H]^+$, the loss of ring D $[M - \text{ring } D + K]^+$ and the loss of ring A $[M - H_2O - \text{ring } A + Na]^+$ (*Supplementary Information*). These data suggest (**1**) to carry a dihyroxyethyl side chain at C18 of ring D and a 6-O-malonyl-glucopyranosyl substituent at $C3^2$.

The elemental composition of *Ep*-PxB-2 was deduced by HR-MS $C_{41}H_{50}N_4O_{15}$, which indicates it to be identical to the PxB identified in senescent leaves of the lime tree (*Tilia cordata*) (Scherl et al., 2012). By comparison of the ESI-MS fragmentation pattern of *Ep*-PxB-2 and *Tc*-PxB and of the HPLC chromatograms of *Ep*-PxB-2, *Tc*-PxB and a 1:1 mixture, which exhibited same elution properties and UV/Vis spectra, *Ep*-PxB-2 could be identified as identical to *Tc*-PxB, carrying a dihydroxyethyl moiety at ring D, and a O-glucopyranosyl unit at $C3^2$.

HR-MS analysis of *Ep*-PxB-3 (**3**) revealed a molecular formula of $C_{35}H_{40}N_4O_{10}$. The same modification pattern has been previously characterized for a PleB isolated from *Spinacia oleracea, So*-PleB-2, with a dihydroxyethyl group at C18 and a hydroxyl group at $C3^2$ (Berghold et al., 2002). In order to verify the structure of (**3**) with co-injection HPLC analysis, *So*-PleB-2 was oxidized to the PxB according to the protocol of Vergeiner et al. (2015) and provisionally named *So*-PxB-2. The identity of *So*-PxB-2 was validated by HR-MS and the PxB chromophore due to its UV characteristics in the HPLC trace. The identical retention behavior and UV/Vis spectra of *So*-PxB-2 and (**3**) allowed to identify the structure of *Ep*-PxB-3 as PxB modified with a dihydroxyethyl moiety at ring D, and a hydroxyethyl motive at ring A.

The elemental composition of *Ep*-PxB-4 was deduced as $C_{44}H_{50}N_4O_{16}$ via HR-MS spectrometry, indicating (**4**) to have the same constitution as the oxidation product of *Nr*-PleB-1, carrying a vinyl side chain at C18 and an additional malonic substituent at the glycosylic side chain at $C3^2$ (Berghold et al., 2004). *Nr*-PleB-1 was oxidized according to the protocol of Vergeiner et al. (2015) and provisionally named *Nr*-PxB-1. ESI-MS and HPLC analyses of co-injections of *Nr*-PxB-1 and (**4**) confirmed (**4**) and *Nr*-PxB-1 as being identical.

HR-MS determined the molecular formula of *Ep*-PxB-5 to be $C_{41}H_{48}N_4O_{13}$. The structure was presumed to contain a sugar moiety at ring A and a dihydroxyethyl side chain at ring D, which is consistent with the structure of the oxidation product of *Nr*-PleB-2, the less polar PleB in tobacco leaves (*Nicotiana rustica*) (Berghold et al., 2004). *Nr*-PleB-2 was oxidized according to the protocol of Vergeiner et al. (2015) and provisionally named *Nr*-PxB-2; co-injections of *Nr*-PxB-2 with (**5**)
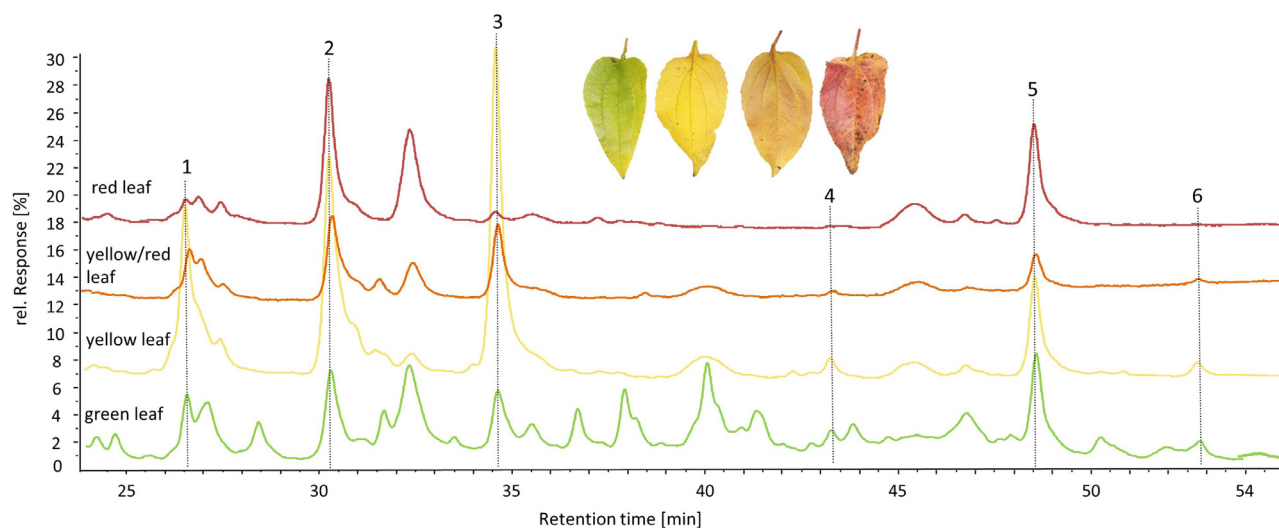
Fig. 2. Analytical HPLC traces (detection at 420 nm) and pictures of the corresponding *Echinacea purpurea* leaves of different colors. Leaves were harvested and immediately used for extraction and subsequent analysis.

demonstrated identical retention times and UV/VIS spectra.

The composition of *Ep*-PxB-6 was determined by HR-MS to be $C_{35}H_{38}N_4O_8$, which indicates it to be identical to the naturally occurring PxB in Katsura tree (*Cercidiphyllum japonicum*) leaves (Moser et al., 2008). HPLC co-injection of the isolated PxBs and a 1:1 mixture of both was performed confirming the two PxBs to be identical. The most apolar PxB identified in *Echinacea purpurea* leaves carries thus a vinyl side chain at ring D and a hydroxyethyl side chain at ring A.

In sum, in extracts of yellow *Echinacea purpurea* leaves, 2 previously characterized PxBs were identified, 3 of the discovered *Ep*-PxBs represent substances previously only identified with a PleB core structure, and 1 *Ep*-PxB featuring a previously unknown modification pattern were identified (Fig. 3).

Ep-PxBs are taken up by human cells

To investigate whether *Ep*-PxBs can be taken up by human cells, HEK cells were incubated for 4 h in medium containing μM concentrations of a representative selection of PxBs of different polarities. After removing the medium, cells were thoroughly washed. After cell lysis and precipitation of proteins, the supernatant was analyzed for *Ep*-PxBs by analytical HPLC (Fig. 4).

All 3 tested *Ep*-PxBs were found in the lysates with unchanged retention times and UV-characteristics compared to the starting material. This experiment not only demonstrates the cellular uptake of the *Ep*-PxBs, it also gives first indications on the stability of the natural products once taken up. Whether the uptake is decreased as a function of higher polarity of the PxBs and if so to what extent, as well as the investigation of metabolic stability, is the subject of future studies.

Ep-PxBs are potent antioxidants

The role of oxidative stress in many human diseases has drawn interest in the last years. Antioxidants as radical scavengers have evolved as valuable components in human nutrition, and antioxidant supplementation has become more and more popular (Kurutas, 2016) (Bendich, 1993). Müller et al. could previously show that a PleB isolated from the peels of apples and pears is a potent inhibitor of autoxidation, underlining the importance of PleBs as natural anti-oxidative constituents of plants (Müller et al., 2007). For the PxBs, an even higher antioxidant activity compared to PleBs is expected, but has not been demonstrated so far.

Antioxidant activity of *Echinacea* preparations is well documented

and, among others, attributed to caffeic acid derivatives, which are among the main constituents. In order to test the anti-oxidative potential of **(1)** - **(6)** *in vitro*, a FRAP assay was performed, determining the absorbance of the reduced Fe^{2+}-$(TPTZ)_2$ – complex at 620 nm with Trolox as a standard. 5 out of 6 *Ep*-PxBs exhibited a significantly stronger anti-oxidative potential relative to Trolox. The anti-oxidative potency decreased in parallel with polarity of the *Ep*-PxBs, from showing the highest activity for *Ep*-PxB-1, more than 3 times higher than Trolox, whereas *Ep*-PxB-6 had comparable anti-oxidative qualities as Trolox. Caffeic acid (CA), an established anti-oxidative constituent of *Echinacea*, had similar effects compared to Trolox and the least effective *Ep*-PxB (**6**, Fig. 5A). Since very potent activities were observed for the *Ep*-PxBs *in vitro*, and it was shown that *Ep*-PxBs are taken up by cells, an anti-oxidative activity assay based on the dye H_2DCF was performed. With this dye, the generation of intracellular ROS upon H_2O_2 stimulation of cells can be monitored and the ROS scavenging activity of potential anti-oxidative compounds can be tested (Yokomizo and Moriwaki, 2006). 3 selected *Ep*-PxBs of different polarities and CA were used to assess the ROS scavenging activity in cells. All 3 tested *Ep*-PxBs and CA were able to scavenge ROS in cells at a concentration as low as 10 μM (Fig. 5B). At this concentration, the cell viability was not affected, neither by the *Ep*-PxBs, nor by CA (Fig. 5C).

The tripeptide glutathione (GSH) is considered to be one of the most important scavengers of reactive oxygen species (ROS) in cells, and total GSH levels are frequently used as marker of oxidative stress (Aquilano et al., 2014). When stimulating HeLa cells with H_2O_2, total GSH levels decreased, as GSH is oxidized in response to the generated ROS. Pre-treatment of the cells with 3 selected *Ep*-PxBs of different polarities and CA resulted in higher cellular GSH levels for all tested *Ep*-PxBs, showing that these compounds are able to protect the cells from oxidative stress. All compounds, *Ep*-PxBs and CA, were used at a low concentration (10 μM), and significant protective effects were observable for all compounds (Fig. 5D).

Conclusion

In the years following their discovery, PBs were considered detoxified forms of no longer needed Chl in autumn. Nowadays, however, PBs are considered to offer potential for explaining bioactivities contributing to health promoting effects of the plants that produce them. We show that yellow PBs, the PxBs, occur in unprecedented abundance and diversity in *Echinacea purpurea*, a plant with undoubted high importance in phytomedicine. PxBs could even be detected in fresh green
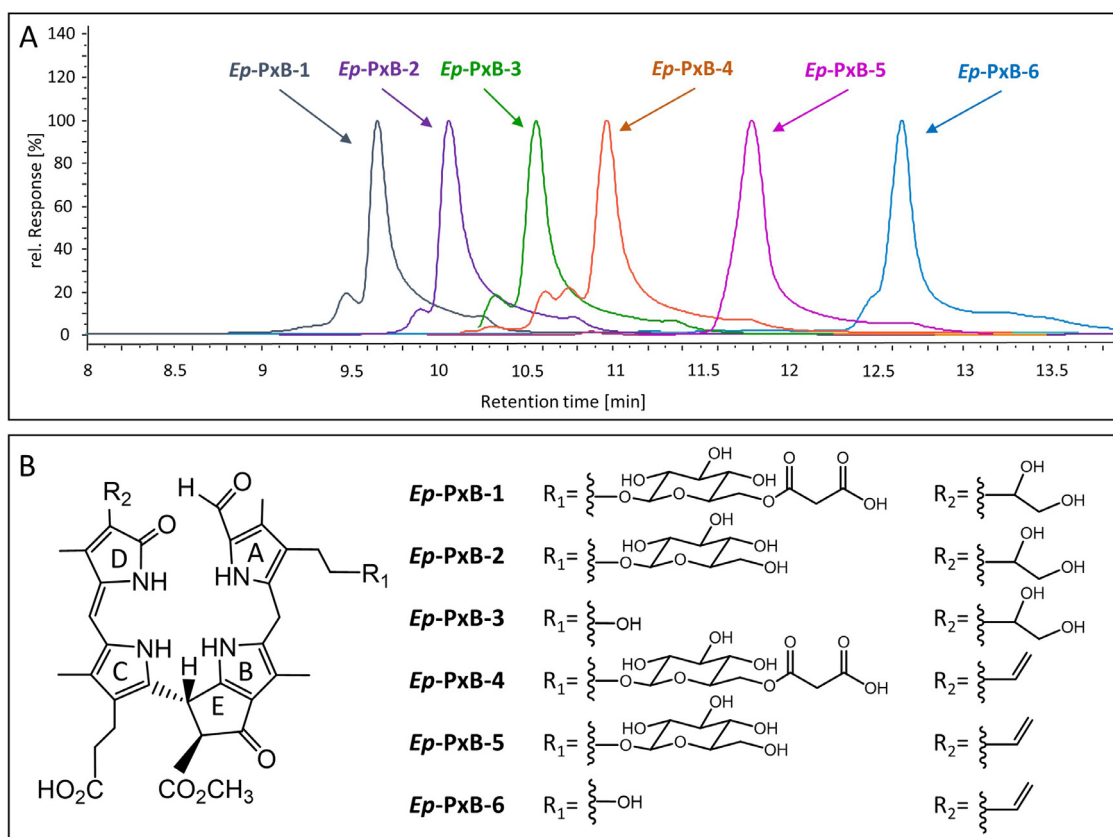
Fig. 3. (A) Overlay of analytical HPLC traces (detection at 420 nm) of purified *Ep*-PxBs (1–6). (B) Structure of the PxB tetrapyrrole core and modification patterns identified for *Ep*-PxBs (1–6).

leaves, without any 'obvious' Chl breakdown. In total, 6 PxBs were identified, of which 2 have been characterized previously, 3 feature known modification motives but are still novel PxBs, and one PxB from *Echinacea* was tentatively identified as having an unprecedented modification pattern. *Echinacea* PxBs are taken up by human cells and appear to be stable over a period of several hours. PxBs turned out to possess potent anti-oxidative activity *in vitro*, are able to scavenge ROS in cells, and can prevent intracellular oxidative stress caused by hydrogen peroxide.

Many different pharmacological activities have been demonstrated for constituents of *Echinacea purpurea*. Among the successes in identifying compounds responsible for pharmacological effects of *Echinacea*

was the demonstration of phagocytosis stimulating activities for alkylamides (Bauer et al., 1988a), as well as the identification of *Echinacea* polysaccharides as immunostimulatory agents, both of which were achieved by Wagner and co-workers (Roesler et al., 1991; Wagner et al., 1988); as was the isolation of a pure polysaccharide from herb material for structural characterization, and proving the phagocytosis activation for the single compound (Proksch and Wagner, 1987).

Nevertheless, the challenge remains of identifying an active principle that can account for all of the efficacies. With our identification of phyllobilins as powerful anti-oxidative constituents in *Echinacea* extracts, we add one missing puzzle piece to the phytochemical repertoire of *Echinacea purpurea*.
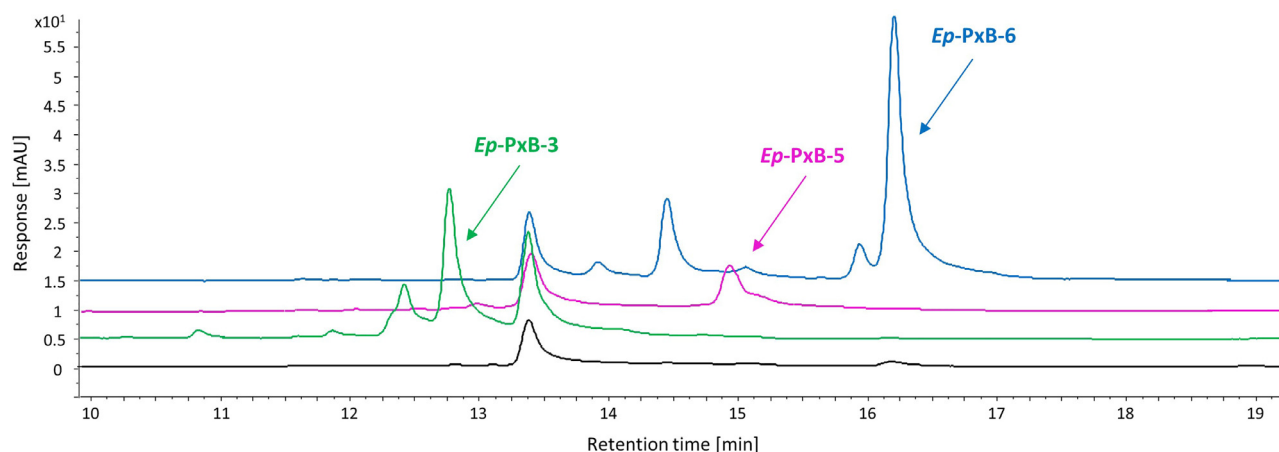
Fig. 4. *Ep*-PxBs are taken up by cells. Cellular uptake of *Ep*-PxBs in HEK cells analyzed by HPLC. Chromatograms of control (black), *Ep*-PXB-3 (green), *Ep*-PxB-5 (pink) and *Ep*-PxB-6 (blue) treated cells are shown. Detection at 420 nm.
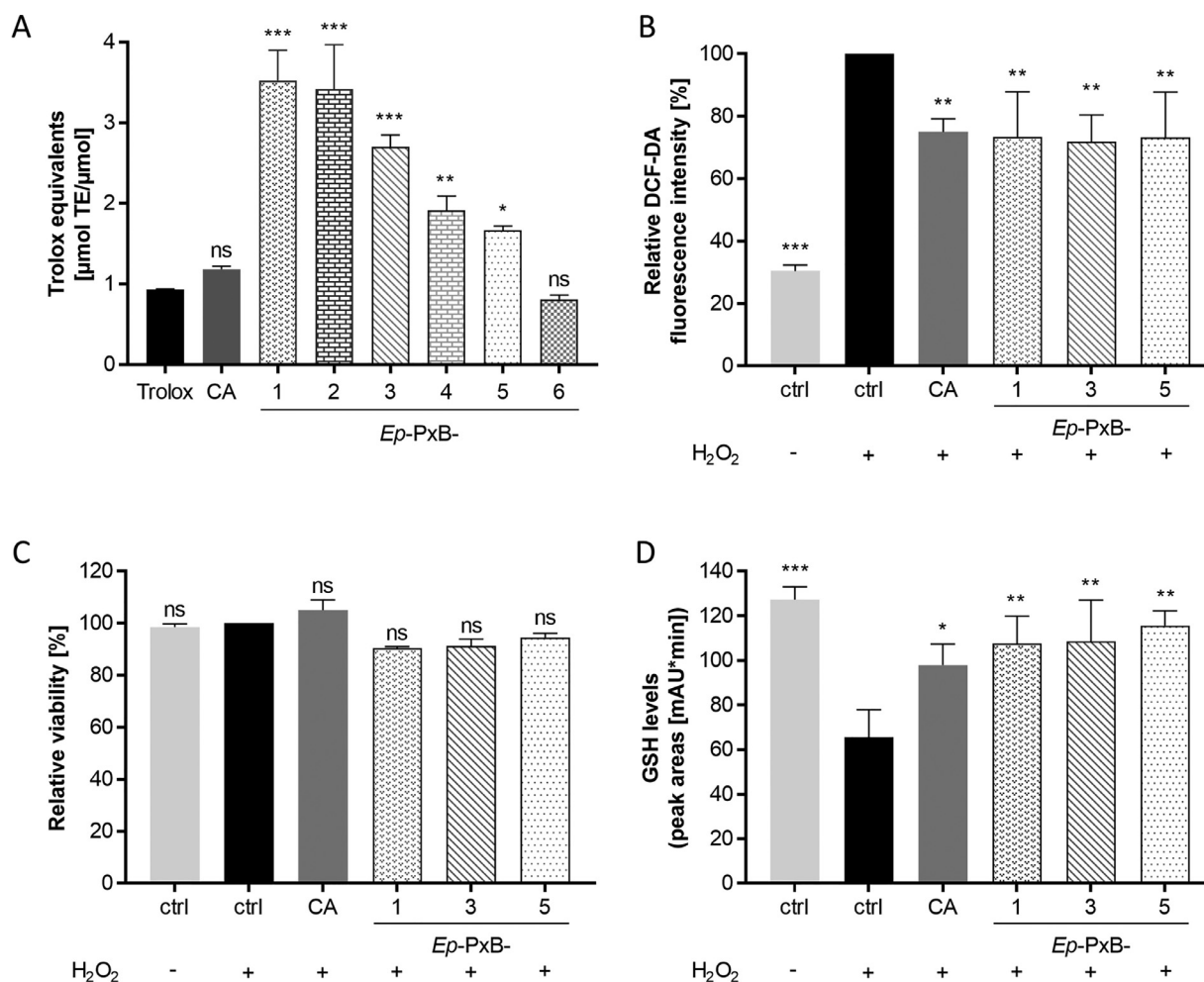
Fig. 5. *Ep*-PxBs possess potent anti-oxidative activities. (**A**) The *in vitro* anti-oxidative potential of *Ep*-PxBs was assessed by a FRAP-Assay, in which anti-oxidative power is expressed as Trolox equivalents (μMol TE/μMol). Up to 3.5-fold higher anti-oxidative power was observed for the more polar *Ep*-PxBs. The known *Echinacea* antioxidant CA and *Ep*-PxB-6 showed anti-oxidative activities comparable with Trolox. (**B**) *Ep*-PxBs can scavenge ROS in cells. HeLa cells were pre-treated with compounds (10 μM) for 24 h before stimulating with 1 mM H_2O_2. The ROS scavenging activity was measured by the prevention of the conversion of the intracellular fluorescein derivative H_2DCF into highly fluorescent DCF. (**C**) *Ep*-PxBs do not affect cell viability at a concentration of 10 μM. Following the DCF measurement, a crystal violet staining was performed as control. (**D**) *Ep*-PxBs can reduce intracellular oxidative stress. HeLa cells were pre-treated with compounds (10 μM) or with DMSO for 24 h, and were then stimulated with 1 mM H_2O_2. GSH levels in cell lysates were analyzed by HPLC. Even at a concentration as low as 10 μM, *Ep*-PxBs can significantly prevent GSH oxidation. Values represent mean ± standard deviation of three independent experiments (ctrl = control, ns = not significant, $p < 0.05$).

Phyllobilins appear to be overlooked constituents with unexplored pharmacological activities. We encourage to take the PxBs into account when performing future phytochemical profiling of *Echinacea* extracts and when testing for efficacies. In appreciation of the pioneer work of Professor Wagner and his co-workers, evaluating the bioactivities of PxBs re-opens the stage for *Echinacea* research, and gives rise to exciting opportunities to continue the investigations on the numerous bioactivities of this medicinal plant with the newly identified substances.

Conflict of interest

The authors declare no conflict of interest.

Supplementary materials

Supplementary material associated with this article can be found, in the online version, at doi:10.1016/j.phymed.2019.152969.

References

Aquilano, K., Baldelli, S., Ciriolo, M.R., 2014. Glutathione: new roles in redox signaling for an old antioxidant. Front. Pharmacol. 5, 196.

Ardjomand-Woelkart, K., Bauer, R., 2014. Echinacea. Zeitschrift für Phytotherapie 35, 2–9.

Barrett, B., 2003. Medicinal properties of *Echinacea*: a critical review. Phytomedicine 10, 66–86.

Barrett, B., Brown, R., Rakel, D., Mundt, M., Bone, K., Barlow, S., Ewers, T., 2010. *Echinacea* for treating the common cold: a randomized trial. Ann. Intern. Med. 153, 769–777.

Bauer, R., 2002. Neue Erkenntnisse zur Wirkung und Wirksamkeit von *Echinacea purpurea*-Preßsaftzubereitungen. Wiener Medizinische Wochenschrift 152, 407–411.

Bauer, R., Remiger, P., Jurcic, K., Wagner, H., 1989. Beeinflussung der Phagozytoseaktivität durch Echinacea-Extrakte. Zeitschrift für Phytotherapie 10, 43–48.

Bauer, R., Remiger, P., Wagner, H., 1988a. Alkamides from the roots of *Echinacea purpurea*. Phytochemistry 27, 2339–2342.

Bauer, R., Wagner, H., 1991. *Echinacea* species as potential immunostimulatory drugs. In: Wagner, H., Farnsworth, N.R. (Eds.), Economic and Medicinal Plant Research.

Academic Press Limited, New York.

Bauer, V.R., Jurcic, K., Puhlmann, J., Wagner, H., 1988b. Immunologic *in vivo* and *in vitro* studies on *Echinacea* extracts. Arzneimittelforschung 38, 276–281.

Bendich, A., 1993. Physiological role of antioxidants in the immune system. J. Dairy Sci. 76, 2789–2794.

Benzie, I.F., Strain, J.J., 1996. The ferric reducing ability of plasma (FRAP) as a measure of "antioxidant power": the FRAP assay. Anal. Biochem. 239, 70–76.

Berghold, J., Breuker, K., Oberhuber, M., Hörtensteiner, S., Kräutler, B., 2002. Chlorophyll breakdown in spinach: on the structure of five nonfluorescent chlorophyll catabolites. Photosynth. Res. 74, 109–119.

Berghold, J., Eichmüller, C., Hörtensteiner, S., Kräutler, B., 2004. Chlorophyll breakdown in tobacco: on the structure of two nonfluorescent chlorophyll catabolites. Chem. Biodivers. 1, 657–668.

Bruni, R., Brighenti, V., Caesar, L.K., Bertelli, D., Cech, N.B., Pellati, F., 2018. Analytical methods for the study of bioactive compounds from medicinally used *Echinacea* species. J. Pharm. Biomed. Anal. 160, 443–477.

Christ, B., Hauenstein, M., Hörtensteiner, S., 2016. A liquid chromatography–mass spectrometry platform for the analysis of phyllobilins, the major degradation products of chlorophyll in Arabidopsis thaliana. Plant J. 88, 505–518.

Clarke, TC, Black, LI., Stussman, BJ, Barnes, PM, Nahin, RL, 2015. Trends in the use of complementary health approaches among adults: United States, 2002–2012. National Center for Health Statistics, Hyattsville, MD National health statistics reports; no 79.

EMA/HMPC/48704/ 2014, European Union herbal monograph on Echinacea purpurea (L.) Moench, herba recens.

Erhart, T., Mittelberger, C., Liu, X., Podewitz, M., Li, C., Scherzer, G., Stoll, G., Valls, J., Robatscher, P., Liedl, K.R., Oberhuber, M., Kräutler, B., 2018. Novel types of hypermodified fluorescent phyllobilins from breakdown of chlorophyll in senescent leaves of grapevine (Vitis vinifera). Chem. Eur. J. 24, 17268–17279.

Erhart, T., Mittelberger, C., Vergeiner, C., Scherzer, G., Holzner, B., Robatscher, P., Oberhuber, M., Kräutler, B., 2016. Chlorophyll catabolites in senescent leaves of the plum tree (Prunus domestica). Chem. Biodiv. 13, 1441–1453.

Gazzin, S., Vitek, L., Watchko, J., Shapiro, S.M., Tiribelli, C., 2016. A novel perspective on the biology of bilirubin in health and disease. Trends Mol. Med. 22, 758–768.

Hendry, G.A.F., Houghton, J.D., Brown, S.B., 1987. The degradation of chlorophyll - a biological enigma (Tansley Review No-11). New Phytol. 107, 255–302.

Konar, N., Dalabasmaz, S., Poyrazoglu, E.S., Artik, N., Colak, A., 2014. The determination of the caffeic acid derivatives of Echinacea purpurea aerial parts under various extraction conditions by supercritical fluid extraction (SFE). J. Supercritic. Fluids 89, 128–136.

Kräutler, B., 2016. Breakdown of chlorophyll in higher plants—phyllobilins as abundant, yet hardly visible signs of ripening, senescence, and cell death. Angew. Chem. Int. Ed. 55, 4882–4907.

Kräutler, B., Jaun, B., Bortlik, K., Schellenberg, M., Matile, P., 1991. On the enigma of chlorophyll degradation - the constitution of a secoporphinoid catabolite. Zum Rätsel des Chlorophyllabbaus: Die Konstitution eines secoporphyinoiden Kataboliten 30, 1315–1318.

Kreft, S., Razinger, B., 2014. Assessment Report on *Echinacea purpurea* (L.) Monch., Herba Recens. European Medicines Agency EMA/HMPC/557979/2013.

Kuai, B., Chen, J., Hörtensteiner, S., 2018. The biochemistry and molecular biology of chlorophyll breakdown. J. Exp. Bot. 69, 751–767.

Kurutas, E.B., 2016. The importance of antioxidants which play the role in cellular response against oxidative/nitrosative stress: current state. Nutr. J. 15, 71.

Lepojević, I., Lepojević, Ž., Pavlić, B., Ristić, M., Zeković, Z., Vidović, S., 2017. Solid-liquid and high-pressure (liquid and supercritical carbon dioxide) extraction of *Echinacea purpurea* L. J. Supercritic. Fluids 119, 159–168.

Melchart, D., Linde, K., Worku, F., Bauer, R., Wagner, H., 1994. Immunomodulation with *Echinacea* — a systematic review of controlled clinical trials. Phytomedicine 1, 245–254.

Moser, S., Scherzer, G., Krautler, B., 2017. On the nature of isomeric nonfluorescent chlorophyll catabolites in leaves and fruit - a study with a ubiquitous phylloleucobilin

and its main isomerization product. Chem. Biodiv. 14, e1700368.

Moser, S., Ulrich, M., Müller, T., Kräutler, B., 2008. A yellow chlorophyll catabolite is a pigment of the fall colours. Photochem. Photobiol. Sci. 7, 1577–1581.

Müller, T., Ulrich, M., Ongania, K.H., Kräutler, B., 2007. Colorless tetrapyrrolic chlorophyll catabolites found in ripening fruit are effective antioxidants. Angew. Chem. Int. Ed. Engl. 46, 8699–8702.

Müller, T., Vergeiner, S., Kräutler, B., 2014. Structure elucidation of chlorophyll catabolites (phyllobilins) by ESI-mass spectrometry—Pseudo-molecular ions and fragmentation analysis of a nonfluorescent chlorophyll catabolite (NCC). Int. J. Mass Spectrom. 365-366, 48–55.

Pellati, F., Benvenuti, S., Magro, L., Melegari, M., Soragni, F., 2004. Analysis of phenolic compounds and radical scavenging activity of *Echinacea* spp. J. Pharm. Biomed. Anal. 35, 289–301.

Proksch, A., Wagner, H., 1987. Structural analysis of a 4-O-methyl-glucuronoarabinoxylan with immuno-stimulating activity from *Echinacea purpurea*. Phytochemistry 26, 1989–1993.

Pružinská, A., Tanner, G., Aubry, S., Anders, I., Moser, S., Müller, T., Ongania, K.-H., Kräutler, B., Youn, J.-Y., Liljegren, S.J., Hörtensteiner, S., 2005. Chlorophyll breakdown in senescent arabidopsis leaves. characterization of chlorophyll catabolites and of chlorophyll catabolic enzymes involved in the degreening reaction. Plant Physiol. 139, 52.

Pugh, N.D., Jackson, C.R., Pasco, D.S., 2013. Total bacterial load within *Echinacea purpurea*, determined using a new PCR-based quantification method, is correlated with LPS levels and *in vitro* macrophage activity. Planta Med. 79, 9–14.

Ríos, J.J., Roca, M., Pérez-Gálvez, A., 2015. Systematic HPLC/ESI-high resolution-qTOF-MS methodology for metabolomic studies in nonfluorescent chlorophyll catabolites pathway. J. Anal. Methods Chem. 2015, 10.

Roesler, J., Emmendörffer, A., Steinmüller, C., Luettig, B., Wagner, H., Lohmann-Matthes, M.-L., 1991. Application of purified polysaccharides from cell cultures of the plant *Echinaca purpurea* to test subjects mediates activation of the phagocyte system. Int. J. Immunopharmacol. 13, 931–941.

Roiser, M.H., Müller, T., Kräutler, B., 2015. Colorless chlorophyll catabolites in senescent florets of broccoli (Brassica oleracea var. italica). J. Agric. Food Chem. 63, 1385–1392.

Scherl, M., Müller, T., Kräutler, B., 2012. Chlorophyll catabolites in senescent leaves of the lime tree (Tilia cordata). Chem. Biodiv. 9, 2605–2617.

Scherl, M., Müller, T., Kreutz, C.R., Huber, R.G., Zass, E., Liedl, K.R., Kräutler, B., 2016. Chlorophyll catabolites in fall leaves of the wych elm tree present a novel glycosylation motif. Chem. Eur. J. 22, 9498–9503.

Stimpel, M., Proksch, A., Wagner, H., Lohmann-Matthes, M.L., 1984. Macrophage activation and induction of macrophage cytotoxicity by purified polysaccharide fractions from the plant *Echinacea purpurea*. Infect. Immun. 46, 845.

Strain, H.H., Cope, B.T., Svec, W.A., 1971. Analytical procedures for the isolation, identification, estimation, and investigation of the chlorophylls. Methods in Enzymology. Academic Press, pp. 452–476.

Vergeiner, C., Ulrich, M., Li, C., Liu, X., Müller, T., Kräutler, B., 2015. Stereo- and regioselective phyllobilane oxidation in leaf homogenates of the peace lily (spathiphyllum wallisii): hypothetical endogenous path to yellow chlorophyll catabolites. Chem. Eur. J. 21, 136–149.

Wagner, H., Stuppner, H., Schäfer, W., Zenk, M., 1988. Immunologically active polysaccharides of *Echinacea purpurea* cell cultures. Phytochemistry 27, 119–126.

Wakana, D., Kato, H., Momose, T., Sasaki, N., Ozeki, Y., Goda, Y., 2014. NMR-based characterization of a novel yellow chlorophyll catabolite, Ed-YCC, isolated from Egeria densa. Tetrahedron Lett. 55, 2982–2985.

Yokomizo, A., Moriwaki, M., 2006. Effects of uptake of flavonoids on oxidative stress induced by hydrogen peroxide in human intestinal Caco-2 cells. Biosci. Biotechnol. Biochem. 70, 1317–1324.

Zahler, S., Kupatt, C., Becker, B.F., 2000. Endothelial preconditioning by transient oxidative stress reduces inflammatory responses of cultured endothelial cells to TNF-alpha. FASEB J. Offic. Pub. Fed. Am. Soc. Exp. Biol. 14, 555–564.

Re-opening the Stage for *Echinacea* Research - Characterization of Phylloxanthobilins as a Novel Anti-oxidative Compound Class in *Echinacea purpurea*

Cornelia A. Karg, Pengyu Wang, Angelika M. Vollmar, Simone Moser

[1]Pharmaceutical Biology, Department Pharmacy

Ludwig-Maximilians University of Munich, Butenandtstraße 5-13, 81377 Munich, Germany

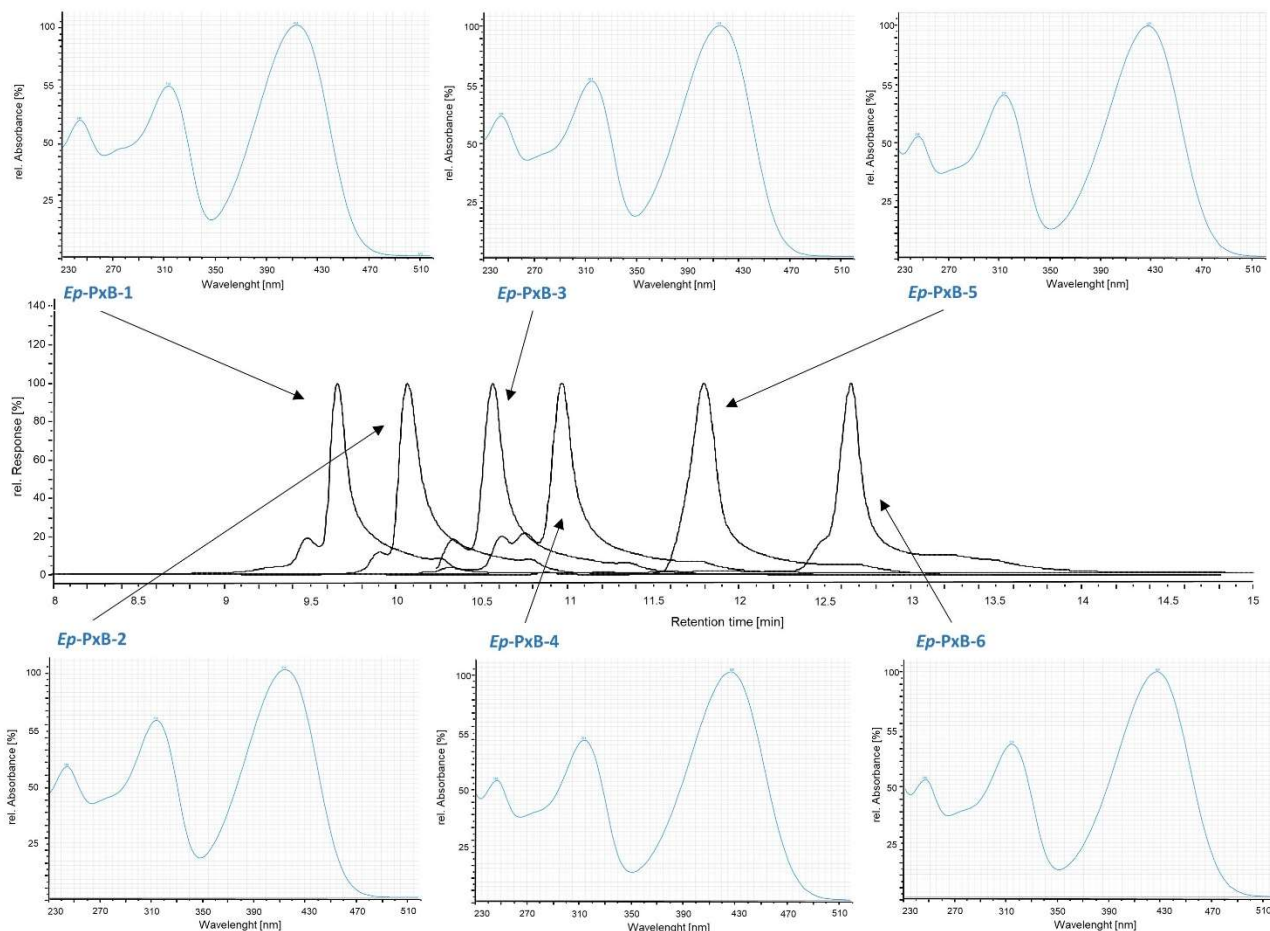e-mail: simone.moser@cup.uni-muenchen.de

Supplementary Information

Figure 1: Overlay of analytical HPLC traces of isolated Ep-PxB-(1-6) and corresponding UV/Vis spectra. Detection at 420 nm.

Table 1: Relative total PxB contents in methanolic extracts of 4 differently colored *Echinacea pupurea* leaves (estimation from one HPLC run each)

Leaf color	Relative PxB content (%)
green	23
yellow	100
yellow/red	12
red	13

In the same samples used for the Chl determination, the relative total PxB contents was estimated; since acetone is a not a good solvent for PxBs, this estimation was only used as qualitative correlation with the Chl contents determined for the same leaf. Acetone was removed on a rotary evaporator and dried by lyophilization, the residue was dissolved in 200 µl of 80% acetone; an aliquot of 20 µl was diluted with 100 µl of PBS and applied to analytical HPLC (injection volume 100 µL). Sums of the peak areas of all six PxBs at 420 nm were calculated and normalized to the sum of peak areas of all six PxBs in the yellow leaves (mean value).

Table 2: Chl a, Chl b, total Chl, and relative total PxB contents in acetone extracts of *Echinacea pupurea* leaves mean (SD standard deviation)

Leaf color	Chl a(ug/cm2)	Chl b(ug/cm2)	Total Chl (ug/cm2)	Relative PxB content
green	33.517 (5.370)	15.290 (1.553)	48.807 (6.806)	0.17 (0.27)
yellow	3.831 (0.832)	3.601 (1.060)	7.432 (1.891)	1.00 (0.1)
red	0.703 (0.130)	0.880 (0.211)	1.583 (0.339)	0.26 (0.14)

Table 3: HR-MS data of *So*-PxB-2, *Nr*-PxB-1 and *Nr*-PxB-2

PxB	m/z [M+H]$^+$
So-PxB-2	891.3143
Nr-PxB-1	677.2679
Nr-PxB-2	805.3307

Figure 2: MS/MS spectra of *Ep*-PxB-1 (m/z 925.0; CID 9%; positive mode). (O-Mal = O-malonyl)
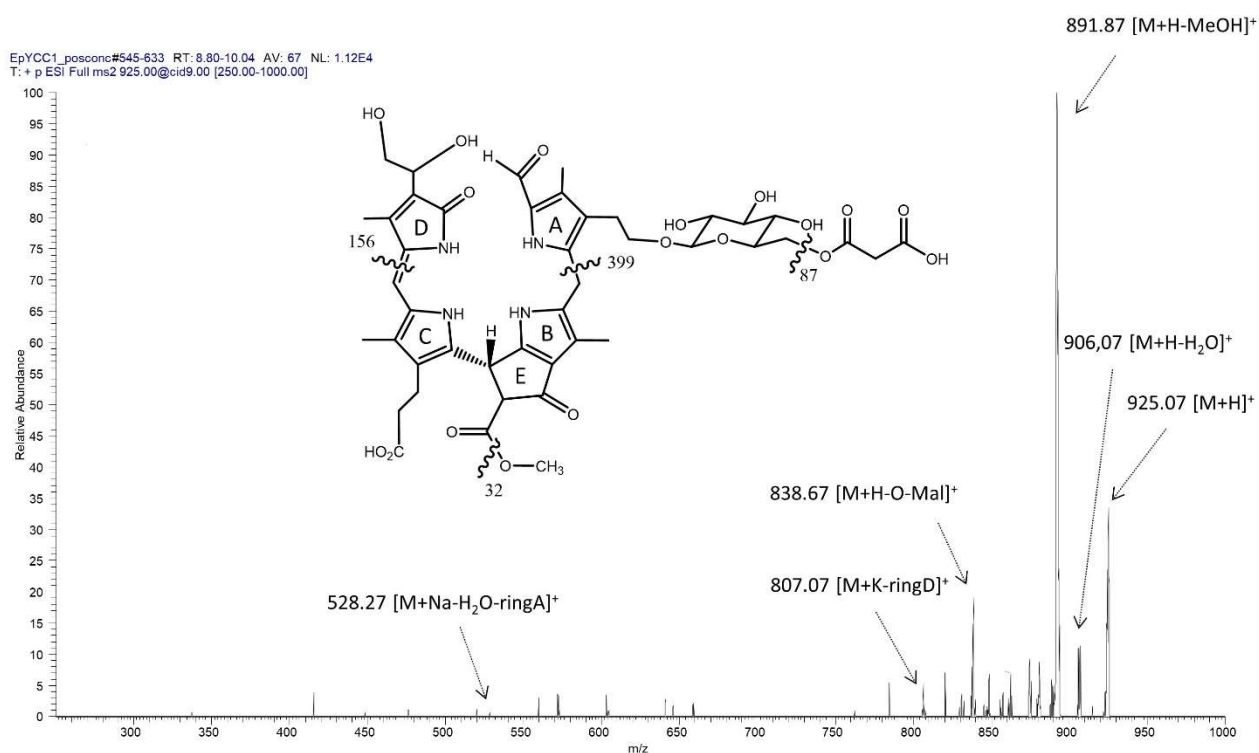
Figure 3: ^{1}H-NMR spectrum of *Ep*-PxB-1 in *d*[4]-MeOH
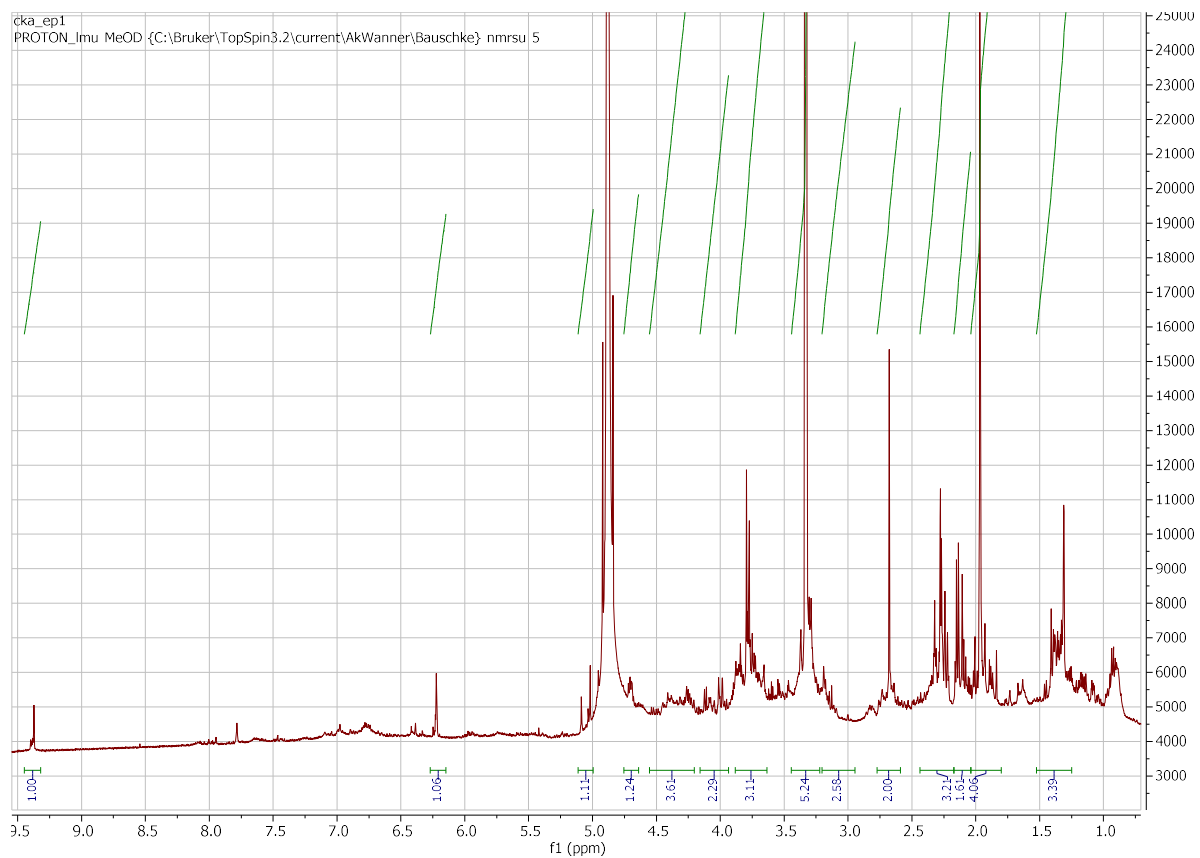
Figure 4: Co-injection analyses of *Ep*-PxBs **(2-6)** by analytical HPLC. (Peak Area = A)
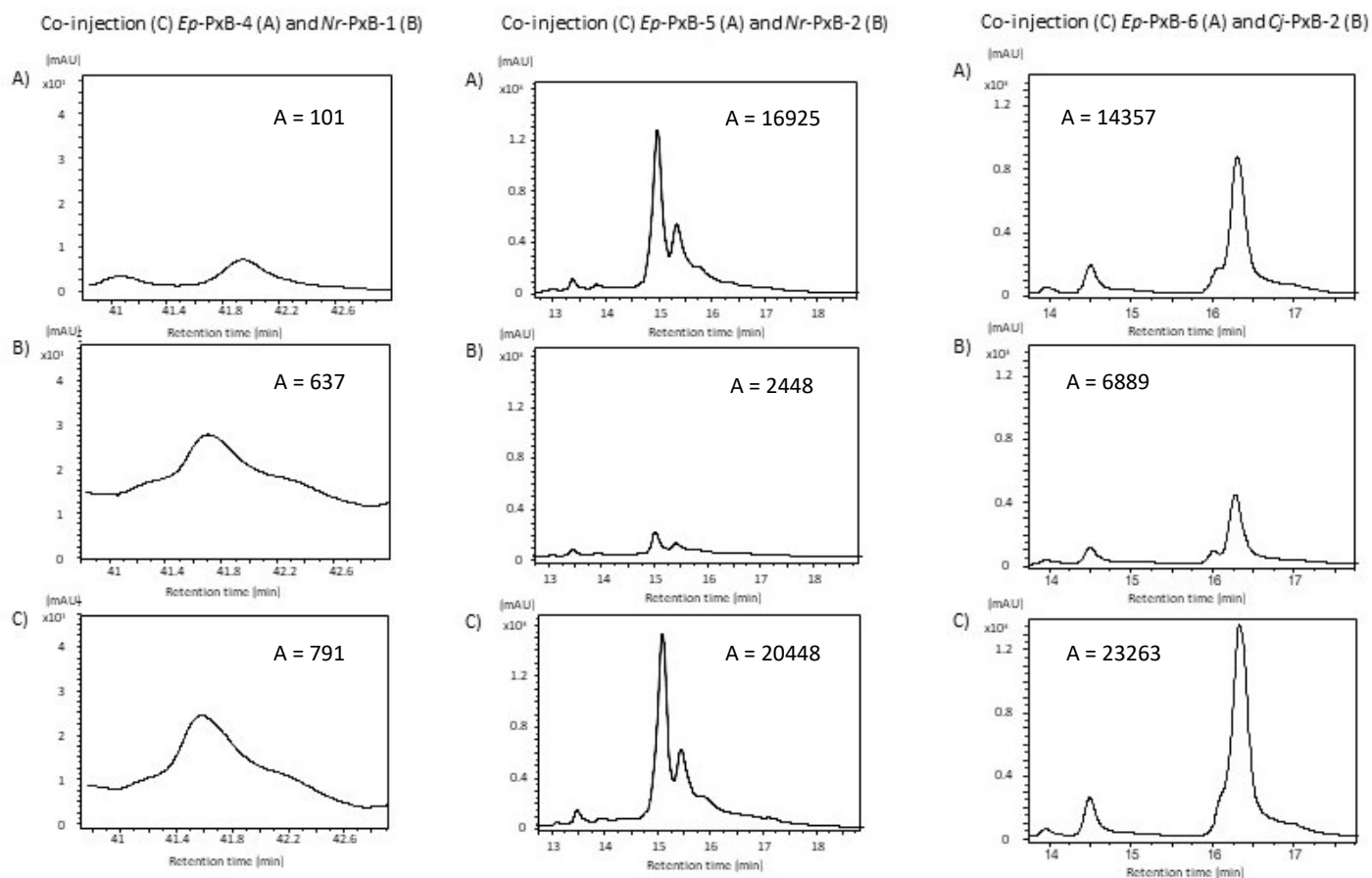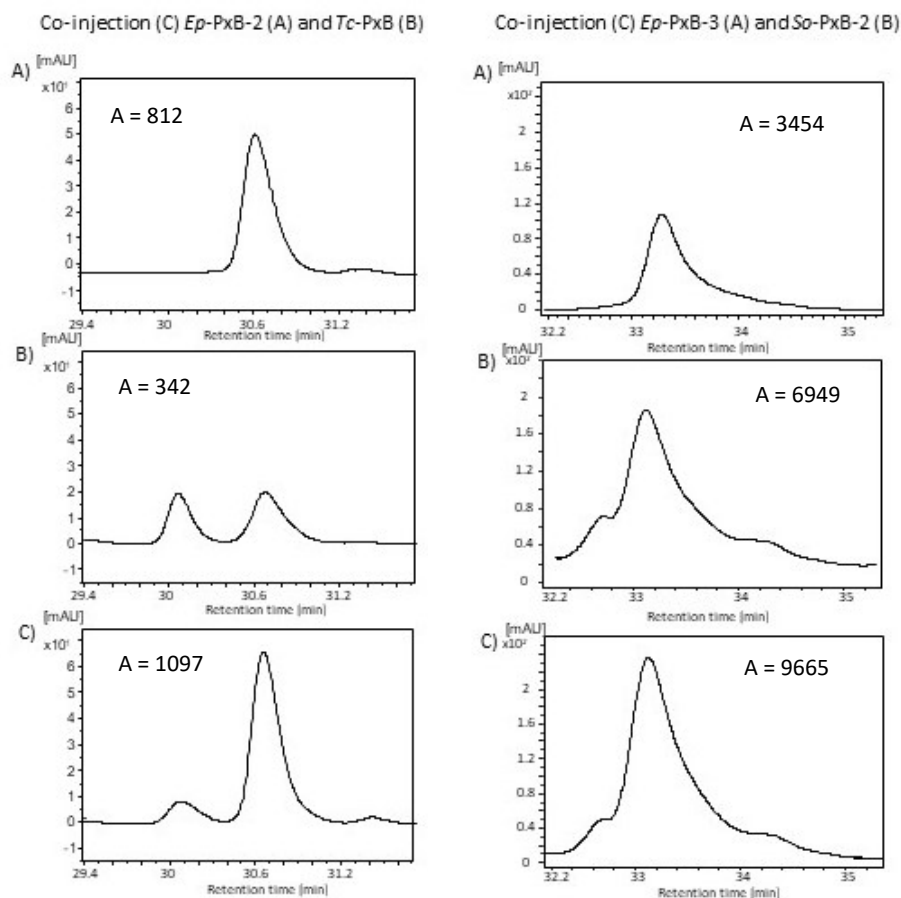
Isolation, characterization, and antioxidative activity of a dioxobilin-type phylloxanthobilin from savoy cabbage

Cornelia A. Karg[a], Charlotte M. Schilling[a], Lars Allmendinger[b], Simone Moser[a]*

[a]*Pharmaceutical Biology, Pharmacy Department, Ludwig-Maximilians University of Munich, Butenandtstraße 5-13, D-81337 Munich, Germany*

[b]*Pharmaceutical Chemistry, Pharmacy Department, Ludwig-Maximilians University of Munich, Butenandtstraße 5-13, D-81337 Munich, Germany*

ABSTRACT: The degradation of the green pigment chlorophyll in plants is known to yield phyllobilins as highly abundant linear tetrapyrroles. Recently, a split path of the degradation pathway has been discovered, leading to so-called dioxobilin-type (or type-II) phyllobilins. The first characterized type-II phyllobilin was colorless featuring four deconjugated pyrrole units; similar to the type-I branch, for which yellow oxidation products of the colorless phyllobilins - the type-I phylloxanthobilins - are known, a type-II phylloxanthobilin has recently been characterized from senescent leaves of grapevine. Type-I phylloxanthobilins appear to be actively produced in the plant, are known to possess interesting chemical properties, and were shown to act as potent antioxidants that can protect cells from oxidative stress. Here we report the isolation and structural characterization of a type-II phylloxanthobilin from de-greened leaves of savoy cabbage, which turned out to be structurally closely related to bilirubin. Bilirubin is known to possess high antioxidative activity, in addition, savoy cabbage is considered to promote health benefits due to its high content in antioxidants. We therefore investigated the *in vitro* antioxidative potential of the newly identified type-II phylloxanthobilin using two different approaches, both of which revealed an even higher antioxidative activity for the type-II phylloxanthobilin from savoy cabbage compared to bilirubin.

*Correspondence to: Simone Moser: email: simone.moser@cup.uni-muenchen.de, phone: +49-89-2180-77175

INTRODUCTION

The disappearance of the green plant pigment chlorophyll (Chl) is a biological phenomenon that we primarily associate with the occurrence of colored leaves in autumn. In recent years, however, Chl degradation products have been identified in the peels of ripe fruit and vegetables [1]. Surprisingly, the biochemical program for Chl degradation appears to be the same in senescent leaves of deciduous trees compared to ripening fruit, each representing a different stage of life. Despite the biological importance of Chl, the degradation products of Chl have remained a mystery for a long time [2]. To date, many linear tetrapyrroles derived from the degradation of Chl in higher plants have been identified, most of which are due to the pioneer work of Kräutler et al [3, 4]. These Chl-derived linear tetrapyrroles are nowadays termed 'phyllobilins' (PBs) due to their structural relationship to the degradation products of heme, the bilins [5]. The first PB to be discovered was colorless [6] - a phylloleucobilin (PleB) - in the meantime, yellow PBs, the phylloxanthobilins [7] (PxBs) have been characterized from a variety of sources.

Although the first steps of Chl degradation seem to be biochemically strictly regulated and controlled, Chl degradation appears to 'branch out' during the later stages depending on the plant species investigated, giving rise to a large structural variety among PBs. The key enzyme of the Chl degradation pathway, pheophorbide A oxygenase (PaO), cleaves the chlorin macrocycle at the 'northern' meso position. In contrast to heme degradation, in which the enzyme heme oxygenase removes the carbon of the methylene bridge in the process of the oxygenolytic ring opening of heme, the reaction of PaO results in a linear tetrapyrrole still containing the C(20), oxidized to an aldehyde [8]. The aldehyde function is retained in the Chl degradation branch leading to type-I PBs (1-formyl-19-oxobilins). In another branch, however, leading to type-II PBs, this aldehyde moiety is removed by the activity of a cytochrome P450 enzyme, CYP89A9 [9] (Scheme 1).

Historically, the type-I PBs were discovered several years before the type-II PBs, both on the stage of the colorless PleBs. Type-I PleBs were for a long time thought to be the final products of Chl degradation, representing a stable storage form of degraded Chl in the vacuoles of the plant cells [5]. Roughly 10 years ago, however, a yellow oxidation product of a type-I PleB, a type-I phylloxanthobilin (PxB), was characterized in senescent leaves of *Cercidiphyllum japonicum* [7]. In the meantime, more PxBs have been identified (for example in *Egeria densa* and in lime tree leaves [10, 11]), in a similar structural variety as their PleB precursors. How the PxBs are formed from PleBs is still under investigation, although the process of PxB formation seems to be actively supported in the plant by a still elusive 'oxidative activity' [12]. Only very recently has a naturally occurring type-II PxB been discovered in senescent grapevine leaves, which was further obtained from a type-II PleB *via* a 'green' semisynthetic approach employing the 'oxidative activity' that also efficiently transforms the type-I PleBs to type-I PxBs [13]. Furthermore, the type-II PxB was shown to possess similar chemical properties as the type-I PxBs, as was recently demonstrated for the ability to act as photoswitches [13, 14]. In addition to being photoswitchable, the type-I PxB was shown to dimerize depending on the lipophilicity of the environment [14], both of which are exciting properties that might be exploited by the plant for yet-to-be identified biological roles.

Scheme 1.

Recently, six different type-I PxBs were identified in the medicinal plant *Echinacea purpurea*, which is of high importance in phytomedicine due to its application as a cold remedy. For the type-I PxBs from *Echinacea*, it was shown that they have very potent antioxidative activities *in vitro,* are able to scavenge reactive oxygen species in a human cell line, and protect the cells from oxidative stress caused by hydrogen peroxide, as was shown by measuring cellular total glutathione levels [15].

Structurally, PxBs are related to bilirubin (BR) [16], whereby the type-II PxBs resemble the catabolite from heme degradation even more than the type-I PxBs due to their 1,19-dioxobilin type structure lacking the aldehyde functionality. BR is known to have cytoprotective functions, most of which are due to its capability to scavenge reactive oxygen and nitrogen species [17, 18]. Since strong antioxidative activities have also been demonstrated for type-I PxBs, we set out to investigate the *in vitro* antioxidative potential of type-II PxBs in comparison to BR.

A type-II PxB has so far only been isolated and characterized from grapevine leaves [13] and was shown to be esterified at the $C8^2$ position at ring E, therefore not sharing the di-propionic acid structural feature of BR. We report here the identification and characterization of a novel type-II PxB from de-greened leaves of savoy cabbage (*Brassica oleracea* var. *sabauda*) that closely resembles BR, as well as studies on the antioxidative activity of the newly identified compound.

RESULTS AND DISCUSSION

HPLC analysis of an extract of senescent savoy cabbage leaves allowed for the tentative assignment of five signals as PBs due to their UV-vis characteristics (Supporting information, Fig. S1); among those, one signal was tentatively identified as type-I PleB, two signals as type-II PleBs, and two signals indicated the presence of *E* and *Z* isomers of a type-II PxB (Fig. 1). HR-MS indicated that the less polar type-II PleB may be the same catabolite that has already been characterized in senescent florets of broccoli [19], and may be the precursor of the type-II PxB (Table S1). For type-II PxBs, only a few reports of the occurrence have been published so far [13, 20]; therefore, the structure of the type-II PxB from savoy cabbage, termed *Bos*-PxB, was characterized in more detail.

Fig. 1

For isolation and structure elucidation of *Bos*-PxB, fresh savoy cabbage was stored in the dark for 5 days and 150 g of the de-greened parts of cabbage leaves were extracted as described in the experimental section. Purification with semi-preparative HPLC yielded 4.56 µmoles (2.8 mg) of *Bos*-PxB. The elemental composition of *Bos*-PxB was deduced as $C_{33}H_{36}N_4O_8$ by HR-MS. ESI-MS analysis confirmed the pseudomolecular ion at *m/z* 617.6 [M+H]$^+$ and MS/MS measurements showed fragment ions at *m/z* 599.3 and *m/z* 573.13 from the loss of H_2O and CO_2, respectively, the latter originating from a free propionic acid side chain (Fig. S2) [21]. Loss of methanol, which is a typical fragmentation for PBs featuring the β-keto ester at ring E [21] was not observed. In addition, the fragment ion at *m/z* 476.87, corresponding to the loss of the ring A [M - ring A + H]$^+$ could be detected, validating the structure of a type-II PxB.

In the ^{1}H NMR spectrum (500 MHz, 25 °C, Fig. S3) of *Bos*-PxB, the high-field singlets of four methyl groups, the signals of an ABX spin system of the vinyl group at ring D, and the singlet at 6.18 ppm (HC15) of

the additional double bond of the typical PxB chromophore stood out. The constitution of *Bos*-PxB was deduced by $^1H,^1H$ homonuclear (COSY and NOESY) and $^1H,^{13}C$ heteronuclear (HSQC and HMBC) NMR correlations (Fig. 2 and Table S2). Three characteristic signals in the intermediate field were assigned to the peripheral vinyl group at ring D. The typical signal in the low field for the formyl group at ring A of type-I PBs was not observed, indicating the presence of a type-II PB. H_2C5 was assigned to the AB spin system at 2.45 and 3.04 ppm, which correlated with C5 at 29.04 ppm (HSQC) and coupled with the multiplet of HC4 at 4.27 ppm ($^1H,^1H$ NOESY), confirming *Bos*-PxB to carry the characteristic type-II lactam moiety at ring A. The signal at 6.18 ppm, from the HC15 of the phylloxanthobilin chromophore correlated with an unsaturated carbon at 101.24 ppm. According to $^1H,^1H$ NOESY correlations, the four singlets at the high field of the methyl groups were assigned as follows: the singlet of H_3C2^1 at 1.72 ppm coupled with the multiplet of H_2C3^1 and the methylene protons of H_2C3^2 of the hydroxyethyl side chain; the singlet of H_3C7^1 at 2.10 ppm coupled with the signal of H_2C5, whereas the signal of H_3C13^1 at 2.09 ppm coupled with the protons of the propanoic acid group (H_2C12^2 and H_2C12^1); and the singlet at 2.15 ppm for H_3C17^1 showed couplings with the signals of the vinyl group at ring D. A singlet of a methyl ester group expected at a shift of about 3.7 ppm was missing, validating the di-propionic acid structural feature of the *Bos*-PxB.

Fig. 2.

On the basis of mass spectrometric and NMR spectroscopic data, the chemical structure of *Bos*-PxB was deduced as a 1,19-dioxo-3^2-hydroxy-$O8^4$-desmethyl-1,4,16,19-tetrahydro-phyllobilane. From all previously discovered structures of PBs, the *Bos*-PxB most resembles the heme-derived yellow bile component BR, with only minor modifications (Fig. 3a). Besides the common tetrapyrrole structure, the 'western hemisphere' of both molecules is identical, including the vinyl group at ring D and the two methyl groups at $C17^1$ and $C13^1$. In contrast to PleBs, which feature four deconjugated pyrrole units, the PxBs (as well as BR) have a conjugated double system extending from ring C to D, leading to a UV-vis absorption maximum above 420 nm (428 nm for *Bos*-PxB, Fig. 3b). Moreover, the *Bos*-PxB shares the di-propionic acid structural feature of BR. Compared to type-I PxBs, the dioxobilin-type *Bos*-PxB as well as BR feature an unsaturated lactam ring instead of an aldehyde group at ring A, resulting in a decreased absorption at 310 nm [13]. In spite of the similar chemical structures of *Bos*-PxB and BR, HPLC analysis of a mixture of both revealed quite different retention times (Fig. S4). *Bos*-PxB eluted after 10.3 min, whereas BR showed a retention time of 19.5 min demonstrating the influence of these minor structural alterations on the polarity, which might also affect, for example, solubility properties.

Fig. 3.

Interestingly, investigation of senescent florets of broccoli (*Brassica oleracea* var. *italica*) [19], revealed a type-II PleB that has the same modification pattern as the newly identified type-II PxB, and may be identical to the type-II PleB identified in savoy cabbage. Past characterizations of PleBs from the same plant family, the *Brassicacea*, showed the occurrence of the same type-II PleB (free acid function at $C8^2$, vinyl group at C18 and hydroxyethyl moiety at C3) in oilseed rape (*Brassica napus*) [22] and in *Arabidopsis thaliana [23]*, which reflects the close phylogenetic relationship on the chlorophyll catabolite level. All PleBs identified in *Arabidopsis thaliana* and all three catabolites from broccoli carry a free acid function at $C8^2$, instead of the methyl ester group that is present in the majority of the identified PleBs as well as the common precursor, the

pPluB [24] (Scheme 1). The removal of the methyl ester functionality at C8^2 is accomplished by the activity of the cytosolic methyl esterase Mes16 in *Arabidopsis thaliana* [25], indicating that an analogue of this enzyme is presumably also present in other *Brassicacea* species, as well as in savoy cabbage. Investigations of enzymes related to Chl degradation in Chinese flowering cabbage (*Brassica rapa* var. parachinensis) showed activities for early Chl degradation steps (among them PaO), the presence of PBs, however, is not reported [26].

Fig. 4.

Alcoholic and hydroalcoholic extracts of savoy cabbage were shown to possess high antioxidative potential; the compounds responsible for the antioxidative activity, however, are still uncharacterized [27]. So far, phytochemical profiling has yielded vitamin C, phenolic compounds such as chlorogenic acid, β-carotene and lutein as active ingredients in terms of antioxidative activity of savoy cabbage extracts [28]. Here we show that alcoholic extracts of savoy cabbage contain a type-II PxB that resembles the established antioxidant BR and exerts strong antioxidative activity *in vitro*. When analyzing the antioxidative activity of both, the type-II PxB and BR in two different *in vitro* approaches (Fig. 4), the type-II PxB showed significantly higher antioxidative potential compared to BR in both assays. The FRAP assay measures antioxidative potential by the ability of the tested compounds to reduce Fe(III)-TPTZ to the corresponding Fe(II) complex. As a standard, the antioxidant compound Trolox, a water-soluble vitamin E derivative, was used, and antioxidative power is expressed relative to Trolox as Trolox equivalents. In contrast to BR, which showed similar antioxidative activity compared to Trolox, the *Bos*-PxB turned out to possess about 2.5-fold higher activity.

The DPPH method is based on the reduction of the stable free radical α,α-diphenyl-β-picrylhydrazyl to the corresponding hydrazine. Again, Trolox was used as a control; the assay showed a scavenging capacity for Trolox as reported in the literature [29]. For the *Bos*-PxB, the DPPH assay showed that the scavenging ability was significantly higher compared to Trolox, confirming the potent antioxidative activity of *Bos*-PxB. BR, which showed a comparable albeit slightly elevated antioxidative potential compared to Trolox in the FRAP assay, exhibited slightly lower scavenging activity than Trolox in the DPPH assay. In both assays, however, the differences between Trolox and BR are not significant and BR can be assumed to have comparable antioxidative activity as Trolox and hence lower activity compared to *Bos*-PxB.

EXPERIMENTAL

General

HPLC grade acetonitrile (MeCN), methanol (MeOH), ethanol (EtOH), dimethylsulfoxide (DMSO) and hydrochloric acid (HCl) were purchased from VWR International GmbH (Ismaning, Germany) and ultra-pure water (18MΩ.cm^{-1}) from a Millipore S.A.S. Milli-Q Academic system (18,2 MΩ cm^{-1}, Molsheim, France). 2,4,6-Tri(2-pyridyl)-s-triazine (TPTZ), potassium phosphate monobasic (KH$_2$PO$_4$), potassium phosphate dibasic (K$_2$HPO$_4$), ammonium acetate (NH$_4$AcO), iron(III)chloride (FeCl$_3$), 2,2-Diphenyl-1-picrylhydrazyl (DPPH), acetic acid 100% (AcOH) were obtained from Merck (Darmstadt, Germany). Bilirubin was bought from Biomol GmbH (Hamburg, Germany) and Trolox from Enzo Life Sciences GmbH (Lörrach, Germany). Fresh, green savoy cabbage (*Brassica oleracea* var. *sabauda*) was bought in a local supermarket (REWE, Großhadern) and

Chl degradation was induced by incubation in the dark at rt for 5 days. Yellow, senescent parts of savoy cabbage leaves were either immediately extracted or stored at -80 °C. A bilirubin stock (10 mM in 0.1 N NaOH) was freshly prepared prior to every experiment under protection from light.

Chromatography

i) Analytical HPLC: Agilent 1260 Infinity II LC system with a 1260 Infinity Degasser, a 1100 Series quaternary pump and 1100 Series diode array detector; Agilent Poroshell column 120EC-C18 4 μm 46 x 150 mm at 15 °C protected by a Phenomenex ODS 4 x 3 mm i.d. pre-column; injection volume: 100 μL. Solvent system for savoy cabbage extract: mobile phase A = ammonium acetate buffer 10 mM pH 7, B = MeOH, flow 0.5 mL/min; Solvent composition: 0-5 min 20% B, 5-35 min 20% to 60% B, 35-37 min 60% to 100% B, 37-40 min 100% B, 40-42 min 100 to 20% B. Solvent system for HPLC analysis of purified type-II *Bos*-PxB and BR: mobile phase A = ammonium acetate buffer 10 mM pH 7, B = MeCN, flow 0.5 mL/min; Solvent composition: 0-2 min 5% B, 2-17 min 5% to 100% B, 17-20 min 100% B, 20-22 min 100 to 5% B. Data were processed with OpenLab CDS Data Analysis.

ii) Semi-preparative HPLC: Gynkotek LC-System with manual sampler, M480 pump, Phenomenex DG-301 online degasser, Gynkotek UVD 640 diode array detector and a Rheodyne injection valve with 5 mL loop; column Phenomenex Luna 5μ C18, 100 Å, with a Phenomenex pre-column ODS 9 x 16 mm; mobile phase A = ammonium acetate buffer 10 mM pH 7, B = MeCN, flow 2.5 mL/min; solvent composition: 0-2 min 12% B, 2-12 min 12% to 20% B, 12-30 min 20% to 80% B, 30-40 min 80% to 100% B. Data were processed with Gynkosoft 5.50.

Spectroscopy

UV-vis: Thermo Spectronic Genesys 5 (336001) UV-visible spectrophotometer; λmax in nm (rel. ε). Concentrations of type-II *Bos*-PxB were calculated using log ε (426 nm) = 4.51 [7]. ESI-MS and MS/MS: Thermo Finnigan LCQ Deca XP Plus mass spectrometer, ESI source, positive ion mode, spray voltage 4.7 kV; ions of selected *m/z* were isolated in the ion trap prior to fragmentation by CID (collision induced dissociation, 15%). High Resolution-Mass Spectra were at the MS facility of the Department of Chemistry, University of Munich. Data were processed with Xcalibur. NMR spectra were recorded on an Avance III HD 500 MHz NMR spectrometer from Bruker BioSpin equipped with a CryoProbe™ Prodigy broadband probe using CD$_3$OD as solvent. The spectral acquisition parameters were as follows: a) ^{1}H NMR spectrum: spectral width: 10 000 Hz, acquisition time: 3.28 s, relaxation delay 1.0 s; b) ^{13}C NMR spectrum: spectral width: 30 864 Hz, acquisition time: 1.06 s, relaxation delay: 2.0 s; c) COSY spectrum: recorded with 16 transients over 128 increments (zero-filled to 1K) and 1K data points with spectral width of 6685 Hz. The recycle delay was 2.0 s. A 0° sine square multiplication was applied in both dimensions; d) the phase sensitive (^{1}H,[13]C) gs-HSQC spectrum: recorded with 64 transients over 256 increments (zero-filled to 512) and 512 data points with spectral widths of 7 000 Hz in F2 and 27 624 Hz in F1. The recycle delay was 1.37 s. A 90° sine square and an additional exponential (10 Hz) multiplication was applied in both dimensions. e) gs-HMBC spectrum: recorded with 128 transients over 128 increments (zero-filled to 512) and 1K data points with spectral widths of 7 000 Hz in F2 and 28 900 Hz in F1. The recycle delay was 1.5 s. A 90° sine square and an additional exponential (10 Hz) multiplication was applied in F2 and a 0° sine bell and an additional exponential (10 Hz) multiplication was applied in F1. f) the phase

sensitive gs-NOESY spectrum with water suppression via excitation sculpting: recorded with 32 transients over 128 increments (zero-filled to 1K) and 1K data points with spectral widths of 7 500 Hz. The mixing time was 0.5 s. The recycle delay was 2.0 s. A 0° sine square multiplication was applied in both dimensions. NMR data were analyzed with Mestre Nova.

Isolation and Characterization

Isolation and Structure Elucidation of type-II Bos-PxB from fresh senescent leaves

Senescent parts of savoy cabbage leaves (150 g) were mixed in a solvent mixture consisting of 60% MeOH and 40% potassium phosphate buffer 50 mM pH 5.2 (500 mL) by a Braun hand blender Model MR 5000 in a 5 L stainless steel beaker. The mixture was incubated at rt for 1 h, then filtered; the filtrate was washed with solvent (200 mL), and filtered again. After acidifying the extract to pH 3.5 by addition of 50% AcOH, the solution was stirred at rt in the dark overnight. Next, the mixture was concentrated (30 mL), centrifuged and filtrated prior to purification by semi-preparative HPLC. The collected yellow fractions were combined, the solvent was removed under reduced pressure on a rotary evaporator, and the solid residue was lyophilized, giving a yield of 4.56 µmoles. The purity of the type-II Bos-PxB was controlled by analytical HPLC. The lyophilized sample was dissolved in DMSO and stored at -20 °C until further use.

UV-vis (MeOH): λ_{max}, nm (relative ε) 226 (1.88), 244 (1.24), 280 (0.64), 428 nm (1.00). HR-ESI-MS: m/z 617.26098 (calcd. for $[M+H]^+$ 617.26059; $\Delta = 0.63$ ppm). ESI-MS/MS: m/z (%) 617.6 (100) $[M+H]^+$; 599.3 (46) $[M-H_2O+H]^+$, 573.1 (56) $[M-CO_2+H]^+$, 476.9 (87) $[M-\text{ring A}+H]^+$. ^{1}H NMR (500 MHz, 25 °C, d_4-MeOH): δ_H, ppm 1.72 (s, H_3C2^1), 2.09 (s, H_313^1), 2.10 (s, H_3C7^1), 2.15 (s, H_3C17^1), 2.32 (m, H_2C12^2), 2.45 (m, H_AC5), 2.60 (m, H_AC12^1), 2.65 (m, H_BC12^1), 2.72 (m, H_2C3^1), 3.04 (dd, $J = 4.6/14.8$, H_BC5), 3.65 (m, H_2C3^2), 4.27 (m, HC4), 4.90 (s, HC10), 5.30 (dd, $J = 2.5/11.7$, H_AC18^2), 6.07 (dd, $J = 2.4/17.7$, H_BC18^2), 6.18 (s, HC15), 6.54 (dd, $J = 11.6/17.6$, $HC18^1$). ^{13}C NMR (500 MHz, 25 °C, d_4-MeOH, signal assignment from HSQC and HMBC spectra): δ_H, ppm 7.1 (2^1), 8.0 (7^1), 8.2 (17^1), 8.3 (13^1), 19.9 (3^1), 19.9 (12^1), 29.0 (5), 37.1 (10), 37.2 (12^2), 59.5 (4), 60.0 (3^2), 70.0 (8^2), 101.2 (15), 111.6 (7), 116.9 (18^2), 118.1 (12), 123.4 (18), 124.3 (8), 124.8 (13), 126.2 (18^1), 129.3 (16), 129.4 (2), 132.4 (11), 132.5 (6), 142.2 (17), 154.9 (3), 159.2 (9), 171.8 (19), 175.2 (8^3), 175.4 (1), 178.1 (12^3).

In vitro Antioxidative assays

Ferric Reducing Antioxidant Potential (FRAP) assay

The FRAP assay was performed according to the protocol of Benzie et al [30] with minor modifications. Briefly, the FRAP reagent was prepared by mixing 10 volumes of 300 mM acetate buffer pH 3.5, 1 volume of 10 mM TPTZ (2,4,6-Tri(2-pyridyl)-s-triazine) in 40 mM HCl and 1 volume of 20 mM iron(III)chloride. Fresh FRAP reagent was incubated with 50 µM of either type-II Bos-PxB, BR, or several concentrations of Trolox for 5 min at 37 °C. The antioxidant power was measured by the absorbance of the reduction product of Fe^{3+}-$(TPTZ)^2$, Fe^{2+}-$(TPTZ)^2$ at 620 nm. A calibration curve was established for Trolox and the antioxidant power of the compounds was calculated as Trolox equivalents.

DPPH radical scavenging activity assay

DPPH radical scavenging activity was performed as described by Pan et al [31] with some adjustments. The control was prepared by mixing 50 µL of EtOH (75% v/v) with 100 µL of DPPH (0.3 mM in 75% EtOH v/v) in

a 96 well plate. 50 µL of either Trolox, type-II *Bos*-PxB, or BR (50 µM) were either mixed with 100 µL of EtOH (75% v/v) for blank groups, or with 100 µL of DPPH solution for sample groups (0.3 mM in 75% EtOH v/v). The plate was incubated for 60 min at 40 °C and the decrease of the absorbance was measured at 505 nm. Blank samples were substracted and the DPPH scavenging activity was calculated as percentage relative to the control.

Statistical analysis

Results represent the mean of at least three independent experiments (means ± standard deviation), which were each carried out in at least three replicates. One-way analysis of variance with post hoc analysis using Dunnett's multiple comparison test was performed to analyze statistical significance; all statistical analyses were performed with GraphPad Prism 7.

CONCLUSION

PBs, and particularly the PxBs, have recently come to our attention as possible bioactive components of plants that could play a role in protecting cells from oxidative stress [15]. Here, we report the isolation and structure elucidation of a novel PxB that closely resembles BR, a potent antioxidative bile pigment, for which antioxidative activity has been proven previously [17, 18]. For the *Bos*-PxB, an even stronger antioxidative *in vitro* activity compared to BR has been revealed, a fact that will be the incentive for further studies on these plant derived tetrapyrroles and their possible roles and potential in protecting cells from oxidative damage.

REFERENCES

1.   Müller T, Ulrich M, Ongania KH and Kräutler B. *Angew. Chem. Int. Ed.* 2007. **46**: 8699-702.
2.   Moser S and Kräutler B. *Isr. J. Chem.* 2019. **59**: 420-431.
3.   Kräutler B. *Photochem. Photobiol. Sci.* 2008. **7**: 1114-1120.
4.   Moser S, Müller T, Oberhuber M and Kräutler B. *Eur. J. Org. Chem.* 2009. 21-31.
5.   Kräutler B. *Angew. Chem. Int. Ed.* 2016. **55**: 4882-4907.
6.   Kräutler B, Jaun B, Bortlik K, Schellenberg M and Matile P. *Angew. Chem. Int. Ed.* 1991. **30**: 1315-1318.
7.   Moser S, Ulrich M, Müller T and Kräutler B. *Photochem. Photobiol. Sci.* 2008. **7**: 1577-1581.
8.   Pružinská A, Tanner G, Anders I, Roca M and Hörtensteiner S. *Proc. Natl. Acad. Sci. U.S.A* 2003. **100**: 15259.
9.   Pružinská A, Tanner G, Aubry S, Anders I, Moser S, Müller T, Ongania K-H, Kräutler B, Youn J-Y, Liljegren SJ and Hörtensteiner S. *Plant Physiol.* 2005. **139**: 52.
10.   Scherl M, Muller T and Krautler B. *Chem. Biodivers.* 2012. **9**: 2605-17.
11.   Wakana D, Kato H, Momose T, Sasaki N, Ozeki Y and Goda Y. *Tetrahedron Lett.* 2014. **55**: 2982-2985.
12.   Vergeiner C, Ulrich M, Li C, Liu X, Müller T and Kräutler B. *Chem. Eur. J.* 2015. **21**: 136-149.
13.   Li C, Erhart T, Liu X and Kräutler B. *Chem. Eur. J.* 2019. **25**: 4052-4057.
14.   Li C, Wurst K, Jockusch S, Gruber K, Podewitz M, Liedl KR and Kräutler B. *Angew. Chem. Int. Ed.* 2016. **55**: 15760-15765.
15.   Karg CA, Wang P, Vollmar AM and Moser S. *Phytomedicine.* 2019. 152969.
16.   Li C and Kräutler B. *J. Porphyrins Phthalocyanines* 2016. **20**: 388-396.
17.   Gazzin S, Vitek L, Watchko J, Shapiro SM and Tiribelli C. *Trends Mol. Med.* 2016. **22**: 758-768.
18.   Mancuso C, Pani G and Calabrese V. *Redox Rep.* 2006. **11**: 207-213.

19.   Roiser MH, Müller T and Kräutler B. *J. Agric. Food. Chem.* 2015. **63**: 1385-1392.
20.   Süssenbacher I, Menghini D, Scherzer G, Salinger K, Erhart T, Moser SV, Clemens, Hörtensteiner S and Kräutler B. *Photosynth. Res.* 2019. https://doi.org/10.1007/s11120-019-00649-2
21.   Müller T, Vergeiner S and Kräutler B. *Int. J. Mass Spectrom.* 2014. **365-366**: 48-55.
22.   Hörtensteiner S and Kräutler B. *Photosynth. Res.* 2000. **64**: 137-146.
23.   Pruzinska A, Tanner G, Aubry S, Anders I, Moser S, Müller T, Ongania KH, Krautler B, Youn JY, Liljegren SJ and Hortensteiner S. *Plant Physiol.* 2005. **139**: 52-63.
24.   Mühlecker W, Ongania K-H, Kräutler B, Matile P and Hörtensteiner S. *Angew. Chem. Int. Ed.* 1997. **36**: 401-404.
25.   Christ B, Schelbert S, Aubry S, Sussenbacher I, Müller T, Krautler B and Hortensteiner S. *Plant Physiol.* 2012. **158**: 628-41.
26.   Zhang X, Zhang Z, Li J, Wu L, Guo J, Ouyang L, Xia Y, Huang X and Pang X. *J. Plant Physiol.* 2011. **168**: 2081-2087.
27.   Quassinti L, Gianfranceschi G, Lupidi G, Miano A and Bramucci M. *J. Food Biochem.* 2016. **40**: 542-549.
28.   Fernández-León MF, Fernández-León AM, Lozano Ruiz M, González-Gómez D, Ayuso Yuste MC and González JA. *Acta Hortic.* 2012. **939**: 295-300.
29.   Mekky H, Sohafy SM, Abu El-Khair R and El-Hawiet A. *Int. J. Pharm. Pharm. Sci.* 2017. **9**: 44.
30.   Benzie IF and Strain JJ. *Anal. Biochem.* 1996. **239**: 70-6.
31.   Pan X, Zhao Y-Q, Hu F-Y and Wang B. *J. Funct. Foods* 2016. **25**: 220-230.
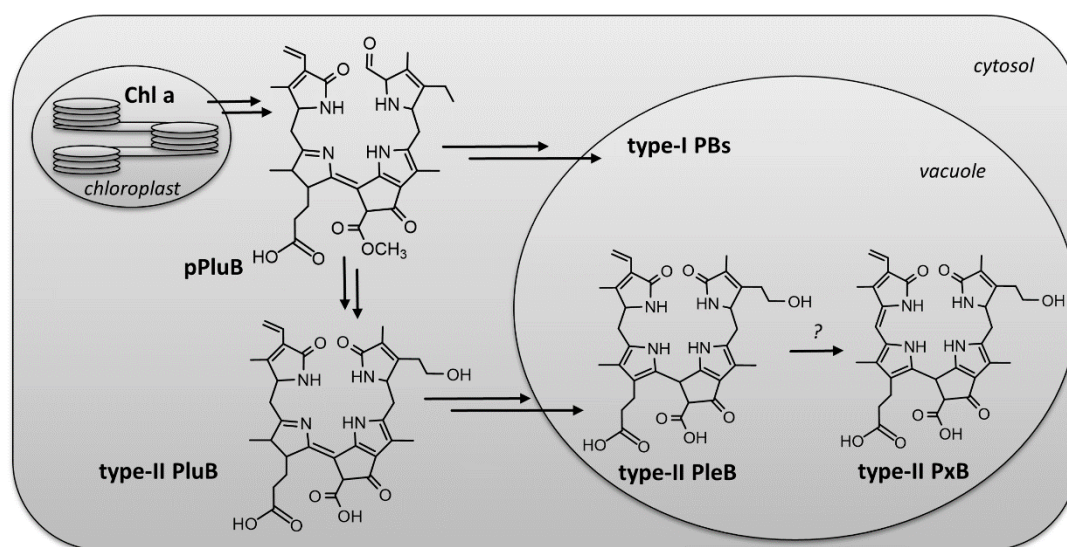
Scheme 1. Topological outline of the degradation of Chl leading to the type-II PxB. Chl a located in the chloroplast is degraded in several steps to a 'primary' PluB (pPluB), which is exported to the cytosol. There, Chl degradation branches out, leading to type-I PBs that are stored in the vacuole, or type-II PBs due to the activity of CYP89A9. How the conversion of the PleB (type-I and type-II) to the corresponding PxB takes place in the plant cell is still not characterized.
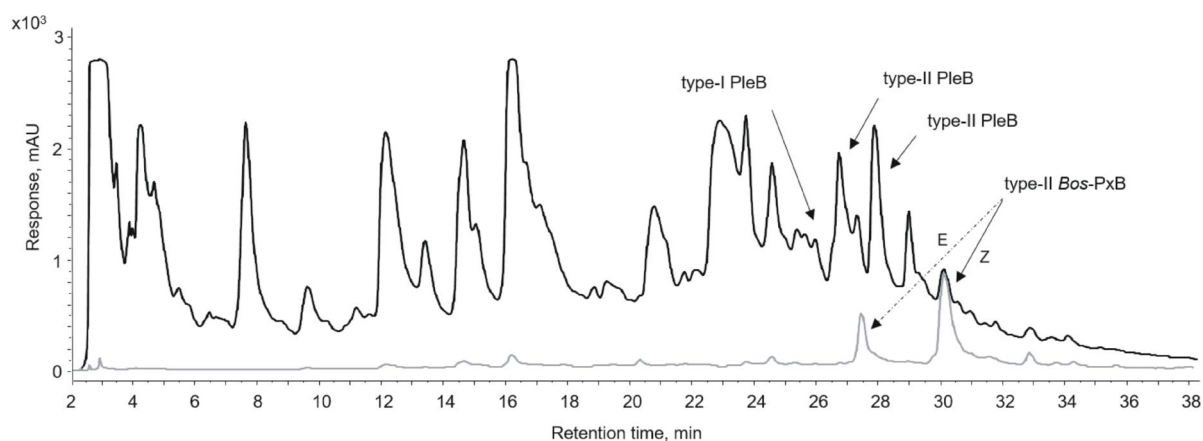
Fig. 1. Analytical HPLC-traces of an extract of senescent savoy cabbage leaves (black = HPLC trace at 254 nm; grey = at 420 nm). PBs were tentatively identified by their UV-vis characteristics.
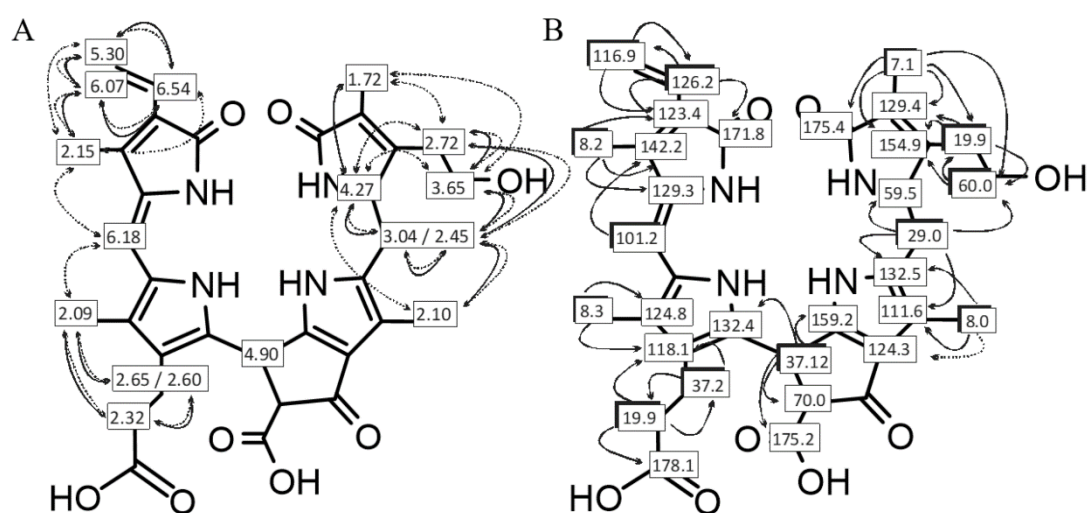
Fig. 2: Graphical representation of the structural characterization of *Bos*-PxB by 1D and 2D NMR spectra (500 MHz, in d_4-MeOH). a) ^{1}H signal assignments from ^{1}H, ^{1}H COSY and ^{1}H, ^{1}H NOESY correlations (represented by bold and dashed arrows). b) ^{13}C signal assignments based on ^{1}H,^{13}C HSQC (represented by shaded boxes) and ^{1}H,^{13}C HMBC (indicated by arrows and open boxes) spectra.
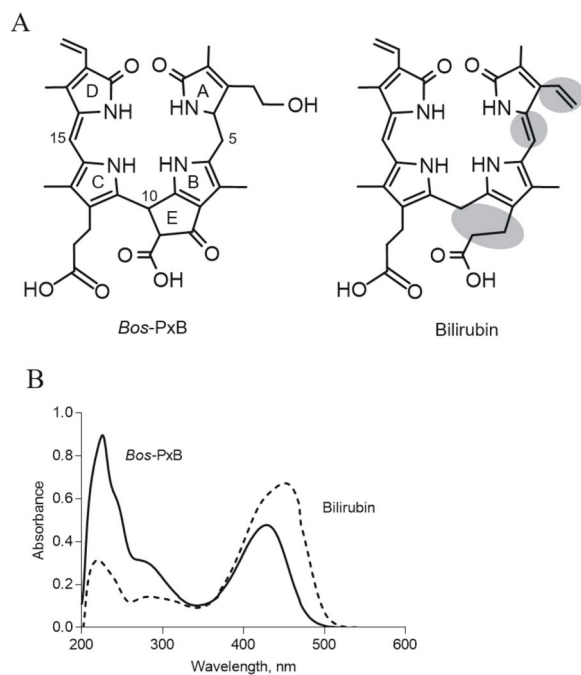
Fig. 3: Characteristics of *Bos*-PxB and BR. Structure highlighting the differences between *Bos*-PxB and BR in grey (a), and UV-vis spectra in methanol (b) of *Bos*-PxB (bold trace) and BR (dashed trace).
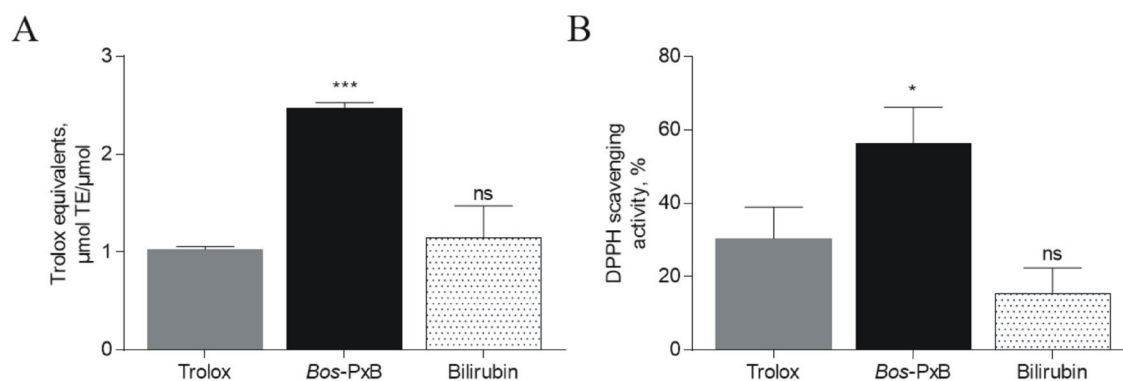
Fig. 4. *Bos*-PxB shows significantly higher *in vitro* antioxidative activity compared to Trolox and BR. a) Ferric reducing antioxidant power (FRAP) assay. b) DPPH free radical scavenging assay.

Isolation, characterization, and antioxidative activity of a dioxobilin-type phylloxanthobilin from savoy cabbage

Supplementary Information

Cornelia A. Karg[a], Charlotte M. Schilling[a], Lars Allmendinger[b], Simone Moser[a]*

[a]*Pharmaceutical Biology, Pharmacy Department, Ludwig-Maximilians University of Munich, Butenandtstraße 5-13, D-81337 Munich, Germany*

[b]*Pharmaceutical Chemistry, Pharmacy Department, Ludwig-Maximilians University of Munich, Butenandtstraße 5-13, D-81337 Munich, Germany*

Figure 1: MS/MS spectrum of type-II *Bos*-PxB (m/z 617.0; CID 15%; positive mode).
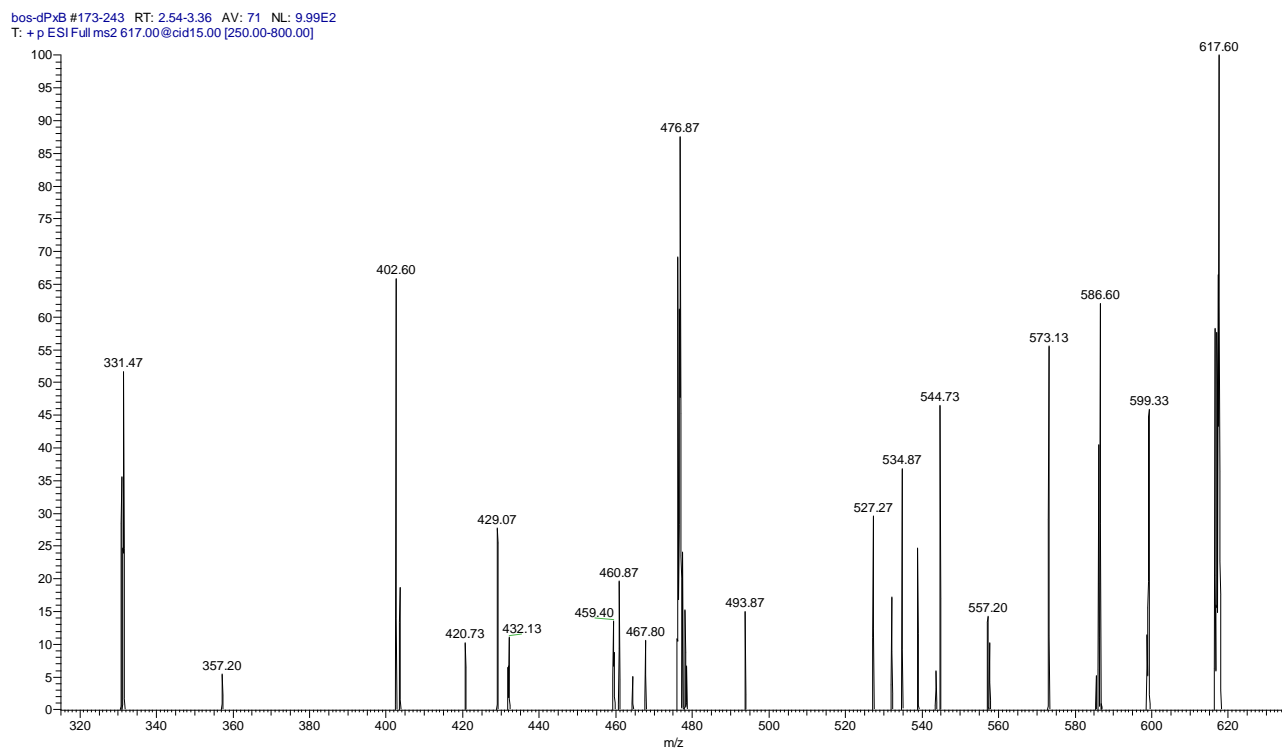
Figure 2: 500 MHz ¹H-NMR spectrum of type-II *Bos*-PxB in d₄-MeOH.

Dioxobilin-type phylloxanthobilin from savoy cabbage - Supplementary Information
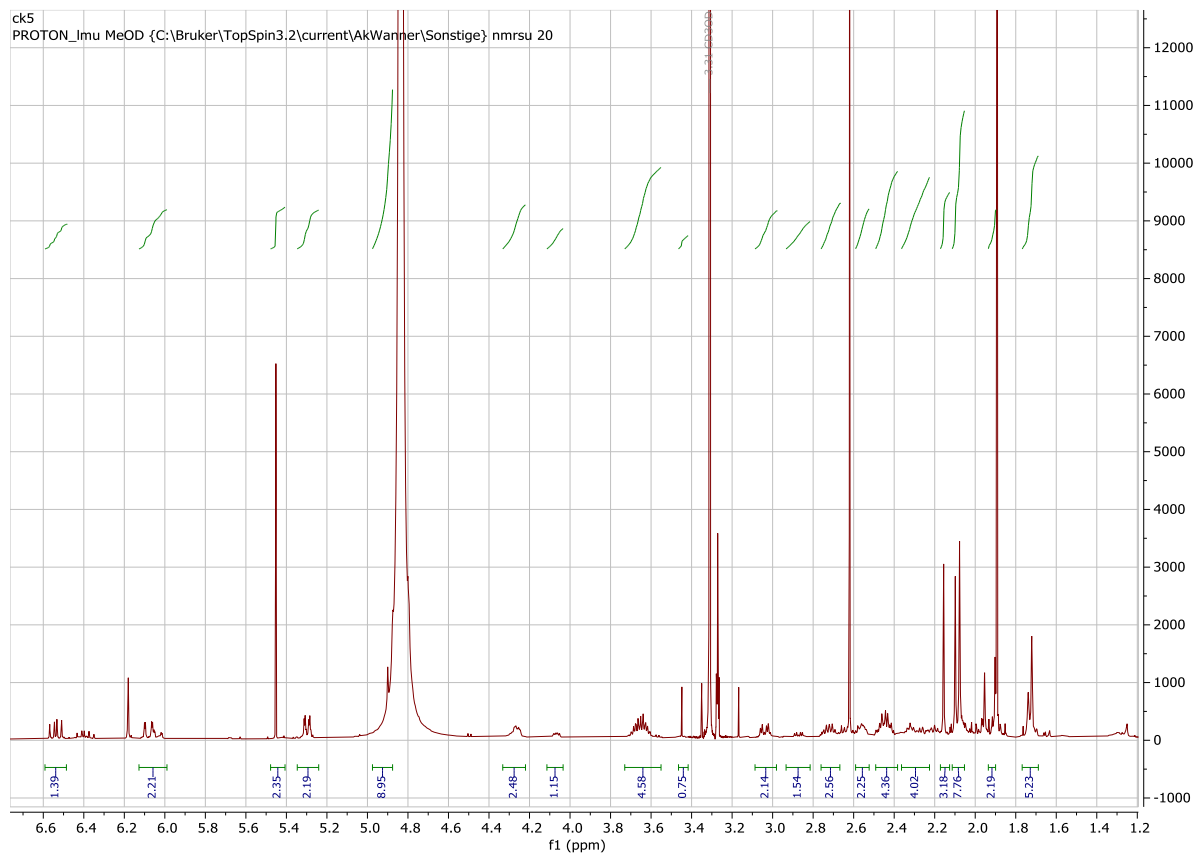
The ^{1}H-NMR showed a signal for the $H_2C(18^1)$ at 6.40 ppm, which comes from the E isomer of the type-II *Bos*-PxB.

Table 1: HR-MS data of the less polar type-II PleB, precursor of the type-II *Bos*-PxB.

	m/z [M+H]$^+$
type-II PleB	619.27647

Table 2: ^{1}H- and ^{13}C-NMR data of type-II *Bos*-PxB in d_4-MeOH (500 MHz, 25°C)

	^{1}H	^{13}C
C1		175.4
C2		129.4
H$_3$C2^1	1.72	7.1
C3		154.9
H$_2$C3^1	2.72	19.9
H$_2$C3^2	3.65	60.0
HC4	4.27	59.5
H$_A$C5	3.04	29.0
H$_B$C5	2.45	
C6		132.5
C7		111.6
H$_3$C7^1	2.10	8.0
C8		124.3
C8^1		
HC8^2		70.0
C8^3		175.2
C9		159.2
HC10	4.90	37.1
C11		132.4
C12		118.1
H$_2$C12^1	2.65 / 2.60	19.9
H$_2$C12^2	2.32	37.2
C12^3		178.1
C13		124.8
HC13^1	2.09	8.3
C14		
HC15	6.18	101.2
C16		129.3
C17		142.2
H$_3$C17^1	2.15	8.2
C18		123.4
HC18^1	6.54	126.2
H$_A$C18^2	5.30	116.9
H$_B$C18^2	6.07	
C19		171.8

Figure 3: HPLC analysis of type-II *Bos*-PxB and bilirubin in MeOH/phosphate buffer 50 mM pH=7 (20/80) (detection at 420 nm).

A yellow chlorophyll catabolite in leaves of *Urtica dioica* L.: An overlooked phytochemical that contributes to health benefits of stinging nettle

Cornelia A. Karg [a], Christian Doppler [b], Charlotte Schilling [a], Franziska Jakobs [a,c], Marlene C. S. Dal Colle [a,d], Nadine Frey [a], David Bernhard [b], Angelika M. Vollmar [a], Simone Moser [a,*]

[a] *Department of Pharmacy, Center for Drug Research, Pharmaceutical Biology, Ludwig-Maximilians-University of Munich, Butenandtstr. 5-13, D-81377 München, Germany*
[b] *Division of Pathophysiology, Institute of Physiology and Pathophysiology, Medical Faculty, Johannes-Kepler-University Linz, Krankenhausstrasse 7a, A-4020 Linz, Austria*
[c] *Department of Chemistry, High Point University, One University Parkway High Point, NC 27268, United States*
[d] *Department of Chemical Sciences, University of Padova, Via Marzolo 1, 35131 Padova, Italy*

ARTICLE INFO

ABSTRACT

Stinging nettle is appreciated for its antioxidant and anti-inflammatory properties, which renders the plant a popular ingredient in a healthy diet in form of salads or smoothies. The most common use, presumably, is of dried leaves as ingredient in tea mixtures. The plant's health benefits are attributed primarily to phenolic phytochemicals. Here we describe the characterization and quantification of a phylloxanthobilin (PxB), a yellow chlorophyll catabolite, in nettle tea. Despite their abundance in the plant kingdom, chlorophyll catabolites have been overlooked as phytochemicals and as part of human nutrition. Our investigations of tea reveal that one cup of nettle tea contains about 50 µg of PxB with large variations depending on the supplier. When investigating the bioactivities of PxB, our observations show that PxB has antioxidative and anti-inflammatory activities comparable to known bioactive small molecules found in nettle, indicating the phylloxanthobilin to be an overlooked ingredient of nettle tea.

1. Introduction

The annual breakdown of chlorophyll (Chl) is one of the most visible signs of life; it is estimated that 1000 million tons of Chl are degraded every year on Earth (Hendry, Houghton, & Brown, 1987). Beside the fascinating color changes of leaves, Chl catabolism also takes place during the ripening of fruits and the de-greening of vegetables (Barry, 2009; Müller, Ulrich, Ongania, & Kräutler, 2007). The discovery of the first non-fluorescent chlorophyll catabolite paved the way for the characterization of a variety of Chl-derived structures, for which the later given term phyllobilins, which points to their structural similarity to the bilins from heme breakdown and their Chl origin (Kräutler, 2014; Kräutler, Jaun, Matile, Bortlik, & Schellenberg, 1991), prevails nowadays.

Additional research has focused on the elucidation of the mechanism of Chl breakdown: The breakdown process turned out to be a strictly controlled and regulated process, which, at least during early steps, appears to be common to all higher plants, and leads to the accumulation of phylloleucobilins (PleBs) in the vacuoles of the plant cell (Scheme 1) (Kräutler, 2014). It was long assumed that these PleBs were the "final" products of Chl degradation. In 2008, however, a new colored structure was detected in fresh extracts of senescent leaves of *Cercidiphyllum japonicum*, a yellow chlorophyll catabolite, called phylloxanthobilin (PxB) (Moser, Ulrich, Müller, & Kräutler, 2008). PxBs are formed from their PleB precursors via a supposed endogenous oxidative process and formally represent a dehydrogenation product of the respective PleBs (Scheme 1) (Vergeiner et al., 2015).

Up to today, >40 constitutionally different phyllobilins (PBs) have been identified, which all share the same tetrapyrrolic core structure but differ in their peripheral substituents. New structures are continuously being discovered from different higher plant sources. In 2007, Müller *et al* discovered PleBs in the peels of apple and pear, which demonstrated the PBs not only to occur in leaves of deciduous trees, but also in large quantities in parts of plants daily ingested by humans (Müller et al., 2007). Further structures were isolated from broccoli (Roiser, Müller, & Kräutler, 2015), spinach (Berghold, Breuker, Oberhuber, Hörtensteiner,

---

* Corresponding author.
  E-mail address: simone.moser@cup.uni-muenchen.de (S. Moser).

& Kräutler, 2002), savoy cabbage (Karg, Schilling, Allmendinger, & Moser, 2019), and olive fruits (Vergara-Domínguez, Ríos, Gandul-Rojas, & Roca, 2016), among others. The characterization of modified PBs also being part of human nutrition has opened the stage for possible physiological properties of these structures, which were originally considered simple detoxification products of Chl. First investigations of biological activities of phyllobilins revealed PleBs being potent antioxidants (Müller et al., 2007). Recently, also PxBs were shown to possess antioxidative activity *in vitro* and in cellular models (Karg, Schilling, et al., 2019; Karg, Wang, Vollmar, & Moser, 2019), and were found to potently inhibit the proliferation of cancer cells (Karg et al., 2020).

Despite the fact that PBs are possible biologically active natural products that are part of our daily diet, pharmacokinetic data on PBs have not been reported yet. As for the fate of chlorophyll during leaf senescence, the fate of phyllobilins in the human body after ingestion is now the puzzle to be solved. Besides *in vitro* studies on the digestive stability of a PleB and its uptake by Caco-2 cells (Roca, 2012), PxBs were found to be taken up by human cells and to be stable in the cells for a time period of at least 5 h (Karg, Wang, et al., 2019).

Urtica dioica L. is an annual plant of the Urticaceae family, which is usually called stinging nettle or common nettle. Since antiquity, stinging nettle is traditionally used as food, fiber, and medicine. It serves as vegetable, and as ingredient or additive of soups, salads, and seasoning (Upton, 2013). Nowadays, the most common usage of nettle leaves are tea-infusions prepared as aqueous extracts of dried leaves, available in every supermarket also in combination with other teas. Indeed, the traditional use of leaf preparations is approved by the European Medicine Agency for the treatment of rheumatic disorders and arthritis and for the usage as diuretic against inflammatory symptoms of the lower urinary tract (EMA/HMPC/508013/2007, 2010).

Phytochemical profiling of the whole plant revealed the main components to be flavonoids, shikimic acid derivatives, as well as carotenoids and polysaccharides (Joshi, Mukhija, & Kalia, 2014). In extracts of nettle leaves, mainly phenolic compounds predominate such as caffeic acid derivatives, chlorogenic acid, caffeoylmalic acid, and flavonoids such as rutin, quercetin, kaempferol, and isorhamnetin (Pinelli et al., 2008). Nettle extracts and their bioactive compounds have been shown to possess antioxidative, anti-inflammatory, analgesic, and immunomodulatory effects, among others (Joshi et al., 2014). Obertreis *et al* demonstrated inhibitory effects of a hydro-ethanolic extract of nettle leaves and caffeic malic acid on the synthesis of prostaglandins derived from the cyclooxygenase-pathway, as well as the secretion of pro-inflammatory cytokines after LPS stimulation (Obertreis, Giller, Teucher, Behnke, & Schmitz, 1996). Gülcin *et al* could prove antioxidant properties for water extracts of the aerial parts of nettle in different experimental setups for testing antioxidative capacities (Gülçin, Küfrevioğlu, Oktay, & Büyükokuroğlu, 2004).

Here we present the identification and structural characterization of a glycosylated PxB from *Urtica dioica* L. leaves, as well as the occurrence and quantification of this PB in nettle tea. We further report studies on the physiological activities, as well as the chemical, digestive, and metabolic stability of the PxB rendering it an until now overlooked plant ingredient, which contributes to the health benefits of nettle used as food, beverage, and medicine.

2. Material and methods

2.1. Chemicals

HPLC grade acetonitrile (ACN) and methanol (MeOH), dichloromethane (CH_2Cl_2), ethanol (EtOH), dimethylsulfoxide (DMSO), sodium pyruvate, potassium chloride (KCl), and hydrochloric acid (HCl) were obtained from VWR International GmbH (Ismaning, Germany); ultrapure water (18MΩ.cm-1) from a Millipore S.A.S. Milli-Q Academic system (18,2 MΩ cm-1, Molsheim, France). 2,4,6-Tri(2-pyridyl)-*s*-triazine (TPTZ), potassium phosphate monobasic (KH_2PO_4), potassium phosphate dibasic (K_2HPO_4), ammonium acetate (NH_4AcO), iron(III) chloride ($FeCl_3$), ammonium carbonate ((NH_4)$_2CO_3$), porcine pepsin, pancreatin from porcine pancreas, uridine 5′-diphosphoglucuronic acid trisodium salt (UDPGA), lipopolysaccharide (LPS), and human liver microsomes were from Sigma-Aldrich (Taufkirchen, Germany). Sodium bicarbonate ($NaHCO_3$), sodium hydroxide (NaOH) and hydrogen peroxide (30%) were obtained from Merck (Darmstadt, Germany); sodium chloride (NaCl), quercetin, chlorogenic acid, caffeic acid, and rutin from Carl Roth (Karlsruhe, Germany) and magnesium chloride hexahydrate ($MgCl_2(H_2O)_6$) and calcium chloride hexahydrate ($CaCl_2(H_2O)_6$) from AppliChem (Darmstadt, Germany). Trolox was from Enzo Life Sciences GmbH (Lörrach, Germany) and SepPak Plus C18 cartridges from Waters Associates (Milford, USA). Bilirubin, alamethicin, nicotinamide adenine dinucleotide phosphate (NADPH) from cayman chemicals were purchased from Biomol GmbH (Hamburg, Germany). Dulbecco's modified Eagle's medium (DMEM) and penicillin/streptomycin 100x were obtained from PAA Laboratories (Pasching, Austria); fetal calf serum was from Biochrom AG (Berlin, Germany); 2′,7′-dichlorodihydrofluorescein diacetate (H_2DCF-DA) was from Thermo Fisher (Waltham, MA, USA), and CellTiter-Blue® reagent was obtained from Promega (Mannheim, Germany). COX-2 monoclonal antibody was purchased from Transduction Labaratories (Lexington, KY) and peroxidase conjugated secondary antibody was from abcam (Cambridge, UK).

2.2. Plant material

Fresh and senescent leaves of *Urtica dioica* L. were collected in
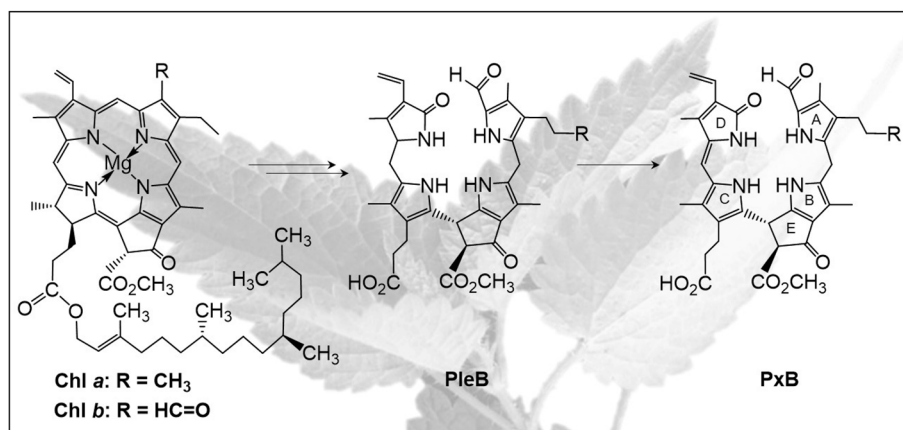
Scheme 1. Schematic overview of selected steps of chlorophyll catabolism. R = O-Glc for PleB and PxB in leaves of *Urtica dioica* L.

Siebnach (Germany, Bavaria, 48°7′59.05′′N, 10°39′39.564′′E) and stored at −20 °C until further use. The identity of the plant material was determined by Prof. Susanne S. Renner (Department of Systematic Botany and Mycology, Faculty of Biology, University of Munich) and the voucher specimen of *Urtica dioica* L. (Moser & Karg 5) has been deposited in the Munich herbarium (acronym M).

Nettle teas from different brands were bought at a local drug store, in local supermarkets, pharmacies, and directly from a supplier of medical herbs. (Alfred Galke GmbH, Bad Grund, Germany; Altapharma Naturprodukte GmbH, Hamburg, Germany; Aurica Naturheilmittel Und Naturwaren GmbH, Schwalbach, Germany; Bad Heilbrunner® Naturheilmittel GmbH & Co. KG, Bad Heilbrunn, Germany; Bombastus Werke AG, Freital, Germany; H&S Tee GmbH & Co. KG, Kressbronn, Germany; dm-drogerie markt GmbH + Co. KG (DAS gesunde PLUS), Karlsruhe, Germany; Meßmer Tee-Gesellschaft mbH, Seevetal, Germany; Sidroga Gesellschaft für Gesundheitsprodukte mbH, Bad Ems, Germany).

2.3. Chromatography

i) Analytical HPLC: Agilent 1260 Infinity II LC system with a 1260 Infinity Degasser, a 1260 Series quaternary pump and 1260 Series diode array detector; Agilent Poroshell column 120EC-C18 (4 μm, 46 × 150 mm) protected by Phenomenex (ODS 5 μm, 4 × 3 mm) pre-column; Column for analysis of nettle tea from Bad Heilbrunner: LiChroCART-LiChrospher100 RP-18 (5 μm, 125 × 4 mm) protected by LiChroCART-LiChrospher100 RP-18 (5 μm, 4 × 4 mm) pre-column; Column for analysis of nettle tea from Altapharma and Meßmer: Phenomenex Hyperclone (ODS 5 μm, 250 × 4.6 mm) protected by Phenomenex (ODS 5 μm, 4 × 3 mm) pre-column; Solvent system: mobile phase A = ammonium acetate buffer 10 mM pH 7, B = ACN, flow 0,5 mL/min; Solvent composition: 0–2 min 5% B, 2–5 min 5% to 20% B, 5–7 min 20% B, 7–22 min 20 to 80% B, 22–25 min 80 to 100% B. Solvent system for assessment of metabolic stability of bilirubin: A = 0.1% (v/v) trifluoroacetic acid, B = ACN, flow 0,5 mL/min; Solvent composition: 0–5 min 20% B, 5–15 min 20% to 75% B, 15–20 min 75% to 95% B, 20–25 min 95% B, 25–30 min 95% to 20% B. Solvent system for assessment of metabolic stability of *Ud*-PxB: A = ammonium acetate buffer 10 mM pH 7, B = ACN, C = 0.1% (v/v) trifluoroacetic acid, flow 0,5 mL/min; Solvent composition: 0–5 min 5% B/ 95% C to 15% A/ 5% B/ 80% C, 5–15 min 15% A/ 5% B/ 80% C to 25% A/ 50 % B/ 25% C, 15–25 min 25% A/ 50 % B/ 25% C to 95% B/ 5% C, 25–30 min 95% B/ 5% C, 30–35 min 95% B/ 5% C to 5% B/ 95% C. Data were processed with OpenLab CDS Data Analysis 2.3.

ii) Semi-preparative HPLC: Gynkotek LC-System with manual sampler, M480 pump, Phenomenex DG-301 online degaser, Gynkotek UVD 640 diode array detector and a Rheodyne injection valve with 5 mL loop; column Phenomenex Luna 5μ C18, 100 Å, with Phenomenex pre-column ODS 9 × 16 mm; mobile phase A = ammonium acetate buffer 10 mM pH 7, B = ACN, flow 2.5 mL/min for injection; solvent composition: 0–2 min 12% B, 2–12 min 12% to 20% B, 12–30 min 20% to 80% B, 30–40 min 80% to 100% B. Data were processed with Gynkosoft 5.50.

2.4. Spectroscopy

UV–Vis: λ_{max} in nm (rel. ε); Thermo Spectronic Genesys 5 (336001) UV–Visible spectrophotometer; Concentrations of *Ud*-PxB were calculated using log ε (426 nm) = 4.51 (Moser et al., 2008).

ESI-MS and MS/MS: Thermo Finnigan LCQ Deca XP Plus mass spectrometer, ESI source, positive ion mode, spray voltage 4.7 kV; ions of selected m/z were isolated in the ion trap prior to fragmentation by CID (collision induced dissociation, 15%). High Resolution-Mass Spectra (HR-MS) were measured in the MS facility of the LMU Department of Chemistry; data were processed with Xcalibur.

NMR spectra were recorded on an Avance III HD 500 MHz NMR spectrometer from Bruker BioSpin equipped with a CryoProbe™ Prodigy broadband probe using d_6-DMSO as solvent. Data were processed

using MestreNova 14.1.1.

2.5. Analysis and quantification of Ud-PxB in nettle tea

One nettle tea bag was poured over with 200 mL of boiling water and brewed for 15 min. The bag was removed and an aliquot of 100 μL was centrifuged and applied to an analytical HPLC. To determine the amount of *Ud*-PxB in one cup of nettle tea, different concentrations of isolated, pure *Ud*-PxB were analyzed by analytical HPLC and used to fit a linear regression of the peak area versus the quantity of compound in mol (Figure S1, Supplementary Information). Teas of nine different brands (Alfred Galke, Altapharma, Aurica, Bad Heilbrunner, Bombastus, dm-Das gesunde PLUS, H&S, Meßmer and Sidroga) were analyzed as described above. The amount of *Ud*-PxB was calculated in μg/200 mL, representing the quantity in one cup of tea and in μg/g, according to the weight of the respective tea bag.

2.6. Isolation and structure elucidation of Ud-PxB from fresh senescent nettle leaves

200 g of fresh senescent leaves of *Urtica dioica* L. were crushed with 800 mL of MeOH by a Braun hand blender Model MR 5000 in a 5 l stainless steel beaker. The plant extract was squeezed through a cotton cloth and dried on a rotary evaporator at 37 °C. The residue was dissolved in 40 mL of potassium phosphate buffer pH 7.4 100 mM and the green suspension was centrifuged at 3000 rpm for 5 min and filtered through a paper filter. The aqueous extract was purified by semi-preparative HPLC. Fractions containing *Ud*-PxB were combined, concentrated, re-dissolved in MeOH/potassium phosphate buffer pH 7.4 100 mM (20/80 v/v) and re-purified by semi-preparative HPLC. After controlling the purity of the PxB by analytical HPLC, the solution was concentrated and lyophilized in a SpeedVac vacuum concentrator.

2.7. Spectroscopic data

Ud-PleB. UV–Vis (HPLC trace, 100 mM aq. ammonium acetate buffer pH 7/ACN), λ_{max}, nm (relative ε) 216 (1.00), 314 (0.63). HR-ESI-MS: m/z_{found} = 807.34390 [M+H]$^+$; $m/z_{calculated}$ ($C_{41}H_{51}O_{13}N_4$) = 807.34471 (Δ = -0.814 ppm).

Ud-PxB. UV–Vis (HPLC trace, 100 mM aq. ammonium acetate buffer pH 7/ACN), λ_{max}, nm (relative ε) 216 (0.84), 246 (0.61), 314 (0.75), 426 (1.00). HR-ESI-MS: m/z_{found} = 803.31349 [M−H]$^-$; $m/z_{calculated}$ ($C_{41}H_{47}O_{13}N_4$) = 803.31451 (Δ = -1.021 ppm). ESI-MS/MS: m/z (%) = 805.11 (100, [M+H]$^+$); 787.28 (18, [M+H-H$_2$O]$^+$); 773.32 (3, [M+H-MeOH]$^+$); 759.14 (4, [M+H-H$_2$O-CO]$^+$), 490.24 (6.5, [M+H-ringA]$^+$). ^{1}H NMR (500 MHz, d_6-DMSO): 2.02 (s, H$_3$C7^1); 2.05 (s, H$_3$C13^1); 2.14 (s, H$_3$C17^1); 2.16 (s, H$_3$C2^1); 2.21 (m, H$_2$C12^2); 2.51 (m, H$_2$C12^1); 2.53 (m, H$_A$C3^1); 2.63 (m, H$_B$C3^1); 2.92 (s, HC2^1); 3.02 (m, HC5′); 3.27 (m, HC4′); 3.32 (m, H$_A$C3^2); 3.40 (m, H$_A$C6′); 3.60 (m, HC3′); 3.62 (m, H$_B$C6′); 3.62 (m, H$_B$C3^2); 3.65 (s, H$_3$C8^4); 3.80 (m, H$_2$C5); 3.86 (m, HC8^2); 4.03 (m, HC1′); 4.81 (m, HC10); 5.29 (m, H$_A$C18^2); 6.05 (s, HC15); 6.17 (m, H$_B$C18^2); 6.55 (dd, J = 18.2 / 12.1, HC18^1); 9.43 (s, HC20). ^{13}C NMR (500 MHz, d_6-DMSO, signal assignment from HSQC and HMBC spectra): 9.33 (2^1); 9.35 (17^1); 9.77 (13^1); 9.78 (7^1); 19.64 (12^1); 24.36 (3^1); 22.65 (5); 34.23 (12^2); 36.37 (10); 52.68 (8^4); 61.26 (6′); 66.40 (8^2); 68.98 (3^2); 70.69 (5′); 74.13 (2′); 74.56 (4′); 77.13 (3′); 99.87 (15); 103.30 (1′); 110.15 (7); 118.31 (18^2); 118.68 (12); 118.91 (3); 123.39 (18); 123.84 (13); 124.52 (14); 124.74 (8); 127.32 (18^1); 128.33 (1); 129.90 (16); 130.80 (11); 131.47 (2); 133.72 (6); 136.41 (4); 142.70 (17); 157.28 (9); 170.30 (8^3); 171.20 (19); 174.11 (12^3); 175.01 (20); 188.25 (8^1).

2.8. Ferric reducing antioxidant potential (FRAP) assay

The antioxidant potential of *Ud*-PxB, rutin, chlorogenic acid, quercetin, and caffeic acid was determined by a FRAP assay according to the

protocol of Benzie *et al* with minor alterations (Benzie & Strain, 1996). Briefly, Trolox and the different compounds were mixed with the freshly prepared FRAP reagent (10 volumes 300 mM acetate buffer pH 3.5, 1 vol 10 mM TPTZ in 40 mM HCl, and 1 vol 20 mM iron(III)chloride) and incubated for 5 min at 37 °C. The reduction of Fe^{3+}-$(TPTZ)_2$ by possible antioxidants generates the complex Fe^{2+}-$(TPTZ)_2$, whose absorbance can be measured at 620 nm. Different concentrations of Trolox were measured to fit a calibration curve, which was used to calculate the antioxidant potential of the compounds expressed as Trolox equivalents.

2.9. Cell culture

Human embryonic kidney derived HEK 293 cells (HEK) were obtained from the *Deutsche Sammlung of Mikroorganismen und Zellkulturen* (DSMZ; Braunschweig, Germany), and the macrophage cell line J774A.1 was a kind gift from Prof. Veit Hornung from the Gene Center Munich. HEK cells were cultured in DMEM supplemented with 10% FCS, and J774A.1 cells were cultivated in DMEM supplemented with 10% FCS, 1% penicillin/streptomycin, and 1% sodium pyruvate. Both cell lines were cultured at 37 °C under 5% CO_2 atmosphere.

2.10. Intracellular reactive oxygen species

The detection of intracellular ROS in HEK cells was performed as published recently (Karg, Wang, et al., 2019). Briefly, 2×10^4 cells/well were seeded in 96 well plates and stimulated with *Ud*-PxB, chlorogenic acid, caffeic acid, quercetin, and rutin for 24 h, before the medium was removed and the cells were incubated with H_2DCF-DA (10 μM) for 30 min. Cells were washed with PBS + Ca^{2+} + Mg^{2+} and incubated for 30 min with hydrogen peroxide (1 mM). Fluorescence intensity of the highly fluorescent 2,7-dichlorofluorescein was measured with a Tecan SpectraFluor plus microplate reader at the excitation wavelength of 485 nm and emission wavelength of 530 nm. Data were normalized to the H_2O_2 treated DMSO control.

2.11. Cyclooxygenase-1 and Cyclooxygease-2 (COX-1/-2) inhibition assay

The COX inhibition assay was performed using Cayman Chemicals COX Fluorescent Inhibitor Screening kit. This assay is based on the conversion of arachidonic acid to a hydroperoxy endoperoxide (PGG2) by the cyclooxygenase component of the bifunctional enzymes COX-1 and COX-2 and the following reduction to prostaglandin H2 by the peroxidase component. The reaction of PGG2 and ADHP results in the fluorescent compound resofurin, whose fluorescence can be detected with an extinction wavelength of 535 nm and an emission wavelength of 595 nm. Briefly, ovine COX-1 and human recombinant COX-2 enzymes were incubated for 5 min with heme and different concentrations of *Ud*-PxB, caffeic acid, and chlorogenic acid, or buffer as a positive control with 100% initial activity. Wells without enzyme were used as negative control. The reaction was initiated by adding arachidonic acid. After subtraction of the negative control, percentages of initial activities were normalized towards the positive control with 100% initial activity and IC_{50} values was calculated.

2.12. Cell treatment for western blot analysis

J774A.1 cells were mechanically scraped, seeded in 12 well plates (2×10^5 cells/well) and allowed to attach for 24 h. Cells were stimulated with LPS (0.5 μg/mL) and compounds for 4 h.

2.13. Western blot analysis

After 4 h of incubation time, cells were washed with ice cold PBS and 100 uL of lysis buffer (50 mM Tris/HCl, 150 mM NaCl, 1% Nonidet NP-40, 0.25% Sodium deoxycholate, 0.1% SDS) were added. Cells were

scraped and cell lysates were frozen at −80 °C until further use. Cell lysates were thawed at 4 °C and centrifuged at 14000 rpm for 10 min at 4 °C, before protein concentrations were determined by Bradford assay using bovine serum albumin as standard. Proteins were denatured at 95 °C for 5 min in SDS sample buffer and equal amounts of protein were separated by sodium dodecyl sulfate polyacrylamide gel electrophoresis (SDS-PAGE) in electrophoresis buffer (100 V, 21 min then 200 V, 43 min) using discontinuous polyacrylamide gels (4–20%). Western blotting was performed by transferring protein to polyvinylidene difluoride (PVDF) membranes at 100 V for 90 min at 4 °C. For COX-2 protein detection, membranes were blocked with 5% non-flat dry milk powder in PBS for 2 h before the primary antibody (1:1000) was incubated overnight at 4 °C. Membranes were washed three times with PBS-T for 5 min, incubated with secondary antibody (anti-mouse IgG-horseradish peroxidase conjugate) (1:1000) for 2 h, before performing another three washing steps and incubating membranes with ECL solution. Chemiluminescence was detected using a ChemiDoc™ Touch Imaging System (Bio-Rad, Munich, Germany). Protein bands were analyzed by comparison with the Page Ruler™ Plus Prestained Protein Ladder and protein levels were analyzed using Image LabTM software (Bio-Rad, Munich, Germany).

2.14. Chemical and digestive stability

The chemical stability of *Ud*-PxB was tested by incubation of *Ud*-PxB (20 μM) in phosphate buffer pH = 2.5 100 mM for 24 h at room temperature in the dark. The stability of *Ud*-PxB was analyzed by analytical HPLC and confirmed by co-elution with Ud-PxB incubated in phosphate buffer pH = 7.4 100 mM.

The stability of *Ud*-PxB in simulated gastric and intestinal digestion fluids was performed according to the protocol of Minekus *et al* with modifications (Minekus et al., 2014). The buffer for the gastric digestion fluid (SGF) was prepared as follows: 6.9 mM KCl, 0.9 mM KH_2PO_4, 25 mM $NaHCO_3$, 47.2 mM NaCl, 0.1 mM $MgCl_2(H_2O)_6$, 0.5 mM $(NH_4)_2CO_3$, 0.075 mM $CaCl_2(H_2O)_2$. HCl was added to the buffer to reach an acidic pH of 3 and porcine pepsin was added to a final concentration of 2000 U/mg. The same volume of SGF buffer was added as negative control without enzyme. The buffer for the intestinal digestion fluid (SIF) was prepared as follows: 6.8 mM KCl, 0.8 mM KH_2PO_4, 85 mM $NaHCO_3$, 38.4 mM NaCl, 0.33 mM $MgCl_2(H_2O)_6$, 0.3 mM $CaCl_2(H_2O)_2$. HCl was added to the buffer to reach a pH of 7; pancreatin was added to a final concentration of 0.25 mg/mL and bile salts to a final concentration of 0.75 mg/mL. Instead of enzyme, the same volume of SIF buffer was added as negative control. Nettle tea (Sidroga) was prepared by brewing two tea bags with 200 mL of water for 15 min. PxB was diluted in SGF or SIF with or without enzyme to a final concentration of 10 μM and tea was diluted 1:1 in SGF or SIF with or without enzyme. All samples were incubated at 37 °C with shaking in a Thermoshake THL 500/THO500 at 100 rpm for 2 h. An aliquot of 100 μL of each sample was mixed with 20 μL of ACN, centrifuged for 5 min at 13000 rpm and analyzed by analytical HPLC. Chromatograms of positive and negative controls were compared and peak areas of *Ud*-PxB were analyzed with OpenLab 2.3.

2.15. Metabolic stability in liver microsomes

The metabolic stability of *Ud*-PxB was determined by incubation with liver microsomes according to the protocol of Ma *et al* with small modifications (Ma et al., 2014). Briefly, 2 μL of test reagent (BR or *Ud*-PxB; 10 mM in DMSO), 5 μL of liver microsomes, 5 μL of $MgCl_2$ (40 mM), and 5 μL of alamethicin (1 mg/mL) were mixed with 168 μL of phosphate buffer pH = 7.4 (100 mM) and incubated for 5 min in the water bath at 37 °C. The same formulation with buffer instead of liver microsomes served as a negative control. 5 μL of UDPGA (200 mM) and 10 μL of NADPH (freshly prepared, 20 mM) were added to initiate the reaction and the reagents were incubated at 37 °C in the dark under gentle agitation. The reaction was stopped after either 75 min or 24 h by adding

200 μL of ACN. Samples were vortexed, centrifuged at 3000 rpm for 5 min at room temperature and an aliquot of 40 μL was mixed with 60 μL of buffer and analyzed by analytical HPLC, each. To verify the evolved glucuronide derivatives of BR, the peaks were collected from an analytical HPLC run and analyzed by ESI-MS.

2.16. Statistical analysis

Results represent the mean of at least three independent experiments (means ± SEM) performed in at least three replicates, unless stated otherwise. Statistical significance was carried out by one-way analysis of variance with post hoc analysis using Dunnett's multiple comparison test or unpaired *t*-test with Welch's correction; all statistical analyses were processed with GraphPad Prism 7.05.

3. Results and discussion

3.1. Characterization of PxB in nettle

Since nettle is primarily consumed as tea which is made from dried leaves, the occurrence of PBs in nettle was studied not only in an extract of a green leaf of freshly collected *Urtica dioica* L., but also in a freshly brewed tea, prepared from one tea bag (from commercial sources) with 200 mL of boiling water. HPLC analysis (Fig. 1, Figure S2, Supplementary Information) revealed two PBs, which were identified due to their characteristic UV–Vis spectra: one signal could be assigned to a PleB due to its maxima at 216 and 314 nm, and one to a PxB due to the additional maximum at 426 nm (Figure S3, Supplementary Information) (Kräutler, 2016). This provides on the one hand first evidence for phyllobilins in dried leaves representing a processed plant product and on the other hand demonstrates the occurrence of *Ud*-PBs in green leaves without any visible sign of chlorophyll catabolism, hinting at a constant chlorophyll turnover, which has recently been shown for *Arabidopsis thaliana*

(Süssenbacher et al., 2019).

In commercially available tea, which consists of processed dried leaves, the PxB seems to withstand the processing procedure of tea production, which usually includes drying leaves in a multistep process and storing them for a long time. The oxidation of PleBs to PxBs is a process for which the underlying mechanisms have not been fully elucidated yet. It is assumed, however, that a possible enzyme-derived 'oxidative activity' seems to be responsible for the transformation including a hydroxylated precursor of the PxB (Vergeiner et al., 2015). Vergeiner *et al* also tested different conditions to elucidate this oxidative activity and demonstrated that the presence of oxygen is critical for the oxidation of PleB. The drying procedure of leaves is usually performed under air, which could be a reason for the high amounts of PxB found in nettle tea.

For structure elucidation, 200 g of fresh, senescent nettle leaves were extracted with methanol. By HR-MS, the formula of the PxB was deduced as $C_{41}H_{48}O_{13}N_4$, and the molecular formula of the PleB as $C_{41}H_{50}O_{13}N_4$, which confirmed the PleB to be the precursor of the PxB. Therefore, structure elucidation focused on the *Ud*-PxB, for which a PxB with the same molecular formula was previously detected in *Echinacea purpurea* and plum species but a detailed structural analysis by NMR spectroscopy is still pending (Erhart et al., 2016; Karg, Wang, et al., 2019; Roca, Ríos, Chahuaris, & Pérez-Gálvez, 2017). The tentative structure of PxB was firstly confirmed by ESI-MS/MS: Collision induced dissociation (CID) of the *Ud*-PxB $[M+H]^+$ at $m/z = 805$ showed diagnostic fragments at $m/z = 773$ corresponding to the loss of methanol. Fragments at $m/z = 787$ corresponding to the loss of water (-18 Da) and $m/z = 759$ corresponding to the loss of water and carbon monoxide (-28 Da) indicated the PxB to carry a free propionic acid side chain. Further, the loss of Ring A and therefore the presence of a glucosyl side chain was validated by the ion fragment at $m/z = 490$ (-315 Da) (Fig. 2D, Figure S4, Supplementary Information).

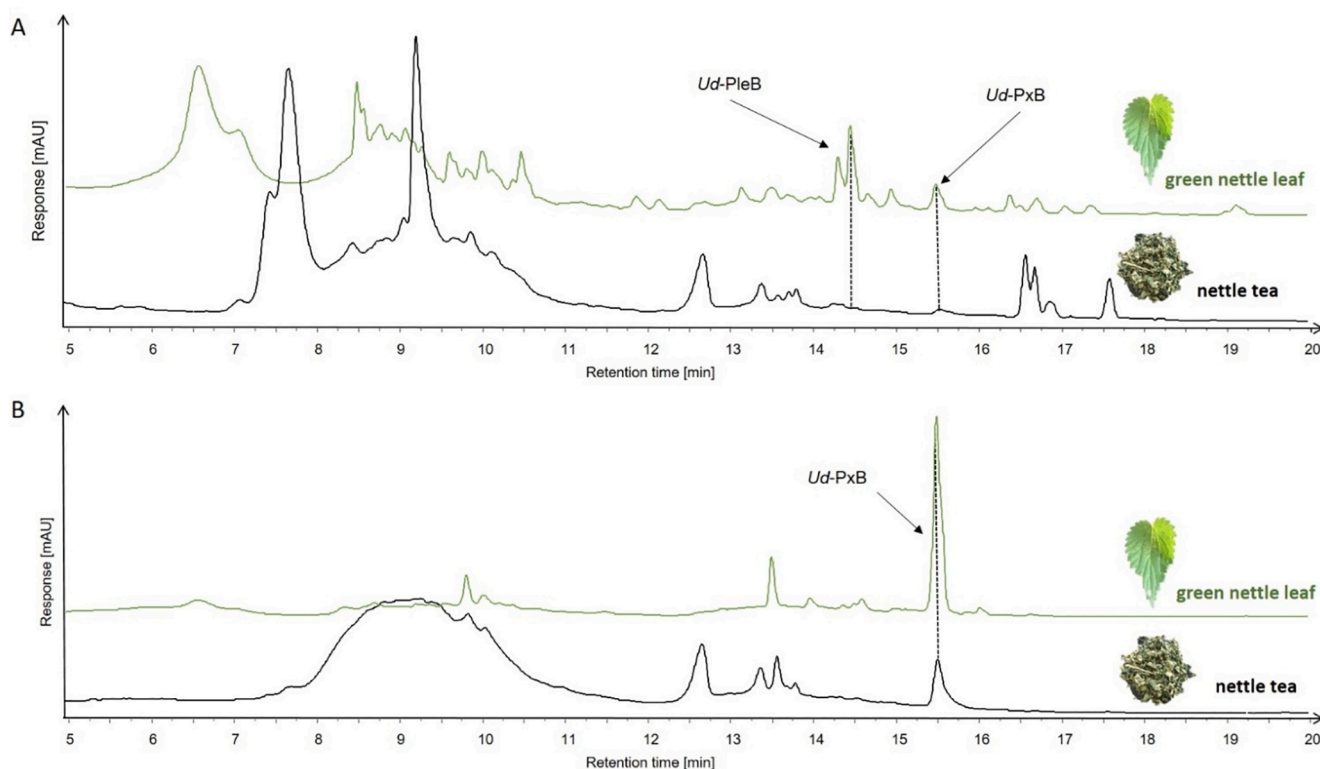Additionally, the structure of the *Ud*-PxB was verified by recording

Fig. 1. HPLC analysis of a freshly prepared nettle tea (black) and a methanolic extract of a green *Urtica dioica* L. leaf (green). Detection at 320 nm (A) and 420 nm (B). (For interpretation of the references to color in this figure legend, the reader is referred to the web version of this article.)
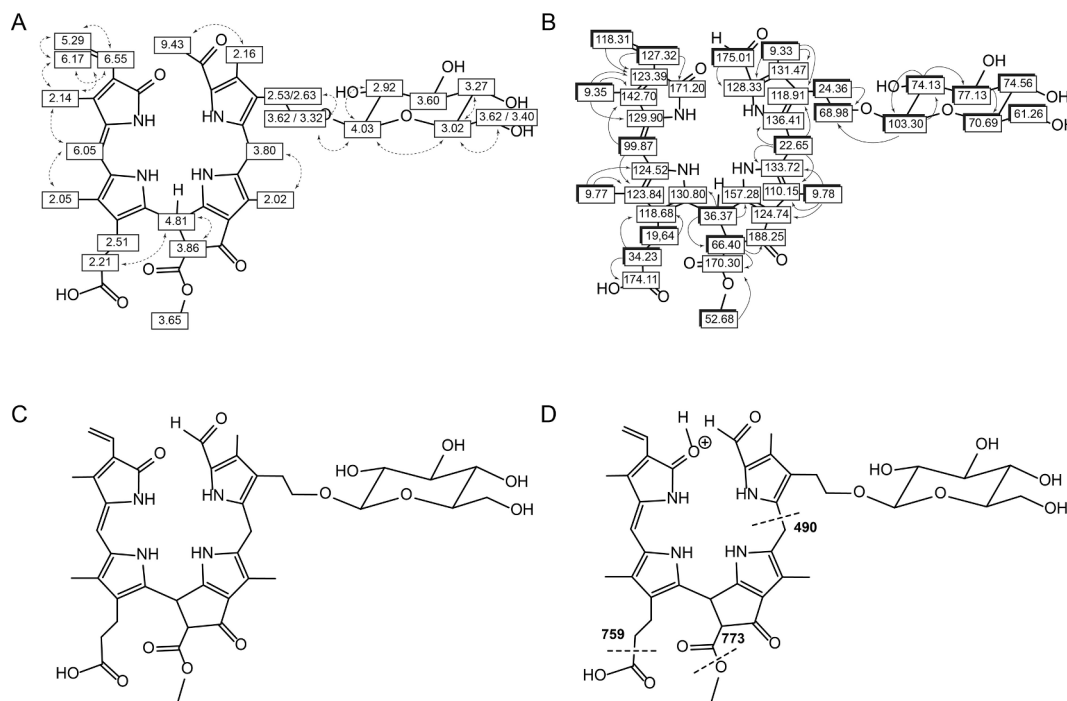
Fig. 2. Graphical analysis of *Ud*-PxB by 1D and 2D NMR spectra. (A) ^{1}H signal assignments from ^{1}H, ^{1}H-ROESY correlations. (B) ^{13}C signal assignments based on ^{1}H,^{13}C-HSQC (represented by shaded boxes) and ^{1}H,^{13}C-HMBC (indicated by arrows and open boxes) spectra. (C) Structure of *Ud*-PxB. (D) MS fragmentation patterns typical for PBs; dashed lines represent formal fragmentation modes of [M+H]$^+$ (Müller, Vergeiner, & Kräutler, 2014); the full MS/MS spectrum can be found in the Supplementary Information (Figure S4).

^{1}H NMR and 2D ^{1}H,^{1}H homonuclear (ROESY) and ^{1}H,^{13}C heteronuclear (HSQC and HMBC) (Fig. 2 A, B) and by comparing the spectra with the spectra of *Nr*-PleB-2, presumably carrying the same modification pattern as the *Ud*-PxB (Figure S5, Table S1, Supplementary Information) (Berghold, Eichmüller, Hörtensteiner, & Kräutler, 2004).

A singlet in the low field was assigned to the α-formyl group at Ring A and the detected characteristic signals for a peripheral vinyl group in the intermediate field confirmed the *Ud*-PxB to carry a vinyl moiety at Ring D. Another singlet at 3.65 ppm correlating with a carbon at 52.68 ppm was observed and could be assigned to a methylester function attached at C8^2 (for numbered structure of *Ud*-PxB see Figure S6, Supplementary Information). Further, the NMR analysis revealed the structure to carry a free propionic acid side chain at Ring C. In contrast to the spectra of *Nr*-PleB-2, which show an AB spin system at HC15 indicating a saturated carbon atom, the NMR analysis of *Ud*-PxB achieved a singlet at HC15 (6.05 ppm) and no signal for HC16 in the ^{1}H or HSQC spectra. Thus, the typical structural pattern of a PxB, featuring a double bond between C15 and C16 could be assigned to the *Ud*-PxB. Four singlets in the high field could be assigned to the four methyl groups in β-pyrrole position. Seven additional signals in the intermediate field suggested the C3^2 to be attached by a O-glucosyl side chain. By comparison with the signals of *Nr*-PleB-2 the peripheral sugar moiety could be identified as a β-gluco-pyranosyl. On the basis of NMR and MS analysis, the chemical constitution of the *Ud*-PxB was characterized as a 3^2-O-glucopyranosyl-1-formyl-19-oxo-16,19-dihydrophyllobilene (Fig. 2C).

3.2. Quantification of Ud-PxB in nettle tea

Not only the occurrence of a PxB in nettle tea itself is striking; besides, it becomes evident that PBs are abundant constituents when analyzing the PxB content in different brands of nettle tea. Teas of nine different brands, obtained from the supermarket, a drug store, the pharmacy, or a supplier of herbal material, were prepared as described in the experimental section and analyzed by analytical HPLC. The amount of PxB in one cup of tea (200 mL) was calculated as described in

the experimental section. The calculation revealed the PxB content to vary greatly. We found PxB contents to range between 11.1 and 100.3 μg per cup of tea and 5.6 to 35.8 μg per g of tea (Fig. 3A, B).

Drying of plants is the most common method to preserve different parts of the plant after harvesting. It prevents the growth of microorganisms due to a decreased water activity and facilitates further handling and storage processes (Hamrouni-Sellami et al., 2013). Several studies showed, however, that the drying procedure might have an influence on the amount and composition of phytochemical compounds (Fernandes, Casal, Pereira, Saraiva, & Ramalhosa, 2018; Hamrouni-Sellami et al., 2013; Lin, Sung, & Chen, 2011). Therefore, different drying procedures including, for instance, either a light protected and heated area or a sun lighted place might cause differences in the amount of PxB in nettle extracts.

In order to find possible explanations for the varying content of PxB in different nettle extracts, analytical HPLC runs of the different teas and extracts of fresh leaves were analyzed for rutin, an already known compound of nettle extracts. Rutin (quercetin-3-rutinoside) is a flavonoid glycoside and known to possess antioxidative, anti-inflammatory, and antimicrobial activity (Sharma, Ali, Ali, Sahni, & Baboota, 2013). It is one of the major bioactive compounds in extracts of nettle leaves. The presence of rutin was tested by comparing the chromatograms and UV–Vis spectra with a rutin standard and the amount of rutin in tea was calculated with a rutin standard (Figure S7, Supplementary Information). The analysis of fresh nettle leaves and of tea from nine different brands revealed rutin not to occur in fresh leaves in detectable amounts (Figure S8, Supplementary Information). Furthermore, the phytochemical could only be detected in six brands of the tested teas and in a varying range from 0.08 to 2.27 mg per cup of nettle tea (200 mL) (Table S2, Supplementary Information). Several studies showed that the content of rutin varied largely among plants from different origin. Dried, methanolic extracts of nettle leaves from different locations in Serbia were found to contain amounts between 1.8 μg and 4.3 mg of rutin per g of extract (Orčić et al., 2014). A similar study revealed rutin to occur in varying amounts between extracts of leaves from different geographical
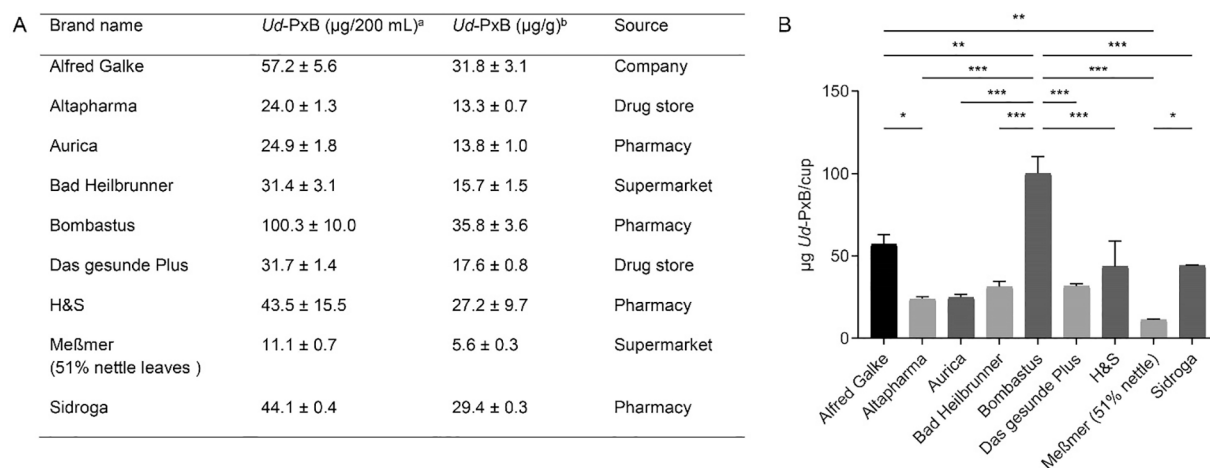
Fig. 3. Quantitative determination of *Ud*-PxB by HPLC analysis in nettle tea from different brands. (A) Data are represented as mean ± SEM of three independent experiments ([a]Analysis of one cup of tea (200 mL) prepared as described in the experimental section. [b]Calculation according to the weight of the respective tea bag). (B) Quantification of *Ud*-PxB in μg per cup of nettle tea represented as bar chart (one-way analysis of variance with post hoc Dunnett's multiple comparison test, ns P > 0.12, *P < 0.05, **P < 0.01, ***P < 0.001).

origin, collected from the Mediterranean area, Aegean area, the Black Sea, and Marmara region. In addition, caffeic acid and chlorogenic acid, further bioactive compounds in nettle extracts, were reported only to be present in 5 out of 19 tested nettle leaf extracts (Otles & Yalcin, 2012).

Thus, the appearance and contents of already known bioactive compounds in nettle might depend on the geographical origin of the plant and the type of the drying process. Furthermore, the solvent used for extraction strongly influences the composition of an extract; in this study, we focus on aqueous extracts (teas), since these are of relevance in a food context. The PxB was present in all tested leaf material, extracted with hot water. This underlines the importance of further studying the possible physiological activities of this overlooked component of nettle tea especially in comparison to already elucidated bioactive reagents.

3.3. Antioxidative and anti-inflammatory effects of Ud-PxB

Previous studies showed that PxBs from *Echinacea purpurea* and savoy cabbage possess antioxidative activities that were similar or even increased, as compared with those of the known antioxidants Trolox or BR (Karg, Schilling, et al., 2019; Karg, Wang, et al., 2019). The quantification of the PBs in nettle tea revealed that the PleB occurred as a

minor fraction in comparison to the PxB. For that reason, only the PxB was further characterized for its physiological activities together with chlorogenic acid (CGA), caffeic acid (CA), rutin, and quercetin, which are known to be among the main bioactive phytochemicals reported in *Urtica dioica* L. leaves (Joshi et al., 2014). Firstly, the antioxidative potential of the PxB from nettle tea was investigated using an *in vitro* FRAP assay (Benzie & Strain, 1996). As shown in Fig. 4A, *Ud*-PxB exhibited a similar antioxidant activity to CGA, CA, and rutin, and a significantly higher activity than Trolox. Further, *Ud*-PxB was shown to be able to scavenge reactive oxygen species in hydrogen peroxide stimulated HEK cells in low concentrations as 20 μM and in a similar range as even higher concentrations of CA, CGA, and rutin (Fig. 4B), without altering the cell viability (Figure S9, Supplementary Information). These data extend the known antioxidative properties of one of the PxBs isolated from *Echinacea purpurea* leaves (*Ep*-PxB-5), which shares the identical structure with *Ud*-PxB (Karg, Wang, et al., 2019), and are comparable with data found in the literature (Apak et al., 2007).

Tea infusions of nettle leaves are commonly used to treat inflammatory diseases such as rheumatic disorders and arthritis and inflammatory symptoms of the lower urinary tract (EMA/HMPC/508013/2007, 2010). After establishing that *Ud*-PxB shows an antioxidative
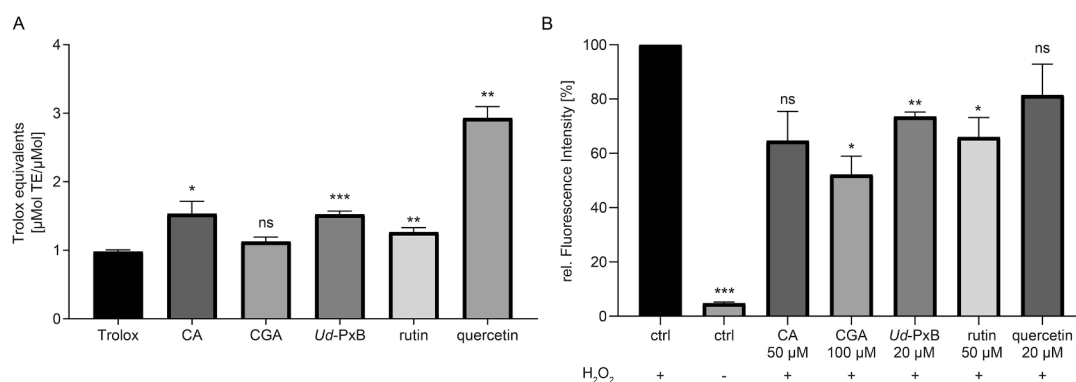

Fig. 4. Antioxidative activity of caffeic acid (CA), chlorogenic acid (CGA), *Ud*-PxB, rutin, and quercetin. (A) *In vitro* antioxidant potential measured by FRAP assay and expressed as Trolox equivalents (μMol TE/μMol). The values are means ± SEM of seven independent experiments for CA, CGA, *Ud*-PxB, and rutin, and of three independent experiments for quercetin (unpaired *t*-test with Welch's correction, ns P > 0.12, *P < 0.05, **P < 0.01, ***P < 0.001). (B) Intracellular antioxidative activity assessed by the detection of intracellular ROS. HEK cells were treated with compounds at indicated concentrations for 24 h before incubating with 1 mM H_2O_2. The ROS scavenging activity was determined by measuring the prevented conversion of the intracellular fluorescein derivative H_2DCF into highly fluorescent DCF. The bar graphs indicate means ± SEM of three independent experiments (unpaired *t*-test with Welch's correction, ns P > 0.12, *P < 0.05, **P < 0.01, ***P < 0.001).

activity to a similar extent as the predominant bioactive components of *Urtica dioica* L. leaves, the question arises whether PxB can also contribute to the anti-inflammatory effects of nettle. Therefore, a fluorometric *in vitro* COX inhibition assay was performed, which measures the effect of substances on the activity of the bifunctional enzymes COX-1 and COX-2. CGA and CA were used as anti-inflammatory positive controls from nettle leaf extracts. The results show that *Ud*-PxB inhibits the initial activity of COX-1 with an IC_{50} of 42.2 μM and of COX-2 with an even lower IC_{50} of 7.5 μM. By comparing these results with the COX-2 inhibitory potencies of CGA and CA, it becomes evident that PxB displays IC_{50} values in a similar low micromolar range. PxB is also capable of inhibiting COX-1 at micromolar concentrations, although being less potent than the positive controls CGA and CA (Fig. 5A). Further, we assessed the effect on protein expression levels of COX-2 in the macrophage cell line J774A.1 as was previously shown for quercetin (Raso, Meli, Di Carlo, Pacilio, & Di Carlo, 2001). According to this protocol, cells were stimulated with LPS to induce COX-2 expression. COX-2 protein levels were analyzed by western blotting after co-stimulation of cells with LPS and different concentrations of *Ud*-PxB, CGA, CA, and quercetin. *Ud*-PxB was found to significantly inhibit COX-2 expression levels at a concentration of 50 μM in a similar range to quercetin. CGA showed only a slight effect and CA could not inhibit COX-2 expression under these conditions (Fig. 5B, C). To underline these results, we measured prostaglandin E2 (PGE2) concentrations using an ELISA assay, which revealed lower PGE2 levels for all four tested nettle phytochemicals and confirmed the anti-inflammatory effect of *Ud*-PxB (Figure S10, Supplementary Information).

3.4. Chemical and digestive stability of Ud-PxB

Having established that *Ud*-PxB shows antioxidative activity as well as inhibitory effects on pro-inflammatory enzymes, questions about the bioavailability of the compound arise, as tea is part of our nutrition. PxBs from *Echinacea purpurea* have been already shown to be taken up by human embryonic kidney cells and to be stable in cell growth

medium supplemented with bovine serum for at least 5 h (Karg, Wang, et al., 2019). This gives the first hint of the PxB being stable towards enzymatic degradation occurring in sera. Roca could also demonstrate that PleBs isolated from pepper fruits are internalized by human intestinal Caco-2 cells and are stable in experimentally prepared gastric and intestinal digestion fluids (Roca, 2012). To elucidate the stability of the PxB isolated from nettle leaves, the phyllobilin was tested for its chemical stability in fluids representing the acidic milieu of the stomach as well as the digestive fluids in the gastrointestinal tract (Minekus et al., 2014).

Incubation of *Ud*-PxB in phosphate buffer pH = 2.5 for a long period of at least 24 h was performed to demonstrate that the PxB is stable in acidic solutions mimicking the conditions of the gastric juice. *Ud*-PxB incubated in phosphate buffer pH = 7.4 served as control. A co-elution experiment by analytical HPLC analysis of *Ud*-PxB in buffer pH = 2.5, in buffer pH = 7.4, and a 1:1 mixture confirmed the chemical stability of the PxB in an acidic milieu (Figure S11, Supplementary Information).

Furthermore, the stability of the PxB was tested during human digestion by imitating physiological conditions of the gastric and intestinal part of the digestive system due to digestive enzymes, pH milieu, digestion time, and specific concentrations of salts. A gastric digestion fluid including pepsin and acidic conditions (pH 3) and an intestinal digestion fluid with pancreatin and bile salts (pH 7) was prepared and freshly brewed nettle tea or isolated PxB (20 μM) were incubated with the simulated fluids for 2 h under shaking. PxB and tea incubated with the digestive fluids without enzymes served as negative control. HPLC analysis revealed no differences of the *Ud*-PxB peak regarding retention time and UV–Vis characteristics between the tea and PxB, incubated with and without enzyme, respectively. Additionally, analysis of the peak areas of PxB showed no significant decrease compared to the negative control (Fig. 6). This indicates the stability of *Ud*-PxB during a simulated gastric and intestinal digestion in a pure form as well as in nettle tea.
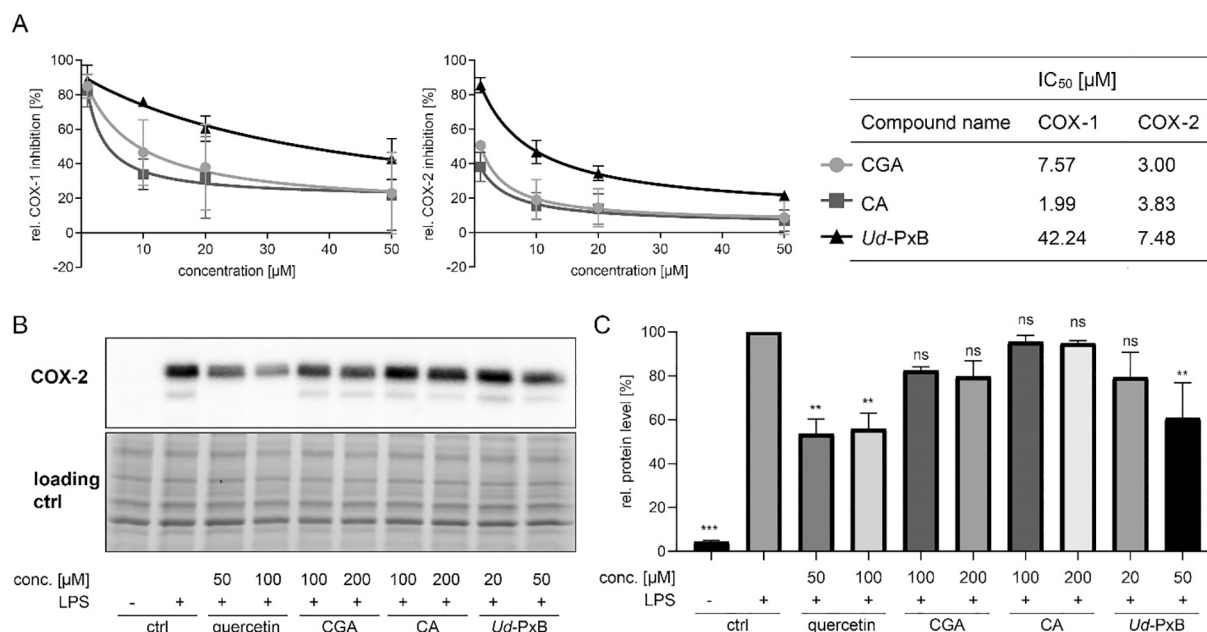

	IC$_{50}$ [μM]	
Compound name	COX-1	COX-2
CGA	7.57	3.00
CA	1.99	3.83
Ud-PxB	42.24	7.48

Fig. 5. Anti-inflammatory activity of *Ud*-PxB and nettle phytochemicals. (A) *In vitro* inhibition of COX-1 and COX-2 by chlorogenic acid (CGA), caffeic acid (CA), and *Ud*-PxB. Data are presented as percentages of initial activities normalized to the positive control with 100% initial activity. IC$_{50}$ values are calculated from three independent experiments. (B) COX-2 expression of LPS and compound stimulated J774A.1 cells. J774A.1 cells were treated with LPS (0.5 μg/mL) and indicated concentrations of compounds for 4 h before cells were lysed and protein levels were analyzed by western blotting. The experiment was performed in triplicate and a representative example is shown. (C) Quantitative evaluation of COX-2 protein levels, normalized to whole lane protein and represented relative to LPS stimulated control (one-way analysis of variance with post hoc Dunnett's multiple comparison test, ns P > 0.12, *P < 0.05, **P < 0.01, ***P < 0.001).
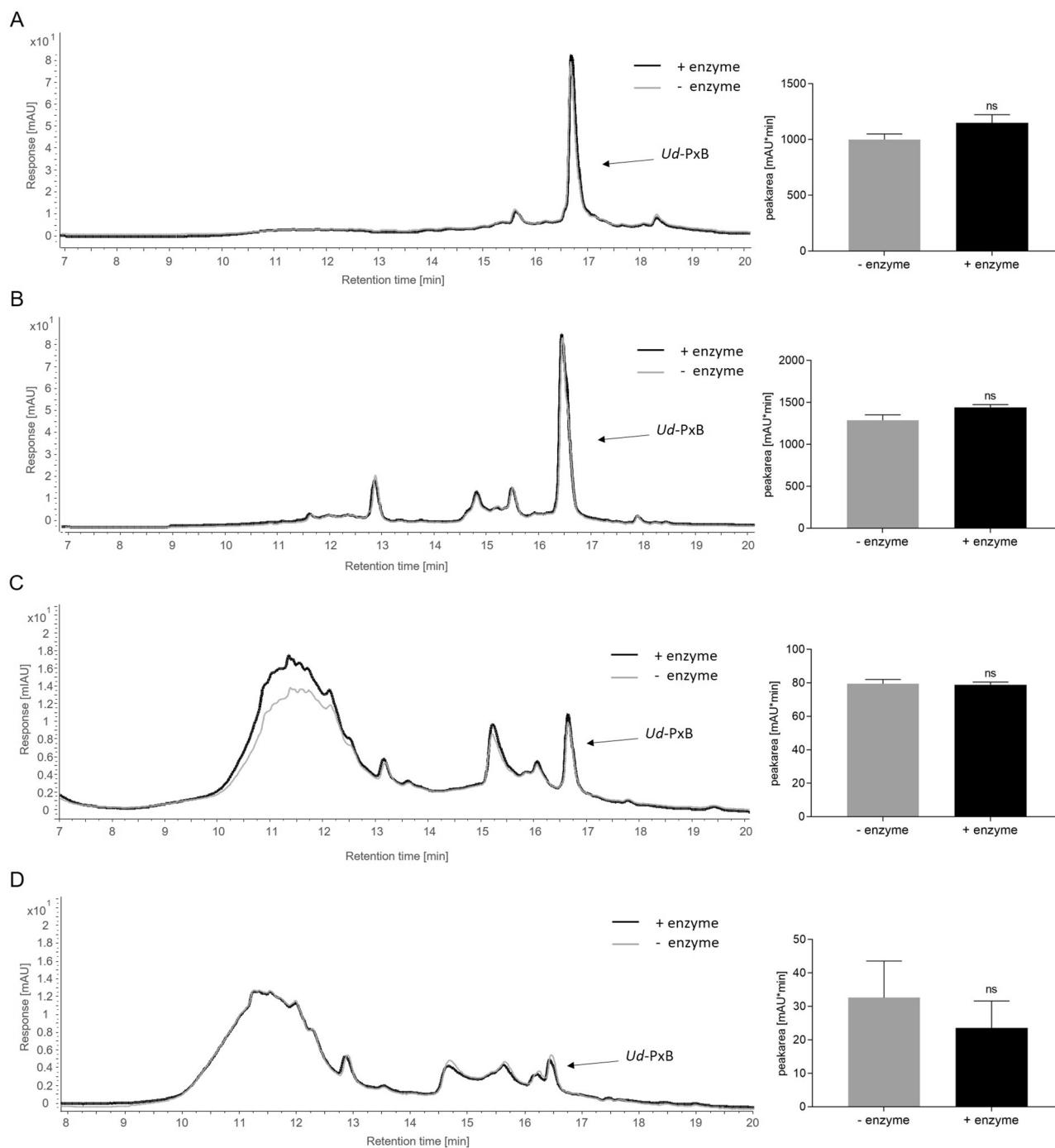
Fig. 6. *In vitro* gastric (A, C) and intestinal (B, D) digestion of isolated *Ud*-PxB (A, B) and nettle tea (C, D). *Ud*-PxB and nettle tea were incubated for 2 h in simulated gastric digestion fluid (A, C) and in simulated intestinal digestion fluid (B, D). Left) HPLC analysis of *Ud*-PxB and nettle tea incubated with digestive fluids with and without enzymes. Detection at 320 nm (A, B) and 420 nm (C, D). The experiment was performed in triplicates and one representative chromatogram is shown. Right) Peak areas of *Ud*-PxB were analyzed in chromatograms of isolated *Ud*-PxB and nettle tea with and without enzymes (unpaired *t*-test with Welch's correction, ns P > 0.12).

3.5. Metabolic stability of Ud-PxB

Beside chlorophyll, bacteriochlorophyll, and vitamin B12, heme is another important and widespread tetrapyrrole in nature (Battersby, 2001). The products of heme catabolism are called bile pigments and include BV and BR. Phyllobilins not only share the tetrapyrrolic structural pattern with bile pigments; in fact, both are the products of a detoxification mechanism and were therefore long thought to be 'mere' waste products. PBs as well as bilirubin (BR) and biliverdin (BV),

however, were shown to have physiological activities (Takemoto, Chang, Chen, & Hinton, 2019).

In contrast to the PBs, bile pigments occur naturally in both, humans and in plants, and BR can cause e.g. damages of the central nervous system at high concentrations, especially in neonates (Takemoto et al., 2019). Therefore, the metabolism of bilirubin has been widely studied. It takes mainly place in the endoplasmic reticulum of hepatocytes, where the enzyme UDP-glucuronosyltransferases 1A1 (UGT1A1) is located. In newborns, the metabolism of BR results mainly in monoglucuronides,

which are created by conjugation of glucuronosyl substituents to one of the propionic acid side chains of BR. In adults, >80% of BR is metabolized to diglucuronides (Ma et al., 2014). By incubating the *Ud*-PxB and BR with human liver microsomes, we tested whether the PxB is also glucuronidated like BR or metabolically resistant against hepatic enzymes. According to the protocol of Ma *et al*, a HPLC method was employed in which BR and its metabolites could simultaneously be detected by UV–Vis (Ma et al., 2014). HPLC analysis of BR showed that in contrast to the negative control without microsomes, new peaks appeared with higher polarity in the formulation incubated with liver microsomes after 75 min and 24 h (Figure S12, Supplementary Information). Those were isolated and verified by ESI-MS giving pseudo-molecular ions of the two bilirubin-monoglucuronides at 761 $[M+H]^+$ and the diglucuronide at 936 $[M+H]^+$ (Figure S13, Supplementary Information). The chromatograms of the PxB solutions showed no differences between the formulation with or without microsomes neither after 75 min nor after 24 h of incubation, indicating that *Ud*-PxB is resistant towards metabolism by the hepatic enzyme UGT1A1.

4. Conclusion

Our study provides first evidence of the occurrence of PBs in dried leaves and in tea, indicating them to be stable during processing procedures of the plant, and making those natural products an even more substantial part of a regular human diet. We establish *Ud*-PxB as important component in nettle tea, as well as in fresh nettle leaves, both of which are widely used as beverage and food. More importantly, we demonstrate potent antioxidant and anti-inflammatory effects for *Ud*-PxB, comparable to the activities of established bioactive components of nettle, such as CA, CGA, and rutin. Using *in vitro* digestive studies, we provide first insights into the bioaccessibility of PxBs, which turned out to be stable under digestive conditions of the human gastric and intestinal system. Our results provide the basis for further studies that involve the screening of other plant-based foods for bioactive PxBs and investigate the bioavailability of these overlooked components of human nutrition in more depth.

CRediT authorship contribution statement

Cornelia A. Karg: Formal analysis, Investigation, Visualization, Writing - original draft. **Christian Doppler:** Methodology, Writing - review & editing. **Charlotte Schilling:** Investigation, Writing - review & editing. **Franziska Jakobs:** Investigation, Writing - review & editing. **Marlene C.S. Dal Colle:** Investigation, Writing - review & editing. **Nadine Frey:** Investigation, Writing - review & editing. **David Bernhard:** Investigation, Writing - review & editing. **Angelika M. Vollmar:** Conceptualization, Supervision, Writing - review & editing. **Simone Moser:** Conceptualization, Project administration, Supervision, Writing - review & editing.

Declaration of Competing Interest

The authors declare that they have no known competing financial interests or personal relationships that could have appeared to influence the work reported in this paper.

Acknowledgements

Appendix A. Supplementary data

Supplementary data to this article can be found online at https://doi.org/10.1016/j.foodchem.2021.129906.

References

Apak, R., Güçlü, K., Demirata, B., Ozyürek, M., Celik, S. E., Bektaşoğlu, B., … Ozyurt, D. (2007). Comparative evaluation of various total antioxidant capacity assays applied to phenolic compounds with the CUPRAC assay. *Molecules, 12*, 1496–1547. https://doi.org/10.3390/12071496.

Barry, C. S. (2009). The stay-green revolution: recent progress in deciphering the mechanisms of chlorophyll degradation in higher plants. *Plant Science, 176*(3), 325–333. https://doi.org/10.1016/j.plantsci.2008.12.013.

Battersby, A. R. (2001). *Tetrapyrroles: The pigments of life. Natural Product Reports, 17*, 507–526. https://doi.org/10.1039/B002635M.

Benzie, I. F. F., & Strain, J. J. (1996). The ferric reducing ability of plasma (FRAP) as a measure of "antioxidant power": the FRAP assay. *Analytical Biochemistry, 239*(1), 70–76. https://doi.org/10.1006/abio.1996.0292.

Berghold, J., Breuker, K., Oberhuber, M., Hörtensteiner, S., & Kräutler, B. (2002). Chlorophyll breakdown in spinach: on the structure of five nonfluorescent chlorophyll catabolites. *Photosynthesis Research, 74*(2), 109–119. https://doi.org/10.1023/a:1020991023248.

Berghold, J., Eichmüller, C., Hörtensteiner, S., & Kräutler, B. (2004). Chlorophyll breakdown in tobacco: On the structure of two nonfluorescent chlorophyll catabolites. *Chemistry & Biodiversity, 1*(4), 657–668. https://doi.org/10.1002/cbdv.200490057.

EMA/HMPC/508013/2007. (2010). Assessment report on Utrica dioica L., Urtica urens L., folium.

Erhart, T., Mittelberger, C., Vergeiner, C., Scherzer, G., Holzner, B., Robatscher, P., & Kräutler, B. (2016). Chlorophyll Catabolites in Senescent Leaves of the Plum Tree (Prunus domestica). *Chemistry & Biodiversity, 13*(11), 1441–1453. https://doi.org/10.1002/cbdv.201600181.

Fernandes, L., Casal, S., Pereira, J. A., Saraiva, J. A., & Ramalhosa, E. (2018). Effects of different drying methods on the bioactive compounds and antioxidant properties of edible Centaurea (Centaurea cyanus) petals. *Journal of Food Technology, 21*. https://doi.org/10.1590/1981-6723.21117.

Gülçin, İ., Küfrevioğlu, Ö. I., Oktay, M., & Büyükokuroğlu, M. E. (2004). Antioxidant, antimicrobial, antiulcer and analgesic activities of nettle (Urtica dioica L.). *Journal of Ethnopharmacology, 90*(2-3), 205–215. https://doi.org/10.1016/j.jep.2003.09.028.

Hamrouni-Sellami, I., Rahali, F. Z., Rebey, I. B., Bourgou, S., Limam, F., & Marzouk, B. (2013). Total phenolics, flavonoids, and antioxidant activity of sage (Salvia officinalis L.) plants as affected by different drying methods. *Food and Bioprocess Technology, 6*(3), 806–817. https://doi.org/10.1007/s11947-012-0877-7.

Hendry, G. A. F., Houghton, J. D., & Brown, S. B. (1987). The degradation of chlorophyll - a biological enigma. *New Phytologist, 107*(2), 255–302. https://doi.org/10.1111/j.1469-8137.1987.tb00181.x.

Joshi, B., Mukhija, M., & Kalia, A. (2014). Pharmacognostical review of Urtica dioica L. *International Journal of Green Pharmacy, 8*, 201–209. https://doi.org/10.4103/0973-8258.142669.

Karg, C. A., Schilling, C. M., Allmendinger, L., & Moser, S. (2019). Isolation, characterization, and antioxidative activity of a dioxobilin-type phylloxanthobilin from savoy cabbage. *J. Porphyrins Phthalocyanines, 23*(07n08), 881–888. https://doi.org/10.1142/s1088424619500718.

Karg, C. A., Wang, P., Vollmar, A. M., & Moser, S. (2019). Re-opening the stage for echinacea research - characterization of phylloxanthobilins as a novel anti-oxidative compound class in echinacea purpurea. *Phytomedicine, 60*, 152969. https://doi.org/10.1016/j.phymed.2019.152969.

Karg, C. A., Wang, P., Kluibenschedl, F., Müller, T., Allmendinger, L., Vollmar, A. M., & Moser, S. (2020). Phylloxanthobilins are abundant linear tetrapyrroles from chlorophyll breakdown with activities against cancer cells. *European Journal of Organic Chemistry, 2020*(29), 4499–4509. https://doi.org/10.1002/ejoc.202000692.

Kräutler, B. (2014). Phyllobilins – the abundant bilin-type tetrapyrrolic catabolites of the green plant pigment chlorophyll. *Chemistry Society Review, 43*(17), 6227–6238. https://doi.org/10.1039/c4cs00079j.

Kräutler, B. (2016). Breakdown of chlorophyll in higher plants-phyllobilins as abundant, yet hardly visible signs of ripening, senescence, and cell death. *Angewandte Chemie International Edition, 55*(16), 4882–4907. https://doi.org/10.1002/anie.201508928.

Kräutler, B., Jaun, B., Matile, P., Bortlik, K., & Schellenberg, M. (1991). On the enigma of chlorophyll degradation: The constitution of a secoporphinoid catabolite. *Angewandte Chemie International Edition, 30*(10), 1315–1318. https://doi.org/10.1002/anie.199113151.

Lin, S.-D., Sung, J. M., & Chen, C.-L. (2011). Effect of drying and storage conditions on caffeic acid derivatives and total phenolics of Echinacea Purpurea grown in Taiwan. *Food Chemistry, 125*(1), 226–231. https://doi.org/10.1016/j.foodchem.2010.09.006.

Ma, G., Lin, J., Cai, W., Tan, B., Xiang, X., Zhang, Y., & Zhang, P. (2014). Simultaneous determination of bilirubin and its glucuronides in liver microsomes and recombinant UGT1A1 enzyme incubation systems by HPLC method and its application to bilirubin glucuronidation studies. *Journal of Pharmaceutical and Biomedical Analysis, 92*, 149–159. https://doi.org/10.1016/j.jpba.2014.01.025.

Minekus, M., Alminger, M., Alvito, P., Ballance, S., Bohn, T., Bourlieu, C., Carrière, F., Boutrou, R., Corredig, M., Dupont, D., Dufour, C., Egger, L., Golding, M., Karakaya, S., Kirkhus, B., Le Feunteun, S., Lesmes, U., Macierzanka, A., Mackie, A., Marze, S., McClements, D. J., Ménard, O., Recio, I., Santos, C. N., Singh, R. P., Vegarud, G. E., Wickham, M. S. J., Weitschies, W., & Brodkorb, A. (2014). A standardised static in vitro digestion method suitable for food – an international

consensus. *Food & Function, 5*(6), 1113–1124. https://doi.org/10.1039/C3FO60702J.

Moser, S., Ulrich, M., Müller, T., & Kräutler, B. (2008). A yellow chlorophyll catabolite is a pigment of the fall colours. *Photochemical & Photobiological Sciences, 7*(12), 1577–1581. https://doi.org/10.1039/b813558d.

Müller, T., Ulrich, M., Ongania, K. H., & Kräutler, B. (2007). Colorless tetrapyrrolic chlorophyll catabolites found in ripening fruit are effective antioxidants. *Angewandte Chemie International Edition, 46*(45), 8699–8702. https://doi.org/10.1002/anie.200703587.

Müller, T., Vergeiner, S., & Kräutler, B. (2014). Structure elucidation of chlorophyll catabolites (phyllobilins) by ESI-mass spectrometry-Pseudo-molecular ions and fragmentation analysis of a nonfluorescent chlorophyll catabolite (NCC). *International Journal of Mass Spectrometry, 365-366*, 48–55. https://doi.org/10.1016/j.ijms.2013.12.028.

Obertreis, B., Giller, K., Teucher, T., Behnke, B., & Schmitz, H. (1996). Anti-inflammatory effect of Urtica dioica folia extract in comparison to caffeic malic acid. *Arzneimittelforschung, 46*(1), 52–56.

Orčić, D., Franciškovic, M., Bekvalac, K., Svirčev, E., Beara, I., Lesjak, M., & Mimica-Dukić, N. (2014). Quantitative determination of plant phenolics in Urtica dioica extracts by high-performance liquid chromatography coupled with tandem mass spectrometric detection. *Food Chemistry, 143*, 48–53. https://doi.org/10.1016/j.foodchem.2013.07.097.

Otles, S., & Yalcin, B. (2012). Phenolic compounds analysis of root, stalk, and leaves of nettle. *The Scientific World Journal, 2012*, 1–12. https://doi.org/10.1100/2012/564367.

Pinelli, P., Ieri, F., Vignolini, P., Bacci, L., Baronti, S., & Romani, A. (2008). Extraction and HPLC analysis of phenolic compounds in leaves, stalks, and textile fibers of urtica dioica L. *Journal of Agricultural and Food Chemistry, 56*(19), 9127–9132. https://doi.org/10.1021/jf801552d.

Raso, G. M., Meli, R., Di Carlo, G., Pacilio, M., & Di Carlo, R. (2001). Inhibition of inducible nitric oxide synthase and cyclooxygenase-2 expression by flavonoids in macrophage J774A.1. *Life Sciences, 68*(8), 921–931. https://doi.org/10.1016/s0024-3205(00)00999-1.

Roca, M. (2012). In vitro digestive stability and uptake by Caco-2 human intestinal cells of nonfluorescent chlorophyll catabolites. *Food Chemistry, 130*(1), 134–138. https://doi.org/10.1016/j.foodchem.2011.07.016.

Roca, M., Ríos, J. J., Chahuaris, A., & Pérez-Gálvez, A. (2017). Non-fluorescent and yellow chlorophyll catabolites in Japanese plum fruits (Prunus salicina, Lindl.). *Food Research International, 100*, 332–338. https://doi.org/10.1016/j.foodres.2017.07.029.

Roiser, M. H., Müller, T., & Kräutler, B. (2015). Colorless Chlorophyll Catabolites in Senescent Florets of Broccoli (Brassica oleracea var. italica). *Journal of Agricultural and Food Chemistry, 63*(5), 1385–1392. https://doi.org/10.1021/jf5055326.

Sharma, S., Ali, A., Ali, J., Sahni, J. K., & Baboota, S. (2013). Rutin: therapeutic potential and recent advances in drug delivery. *Expert Opinion on Investigational Drugs, 22*(8), 1063–1079. https://doi.org/10.1517/13543784.2013.805744.

Süssenbacher, I., Menghini, D., Scherzer, G., Salinger, K., Erhart, T., Moser, S., & Kräutler, B. (2019). Cryptic chlorophyll breakdown in non-senescent green Arabidopsis thaliana leaves. *Photosynthesis Research, 142*(1), 69–85. https://doi.org/10.1007/s11120-019-00649-2.

Takemoto, J. Y., Chang, C.-W. T., Chen, D., & Hinton, G. (2019). Heme-derived bilins. *Israel Journal of Chemistry, 59*(5), 378–386. https://doi.org/10.1002/ijch.201800167.

Upton, R. (2013). Stinging nettles leaf (Urtica dioica L.): Extraordinary vegetable medicine. *Journal of Herbal Medicine, 3*(1), 9–38. https://doi.org/10.1016/j.hermed.2012.11.001.

Vergara-Domínguez, H., Ríos, J. J., Gandul-Rojas, B., & Roca, M. (2016). Chlorophyll catabolism in olive fruits (var. Arbequina and Hojiblanca) during maturation. *Food Chemistry, 212*, 604–611. https://doi.org/10.1016/j.foodchem.2016.06.020.

Vergeiner, C., Ulrich, M., Li, C., Liu, X., Müller, T., & Kräutler, B. (2015). Stereo- and regioselective phyllobilane oxidation in leaf homogenates of the peace lily (Spathiphyllum wallisii): Hypothetical endogenous path to yellow chlorophyll catabolites. *Chemistry – A European Journal, 21*(1), 136–149. https://doi.org/10.1002/chem.201404783.

A Yellow Chlorophyll Catabolite in Leaves of *Urtica dioica* L.: An Overlooked Phytochemical that Contributes to Health Benefits of Stinging Nettle

Cornelia A. Karg[a], Christian Doppler[b], Charlotte Schilling[a], Franziska Jakobs[a,c], Marlene C. S. Dal Colle[a,d], Nadine Frey[a], David Bernhard[b], Angelika M. Vollmar[a], Simone Moser[a*]

[a]Department of Pharmacy, Center for Drug Research, Pharmaceutical Biology, Ludwig-Maximilians-University of Munich, Butenandtstr. 5-13, D-81377 München, Germany

[b]Division of Pathophysiology, Institute of Physiology and Pathophysiology, Medical Faculty, Johannes-Kepler-University Linz, Krankenhausstrasse 7a, A-4020 Linz, Austria

[c]Department of Chemistry, High Point University, One University Parkway, High Point, NC 27268, United States

[d]Department of Chemical Sciences, University of Padova, Via Marzolo 1, 35131 Padova, Italy

[*]Corresponding author at: Department of Pharmacy, Center for Drug Research, Pharmaceutical Biology, Ludwig-Maximilians-University of Munich, Butenandtstr. 5-13, D-81377 München, Germany, Email address: simone.moser@cup.uni-muenchen.de

Supplementary Information

Content:

29   Figure S10: HPLC analysis of *Ud*-PxB incubated in phosphate buffer pH=2.5

30   Figure S11: Metabolic stability of bilirubin and *Ud*-PxB

31   Figure S12: ESI MS/MS spectra of bilirubin-glucuronides

32

33

34

35

36

37

38

39

40

41

42

43

44

45

46

47

48
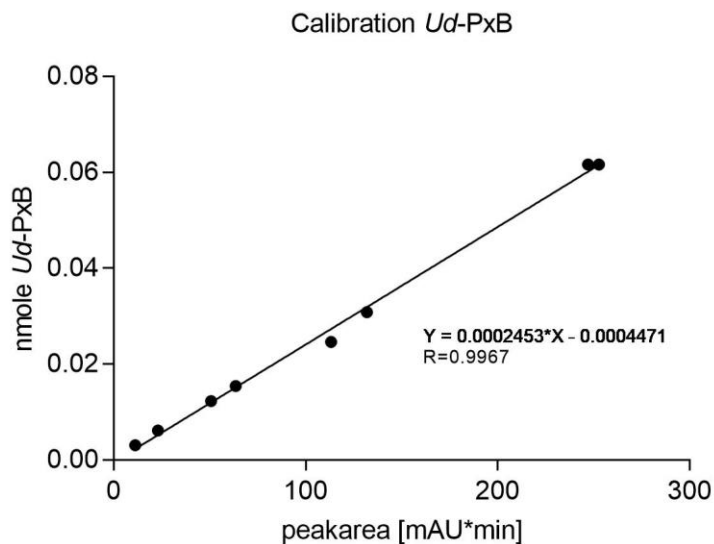
Figure S1: Calibration linear of isolated, pure *Ud*-PxB for quantification of *Ud*-PxB in nettle tea.
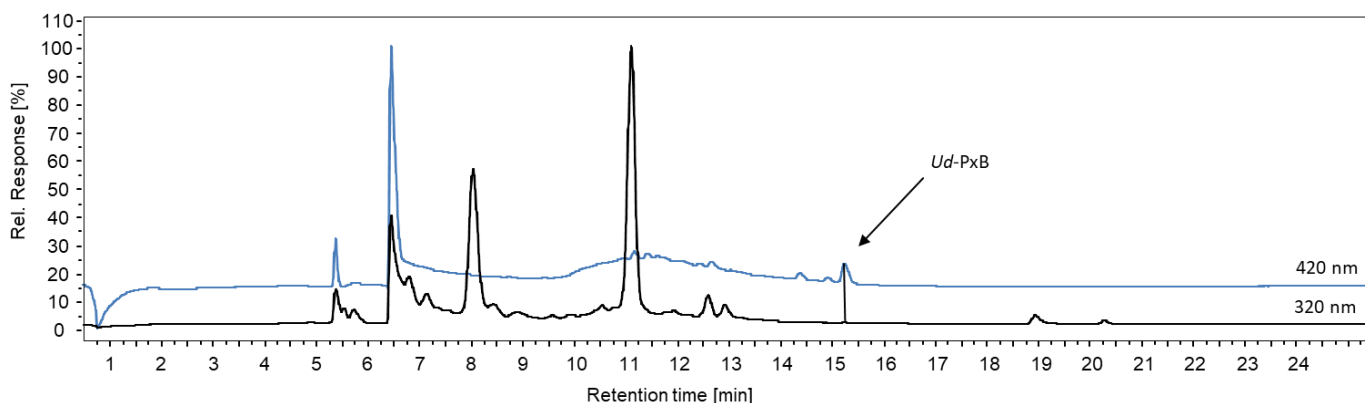
Figure S2: HPLC analysis of commercially available nettle tea (Bad Heilbrunner), which was prepared as described in the experimental section. Detection at 320 nm (black line) and 420 nm (blue line). (LiChroCART-LiChrospher100 RP-18 (5 μm, 250 x 4 mm) protected by LiChroCART-LiChrospher100 RP-18 (5 μm, 4 x 4 mm) pre-column; Solvent system: mobile phase A = 0.1% TFA, B = ACN, flow 0,5 mL/min; Solvent composition: 0-2 min 20 % B, 2-22 min 20 % to 100 % B, 22-23 min 100 % B, 23-25 min 100 to 20 % B)
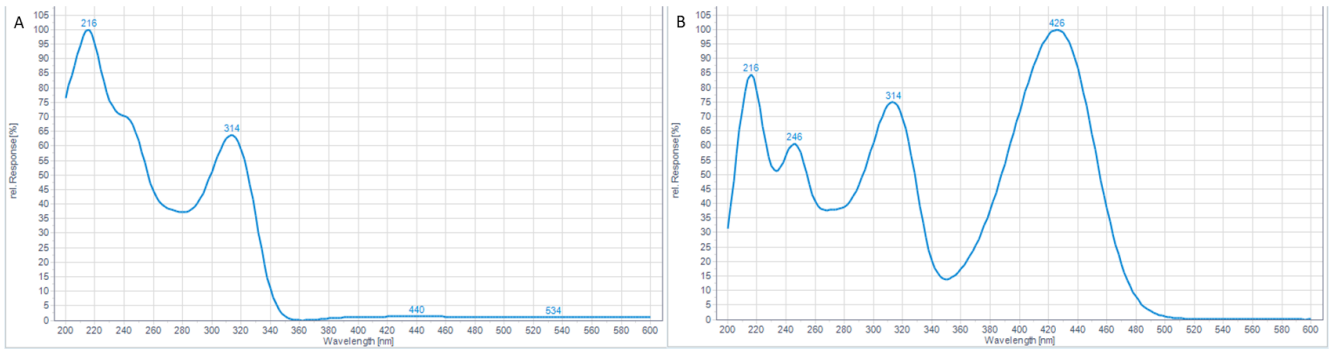
Figure S3: UV-Vis online spectra of *Ud*-PleB (**A**) and *Ud*-PxB (**B**).
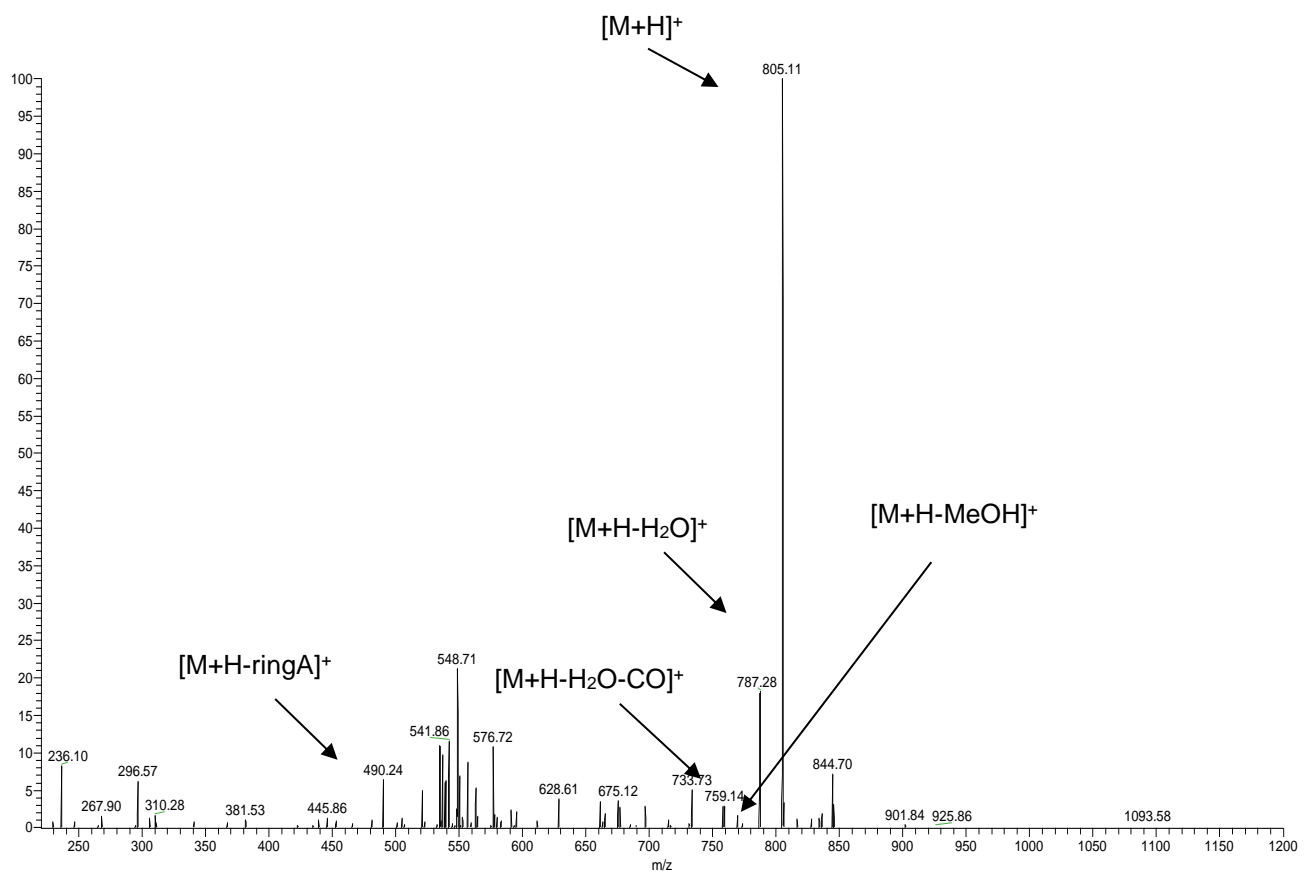
Figure S4: ESI MS/MS mass spectrum of *Ud*-PxB.

74
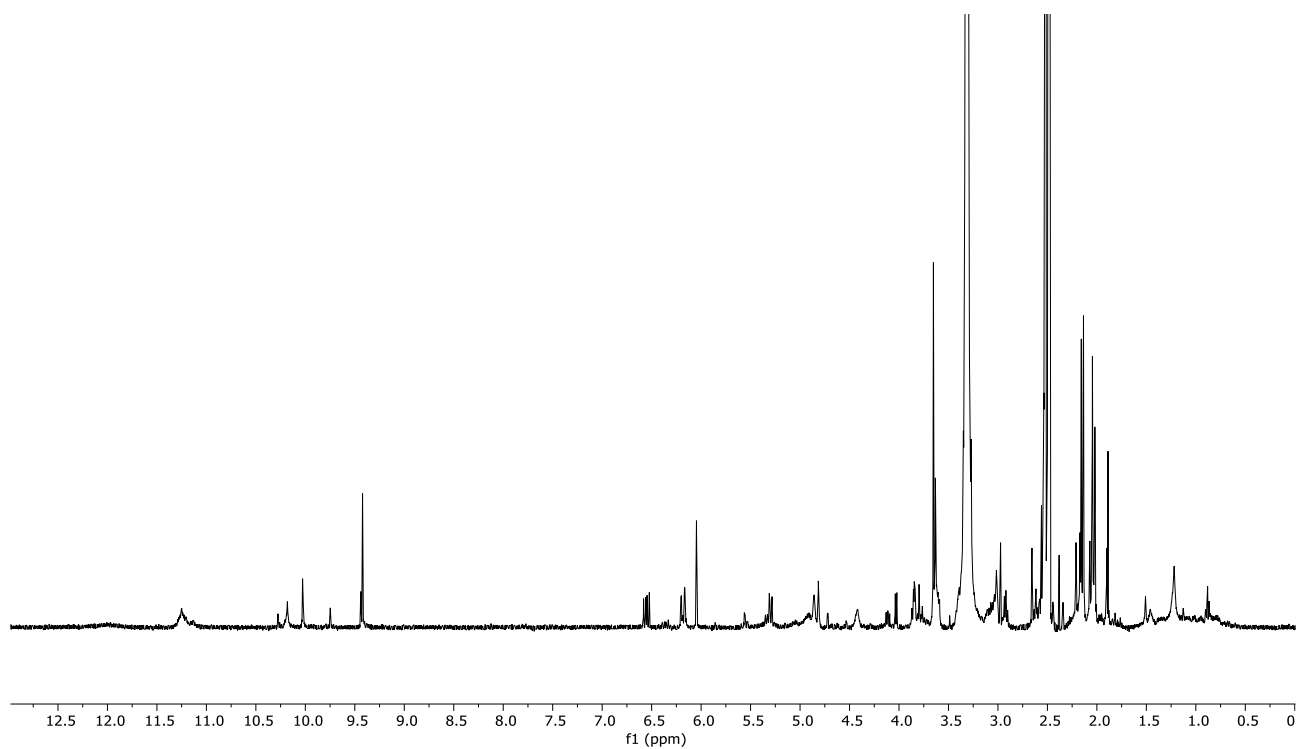
Figure S5: ¹H NMR spectrum of *Ud*-PxB in d_6-DMSO

75

76

	Ud-PxB		*Nr*-PleB-2	
	δ(¹H)	δ(¹³C)	δ(¹H)	δ(¹³C)
C(1)		128.33		129.2
C(2)		131.47		135.4
C(2^1)	2.16, s	9.33	2.24	8.9
C(3)		118.91		120.8
C(3^1)	2.53, m; 2.63, m	24.36	2.68	25.2
C(3^2)	3.62, m; 3.32, m	68.98	3.47; 3.82	70.1
C(4)		136.41		139.1
C(5)	3.80, m	22.65		23.8
C(6)		133.72		134.1
C(7)		110.15		112.8
C(7^1)	2.02, s	9.78	2.12	9.2
C(8)		124.74		126.2
C(8^1)		188.25		
C(8^2)	3.86, m	66.40		68.1
C(8^3)		170.30		171.7
C(8^4)	3.65, s	52.68	3.77	52.9
C(9)		157.28		160.7
C(10)	4.81, m	36.37	4.85	37.3
C(11)		130.80		124.6
C(12)		118.68		120.1
C(12^1)	2.51, m	19.64	2.65	21.0

C(12²)	2.21, m	34.23	2.26; 2.37	37.1
C(12³)		174.11		178
C(13)		123.84		114.5
C(13¹)	2.05, s	9.77	1.91	9.2
C(14)		124.52		124.5
C(15)	6.05, s	99.87	2.50; 2.89	30.1
C(16)		129.90	4.01	61.6
C(17)		142.70		155.9
C(17¹)	2.14, s	9.35	1.98	12.5
C(18)		123.39		128.8
C(18¹)	6.55, dd, *J*=18.2/12.1	127.32	6.45	127.0
C(18²)	5.29, m; 6.17, m	118.31	5.36; 6.12	119.3
C(19)		171.20		174.8
C(20)	9.43, s	175.01	9.31	177.8
C(1')	4.03, m	103.30	2.50; 2.89	104.1
C(2')	2.92, s	74.13	4.2	74.9
C(3')	3.60, m	77.13	3.16	78.0
C(4')	3.27, m	74.56	3.31	71.5
C(5')	3.02, m	70.69	3.24	77.9
C(6')	3.62, m; 3.40, m	61.26	3.63; 3.84	62.6

77 **Table S1**. ^{1}H- and ^{13}C-NMR data of *Ud*-PxB (500 MHz, d$_6$-DMSO) and their comparison with ^{1}H- and ^{13}C-NMR

78 data of *Nr*-PleB-2 (500 MHz, CD$_3$OD, 26°C) (Berghold, Eichmüller, Hörtensteiner, & Kräutler, 2004).

79
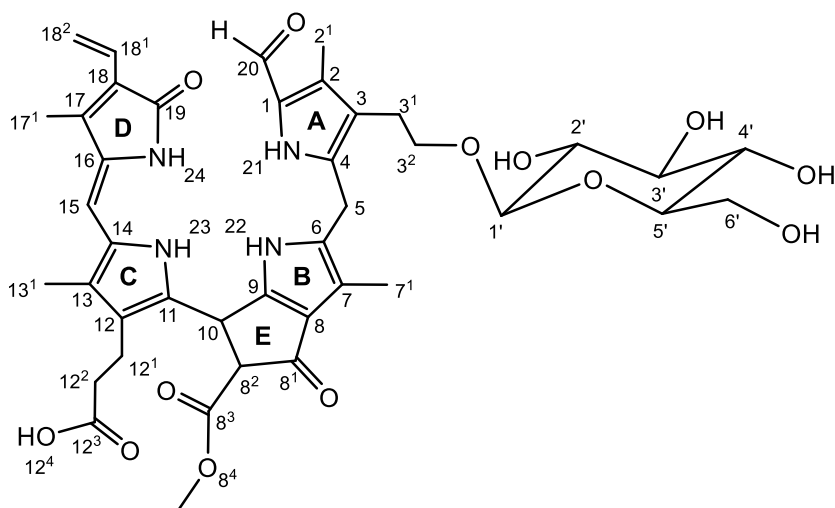
80

81 **Figure S6:** Numbered structure of *Ud*-PxB.

82

83

84

Calibration rutin

$Y = 0.005698*X - 0.01073$
$R=0.9998$

85
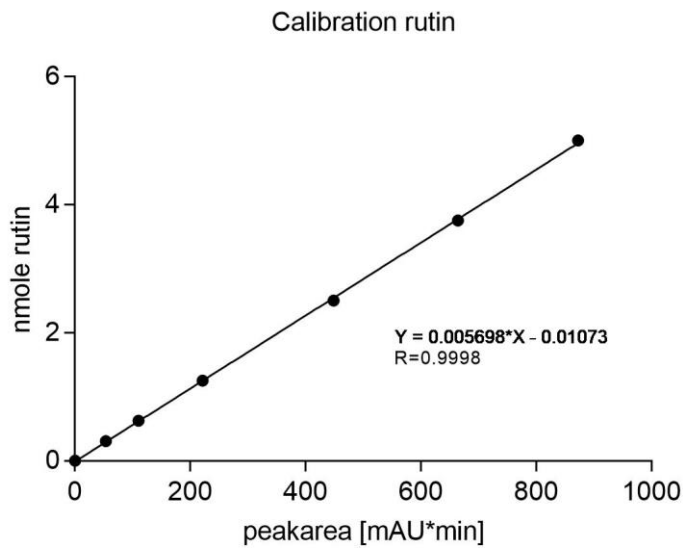
Figure S7: Calibration linear of a rutin standard for quantification of rutin in nettle tea.
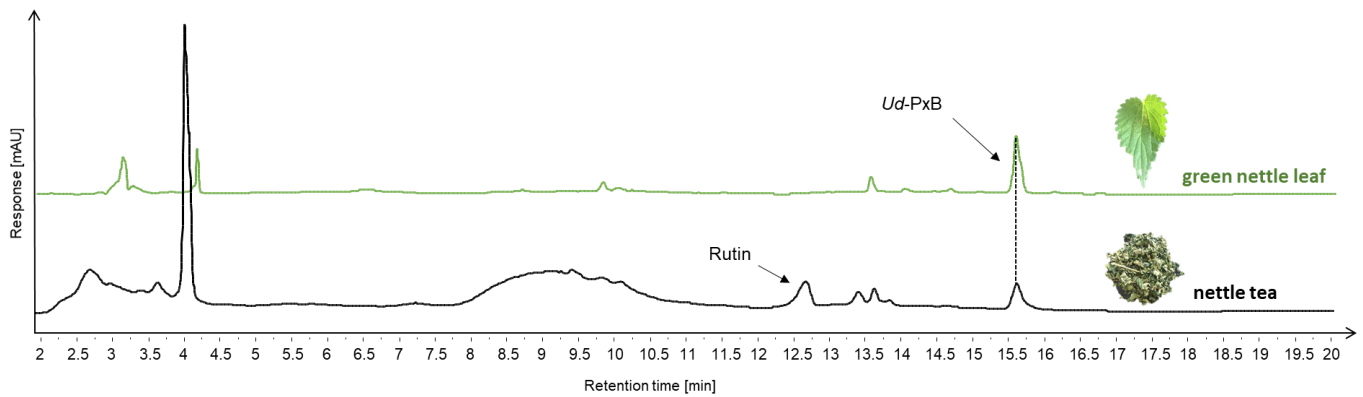
87
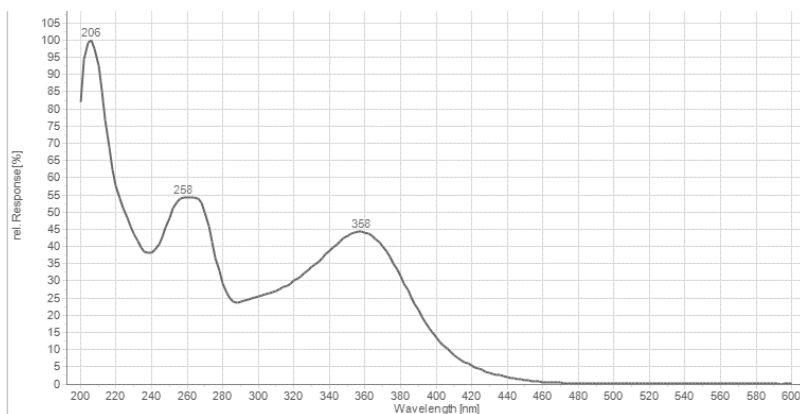
88

89 **Figure S8:** Representative chromatograms and UV-Vis spectrum of rutin for quantification in a fresh green
90 leaf extract and nettle tea (Bombastus) by analytical HPLC. Detection at 420 nm.

91

92

Brand name	rutin (mg/200 mL)[a]	rutin (mg/g)[b]	Source
Alfred Galke	-[c]	-[c]	Company
Altapharma	-[c]	-[c]	Drug store
Aurica	2.27 ± 0.11	1.26 ± 0.06	Pharmacy
Bad Heilbrunner	0.84 ± 0.11	0.47 ± 0.06	Supermarket
Bombastus	1.98 ± 0.2	0.71 ± 0.07	Pharmacy
Das gesunde Plus	1.56 ± 0.12	0.87 ± 0.06	Drug store
H&S	-[c]	-[c]	Pharmacy
Meßmer (51% nettle leaves)	0.08[d]	0.05[d]	Supermarket
Sidroga	1.07 ± 0.06	0.71 ± 0.04	Pharmacy

Data are means ± SEM, n=3

Table S2: Quantitative determination of rutin by HPLC analysis in nettle tea from different brands. [a]Analysis of one cup of tea (200mL) prepared as described in the experimental section. [b]Calculation according to the weight of the respective tea bag. [c]Rutin was not detected. [d]Rutin was only detected in one replicate.
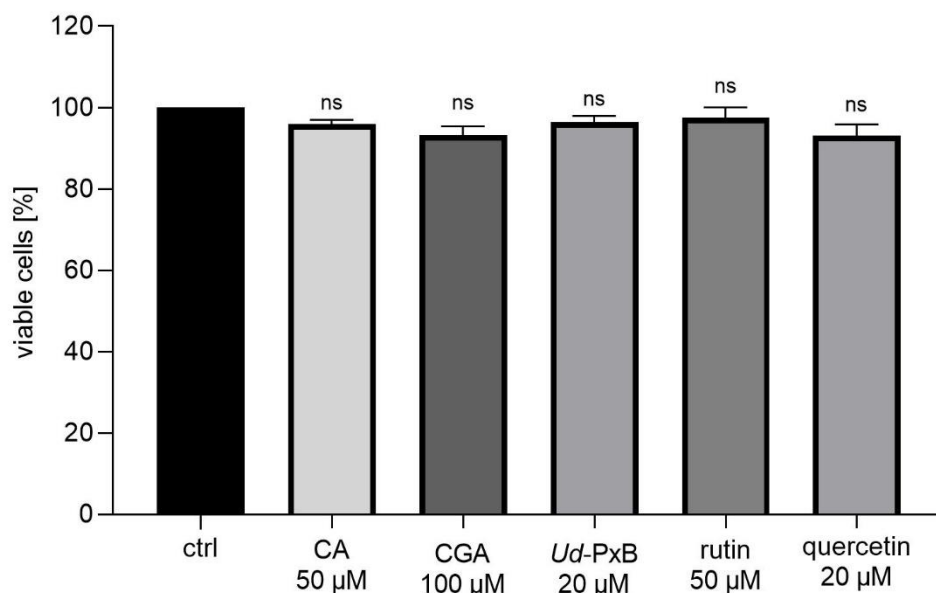
Figure S9: Cell viability assay of HEK cells treated with caffeic acid (CA), chlorogenic acid (CGA), *Ud*-PxB, and rutin. Cell viability was determined by a CellTiter-Blue® assay in HEK cells, which were seeded and stimulated with the same conditions as the intracellular ROS assay. 4 h before the end of 24 h stimulation time, 20 µL of CellTiter-Blue® reagent was added to the cells and fluorescence was detected after 4 h incubation at 37°C with a Tecan SpectraFluor plus microplate reader at 590 nm. Data were normalized to the DMSO control.

105 Compounds do not affect cell viability at indicated concentrations. In parallel to the DCF measurement, a
106 CellTiterBlue® cell viability assay was performed to exclude any cytotoxic effects that could influence
107 intracellular ROS levels (unpaired t-test with Welch's correction, ns $P > 0.12$).

108
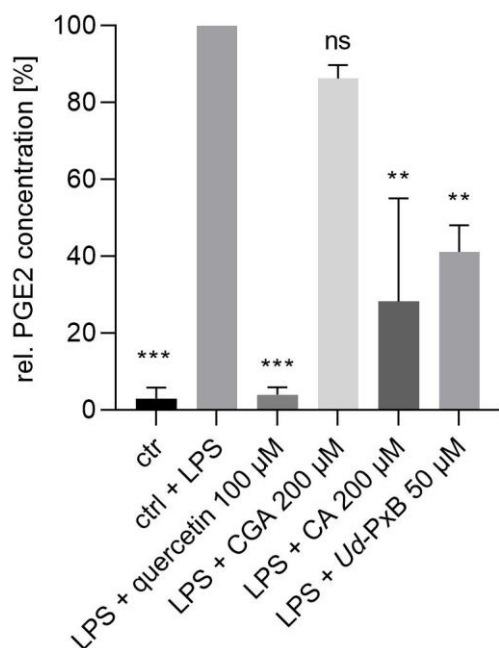
109

110 **Figure S10:** Effect of nettle phytochemicals on PGE2 production in LPS stimulated J774A.1 cells was
111 assessed using a commercial ELISA kit (cayman chemicals PGE2-ELISA-Kit) following the manufacturer's
112 instructions. J774A.1 cells were stimulated for 4 h with LPS (0.5 µg/mL) and nettle phytochemicals, before the
113 supernatant was analyzed for the concentration of prostaglandin E2. PGE2 concentration in pg/mL was
114 normalized to the LPS stimulated control. Data represent means ± SEM of two independent experiments (one-
115 way analysis of variance with post hoc Dunnett's multiple comparison test, ns $P > 0.12$, **$P < 0.01$, ***$P < $
116 0.001).

117

118

119

120

121

122
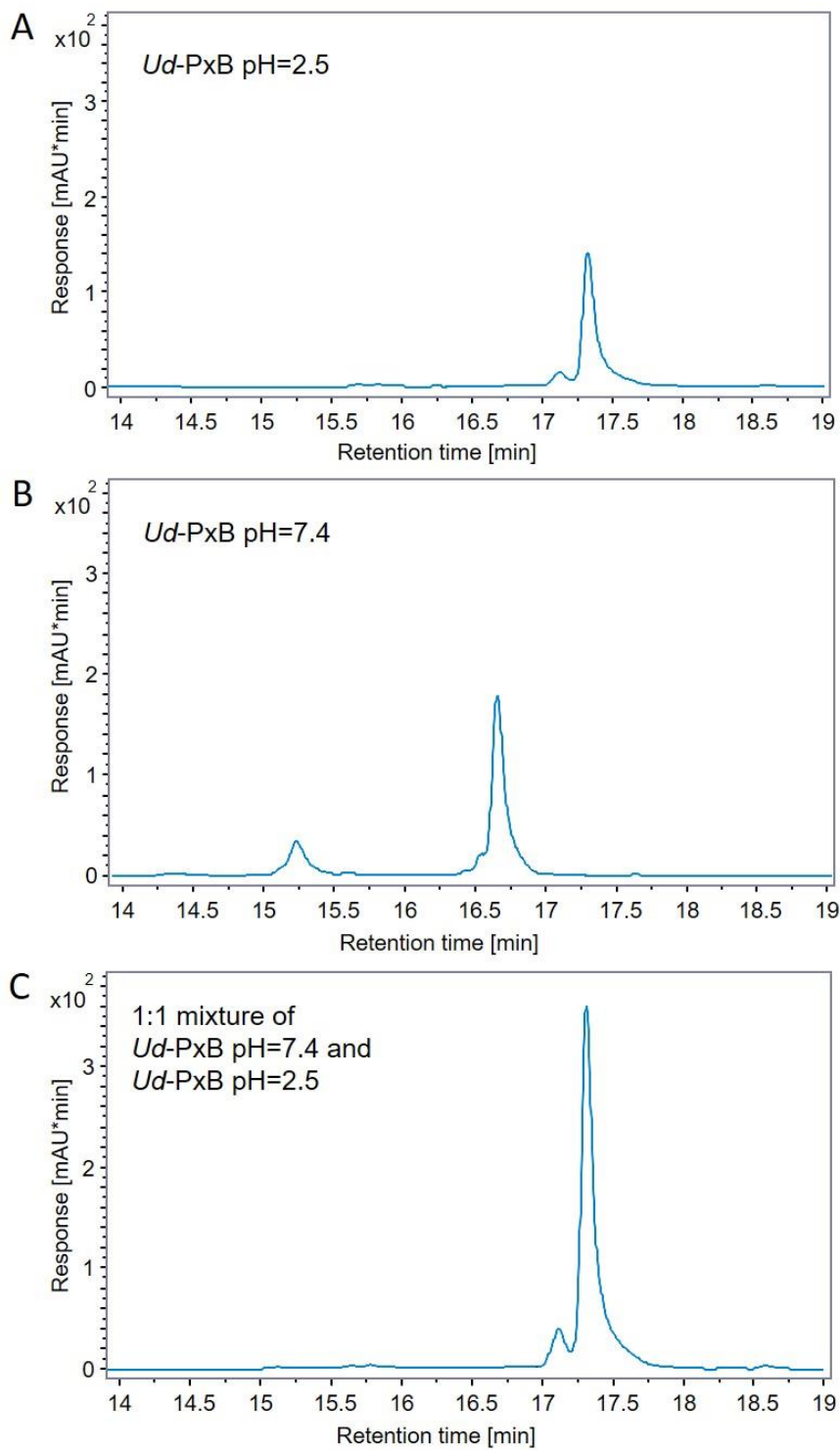
Figure S11: Co-elution HPLC analysis of *Ud*-PxB incubated in phosphate buffer pH=2.5 for 24h (**A**), *Ud*-PxB incubated in phosphate buffer pH=7.4 for 24h (**B**) and a 1:1 mixture (**C**).
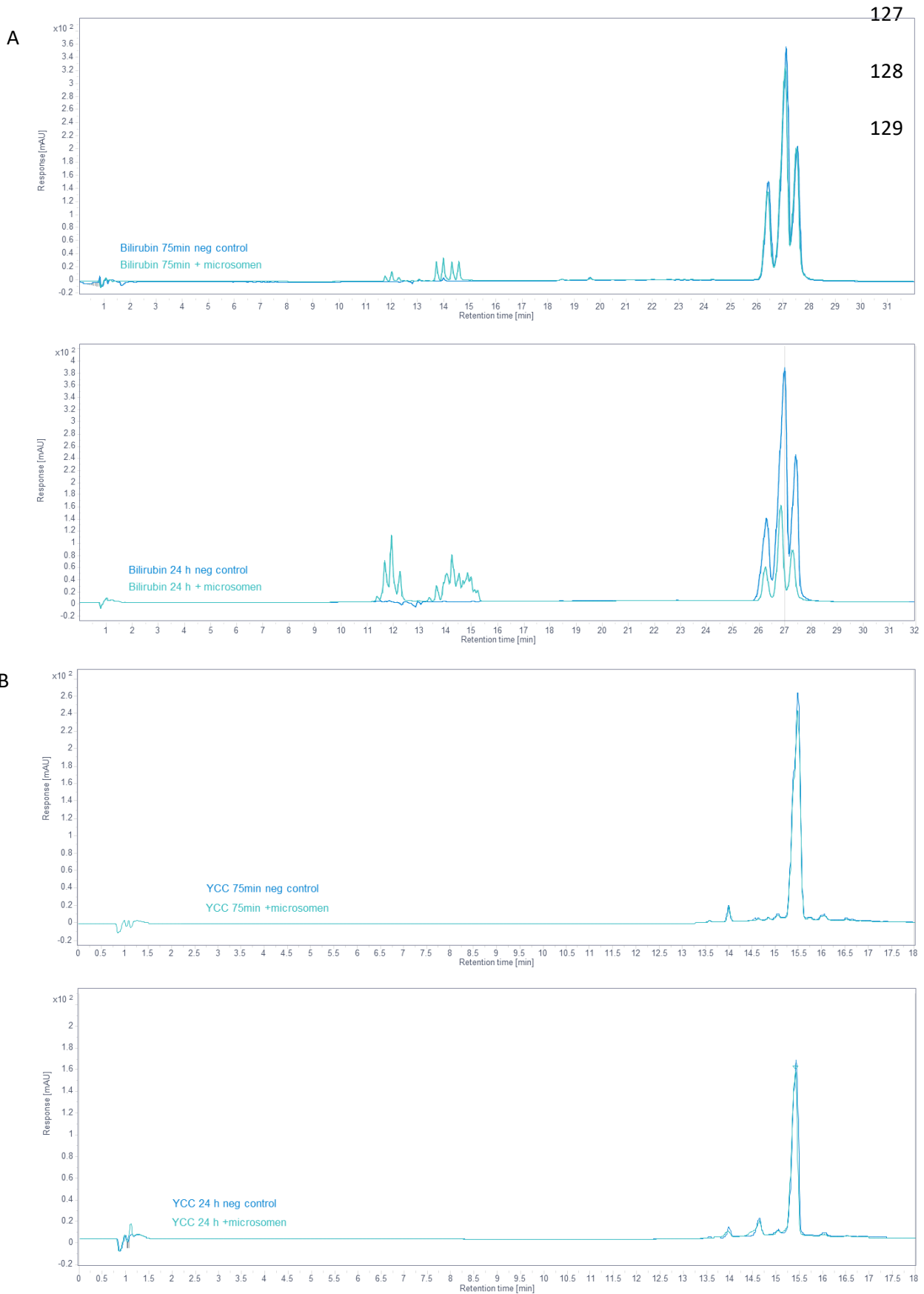
Figure S12: Metabolic stability of bilirubin and *Ud*-PxB. HPL-Chromatograms of bilirubin (A) and *Ud*-PxB (B) incubated for 75 min and 24 h, respectively, and with or without liver microsomes.
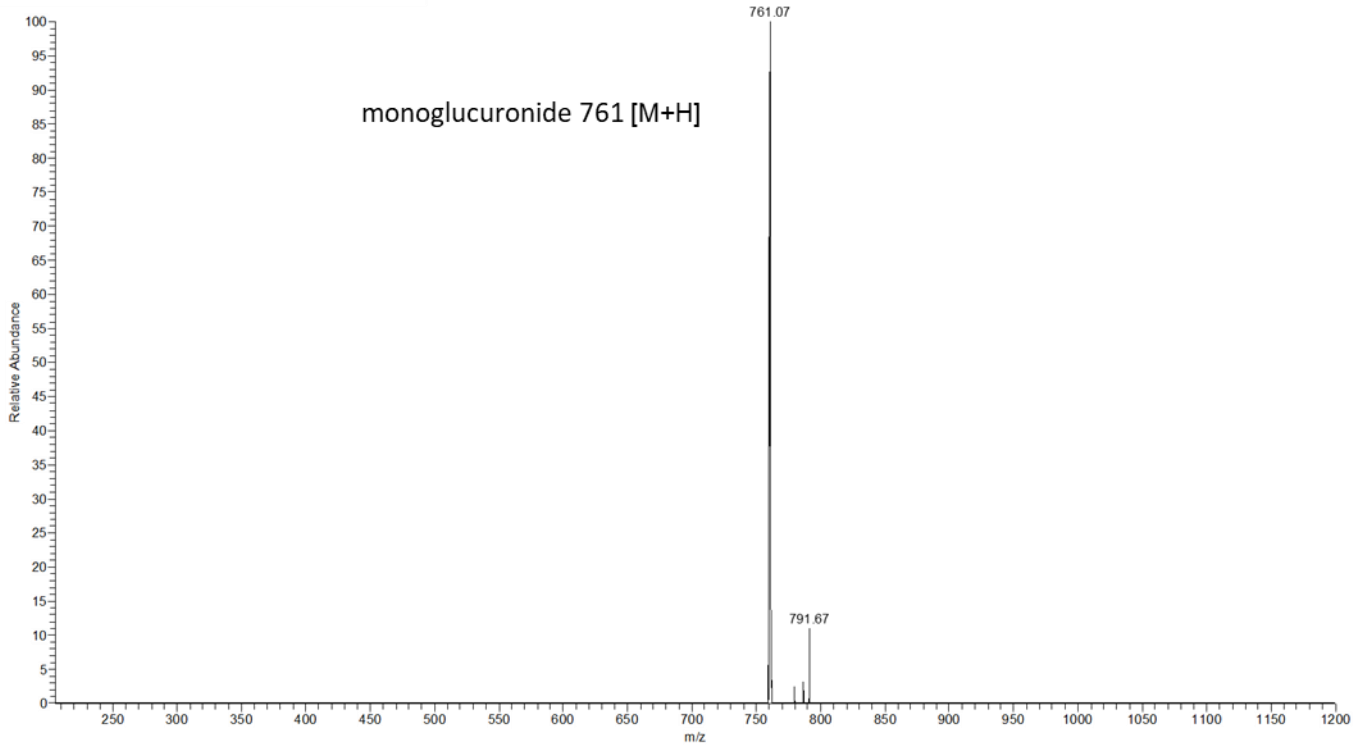
133
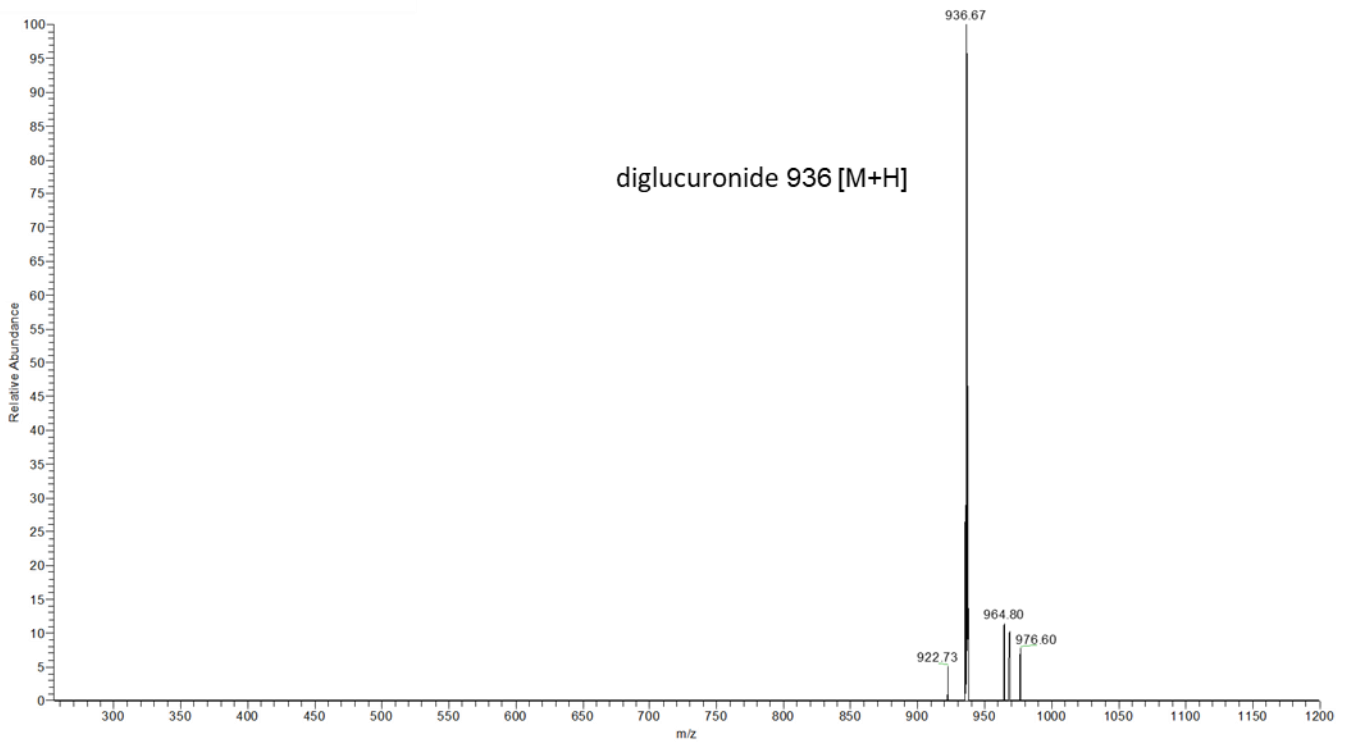
134

135 **Figure 13:** ESI-MS/MS spectra of bilirubin glucuronides derived from incubation with liver microsomes.

136

137

138   **References**

139   Berghold, J., Eichmüller, C., Hörtensteiner, S., & Kräutler, B. (2004). Chlorophyll Breakdown in Tobacco: On
140   the Structure of Two Nonfluorescent Chlorophyll Catabolites. *Chemistry & Biodiversity, 1*(4), 657-
141   668.

142

Rising levels of antioxidative phyllobilins in stored agricultural produce and their impact on consumer acceptance

Cornelia A. Karg[a], Christina M. Neubig[b], Jutta Roosen[b], Simone Moser[a,*]

[a]Ludwig-Maximilians University of Munich, Pharmaceutical Biology, Department of Pharmacy, Butenandtstraße 5-13, D-81377 Munich, Germany

[b]Technical University of Munich, TUM School of Management, Chair of Marketing and Consumer Research, Alte Akademie 16, 85354, Freising, Germany

*Email: simone.moser@cup.uni-muenchen.de

Abstract

Consumers often throw away faded greens, because taste and appearance are less appealing as in fresh ones. We report here a family of antioxidants, the phyllobilins, which increase during storage in iceberg lettuce and cucumber. We show that informing consumers about rising levels of phyllobilins leads to a longer willingness to consume faded lettuce and to an improved health and safety perception.

Currently 11% of the world population suffer from poverty and hunger while one third of the food produced for human nutrition worldwide (roughly 1.3 billion tons) is wasted every year[1]. Especially in these times, in a worldwide pandemic, when food systems are stressed and produce accessibility may be limited, finding means to achieve a more sustainable use of food resources is of utmost importance.

In the long term, reducing food waste is crucial for preventing food insecurity in addition to curbing environmental harm, since when food is wasted the resources for its production are wasted as well. Handling and transportation of agricultural produce adds to the total of wasted resources when food is thrown away at the end of the supply chain. The awareness of wasted food has already reached the population, as can be seen by the discussion about

the phenomenon of 'Dumpster Diving' (salvaging dumped food from large industrial or commercial dumpsters), which is illegal in many countries[2]. While Dumpster Diving can be mainly seen as a consumer demand towards retailers to reduce their food waste, it is important to note that in Europe, more than 50% of food waste is caused by the consumer[3], stressing the immense potential of changing consumer behavior. Fruits and vegetables are among the food items that are most often wasted by the end consumer[4]. This waste occurs for a variety of reasons including cosmetic issues. Fresh and more chromatic colored foods are often preferred, especially for red and green produce[5]. Consequently, changes in shape or color (e.g. withering or yellowing of lettuce) can influence food practice at home. Consumers often throw away perishable food when it appears to be less fresh, although it is still safe to eat[6]. While there is extensive research concerning preferences regarding how suboptimal looking produce (such as curved cucumbers) may influence food waste, there is little research into how reduced freshness and yellowing of lettuce impact consumer food waste.

With the aim of reducing food waste, what if one could shift consumer behavior towards judging aged produce as still valuable and too good to be thrown away? By informing consumers about a family of antioxidants that occur in food stored for a couple of days, we were able to initiate a revaluing of stored lettuce by consumers.

The loss of green color is the result of a detoxification process employed by plants to get rid of chlorophyll. The biochemical degradation of the green plant pigment chlorophyll takes place in all higher plants, and is triggered by environmental or biotic factors, such as drought or pest infestation[7], in addition to senescence. At the end of this multi-step program, more water-soluble and stable chlorophyll catabolites called phyllobilins accumulate[7,8] (Supplementary Figure 1). Phyllobilins are linear tetrapyrroles and, unlike chlorophyll and its early degradation products such as pheophytin or pheophorbide a[9], not phototoxic. Recently, phyllobilins were even shown to possess relevant bioactivities: our research revealed strong antioxidative effects *in vitro* and in cells, even superior to known antioxidants such as bilirubin, Trolox, and caffeic acid. In addition, phyllobilins were shown to be free radical

scavengers and to protect cells from oxidative stress[10,11]. Although phyllobilins are ubiquitous in plants, they have not yet been considered as antioxidants in foods, and appear to be completely overlooked components of our nutrition. Phyllobilins are related to phycocyanobilin from the blue-green algae spirulina, which has recently been recognized to have health-promoting effects[12,13]. Consequently, spirulina products have conquered the market and spirulina itself is now considered a 'superfood'.

Vegetables are major dietary sources of micronutrients (i.e. vitamins and minerals) and bioactive compounds (e.g. carotenoids, flavonoids); however, the contents of bioactive phytochemicals can vary over time, and many studies focus on the analysis of post-harvest composition of bioactive compounds in plant based food. Levels of flavonoids, for example, have been found to be stable during storage in spinach[14]; for glucosinolates in broccoli, even an increase was identified during short-time storage[15]; whereas losses of carotenoids and folate contents were reported for packaged spinach[16]. High quantities of phyllobilins have been detected in stored plant-based foods[17,18], indicating the biochemical chlorophyll degradation program to be active post-harvest.

We selected iceberg lettuce and cucumbers for our studies since they are commonly consumed all over the world. Although lettuce is a source of fiber, vitamins, and folate, amounts in iceberg lettuce were found to be comparably low in regard to other types of lettuce[19]; in general, lettuce and cucumber are lower in nutrients as some other greens[20,21]. In contrast, high amounts of phyllobilins were detected in these two vegetables in a preliminary screening of a variety of plant-based foods. Using time-lapse photography, we monitored the aging process of iceberg lettuce and cucumbers during a storage time of 7 and 12 days, respectively, until the food appeared faded but still edible (Figure 1a). To ensure that aged lettuce and cucumbers were still safe to consume, we confirmed a lack of microbial increase at the end of storage. Furthermore, isolated phyllobilins were tested for chemo- and genotoxicity and were found to be innocuous (Supplementary Figures 2, 3, 4).

Each day, samples of lettuce and cucumber peels were collected and phyllobilin contents were analyzed (Supplementary Figure 5). On day 1, when the lettuce and cucumber still

appeared fresh and green (Supplementary Figure 6), only low levels of phyllobilins were detected; however, the amount of phyllobilins increased significantly over time. For lettuce, phyllobilin content increased significantly throughout days 3 through 7 compared to day 1. For cucumbers, phyllobilin content started to increase significantly on day 9 and reached its maximum level on day 12 (Figure 1b). Next, we compared the antioxidant potential of lettuce and cucumber extracts at the beginning and end of storage. Although phyllobilins are formed in the expense of chlorophyll, which is connected to biological activities[22], extracts of aged produce enriched in phyllobilins showed significantly higher antioxidative activity compared to extracts of fresh ones (Figure 1c). Furthermore, we performed targeted cellular biological assays using phyllobilins isolated from aged lettuce and cucumber, which demonstrated a similar or higher antioxidative potential than Trolox and revealed radical scavenging activities, protecting cells upon oxidative stress (Supplementary Figure 7).

Phyllobilins are therefore potent antioxidants that could – depending on storage time – constitute a noteworthy part of human nutrition. Phyllobilin levels rise from 0.07 to 2.77 $\mu g/cm^2$ in lettuce and from 1.34 to 4.52 $\mu g/cm^2$ in cucumber, as calculated from the data of the time-lapse study (Supplementary Figure 8). We investigated whether educating consumers about strong antioxidative components that occur nearly exclusively in aged produce has the potential to shift consumer behavior towards eating stored produce longer, which holds a large promise of preventing unnecessary food waste.

Using an online experiment, we show that consumers who received information about health benefits and occurrence of phyllobilins in aged iceberg lettuce ('phyllobilin condition') were willing to eat the lettuce significantly longer (by 0.56 days, p=0.001, Supplementary Table 3) than consumers who received a non-relevant information about chlorophyll ('control condition'). While similar in the beginning, willingness to consume the lettuce dropped quickly in the control condition after day 3, while decreasing significantly more slowly in the phyllobilin condition (Figure 2a). Moreover, consumers in the phyllobilin condition rated the lettuce significantly healthier and safer than those in the control condition on days 4 to 7 (Figure 2b,c). Compared to a safety condition, in which consumers were informed that seven

days old lettuce is still safe to eat, the phyllobilin condition rated the lettuce significantly healthier on days 6 and 7; and even though the lettuce's safety was emphasized in the information given to subjects in the safety condition, consumers in the phyllobilin condition perceived the lettuce as significantly more safe on day 6 (Supplementary Tables 4, 5). Interestingly, an increased health perception in the phyllobilin group compared to the safety group led to a comparable behavior, as reflected in similar results for the willingness to consume the stored lettuce between the two groups. Considering this fact, the highest impact on food waste might be achieved by combining safety and health, and educate people that aged, stored lettuce is not only safe to eat but has even higher antioxidative potential than fresh lettuce.

The knowledge about phyllobilins has the potential to upgrade longer stored greens, and initiate a rethinking in consumers. Our results indicate that informing consumers about phyllobilins can change their health and safety perception of produce and leads to a longer willingness to eat perishable produce (even though they may be wrinkly or yellow instead of fresh and green), which has great potential to reduce food waste at home. In Germany, for instance, roughly 188.000 tons of lettuce are consumed per year[23]. Regarding this high number, prolonging willingness to consume lettuce by only an average of half a day (as indicated by our results) will already make a substantial contribution to reducing food waste. Phyllobilins are ubiquitous in plants and have been overlooked as food components for far too long: with this report and its implications in consumer behavior, we aim at raising awareness of these compounds in the food science community - we hope to initiate in-depth evaluations of phyllobilins in terms of animal and human studies, which will be necessary to substantiate their use in health claims and dietary recommendations. Eventually, educating consumers about this class of powerful antioxidants can lead to a more sustainable consumer behavior and hence has a huge potential in reducing consumer food waste at home.

Methods

Time-lapse photography and phyllobilin content quantification

Iceberg lettuce and cucumbers were bought at a local supermarket and stored for indicated times at room temperature (22 °C, 26% relative humidity) protected from light. Pictures were taken every 90 min with a fixedly installed GoPro HERO4 camera. Data were processed with ImageJ. Each day during the storage time, samples of lettuce leaves and cucumber peels were collected, and extracts were prepared using methanol / potassium phosphate buffer 100 mM pH 7. Extracts were analyzed by analytical HPLC. Phyllobilins were identified by their characteristic UV VIS online spectra using a diode array detector and LC-HR MS measurements (Supplementary Figures 9, 10, Supplementary Table 1), and the peaks were integrated with the Agilent software OpenLab CDS. The sum of all peak areas, corrected for the differences of the size of each sample (area) and normalized to the sum of all phyllobilins at the day with the highest phyllobilin content, is represented. A correction factor to account for the loss of volume due to dehydration effects was determined by analyzing the area of lettuce and cucumbers on the snap-shots of the time-lapse images by Matlab software R2018b. For iceberg lettuce, three series with three lettuces each were performed; samples of one of the series were collected on day 1, 2, 3, 6, and 7. Three cucumbers were analyzed each day during storage. Statistical significance was evaluated by one-way ANOVA followed by Dunnett's multiple comparison test. Other detailed methods are available as Supplementary Information.

Antioxidative assay

The *in vitro* antioxidative activity was assessed by a Ferric reducing antioxidative power (FRAP) assay using the method from Benzie et al.[24] Briefly, FRAP reagent was freshly prepared. Extracts or isolated compounds and varying concentrations of Trolox were incubated with FRAP reagent for 5 min at 37°C. The antioxidative activity was measured colorimetrically with a Tecan SpectraFluor plus microplate reader at 620 nm and antioxidant potential of the extracts and isolated compounds was expressed as Trolox equivalents (µmol

TE/µM or µmol TE/g/mL extract). Statistical significance was evaluated by an unpaired t-test. Other detailed methods are available as Supplementary Information.

Consumer behavior study

The study was carried out in accordance to the Technical University of Munich guidelines for good scientific practice. Data were collected in July 2020 through an online experiment with a between-subjects design in Germany (N=1103, Supplementary Table 2). The sample was quota-sampled to ensure representativeness for the German population regarding age, gender, region, and education. Informed consent was obtained from all participants. Subjects were randomly assigned to three different treatment groups (control, safety, phyllobilin). First, subjects provided demographical information and answered questions about food consumption and habits. Next, all groups were shown the same time-lapse video of an iceberg lettuce head aging for seven days, but received different information with the video. The safety group (N=376) learned that even seven days old iceberg lettuce is still safe to eat. The phyllobilin group (N=360) learned about phyllobilins, their health benefits, and occurrence in aged iceberg lettuce. The control group (N=367) was given information that was not expected to change their perception and willingness to consume the lettuce (i.e., they learned about chlorophylls and photosynthesis). In order to ensure that subjects had read the information, they were asked to answer three knowledge questions. In the final part of the questionnaire, subjects were shown up to seven pictures of the aging iceberg lettuce taken on consecutive days. For each picture and day, they indicated on a scale from 1 to 5 how healthy and how safe to eat they judged the respective lettuce (1=very healthy/safe; 5=very unhealthy/unsafe). Moreover, they indicated whether they would still eat the lettuce (yes/no) (Supplementary Table 3, Supplementary Figure 11). Data were analyzed in IBM SPSS Statistics 26 using descriptive statistics and One-way Analyses of Variance. Due to the large sample size, normal distribution of variables was assumed. Other detailed methods are available as Supplementary Information.

Data availability

The datasets generated during and/or analyzed during the current study are available from the corresponding author on reasonable request.

Acknowledgments

We would like to thank Prof. Dr. Angelika Vollmar for her expertise and support, Kerstin Schmid and Rita Socher for technical support, Maibritt Kretschmer for analyzing data with Matlab and Assoc. Prof. Dr. Thomas Müller and Christian Nadegger for performing LC-MS measurements.

Author contributions

S.M. and C.A.K. developed the project and the main conceptual idea. S.M. and J.R. designed the study. C.A.K. performed time-lapse, chemical, and biological experiments and C.A.K. and S.M. evaluated data. C.M.N. and J.R. set up the consumer survey. Data were analyzed by C.M.N. with feedback by J.R. The manuscript was written with input from all authors. All authors discussed the results and commented on the manuscript.

Competing interest

The authors declare no competing interests.

References

1   FAO Food and Agriculture Organization of the United Nations, Global food losses and food waste: Extent, causes and prevention. http://www.fao.org/food-loss-and-food-waste/flw-data (2011).

2   Vinegar, R., Parker, P. & McCourt, G. More than a response to food insecurity: demographics and social networks of urban dumpster divers. *Local Environ.* **21**, 241-253 (2016).

3   Stenmarck, A., Jensen, C., Quested, T., Moates, G. Estimates of European Food Waste Levels. IVL Swedish Environmental Research Institute, Stockholm. https://www.eu-fusions.org/phocadownload/Publications/Estimates%20of%20European%20food%20waste%20levels.pdf (2016).

4   Braeutigam, K.-R., Jörissen, J. & Priefer, C. The extent of food waste generation across EU-27: Different calculation methods and the reliability of their results. *Waste Manag. Res.* **32**, 683-694 (2014).

5   Lee, S.-M., Lee, K.-T., Lee, S.-H. & Song, J.-K. Origin of human colour preference for food. *J. Food Eng.* **119**, 508-515 (2013).

6   Aschemann-Witzel, J., de Hooge, I., Amani, P., Bech-Larsen, T. & Oostindjer, M. Consumer-Related Food Waste: Causes and Potential for Action. *Sustainability* **7**, 6457-6477 (2015).

7   Moser, S., Erhart, T., Neuhauser, S. & Kräutler, B. Phyllobilins from Senescence-Associated Chlorophyll Breakdown in the Leaves of Basil (Ocimum basilicum) Show Increased Abundance upon Herbivore Attack. *J. Agric. Food Chem.* **68**, 7132-7142 (2020).

8   Kräutler, B. Breakdown of Chlorophyll in Higher Plants—Phyllobilins as Abundant, Yet Hardly Visible Signs of Ripening, Senescence, and Cell Death. *Angew. Chem. Int. Ed.* **55**, 4882-4907 (2016).

9   Jonker, J. W. *et al.* The breast cancer resistance protein protects against a major chlorophyll-derived dietary phototoxin and protoporphyria. *Proc. Natl. Acad. Sci. USA* **99**, 15649-15654 (2002).

10   Karg, C. A., Schilling, C. M., Allmendinger, L. & Moser, S. Isolation, characterization, and antioxidative activity of a dioxobilin-type phylloxanthobilin from savoy cabbage. *J. Porphyr. Phthalocyanines* **23**, 881-888 (2019).

11   Karg, C. A., Wang, P., Vollmar, A. M. & Moser, S. Re-opening the stage for Echinacea research - Characterization of phylloxanthobilins as a novel anti-oxidative compound class in Echinacea purpurea. *Phytomedicine* **60**, 152969 (2019).

12   Capelli, B. & Cysewski, G. Potential health benefits of spirulina microalgae. *Nutrafoods* **9** (2010).

13   McCarty, M. F. Clinical potential of Spirulina as a source of phycocyanobilin. *J. Med. Food.* **10**, 566-570 (2007).

14   Gil, M. I., Ferreres, F. & Tomás-Barberán, F. A. Effect of Postharvest Storage and Processing on the Antioxidant Constituents (Flavonoids and Vitamin C) of Fresh-Cut Spinach. *J. Agric. Food Chem.* **47**, 2213-2217 (1999).

15   Ilahy, R. *et al.* Pre- and Post-harvest Factors Affecting Glucosinolate Content in Broccoli. *Front. Nutr.* **7**, 147 (2020).

16   Pandrangi, S. & LaBorde, L. F. Retention of Folate, Carotenoids, and Other Quality Characteristics in Commercially Packaged Fresh Spinach. *J. Food Sci.* **69**, C702-C707 (2004).

17   Moser, S. *et al.* Blue Luminescence of Ripening Bananas. *Angew. Chem. Int. Ed.* **47**, 8954-8957 (2008).

18   Roiser, M. H., Müller, T. & Kräutler, B. Colorless Chlorophyll Catabolites in Senescent Florets of Broccoli (Brassica oleracea var. italica). *J. Agric. Food. Chem.* **63**, 1385-1392 (2015).

19   Kim, M. J. *et al.* Nutritional Value of Crisphead 'Iceberg' and Romaine Lettuces (Lactuca sativa L.). *J. Agric. Food Chem.* **Vol. 8, No. 11**, 1 (2016).

20   Kevers, C. *et al.* Evolution of Antioxidant Capacity during Storage of Selected Fruits and Vegetables. *J. Agric. Food Chem.* **55**, 8596-8603 (2007).

21   US Department of Agriculture, A. R. S. USDA National Nutrient Database for Standard Reference, Release 28 (Slightly revised). *Nutrient Data Laboratory* **Version Current: May 2016** (2016).

22   Ferruzzi, M. G., Böhm, V., Courtney, P. D. & Schwartz, S. J. Antioxidant and Antimutagenic Activity of Dietary Chlorophyll Derivatives Determined by Radical Scavenging and Bacterial Reverse Mutagenesis Assays. *J. Food Sci.* **67**, 2589-2595 (2002).

23   Bundesministerium für Ernährung und Landwirtschaft, Versorgungsbilanzen Obst, Gemüse, Zitrusfrüchte, Schalen- und Trockenobst. Versorgung mit Gemüse nach Arten. https://www.bmel-statistik.de/ernaehrung-fischerei/versorgungsbilanzen/ (2019).

24   Benzie, I. F. & Strain, J. J. The ferric reducing ability of plasma (FRAP) as a measure of "antioxidant power": the FRAP assay. *Anal. Biochem.* **239**, 70-76 (1996).
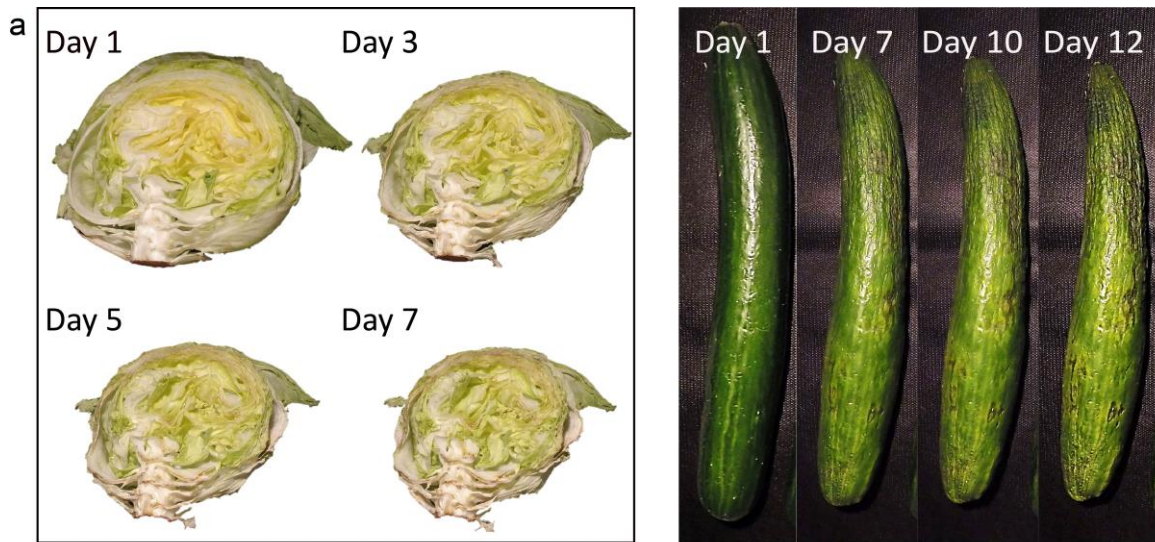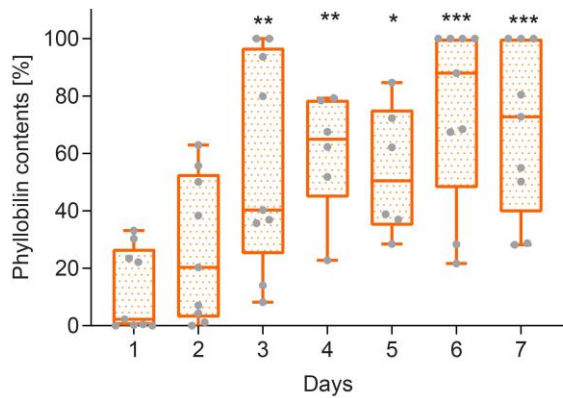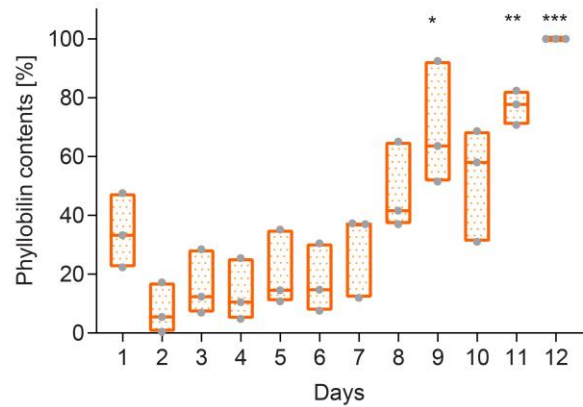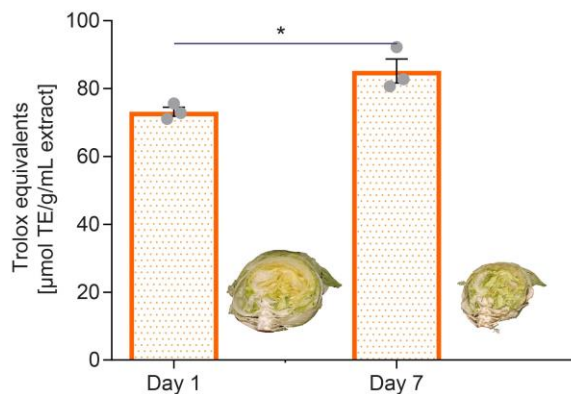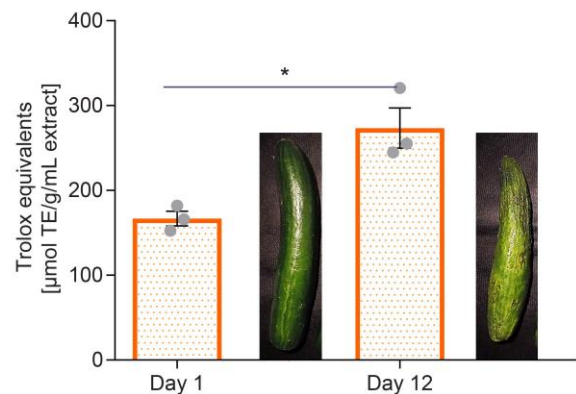
Figure 1: Analyses of stored greens. **a**) Snapshots of a time-lapse study (videos available as Supplementary Material) showing the aging progress of iceberg lettuce and cucumbers during home storage. **b**) Phyllobilin contents in lettuce and cucumbers significantly increased

with storage time (box-and-whiskers plot (lettuce): box 25-75 percentile, whiskers min-max, line at median; floating bars (cucumber): min-max, line at mean value; *p < 0.05, **p < 0.01, ***p < 0.001). **c**) End-of-storage extracts of the lettuce and cucumbers have significantly higher antioxidative *in vitro* activity compared to freshly bought produce. Values expressed relative to the antioxidant Trolox (*p<0.05). Mean values +/- s.e.m are shown.

a   Willingness to consume lettuce
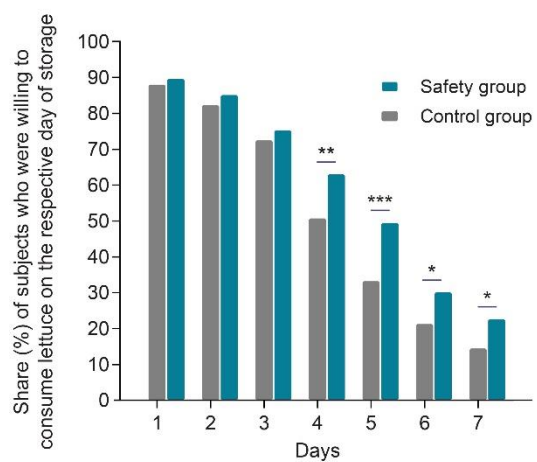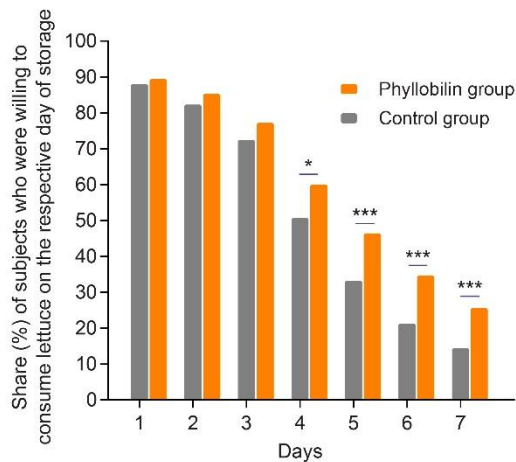
b   Health perception
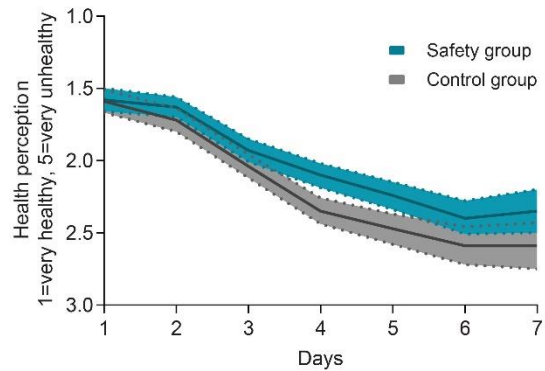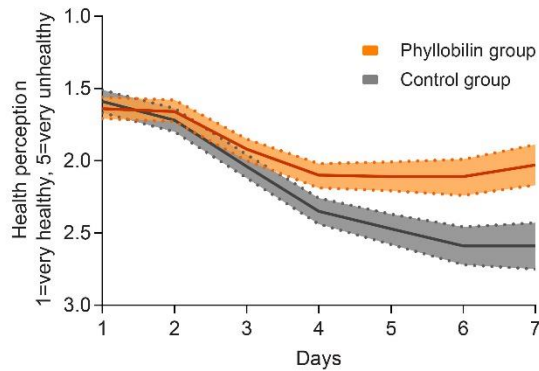
c   Safety perception
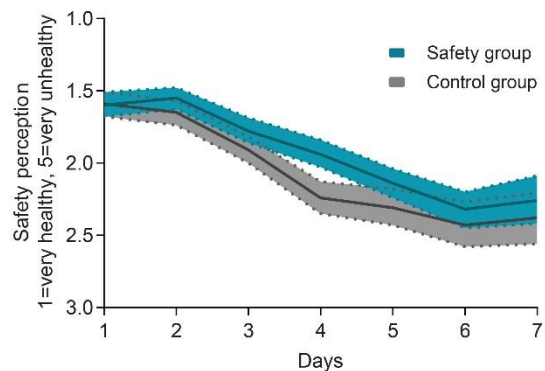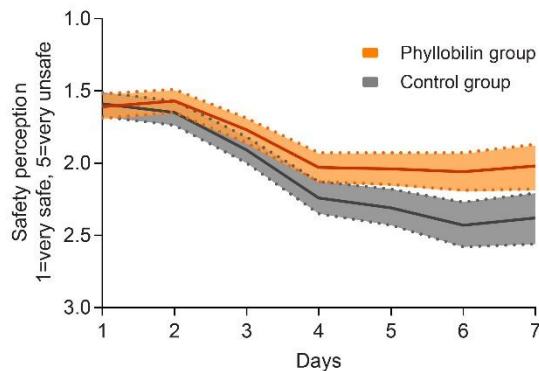
Figure 2: Results of consumer online experiment (N=1103). **a**) Share (%) of subjects in the phyllobilin and control condition (left panel) and safety and control condition (right panel) who stated to be willing to consume the lettuce on days 1 to 7 of storage (bars, *p < 0.05, **p < 0.01, ***p < 0.001, statistical analysis see Supplementary Table 3). **b**) Health and **c**) safety perception of the lettuce on a 5-point Likert scale on days 1 to 7 (mean values and 95% CI, statistical evaluation see Supplementary Tables 4, 5).

Rising levels of antioxidative phyllobilins in stored agricultural produce and their impact on consumer acceptance

Cornelia A. Karg[a], Christina M. Neubig[b], Jutta Roosen[b], Simone Moser[a,*]

[a]Pharmaceutical Biology, Department Pharmacy, Ludwig-Maximilians University of Munich, Butenandtstraße 5-13, D-81377 Munich, Germany

[b] Technical University of Munich, TUM School of Management, Chair of Marketing and Consumer Research, Alte Akademie 16, D-85354 Freising, Germany

*Email: simone.moser@cup.uni-muenchen.de

Supplementary Information

1. Supplementary Methods
2. Supplementary Figures
3. Supplementary Figures Consumer Study
4. Supplementary References

1. Supplementary Methods

1.1 Reagents and chemicals

HPLC grade acetonitrile (MeCN), methanol (MeOH), ethanol (EtOH), dimethylsulfoxide (DMSO), hydrochloric acid (HCl) and filter paper (110 mm pore size) were obtained from VWR International GmbH (Ismaning, Germany) and ultra-pure water (18MΩ.cm-1) from a Millipore S.A.S. Milli-Q Academic system (18,2 MΩ cm-1, Molsheim, France); 2,4,6-Tri(2-pyridyl)-s-triazine (TPTZ), potassium phosphate monobasic (KH_2PO_4), potassium phosphate dibasic (K_2HPO_4), ammonium acetate (NH_4AcO), iron(III) chloride ($FeCl_3$), hydrogen peroxide (30%) were from Merck KGaA (Darmstadt, Germany). Yeast extract, peptone and MEM Non-essential amino acid solution were obtained from Sigma-Aldrich (Taufkirchen, Germany) and collagen G from Biochrom AG (Berlin, Germany). Trolox was from Enzo Life Sciences GmbH (Lörrach, Germany), 2′,7′-dichlorodihydrofluorescein diacetate (H_2DCF-DA) and LB Broth Base were from Thermo Fisher (Waltham, MA, USA). DMEM medium was from PAN-Biotech GmbH (Aidenbach, Germany); MEM medium was from PromoCell (Heidelberg, Germany) and HEPES from AppliChem GmbH (Darmstadt, Germany). Fetal calf serum (FCS) was from PAA Laboratories GmbH (Pasching, Austria) and L-glutamine, agar and glucose were obtained from Carl Roth (Karlsruhe, Germany). Iceberg lettuce and cucumber were bought at a local supermarket and immediately used.

1.2 Chromatography

i) Analytical HPLC: Agilent 1260 Infinity II LC system with a 1260 Infinity Degasser, a 1100 Series quaternary pump and 1100 Series diode array detector; column: Phenomenex Hyperclone (ODS 5 μm, 250x4,6 mm i.d.) at 15°C protected by Phenomenex ODS 4x3 mm i.d. pre-column; injection volume: 100 μL, flow rate 0.5 mL/min. Solvent system: mobile phase A = 10 mM ammonium acetate in water, B = MeCN; Solvent composition A/B (v/v): 0-5 min: 95/5, 5-45 min: 95/5 to 40/60, 45-51 min: 40/60 to 0/100, 51-53 min: 0/100, 53-55 min: 0/100 to 95/5. Data were collected and processed using OpenLab CDS Data Analysis 2.3.

ii) Semi-preparative HPLC: Gynkotek LC-System with manual sampler, M480 pump, Phenomenex DG-301 online degasser, Gynkotek UVD 640 diode array detector and a Rheodyne injection valve with a 5 mL loop; column: Phenomenex Luna 5μm C18, 100 Å protected by Phenomenex pre-column ODS 9x16 mm, flow rate 2.5 mL/min. Solvent system: mobile phase A = 10 mM ammonium acetate in water, B = MeCN; solvent composition A/B (v/v): 0-2 min: 88/12, 2-12 min: 88/12 to 80/20, 12-30 min: 80/20 to 20/80, 30-40 min: 20/80 to 0/100. Data were collected and processed using Gynkosoft 5.50.

iii) Analytical HPLC LC/MS: Shimadzu HPLC system equipped with an LC-20AD pump, a DGU-20A5 online degasser unit and an SPD-M20A diode array detector, a Rheodyne injection valve with a 200 µl loop; column: Phenomenex Hyperclone (ODS 5 µm 250x4.6 mm i.d.), protected by Phenomenex ODS 4x3 mm i.d. pre-column; flow rate 0.5 mL/min. Solvent system: mobile phase A = 4 mM ammonium acetate in water, B = 4 mM ammonium acetate in MeOH; solvent composition A/B (v/v): 0-5 min: 80/20; 5-60 min: 80/20 to 0/100; 60-70 min: 0/100; 70-75 min: 0/100 to 80/20. Data were collected and processed using Shimadzu LC Solution software (version 1.24 SP1).

1.3 Spectroscopy

UV/Vis: λ_{max} [nm] (ε_{rel}), Thermo Spectronic Genesys 5 (336001) UV-Visible spectrophotometer. Concentrations of the PBs were calculated using log ε (312 nm) = 4.23 for the PleB[1], log ε (426 nm) = 4.51 for the PxB[2], and log ε (237 nm) = 4.49 for the iceberg lettuce fraction[3].

High resolution (HR) mass spectrometry (MS) (LC-HR MS system): ThermoScientific QExactive Orbitrap mass spectrometer, equipped with an ESI source (positive-ion mode, spray voltage 3.7 kV. Data were collected and processed with Xcalibur 4.1 software.

1.4   Time-lapse photography

To record the aging process of stored iceberg lettuce and cucumbers, iceberg lettuces were stored for seven days and cucumbers for twelve days at 22°C, 38 % RH, and protected from light, until the plant produce appeared wrinkly and de-greened but still edible. Pictures were taken during the storage every 90 min with a fixedly installed GoPro HERO4 camera. Data were processed using ImageJ 1.45s.

1.5   Determination of phyllobilin contents

Each day during the storage time of seven days for iceberg lettuce and twelve days for cucumber, samples of the same size of lettuce leaves and cucumber peels were collected and stored at -20°C until further use. Before analysis, samples were thawed, cut into halves and one part was used for the analysis of the phyllobilin contents. Photos of the specimens were taken with a Canon DS126181 camera and the areas of the samples were determined by using Matlab software R2018b. The samples were ground with 700 µL of MeOH/ potassium phosphate buffer 100 mM pH 7 (PBS) (20/80) in a mortar and centrifuged several times at 14000 rpm for 4 min, before an aliquot of 120 µL was analyzed by analytical HPLC. Phyllobilins were tentatively identified by their characteristic UV Vis online spectra[4] using a diode array detector and integrated with the Agilent software OpenLab CDS; further, identified phyllobilins

were confirmed by mass spectrometry (MS) and liquid-chromatography-high resolution mass-spectrometry (LC-HR MS). Peak areas of all detected phyllobilins were summarized, corrected for the differences of the area of each sample. A correction factor, which accounts for the loss of volume due to dehydration effects, was determined by analyzing the area of lettuce and cucumbers on the snap-shots of the time-lapse images by Matlab software R2018b. The values were multiplied with the calculated factor and normalized to the sum of all phyllobilins at the day with the highest PB amount. For iceberg lettuce three series with three lettuce each were performed; samples of one of the series were collected on day 1, 2, 3, 6 and 7. Three cucumbers were analyzed each day during storage.

1.6 Extraction of iceberg lettuce and cucumbers

Extracts of three iceberg lettuces and cucumbers at day 1, when they appeared fresh and green, and at the last day of storage (7 and 12, respectively) at a more aged and de-greened state, were prepared as follows: iceberg lettuces (without the stem) were weighed and crushed with a Kenwood CH580 Food Processor. The slurry was then extracted with 500 mL of ethanol and again mixed with a Braun hand blender Model MR 5000. The mixture was first filtered through a coffee filter and then again filtered through a filter paper (110 mm pore size). The residue was washed with 200 mL of ethanol and again filtered. Cucumbers were completely peeled; the peel was weighed and crushed with a Braun hand blender Model MR 5000 with 100 mL of ethanol. The mixture was filtered through a filter paper (110 mm pore size) and the residue was washed with 100 mL of ethanol. Extracts of iceberg lettuce and cucumber were stored at -20°C and used for determination of the *in vitro* antioxidative activity.

1.7 Isolation of phyllobilins from stored iceberg lettuce and cucumber

Iceberg lettuces and cucumbers used for the time-lapse photography studies were extracted after 7 and 12, respectively, days of monitoring the aging process. The lettuces and cucumber peels were crushed with a Kenwood CH580 Food Processor, mixed with 500 mL of ethanol each, and again crushed with a Braun hand blender Model MR 5000. The extracts were filtered through a coffee filter and dried on a rotary evaporator. The residue was re-dissolved in 20/80 MeOH/ PBS 100 mM pH 7 and centrifuged prior to purification by semi-preparative HPLC using a diode array detector. A phyllobilin-enriched fraction was isolated from the extract of iceberg lettuce (LF) and two phyllobilins, a phylloleucobilin (PleB) and a phylloxanthobilin (PxB), were isolated from the peels of cucumber. The purity of the PleB, the PxB and the lettuce fraction (LF) was confirmed by analytical HPLC. The samples were lyophilized, dissolved in DMSO and stored at -20°C until further use. The concentrations were determined spectrophotometrically by using the extinction factors as described above.

1.8   Cell culture

Human embryonic kidney derived HEK293 cells were obtained from the German Collection of Microorganisms and Cell Cultures (DSMZ) and Caco-2 cells were a kind gift of Prof. Wagner from the Chair of Pharmaceutical Biology and Biotechnology at the LMU Munich. HEK293 cells were cultured in DMEM Medium with 10% fetal calf serum (FCS) and Caco-2 cells in MEM Medium with 10% FCS, 1% non-essential amino acids (NEAA), 1 M HEPES and 1% glutamine. All cells were cultivated at a constant humidity with 5% CO_2 at 37 °C. The culture flasks and multiwell plates for HEK293 cells were coated with collagen G (0.001% in PBS).

1.9   Ferric Reducing Antioxidant Power (FRAP) assay

The Ferric Reducing Antioxidant Power (FRAP) assay allows for the determination of the antioxidant capacity of biological samples *in vitro* and was performed according to the protocol of Benzie et al.[5] with minor adaptations. Briefly, FRAP reagent was prepared freshly by combining 10 volumes of 300 mM acetate buffer pH 3.5, 1 volume of 10 mM TPTZ (2,4,6-Tri(2-pyridyl)-s-triazine) in 40 mM HCl and 1 volume of 20 mM iron(III)chloride. The prepared extracts or isolated compounds and varying concentrations of Trolox were incubated with FRAP reagent for 5 min at 37°C. The reduction of the Fe^{3+}-(TPTZ)$_2$-complex by a possible antioxidative activity is measured colorimetrically with a Tecan SpectraFluor plus microplate reader at 620 nm. A calibration curve with different Trolox concentrations was calculated and antioxidant potential of the extracts and isolated compounds was expressed as Trolox equivalents (µmol TE/µM or µmol TE/g/mL extract).

1.10   Detection of intracellular radical oxygen species (ROS)

The antioxidative activity of isolated phyllobilins in cells was determined as described[6] with minor modifications: In brief, cells were seeded in 96 well plates and allowed to adhere for 24 h. Then, diluted compounds (PleB 10, 20, 50 µM; PxB 10, 20 µM; LF 20, 50 µM) and a vehicle control were added to the cells and incubated for 24 h. Medium was discarded and cells were treated with H_2DCF-DA (10 µM) for 30 min, before washing cells with PBS +Ca^{2+}+ Mg^{2+} and adding hydrogen peroxide (1 mM) for 30 min. Cells treated with a vehicle control and without H_2O_2 served as negative control. The fluorescence of oxidized H_2DCF-DA, the highly fluorescent 2′,7′-dichlorofluorescein (DCF), was detected with a Tecan SpectraFluor plus microplate reader (excitation wavelength 485 nm; emission wavelength 530 nm). Data were normalized to the positive control, which was treated with hydrogen peroxide and a vehicle control.

1.11 Cell viability assay

Isolated phyllobilins were probed for their toxicity in cells. Thus, cell viability of treated HEK293 and Caco-2 cells was determined by a CellTiter-Blue® assay (Promega). The assay allows to determine cell viability as viable cells are able to reduce the dye resazurin into the fluorescent reagent resorufin and nonviable cells show reduced metabolic capacity, which results in a reduced or no fluorescence signal. Cells were treated as described above with isolated compounds for 24 h. 4 h before the end of stimulation time, CellTiter-Blue® reagent was added and after 4 h of incubation at 37°C, fluorescence of resorufin at 590 nm was measured with a Tecan SpectraFluor plus microplate reader. The number of viable cells was normalized to a DMSO control.

1.12 Alkaline comet assay

Oxidative and environmental stress in cells often leads to degradation and oxidation of genomic DNA. The alkaline comet assay was performed as a biomarker to confirm that isolated phyllobilins cause no genotoxic effects. A commercial Comet SCGE assay kit from Enzo Life Sciences GmbH (Lörrach, Germany) was used, which detects DNA damage by determination of the integrity of DNA release from cells immobilized in agarose. When DNA gets fragmented, the small parts move more easily in the gel than undamaged DNA, which creates a characteristic "comet" shaped tail. With a specific dye, nucleic acid can be stained and tail formation can be analyzed by CometScore software and compared to controls. Cells were treated with PxB (20 µM), PleB (50 µM), LF (50 µM) and a vehicle control for 24 hours. H_2O_2 treated cells (4°C, 20 min) served as a positive control. Cells were then seeded in low melting agarose at 37°C on pre-coated glass slides and lysed overnight in lysis buffer at 4 °C. Slides were incubated in alkaline solution electrophoresis was performed at 35V, 300mA for 30min in alkaline electrophoresis buffer. Glass slides were washed in water, fixed in 70% ethanol for 5 min and completely dried. DNA was then stained with CYGREEN® Nucleic acid dye for 30 min in the dark before slides were washed and again dried at 37°C. Images were taken with a Leica TCS SP8 SMD microscope (Leica Microsystem, Wetzlar, Germany). Additionally, tail moments (% DNA in tail * tail length) of 20 cells per condition were analyzed with CometScore.

1.13 Microbial load

The microbial load of iceberg lettuce and cucumber was determined to confirm that even after seven days or twelve days of storage, the plant produce showed no increased microbial contamination and could still be safely consumed. Three iceberg lettuces and cucumbers were bought at a local supermarket and microbial load was assessed at day 1 and day 7 for the lettuce and at day 1 and day 12 for the cucumber as follows: Vegetables were washed

thoroughly. A small piece of the outer leaf of each lettuce and a small slice of each cucumber was weighed under sterile conditions. Each sample was soaked in 15 mL of sterile water for 30 min and the solution was diluted 1:100 or 1:10 before three aliquots of 100 µL of each sample were inoculated on plates with LB medium (2% LB broth base, 3.2% agar) and Yeast Extract–Peptone–Dextrose (YPD) medium (1% yeast extract, 2% peptone, 2% agar, 20% glucose). LB medium was used to cultivate bacteria and YPD medium to cultivate fungi. Plates were incubated at 29°C for 24 h for lettuce and 68 h for cucumber, colonies were counted, and Colony Forming Units (CFU) per mL, corrected for the weight of the sample, were calculated.

1.14   Statistics

All experiments were performed three times in triplicates unless stated otherwise. The data represent means ± SEM. Statistical differences were assessed by using an unpaired t-test, a one-way analysis of variance with post hoc analysis using Dunnett's multiple comparison test. Statistical analyses were carried out with GraphPad Prism software version 7.05.

2.   Supplementary Figures

Phyllobilins (PBs) are linear tetrapyrroles, which arise from the degradation of the green plant pigment chlorophyll. Scheme 1 shows the most important phyllobilin core structures, which are generated during chlorophyll degradation: a phylloleucobilin (PleB) or non-fluorescent chlorophyll catabolite (NCC), which was the first elucidated structure of chlorophyll catabolites and was found to accumulate in the vacuoles of the plant cell; a phylloxanthobilin (PxB) or yellow chlorophyll catabolite (YCC), first characterized in 2008 and representing an oxidation product of the PleB; and a dioxobilin-type PleB (DPleB), resulting from another branch of chlorophyll breakdown and carrying a lactam group instead of an aldehyde moiety at the north-eastern hemisphere[4].
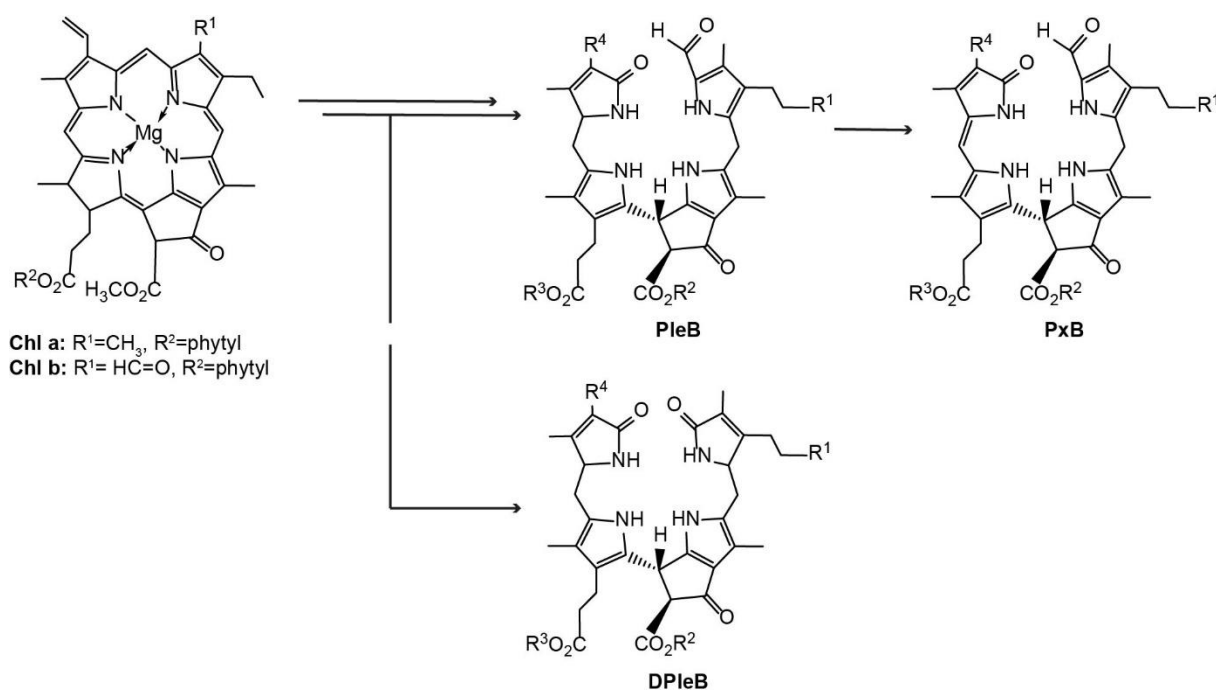
Supplementary Figure 1: Overview of phyllobilin key structures formed during chlorophyll breakdown.

Since the first structure of a PB was elucidated in 1991, more than 30 constitutionally different structures were identified, which, however, all share the same tetrapyrrolic core pattern. The extensive characterization of PBs by mass spectrometry led to the creation of a MS database and mass spectrometry was established as tool for the structural elucidation of PBs with known modification patterns[7,8]. Therefore, phyllobilins in extracts of iceberg lettuce and cucumber were identified by liquid-chromatography-high resolution mass-spectrometry (LC-HR MS), due to characteristic UV Vis spectra and known mass patterns from the library.
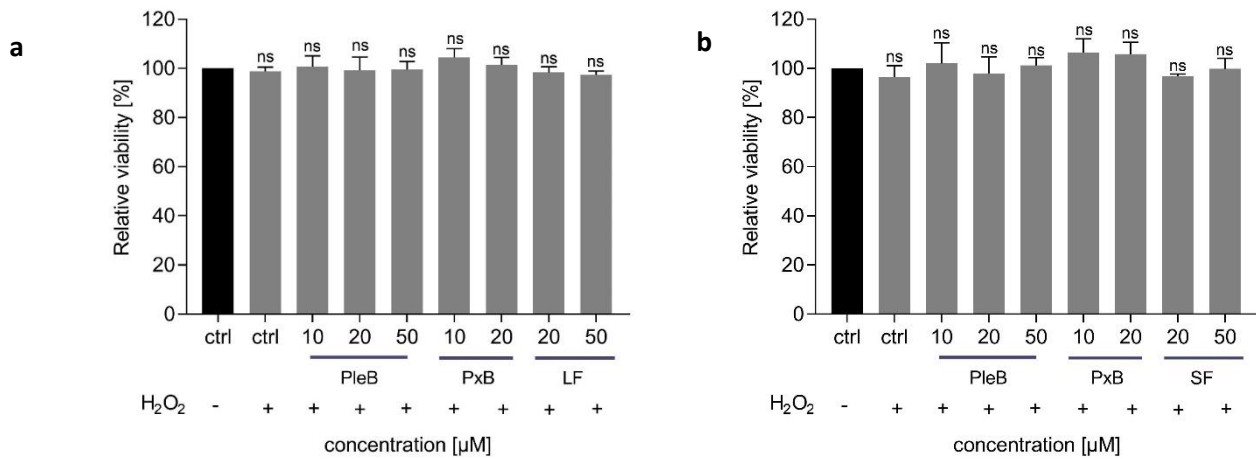
Supplementary Figure 2. Isolated phyllobilins do not alter cell viability at indicated concentrations. Cell viability was determined by a CellTiter-Blue® assay in HEK293 (**a**) and Caco-2 (**b**) cells. Values represent mean ± SEM of three independent experiments. One-Way ANOVA followed by Dunnett's multiple comparison test, *p < 0.05, **p < 0.01, ***p < 0.001, ns = not significant.
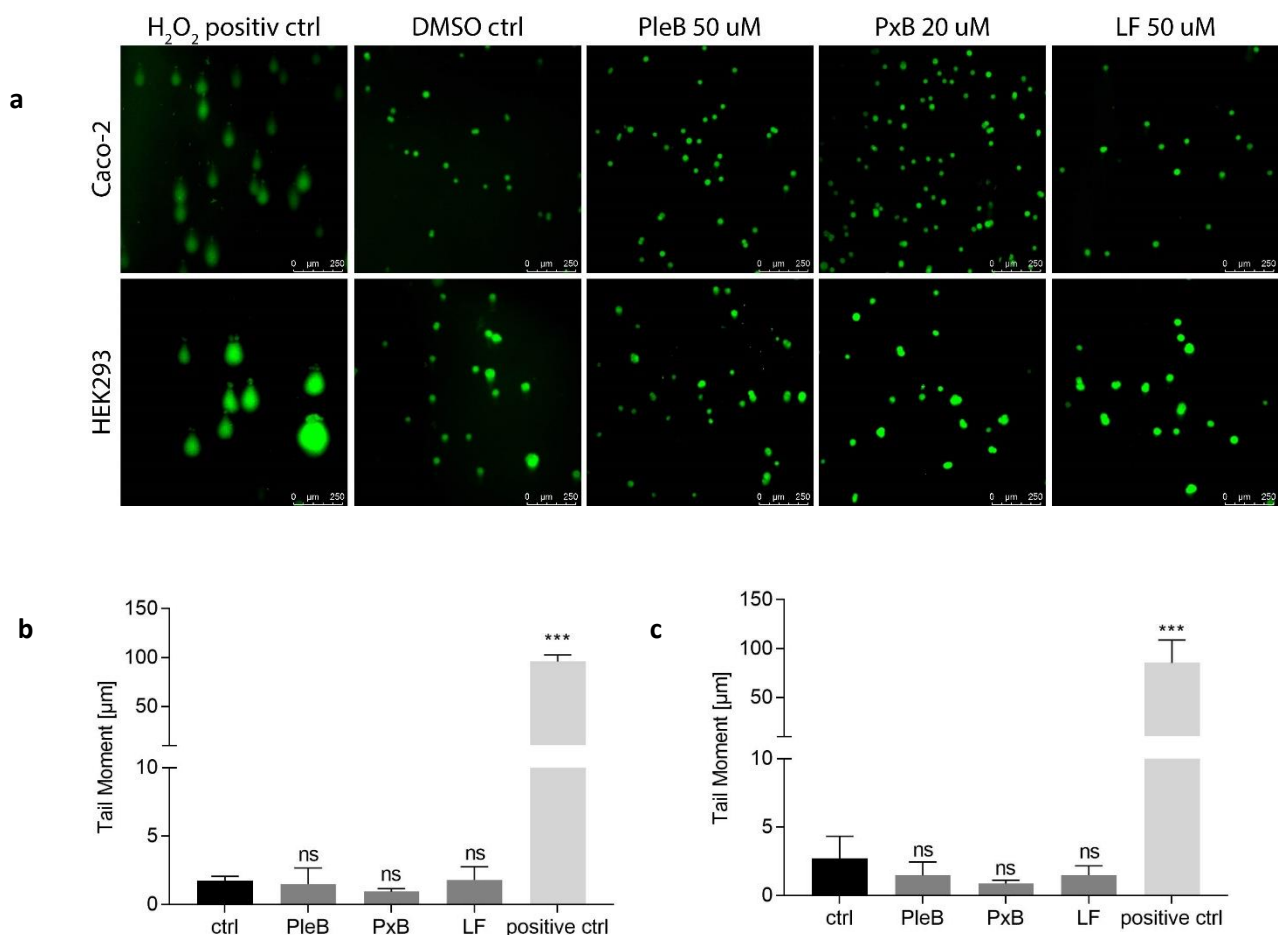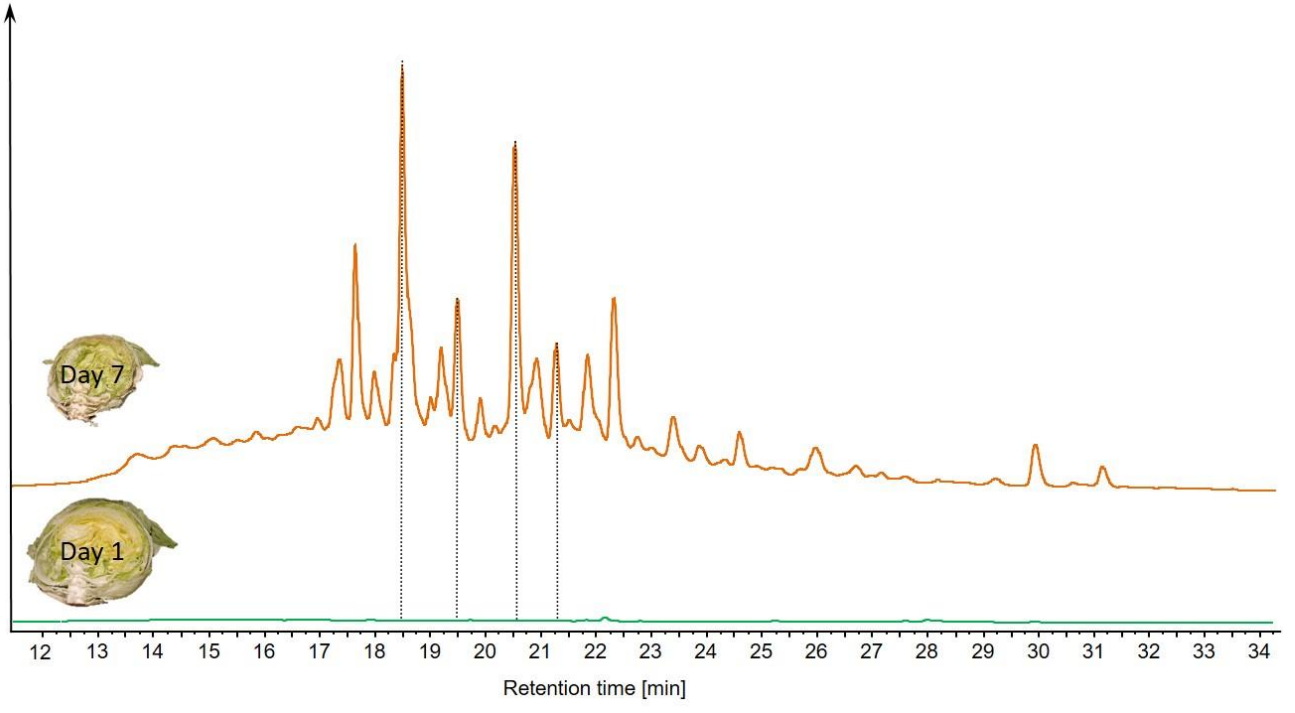

Supplementary Figure 3: Isolated phyllobilins show no DNA damaging effects. Isolated PleB (50 µM) and PxB (20 µM) from cucumber peels and a phyllobilin enriched fraction (LF) (50 µM) from iceberg lettuce were tested for a possible genotoxic effect using an alkaline comet

assay in HEK293 and Caco-2 cells. In contrast to the positive control, which was treated with hydrogen peroxide for 20 min at 4 °C, isolated PBs showed no effect on DNA fragmentation. Three independent experiments were performed (one representative image is shown, **a**). Additionally, tail moments (% DNA in tail * tail length) of 20 cells per condition were analyzed with CometScore in HEK293 (**b**) and Caco-2 (**c**) cells. One-Way ANOVA followed by Dunnett's multiple comparison test, ***p < 0.001, ns = not significant.
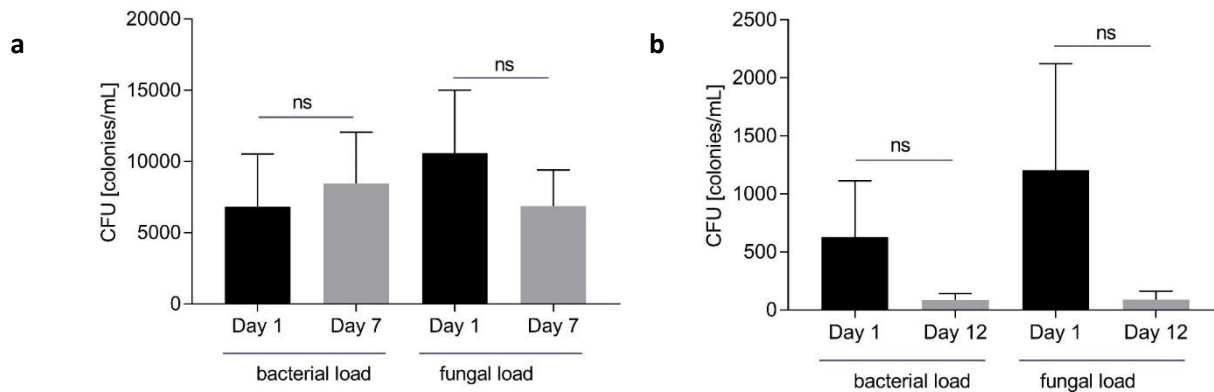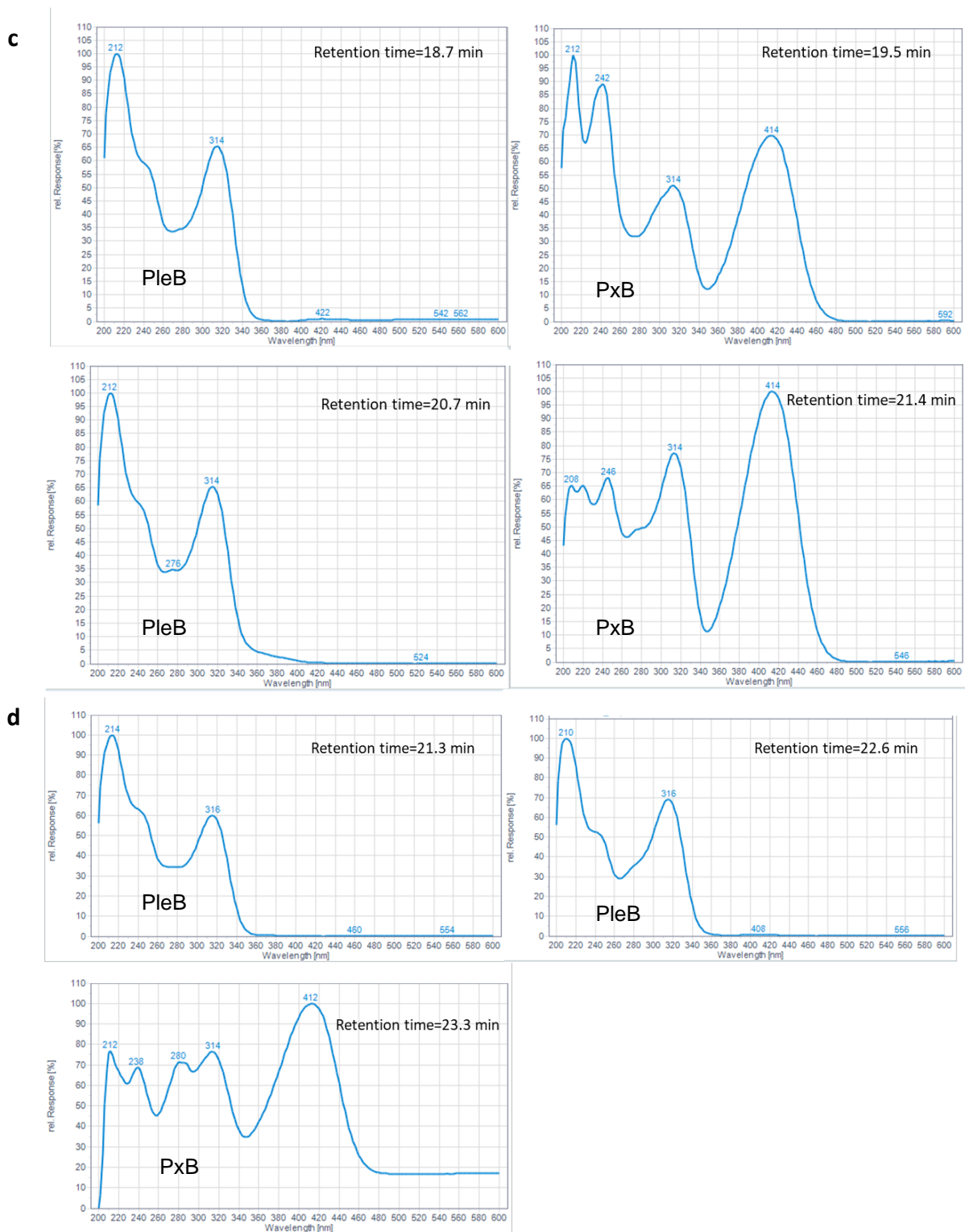

Supplementary Figure 4: Stored iceberg lettuce and cucumber show no increased microbial load. A piece of iceberg lettuce (**a**) and cucumber (**b**) at day 1 and at the last day of storage time was soaked in sterile water for 30 min. The solution was inoculated on agar plates for bacterial growth and fungal growth and incubated for 24 h (iceberg lettuce) and 68 h (cucumber) at 29 °C. Colonies were counted and colony-forming units (CFU) per mL were calculated and corrected for the weight of the respective sample (Unpaired t-test p< 0.05).

a

Day 7

Day 1

Retention time [min]

b

Day 12

Day 1

Retention time [min]
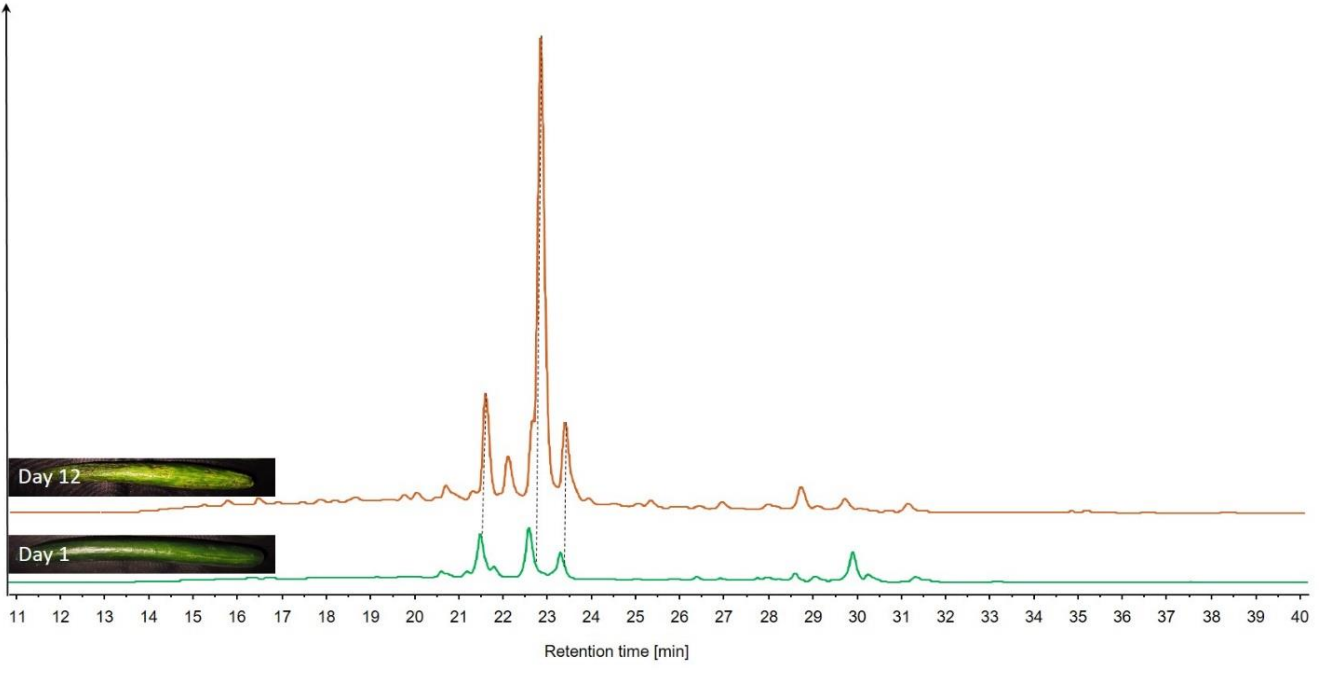
Supplementary Figure 5: Phyllobilin content increases with storage time and progressive age of iceberg lettuce and cucumber. Analytical HPLC traces of extracts of iceberg lettuce (**a**) of day 1 and day 7 and cucumber peels (**b**) of day 1 and day 12 and UV Vis online spectra of identified phyllobilins for iceberg lettuce (**c**) and cucumber (**d**). Iceberg lettuce and cucumber were stored at room temperature and light protected until a progressed aging of the vegetables, although the plant produce still appeared edible. Phyllobilins were tentatively identified by their characteristic UV Vis online spectrum[4] using a diode array detector and

confirmed by LC-HR MS; phyllobilin signals are highlighted with dashed lines. Chromatograms show detection at 320 nm.
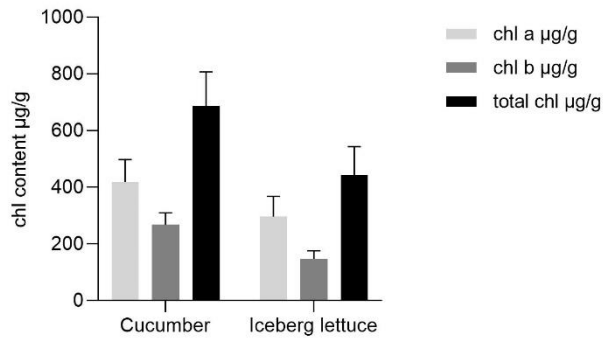

Supplementary Figure 6: Chlorophyll a, chlorophyll b, and total chlorophyll contents in freshly bought cucumber and iceberg lettuce. Samples of cucumber peel and iceberg lettuce of equal weight were extracted four times with 1 ml of 80% acetone containing 1mM KOH[9]. Extracts were combined and chlorophyll content was determined spectrophotometrically as described[10]. For a rough estimation of the chlorophyll content, experiment was performed in triplicates of one specimen each.

b
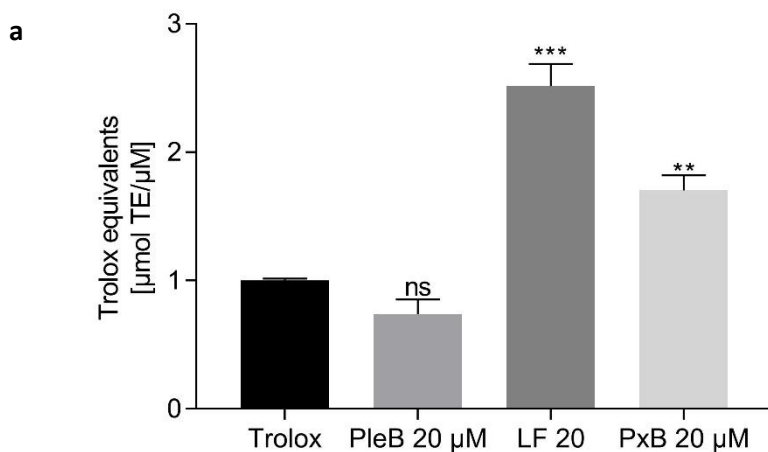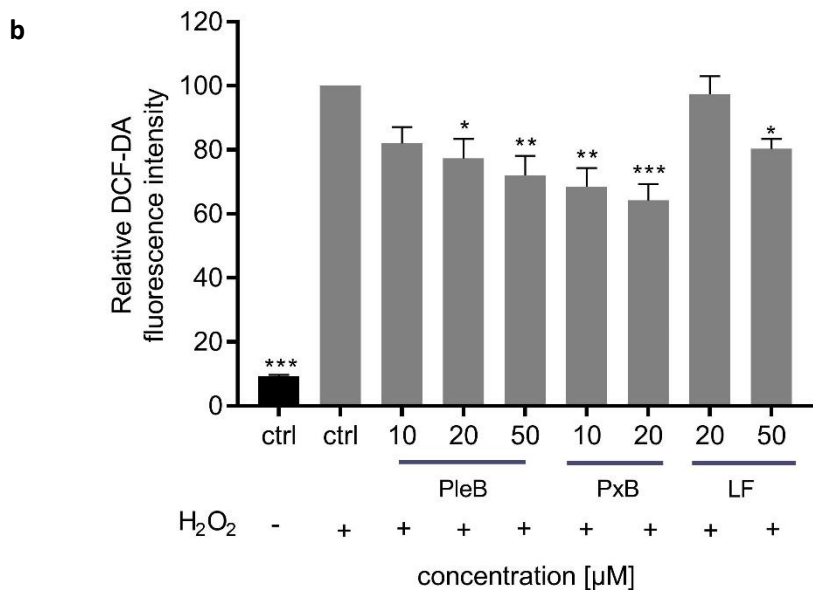
Supplementary Figure 7: Phyllobilins possess antioxidative activities. (**a**) *In vitro* antioxidative potential of a phylloleucobilin (PleB) and a phylloxanthobilin (PxB), isolated from de-greened cucumber peels as described in the materials section, and a phyllobilin-enriched fraction (LF) isolated from aged iceberg lettuce (LF). Antioxidant power was determined by FRAP assay with Trolox as a control and expressed as Trolox equivalents (µmol TE/µM). Phyllobilins showed similar or higher antioxidative activity as the vitamin E derivative Trolox, known for its strong antioxidative effects. One-Way ANOVA followed by Dunnett's multiple comparison test, **$p < 0.01$, ***$p < 0.001$, ns = not significant. (**b**) Phyllobilins show *in cellulo* antioxidative activity by scavenging intracellular oxidative stress in a dose dependent manner. HEK293 cells were incubated with PleB, PxB or LF at indicated concentrations for 24 h before stimulating with 1 mM H_2O_2. ROS scavenging activity was determined by the prevented oxidation of the intracellular fluorescein derivative H_2DCF into highly fluorescent DCF. One-Way ANOVA followed by Dunnett's multiple comparison test, *$p < 0.05$, **$p < 0.01$, ***$p < 0.001$.
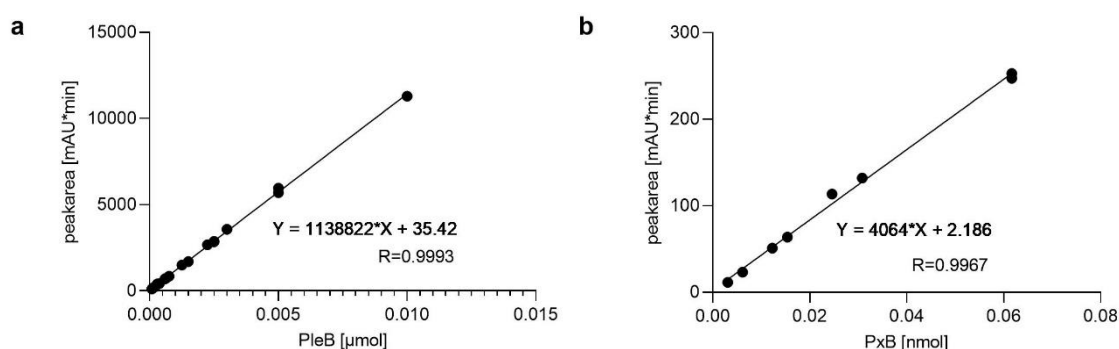
Supplementary Figure 8: Calibration linear of PleB (A) and PxB (B). Different concentrations of PleB and PxB were analyzed by analytical HPLC to fit a calibration linear of PleB and PxB, which were used to estimate the maximum phyllobilin content in cucumber peels and iceberg lettuce after storage, respectively.
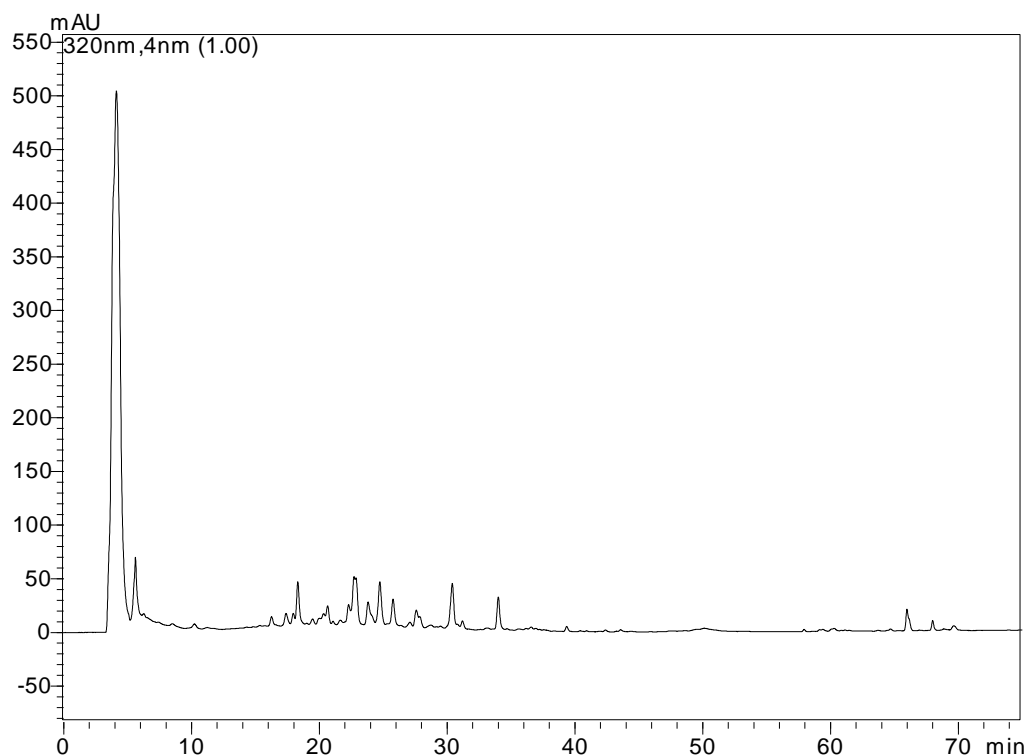
Supplementary Figure 9: HPL-chromatogram of iceberg lettuce recorded during LC-HR MS analysis. Lettuce was stored for seven days in the dark and extracted as described in the methods section. (Detection at 320 nm)
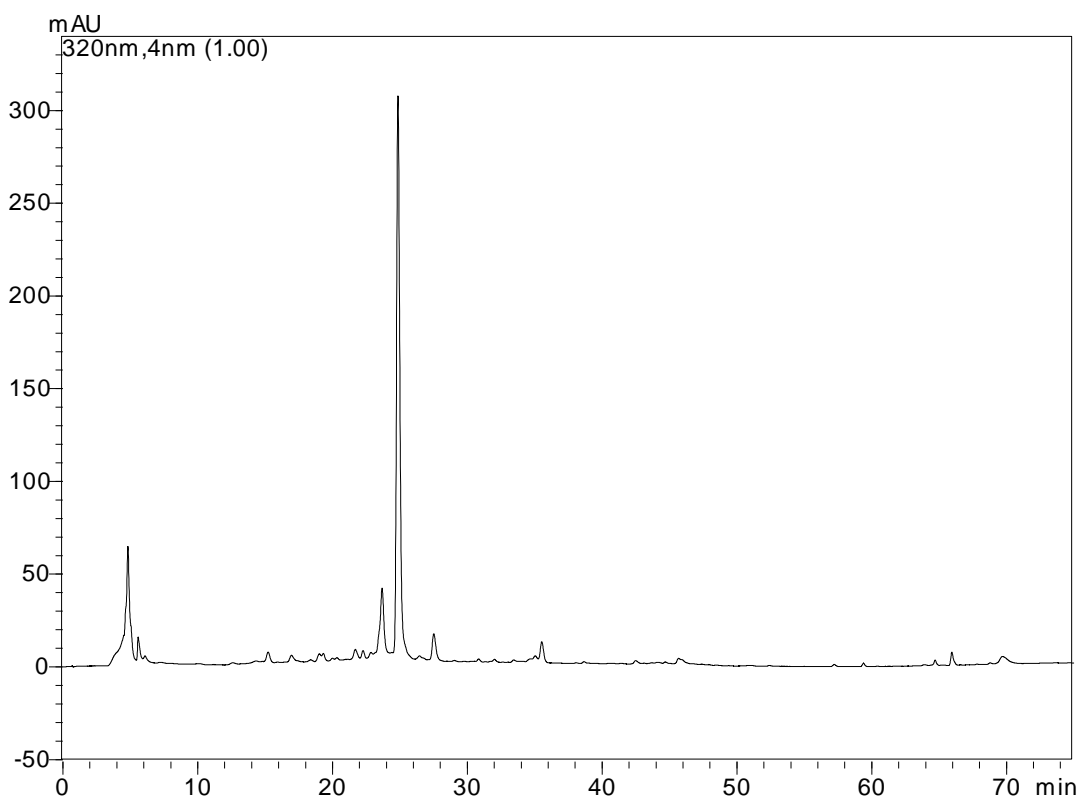
Supplementary Figure 10: HPL-chromatogram of cucumber peels recorded during LC-HR MS analysis. Cucumber was stored twelve days in the dark and the peel was extracted as described in the methods section. (Detection at 320 nm)

Source	type	Retention time LC-HR MS	Retention time LC	R1	R2	R3	R4	published PleB structures	published PxB structures
iceberg lettuce	PleB	14,45	20,7	O-Glc	CH$_3$	H	CH(OH)-CH$_2$OH	Zm-PleB-1, Tc-PleB-1, Co-PleB-1, Ug-PleB-27, Pd-PleB-35	
	PxB	14,9	21,4	O-Glc	CH$_3$	H	CH(OH)-CH$_2$OH		Tc-PxB-1, Ep-PxB-2
	PxB		19,5	O-(6'-OMal)Glc	CH$_3$	H	CH(OH)-CH$_2$OH		Ep-PxB-1
	PleB	9,58	18,7	O-(6'-OMal)Glc	CH$_3$	H	CH(OH)-CH$_2$OH		

Source	type	Retention time LC-HR MS	Retention time LC	R1	R2	R3	R4	published PleB structures	published PxB structures
Cucumber	PleB	13,73	21,3	O-Glc	CH$_3$	H	CH(OH)-CH$_2$OH	Zm-PleB-1, Tc-PleB-1, Co-PleB-1, Ug-PleB-27, Pd-PleB-35	
	PleB	15,9	22,6	OH	CH$_3$	H	CH(OH)-CH$_2$OH	So-PleB-2, Mc-PleB-42, Pd-PleB-40, Cl-PleB-2, Ej-PleB-1	
	PxB	19,65	23,3	OH	CH$_3$	H	CH(OH)-CH$_2$OH		Ep-PxB-3

Supplementary Table 1: Identified phyllobillins by UV Vis online spectra and LC-HR MS analysis. (R[1-4] see Scheme 1; *Zm=Zea mays*, *Tc=Tilia cordata*, *Co=Cydonia oblonga*, *Ug=Ulmus glabra*, *Pd=Prunus x domestica*, *Ep=Echinacea purpurea*, *So=spinacia oleracea*, *Mc=Musa cavendish*, *Ej=Eribotrya japonica*)

3. Supplementary Figures Consumer Study

3.1 Tables and Figures

	Total	Control	Safety	Phyllobilin
Gender in %				
Female	50.6	49.0	50.5	52.2
Male	49.3	51.0	49.5	47.5
Other	0.1	0.0	0.0	0.3
Age in %				
18 – 22	4.9	5.2	5.1	4.4
23 – 35	19.4	19.1	18.1	21.2
36 – 55	37.0	37.3	38.8	34.7
56 +	38.7	38.4	38.0	39.7
Education in %				
No education completed (yet)	1.7	1.7	1.6	1.7
Primary education	32.4	31.0	32.3	33.8
Secondary education	32.0	31.9	32.1	32.1
University entrance qualification	33.9	35.5	34.0	32.4
Household Size in %				
1	33.1	33.8	32.2	33.3
2	39.8	37.3	38.6	43.6
3	14.0	15.3	15.2	11.4
4 +	13.1	13.6	14.1	11.7
Income in %				
Less than 1500€	27.4	24.6	29.7	27.9
1500 – 2500€	28.5	30.3	24.1	31.1

2500 – 3500€	19.5	17.6	22.7	18.0
3500 – 4500€	14.8	16.5	14.0	14.0
4500 – 5500€	6.2	6.9	5.9	5.8
More than 5500€	3.6	4.0	3.6	3.2
Region in %				
Baden-Württemberg	12.6	12.8	13.3	11.7
Bavaria	15.0	13.9	16.2	15.0
Berlin	4.6	3.5	5.9	4.4
Brandenburg	3.0	4.4	2.4	2.2
Bremen	0.8	0.5	1.1	0.8
Hamburg	3.3	2.5	4.5	2.8
Hesse	7.3	7.1	6.9	7.8
Mecklenburg Western Pomerania	2.0	3.0	1.9	1.1
Lower Saxony	10.0	12.0	8.2	9.7
Northrhine-Westphalia	21.8	22.3	19.7	23.3
Rhineland Palatinate	4.1	3.8	4.3	4.2
Saarland	1.8	2.5	0.5	2.5
Saxony	5.5	4.6	6.9	5.0
Saxony-Anhalt	2.5	2.7	2.1	2.8
Schleswig-Holstein	2.7	2.2	2.7	3.3
Thuringia	3.0	2.2	3.5	3.3

Supplementary Table 2: Sample Description (Total and Conditions)
a

Number of days on which subjects were willing to consume the lettuce (ANOVA):

	N	Mean	SD	95%-CI	F	p
Control	367	3.62	2.15	3.40; 3.84		
Safety	376	4.15	2.26	3.92; 4.38		
Phyllobilin	360	4.19	2.31	3.95; 4.43		
Total	1103	3.99	2.25	3.85; 4.12	7.270	0.001

b

Significance of Mean Differences (MD) between Groups Post-hoc Test:

		MD	p
Control	**Safety**	-.53[*]	0.004
	Phyllobilin	-.56[*]	0.002
Safety	**Phyllobilin**	-.03	0.976

* The difference is significant on the 1% level

Supplementary Table 3: Main Effect Information Treatment. (**a**) Means, Standard Deviations (SD), 95%-Confidence Interval (CI) of the Mean and Results from One-way Analysis of Variance (ANOVA). (**b**) Post-hoc Test for the Main Effect (Tukey-HSD).

Day	Condition	N	Mean	SD	95%-CI	F	p
1	Control	367	1.59	0.80	1.51; 1.67		
	Safety	376	1.58	0.78	1.50;1.66		
	Phyllobilin	360	1.64	0.73	1.56; 1.71		
	Total	1103	1.60	0.77		0.588	0.555
2	Control	323	1.72	0.72	1.64; 1.80		
	Safety	337	1.63	0.66	1.56; 1.70		
	Phyllobilin	322	1.66	0.65	1.58; 1.73		
	Total	982	1.67	0.68		1.587	0.205
3	Control	302	2.04	0.71	1.96; 2.12		
	Safety	320	1.93	0.75	1.85; 2.01		
	Phyllobilin	307	1.92	0.65	1.85; 2.00		
	Total	929	1.96	0.70		2.894[a]	0.056
4	Control	266	2.35 (a)	0.78	2.26; 2.44		
	Safety	283	2.10 (b)	0.73	2.02; 2.19		
	Phyllobilin	278	2.10 (b)	0.76	2.02; 2.19		
	Total	827	2.18	0.76		9.217[a]	0.000
5	Control	186	2.47 (a)	0.72	2.37; 2.58		
	Safety	237	2.24 (b)	0.75	2.15; 2.34		
	Phyllobilin	216	2.11 (b)	0.76	2.01; 2.21		
	Total	639	2.27	0.76		11.868	0.000
6	Control	122	2.59 (a)	0.74	2.46; 2.72		
	Safety	186	2.40 (a)	0.80	2.28; 2.51		
	Phyllobilin	167	2.11 (b)	0.80	1.99; 2.24		
	Total	475	2.35	0.81		13.612	0.000
7	Control	78	2.59 (a)	0.71	2.43; 2.75		
	Safety	113	2.35 (a)	0.80	2.20; 2.50		
	Phyllobilin	125	2.03 (b)	0.79	1.89; 2.17		
	Total	316	2.28	0.81		13.097	0.000

Supplementary Table 4: Health Perception of Lettuce by Group on Days 1 to 7: Means, Standard Deviations (SD), 95%-Confidence Interval (CI) of the Mean and Results from One-way ANOVA incl. Post-hoc Test. Scale: 1 = very healthy to 5 = very unhealthy.
[a] Welch's F used for data that violated the assumption of homogeneity of variance
(a) (b) – different letters indicate significant mean differences ($p<.05$) between the respective groups, evaluated by Tukey-HSD Post-hoc Test (for data that violated the assumption of homogeneity of variance Games Howell Post-hoc Test was used).

Day	Condition	N	Mean	SD	95%-CI	F	p
1	Control	367	1.59	0.81	1.51; 1.68		
	Safety	376	1.60	0.83	1.51; 1.68		
	Phyllobilin	360	1.61	0.81	1.52; 1.69		
	Total	1103	1.60	0.81	1.55; 1.65	0.029	0.971
2	Control	323	1.65	0.76	1.57; 1.74		
	Safety	337	1.55	0.70	1.48; 1.63		
	Phyllobilin	322	1.57	0.70	1.49; 1.65		
	Total	982	1.59	0.72	1.55; 1.64	1.815	0.163
3	Control	302	1.91	0.81	1.82; 2.00		
	Safety	320	1.78	0.78	1.69; 1.86		
	Phyllobilin	307	1.77	0.75	1.69; 1.86		
	Total	929	1.82	0.78	1.77; 1.87	3.055	0.048
4	Control	266	2.24 (a)	0.89	2.13; 2.35		
	Safety	283	1.94 (b)	0.79	1.84; 2.03		
	Phyllobilin	278	2.03 (b)	0.85	1.93; 2.13		
	Total	827	2.07	0.85	2.01; 2.12	9.082^a	0.000
5	Control	186	2.31 (a)	0.87	2.18; 2.43		
	Safety	237	2.14	0.79	2.04; 2.24		
	Phyllobilin	216	2.04 (b)	0.82	1.93; 2.15		
	Total	639	2.15	0.83	2.09; 2.22	5.092^a	0.007
6	Control	122	2.43 (a)	0.85	2.27; 2.58		
	Safety	186	2.32 (a)	0.85	2.20; 2.45		
	Phyllobilin	167	2.06 (b)	0.84	1.93; 2.19		
	Total	475	2.26	0.86	2.18; 2.33	7.531	0.001
7	Control	78	2.38 (a)	0.76	2.21; 2.56		
	Safety	113	2.26	0.87	2.09; 2.42		
	Phyllobilin	125	2.02 (b)	0.89	1.87; 2.18		
	Total	316	2.20	0.87	2.10; 2.29	4.709	0.010

Supplementary Table 5: Safety Perception of Lettuce by Group on Days 1 to 7: Means, Standard Deviations (SD), 95%-Confidence Interval (CI) of the Mean and Results from One-way ANOVA incl. Post-hoc Test. Scale: 1 = very safe to 5 = very unsafe.
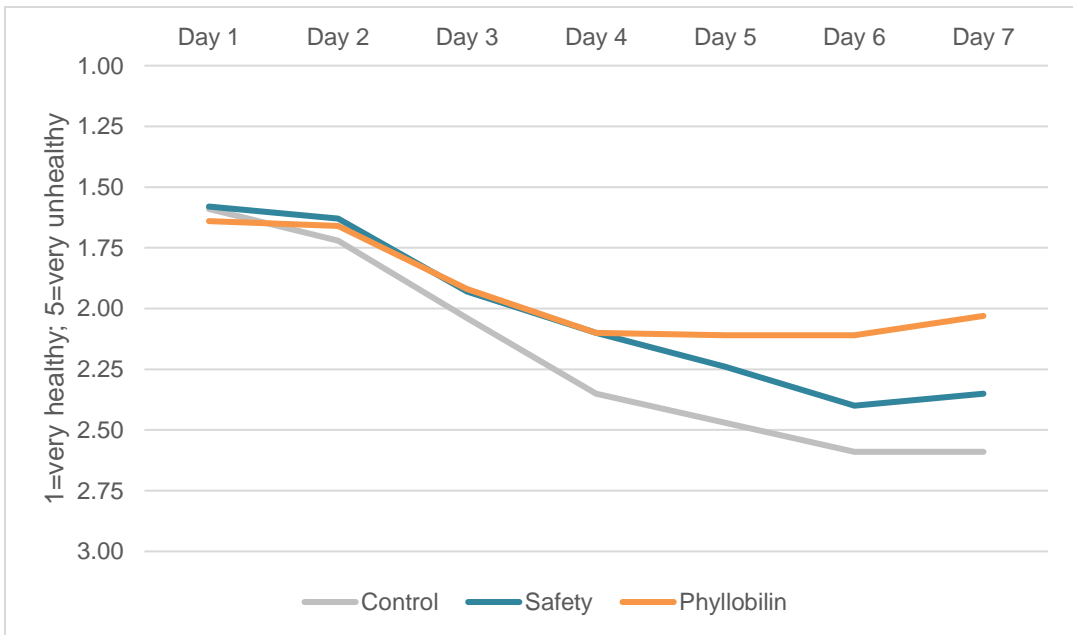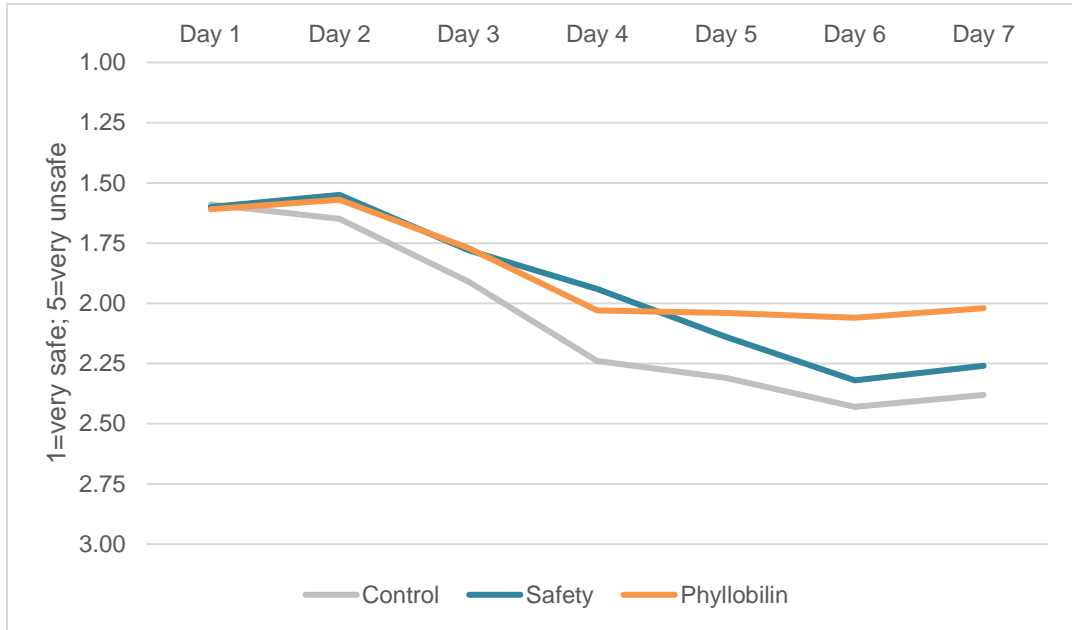
[a] Welch's F used for data that violated the assumption of homogeneity of variance

(a) (b) – different letters indicate significant mean differences (p<.05) between the respective groups, evaluated by Tukey-HSD Post-hoc Test (for data that violated the assumption of homogeneity of variance Games Howell Post-hoc Test was used).

a
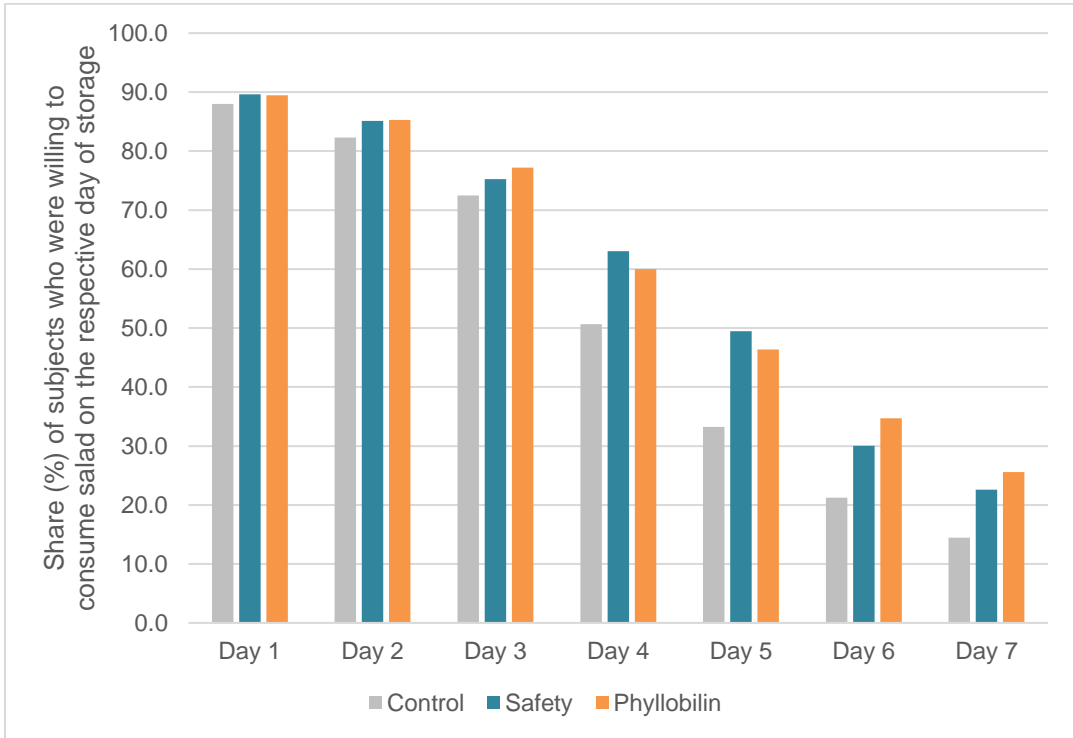
b

c

Supplementary Figure 11: Graphical Depiction of Results for Phyllobilin, Safety and Control Condition. (**a**) Share (%) of subjects in the phyllobilin, safety and control condition who stated to be willing to consume the lettuce on days 1 to 7 of storage. (**b**) Health perception of the lettuce (on 5-point Likert scale) on days 1 to 7 of storage by group. (**c**) Safety perception of the lettuce (on a 5-point Likert scale) on days 1 to 7 of storage by group.

3.2 Picture Material of the Lettuce shown to Subjects (one picture for each day)

Tag 1

Tag 2

Tag 3

Tag 4

Tag 5

Tag 6

Tag 7

3.3 Extract from the Consumer Questionnaire: Questions regarding willingness to consume lettuce, health perception, and safety perception.

<u>Example Day 1</u>
(Questions were repeated for each day, until subject stated to no longer be willing to eat the lettuce)

What do you think – how healthy or unhealthy is this lettuce?
o   Very healthy
o   Rather healthy
o   Neither
o   Rather unhealthy
o   Very unhealthy

In terms of potential health risks, how safe or unsafe would you consider it to eat this lettuce?
o   Very safe
o   Rather safe
o   Neither
o   Rather unsafe
o   Very unsafe

Would you still eat the lettuce?
o   Yes
o   No
o   Don't know

3.4 Information Treatments provided to subjects before they answered the lettuce questions (see F.). Above the info, there was a time-lapse video of the lettuce aging over 7 days.

3.4.1 Control Treatment

The video (no sound) uses the example of lettuce to show how foods may change with ripening and aging. At the top left you can see the respective day and time.

As green foods, such as lettuce, age, the green pigment (chlorophyll) in the plant cells is broken down.

Chlorophylls are color pigments that are responsible for the absorption of light during photosynthesis and thus for the conversion of light energy into chemical energy. In this process, carbon dioxide and water are turned into oxygen and sugar. Chlorophylls are therefore essential components of one of the most important processes on earth, without which higher life would not be possible.

The amount of chlorophyll in the plant cells changes with the aging process. The result can be seen in the video: With the breakdown of chlorophyll, the lettuce becomes less and less green over time and takes on a brownish color.

3.4.2 Phyllobilin Treatment

The video (no sound) uses the example of lettuce to show how foods may change with ripening and aging. At the top left you can see the respective day and time.

As green foods, such as lettuce, age, the green pigment (chlorophyll) in the plant cells is broken down. As you can see in the video, the lettuce becomes less and less green over time and takes on a brownish color.

However, other chemical substances are produced during the breakdown of the green pigment. Among them are so-called phyllobilins. Phyllobilins are powerful antioxidants that protect our cells from oxidative stress. Oxidative stress can occur, for example, through inflammatory processes or environmental influences such as UV radiation or exhaust gases and contribute to the development of many different diseases. Antioxidants help our bodies deal with this stress.

Since phyllobilins arise with the aging of green vegetables, the content of phyllobilins is higher the older e.g. a cucumber or a salad is. For example, an iceberg lettuce stored for seven days contains up to 1000 times more phyllobilins than a freshly purchased one. So we take in certain amounts of phyllobilins with our diet every day. However, by eating vegetables that are no longer quite as fresh, we can significantly increase these quantities.

Studies of the lettuce shown in the video in the laboratory have also shown that the bacterial load does not increase between day 1 and day 7. Slightly brown and wilted lettuce is therefore not always bad, but can usually be consumed without hesitation and even benefit our health due to the increased phyllobilin content.

3.4.3 Safety Treatment

The video (no sound) uses the example of lettuce to show how foods may change with ripening and aging. At the top left you can see the respective day and time.

As green foods, such as lettuce, age, the green pigment (chlorophyll) in the plant cells is broken down. As you can see in the video, the lettuce becomes less and less green over time and takes on a brownish color. The brownish color and the wilting of the lead to the salad appearing less appetizing and often makes us worry whether we can still eat it without hesitation.

To answer this question, the microbial contamination of the lettuce shown in the video was measured in the laboratory. The results show that the bacterial load does not increase between day 1 and day 7. Slightly brown and wilted lettuce is therefore not necessarily bad and dangerous to eat, but can usually be eaten without hesitation.

Tip: rely on your senses! For example, if the salad is moldy or smells musty, it is better to throw it away. If this is not the case, you can still eat it!

4. Supplementary References

1   Scherl, M. *et al.* Chlorophyll Catabolites in Fall Leaves of the Wych Elm Tree Present a Novel Glycosylation Motif. *Chem. Eur. J.* **22**, 9498-9503 (2016).
2   Moser, S., Ulrich, M., Müller, T. & Kräutler, B. A yellow chlorophyll catabolite is a pigment of the fall colours. *Photochem. Photobiol. Sci.* **7**, 1577-1581 (2008).
3   Müller, T., Rafelsberger, M., Vergeiner, C. & Kräutler, B. A Dioxobilane as Product of a Divergent Path of Chlorophyll Breakdown in Norway Maple. *Angew. Chem. Int. Ed.* **50**, 10724-10727 (2011).
4   Kräutler, B. Breakdown of Chlorophyll in Higher Plants—Phyllobilins as Abundant, Yet Hardly Visible Signs of Ripening, Senescence, and Cell Death. *Angew. Chem. Int. Ed.* **55**, 4882-4907 (2016).
5   Benzie, I. F. & Strain, J. J. The ferric reducing ability of plasma (FRAP) as a measure of "antioxidant power": the FRAP assay. *Anal. Biochem.* **239**, 70-76 (1996).
6   Yokomizo, A. & Moriwaki, M. Effects of uptake of flavonoids on oxidative stress induced by hydrogen peroxide in human intestinal Caco-2 cells. *Biosci. Biotechnol. Biochem.* **70**, 1317-1324 (2006).
7   Christ, B., Hauenstein, M. & Hörtensteiner, S. A liquid chromatography–mass spectrometry platform for the analysis of phyllobilins, the major degradation products of chlorophyll in Arabidopsis thaliana. *Plant J.* **88**, 505-518 (2016).
8   Müller, T., Vergeiner, S. & Kräutler, B. Structure elucidation of chlorophyll catabolites (phyllobilins) by ESI-mass spectrometry—Pseudo-molecular ions and fragmentation analysis of a nonfluorescent chlorophyll catabolite (NCC). *Int. J. Mass Spectrom.* **365-366**, 48-55 (2014).
9   Pružinska, A., Tanner, G., Anders, I., Roca, M. & Hörtensteiner, S. Chlorophyll breakdown: Pheophorbide *a* oxygenase is a Rieske-type iron-sulfur protein, encoded by the *accelerated cell death 1* gene. *Proc. Natl. Acad. Sci. USA* **100**, 15259-15264 (2003).
10   Strain, H. H., Cope, B. T. & Svec, W. A. in *Methods in Enzymology* Vol. 23   452-476 (Academic Press, 1971).

Bioactivities of Natural Products

Phylloxanthobilins are Abundant Linear Tetrapyrroles from Chlorophyll Breakdown with Activities Against Cancer Cells

Cornelia A. Karg,[a] Pengyu Wang,[a] Florian Kluibenschedl,[b] Thomas Müller,[b] Lars Allmendinger,[c] Angelika M. Vollmar,[a] and Simone Moser*[a]

Abstract: Linear tetrapyrroles, called phyllobilins, are obtained as major catabolites upon chlorophyll degradation. Primarily, colorless phylloleucobilins featuring four deconjugated pyrrole units were identified. Their yellow counterparts, phylloxanthobilins, were discovered more recently. Although the two catabolites differ only by one double bond, physicochemical properties are very distinct. Moreover, the presence of the double bond seems to enhance physiologically relevant bioactivities: in contrast to phylloleucobilin, we identified a potent anti-proliferative activity for a phylloxanthobilin, and show that this natural product induces apoptotic cell death and a cell cycle arrest in cancer cells. Interestingly, upon modifying inactive phylloleucobilin by esterification, an anti-proliferative activity can be observed that increases with the chain lengths of the alkyl esters. We provide first evidence for anti-cancer activity of phyllobilins, report a novel plant source for a phylloxanthobilin, and by using paper spray MS, show that these bioactive yellow chlorophyll catabolites are more prevalent in Nature than previously assumed.

Introduction

Despite its visibility, the biochemical degradation of the green plant pigment chlorophyll (Chl) has remained unresolved for a long time, until abundant linear tetrapyrroles, now called phyllobilins (PBs), were discovered as stable degradation products accumulating in the vacuoles of the plant cell.[1] In the meantime, Chl breakdown has revealed many of its mysteries, and we now have a well-defined picture of the biochemical program of Chl breakdown, called pheophorbide a oxygenase (PaO)/phyllobilin pathway. The most commonly identified "final" breakdown product is a 3^2-hydroxylated phylloleucobilin (PleB), 3^2-OH-PleB. Colorless PleBs were the first PBs to be discovered and were believed to represent the "last stage" of Chl breakdown.

For the plant *Cercidiphyllum japonicum*, in addition to 3^2-OH-PleB (*Cj*-PleB (**1**)),[2] a yellow colored oxidation product, a phylloxanthobilin (*Cj*-PxB (**2**)), was discovered for the first time 10 years ago[3] (Scheme 1).

The formation of PxBs in plants has not yet been fully clarified, but it is assumed that plants with PxB content show an endogenous "oxidative activity", likely caused by enzymes.[4] In contrast to PleBs, PxBs feature a double bond system extending from ring C to ring D, resulting not only in an intense yellow color, but also in interesting chemical properties. PxBs were shown to be reversible photoswitches and to dimerize depending on the lipophilicity of the environment in a formal [2+2] cycloaddition.[5]

Chl breakdown has been and still is regarded primarily as a detoxification process; the discovery of the PxBs, however, points towards yet to be elucidated physiological roles of these metabolites for the plant. Up to the stage of the PleBs, the efforts of the PaO/phyllobilin pathway, using metabolic energy and specific enzymes to detoxify photoactive Chl, yields non-photoactive, more water-soluble molecules with four isolated tetrapyrrole units. The discovery of PxBs, however, contradicts the detoxification paradigm. PxBs were found to be photoactive compounds[5] and are, compared to PleBs, less hydrophilic, seemingly reverting the efforts of the detoxification pathway and raising the question of a potential relevance of PxBs in physiological roles for the plant.

For humans, PxBs are suspected to have yet un-identified bioactivities, too.[6] We could recently show that the PxBs from *Echinacea purpurea* have a very potent in vitro antioxidative activity, a high radical scavenging potential in human cells, and can protect the cells from oxidative stress. Furthermore, metabolic studies indicated the PxBs to be stable in the cell.[7] An-
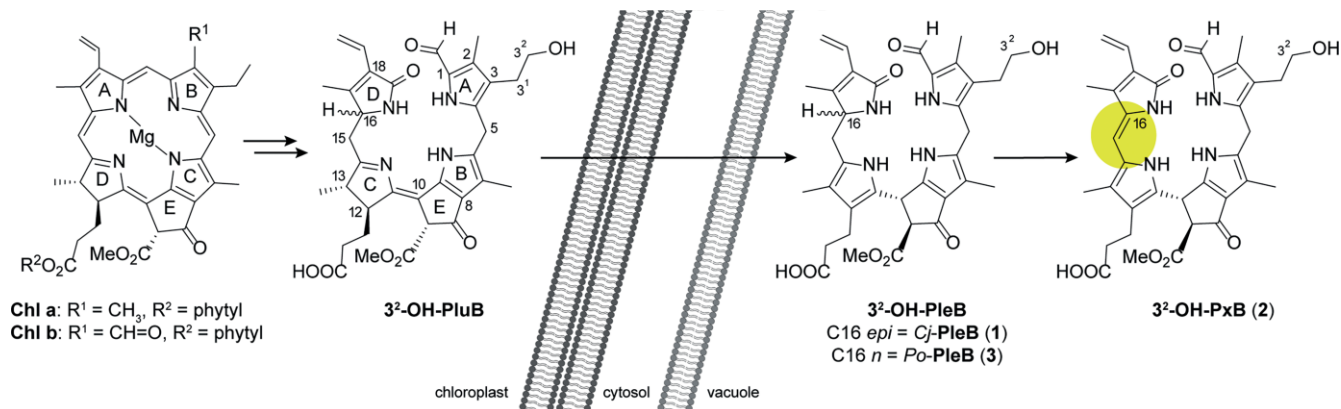
[a] C. A. Karg, P. Wang, Prof. Dr. A. M. Vollmar, Dr. S. Moser
Pharmaceutical Biology, Pharmacy Department, Ludwig-Maximilians University of Munich,
Butenandtstraße 5-13, 81377 Munich, Germany
E-mail: simone.moser@cup.uni-muenchen.de
https://www.pharmbiol.cup.uni-muenchen.de/staff/group-leaders/moser1/
[b] F. Kluibenschedl, Assoz. Prof. Dr. T. Müller
Institute of Organic Chemistry, University of Innsbruck,
Innrain 80-82, 6020 Innsbruck, Austria
[c] L. Allmendinger
Pharmaceutical Chemistry, Pharmacy Department, Ludwig-Maximilians University of Munich,
Butenandtstraße 5-13, 81377 Munich, Germany

EurJOC
European Journal of Organic Chemistry

Full Paper
doi.org/10.1002/ejoc.202000692

Chemistry Europe
European Chemical Societies Publishing

Chl a: R^1 = CH$_3$, R^2 = phytyl
Chl b: R^1 = CH=O, R^2 = phytyl

Scheme 1. Overview on key structures of chlorophyll catabolism leading - via a transient 3^2-phyllolumibilin (3^2-OH-PluB) – to the most commonly identified 3^2-hydroxylated phylloleucobilin (3^2-OH-PleB). While the absolute configuration at the stereocenter at C16 of PluBs and PleBs is not known, these catabolites can be classified as either n or epi, depending on the plant species. 3^2-OH-PleB accumulates in the vacuoles; oxidation of the 3^2-OH-PleB leads to the colored 3^2-hydroxylated phylloxanthobilin (3^2-OH-PxB (**2**)).

other PxB was isolated from de-greened leaves of savoy cabbage, which is thought to exert its health promoting effects via antioxidants. Also for this PxB, its potent in vitro antioxidative activity was proven by two different approaches.[8]

Cornelia A. Karg studied pharmacy at the Ludwig-Maximilians-University of Munich and received her approbation in pharmacy in 2017. She then started her PhD under the supervision of Prof. Angelika Vollmar and Dr. Simone Moser at the Department of Pharmaceutical Biology at the LMU. Her research topics include the structural characterization of natural products in plants and investigations on their bioactivities and molecular mode of action in cells.

Pengyu Wang received his Master's degree in Pharmaceutical Chemistry from Wuhan University, China in 2018. He then pursued his PhD degree under the guidance of Prof. Angelika Vollmar and Dr. Simone Moser at Ludwig-Maximilians-University, Munich, Germany. His research mainly focuses on discovery, modification and bioactivity evaluation of natural products from plants.

Florian Kluibenschedl is studying chemistry and physics at the University of Innsbruck, Austria. He discovered his interest in mass spectrometry in the course of two internships at the Institute of Organic Chemistry, University of Innsbruck. It was then when he performed Leaf Spray mass spectrometry experiments. He now is pursuing his bachelor thesis as a member of the Müller research group.

Thomas Müller is an Associate Professor at the Institute of Organic Chemistry, University of Innsbruck, Austria. He obtained his PhD at the Medical University of Innsbruck. During his post-doctoral period with Prof. Bernhard Kräutler (University of Innsbruck) he worked on structure elucidation of natural products isolated from plants. As a visiting scientist at Prof. R. Graham Cooks' lab (Purdue University, West Lafayette, IN, USA), he started to focus on ambient ionization techniques. The utilization of ambient ionization for structure elucidation and imaging mass spectrometry is still his main research interest.

Lars Allmendinger received his PhD degree in 2004 from the Ludwig-Maximilians-University (LMU), Munich (Germany), working on the total synthesis of a natural occurring antibiotic under the supervision of Dr. Franz Paintner. He has then overtaken the management of the NMR facility belonging to the Medici nal Chemistry unit of the Department of the LMU. In April 2020 he joined the research group of Prof Ivan Huc at the LMU in order to seek new challenges in the field of Chemical Biology.

Angelika M. Vollmar is Dean of the Faculty of Chemistry and Pharmacy and full professor at the Ludwig-Maximilians-University of Munich. She obtained her doctorate in pharmaceutical biology in 1984. After a post-doctoral stay at UCLA, USA (1985–1987), she habilitated in clinical pharmacology and pharmacy at the Faculty of Veterinary Medicine at LMU Munich in 1991. In 1991, she has been visiting researcher at the Clinical Research Institute, Montreal, followed by a professorship in pharmacology in 1994. Since 1998, she has held the Chair of Pharmaceutical Biology in the Department of Pharmacy at LMU Munich. Her research activities are in the field of drug development and focus on natural compounds as tools and leads in cancer biology and therapy. In addition to various scientific awards, she received the Federal Cross of Merit on Ribbon of Germany in 2011.

Simone Moser studied chemistry at the University of Innsbruck, Austria. She pursued doctoral studies with Prof. Kräutler at the Institute of Organic Chemistry (Innsbruck), working on structure elucidation of natural products. After postdoctoral studies as a Marie-Curie postdoctoral fellow in the group of Prof. Johnsson at EPFL, Switzerland and as Swiss National Science Foundation Fellow at MIT, USA with Prof. Nolan, she returned to Austria and worked in the pharmaceutical industry (Novartis). After a short stay at her alma mater, she moved to Munich and is currently leading a research group at LMU, working on bioactivities of natural products.

EurJOC
European Journal of Organic Chemistry

Full Paper
doi.org/10.1002/ejoc.202000692

Chemistry Europe
European Chemical
Societies Publishing

Since PxBs appear to be overlooked bioactive constituents of plants, and compounds with structures related to PBs, such as bilirubin, have a reported anti-cancer activity,[9] we set out to test the cytotoxicity of PBs against cancer cells. We focused on the most common PB motif, the 3^2-hydroxylated core structure, 3^2-OH-PleB (**1** and **3**), and its PxB oxidation product **2**. The PxB (**2**) showed promising cytotoxicity and apoptosis-inducing properties in bladder and breast cancer cells. The PleB precursors **1** and **3**, in contrast, were revealed not to be toxic against cancer cells; we could show, however, that esterification of the propionic acid side chain by chemical synthesis led to tunable cytotoxicity, which could be partially explained by uptake studies.

Results and Discussion

Isolation and Structure Elucidation of PleB (3) and PxB (2) from Plane Tree (*Platanus occidentalis*)

The analytical HPLC analysis of a senescent plane tree leaf revealed two signals with UV spectra characteristics for phyllobilins (Figure 1, Figure S1). One signal was tentatively identified as PleB with absorption maxima at around 240 nm and 312 nm and one as a PxB featuring an additional maximum at 426 nm.[3] The *Po*-PleB (**3**) was isolated from 300 g of leaves as described in the experimental section, giving 50 mg of pure **3**. In order to obtain large amounts of **2**, the latter was synthesized from **3** via light assisted oxidation on silica gel.[10] Using the published protocol, 2 mg of the PxB (**2**) were obtained from 10 mg of **3**. HRMS analysis of purified compounds allowed for the deduction of the molecular formulae as $C_{35}H_{41}O_8N_4$ for **3**, and $C_{35}H_{39}O_8N_4$ for **2**, revealing them to have an identical molecular composition as PleB (**1**) and PxB (**2**) from katsura tree leaves. PBs from katsura tree, *Cercidiphyllum japonicum*, have been thoroughly characterized by spectroscopic methods; the major PleB (**1**) was identified as 3^2-OH PleB.[2] Furthermore, the Z and E conformers of 3^2-OH-PxB (**2**) were identified.[3]
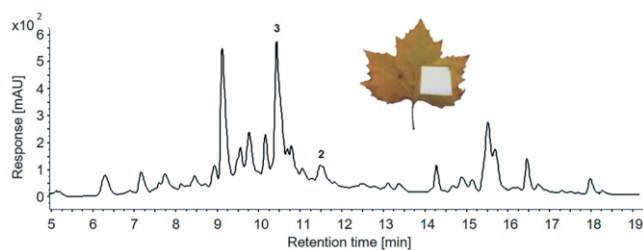

Figure 1. Analytical HPLC trace of a methanolic extract of a fresh, senescent plane tree leaf (detection at 320 nm) indicated the presence of *Po*-PleB (**3**) and *Po*-PxB (**2**).

In a co-elution experiment, in which isolated pure *Po*-PleB (**3**) and *Cj*-PleB (**1**), and a mixture of the two pure compounds, were applied to analytical HPLC, the two PleB signals showed similar but not identical retention times (Figure S2 A–C). Since the mass spectra of the two compounds revealed them to have an identical molecular formula, we conclude that the two PleBs **1** and **3** are epimers featuring a different configuration at the

stereocenter at C16. Two "classes" of PleBs, i.e. C16 epimers, result from the stereospecificity of an enzyme that introduces a new stereocenter in the PleB precursor primary phyllolumibilin (*p*PluB) either in the "*n*" or "*epi*" configuration, depending on the plant species.[11] The *p*PluB is then hydroxylated resulting in a 3^2-OH PluB, which is converted into the respective PleB by acid-induced tautomerization in the vacuoles of the senescent plant cell.[12]

The elemental composition of *Po*-PxB (**2**) was deduced via HRMS as $C_{35}H_{39}O_8N_4$ and revealed the structure to be identical with *Cj*-PxB (**2**) from katsura. A co-elution experiment was performed, in which the isolated compounds *Cj*-PxB (**2**), *Po*-PxB (**2**), and a mixture of both compounds, were analyzed by analytical HPL-chromatography. The chromatograms showed identical peaks and chromatographic characteristics (Figure S2 D–F). Moreover, these findings were confirmed by ^1H NMR spectroscopy. By comparing the ^1H NMR spectrum of *Po*-PxB (**2**) with the spectrum of *Cj*-PxB (**2**),[3] the same typical signals for a tetrapyrrolic PxB stood out: the characteristic signal pattern for the spin system of the peripheral vinyl group at the intermediate field; four singlets at high field of the methyl groups H_3C2^1, H_3C7^1, H_3C13^1, and H_3C17^1 near 2 ppm, and one singlet of the methyl ester group at 3.7 ppm. Moreover, one singlet at the low field for the formyl group was detected, as well as the characteristic signal for the additional double bond in a PxB core in Z conformation,[3] a singlet of HC15 at 6.19 ppm (Figure S5, Table S2). In conclusion, the spectroscopic data clearly show the PxB from *Platanus* to be identical to the PxB (**2**) from *Cercidiphyllum japonicum*.

Analysis of PBs in Senescent Leaves by Paper Spray Mass Spectrometry

Since the discovery of the first linear chlorophyll catabolite, a PleB, 29 years ago in the leaves of barley,[1] the list of PleBs identified from different plant species has grown considerably; PleBs were shown to occur in a large structural variety arising from the conjugation of the tetrapyrrole core to hydrophilic residues.

With the first PxB (**2**), detected in leaves of katsura,[3] the spectrum of chlorophyll catabolites was extended beyond PleBs. Following the PxB (**2**) from katsura, investigations on other plant species have yielded PxBs; PxBs have been identified in leaf extracts of *Egeria densa*,[13] *Tilia cordata*,[14] plum tree,[15] and wych elm.[16] The abundances of PxBs compared to their PleB precursors, however, appeared to be lower. Exceptions to this observation are the PxBs discovered in the medicinal plant *Echinacea purpurea*, in which PxBs were detected in unprecedented abundance and diversity.[7] These findings raised the question of a broader occurrence of PxBs; since many plant species have been investigated before the discovery of PxBs, only PleBs are reported for those. The most common 3^2-OH PleB has been identified, among others, in *Cercidiphyllum japonicum,* spinach *(Spinacia oleracea),* and *Spathiphyllum wallisii*.[17] Taken into account that PxBs hold a large promise of yet unexplored bioactivities, we re-investigated *Spinacia oleracea* and *Spathiphyllum wallisii*, reportedly containing 3^2-OH-PleB (**1**

EurJOC
European Journal of Organic Chemistry

Full Paper
doi.org/10.1002/ejoc.202000692

Chemistry
Europe
European Chemical
Societies Publishing

and **3**, respectively), but specifically looking for the presence of the 3^2-OH PxB (**2**).

A characteristic feature of PleBs, which originally led to the term "rusty pigments", is that when applied to thin-layer chromatography on silica gel, the colorless PleB spots developed first into yellow spots, and eventually into rust-colored spots under exposure to daylight.[3] Since the oxidation of PleBs to PxBs is influenced by air and light, higher apparent abundances of PxBs might be artifacts of the extraction procedure. We, therefore, used a combination of paper spray and leaf spray mass spectrometry which allowed the rapid and direct analysis of the leaf tissue without any sample preparation. Paper spray as well as leaf spray are rather new applications in the field of ambient mass spectrometry, which were first described by Liu et al. in 2010[18] and 2011.[19] In general, mass spectrometry has been developed into an efficient tool for identification and structural elucidation of phyllobilins with known modification patterns. The core structure of the linear tetrapyrroles has been characterized extensively for more than 20 different examples leading to the creation of an MS database for phyllobilins.[20] Due to characteristic fragmentation patterns of phyllobilins, MS and MS/MS are straightforward tools for the characterization of this family of linear tetrapyrroles.[21]

Paper spray MS analysis of freshly collected, senescent leaves (Figure 2 and Figure 3) clearly revealed the presence of both types of chlorophyll catabolites, colorless PleB and yellow PxB, in the intact senescent leaves of *Cercidiphyllum japonicum* as well as *Platanus occidentalis, Spinacia oleracea,* and *Spathiphyllum wallisii*. PleBs and PxBs were identified with respect to the fragmentation behavior of their isolated molecular ions in the gas phase.[21] Collision induced dissociation (CID) of the monoisotopic, potassiated molecular ions ([M + K]⁺) of 3^2-OH PleB (**1** and **3**) at $m/z = 683$ showed diagnostic fragments at $m/z = 651$, which correspond to the characteristic loss of methanol (–32 Da). Interestingly, the two most abundant fragment ions of monoisotopic, potassiated molecular ions ([M + K]⁺) of 3^2-OH PxB (**2**) at $m/z = 681$ correspond to the loss of methanol (–32 Da) as well as to the loss of water (–18 Da). The paper spray confirms the occurrence of PxB (**2**) in all four investigated plant species, for which only the PleB precursor (**1** or **3**) was reported before.
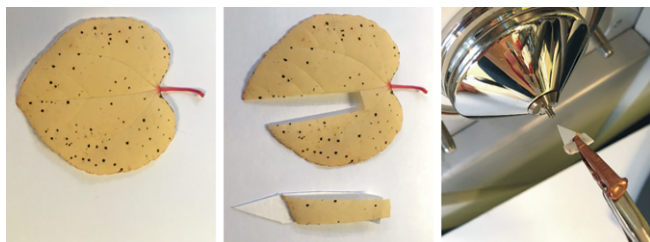

Figure 2. Example of a paper spray setup. The yellow, freshly collected senescent leaf from katsura tree (*Cercidiphyllum japonicum*, left) was cut using razor blade (center). The 0.5 cm × 3 cm slice was wrapped using a tapered piece of filter paper and mounted in front of the MS inlet (right). A potential of 3.5 kV was applied to the wrapped leaf, and the MSⁿ data were recorded within 30 s while applying 20 μL of methanol.
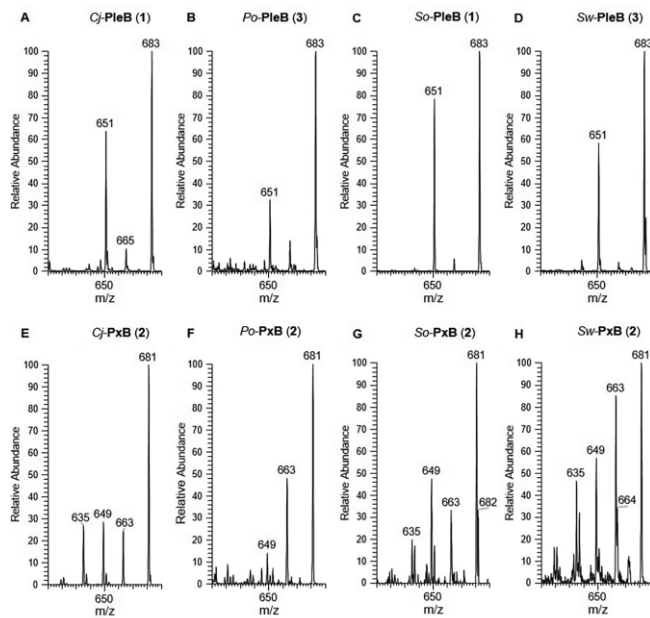

Figure 3. Direct mass spectrometric identification of PleB (**1** or **3**), and PxB (**2**) in senescent leaves of *Cercidiphyllum japonicum* (A, E), *Platanus occidentalis* (B, F), *Spinacia oleracea* (C, G) and *Spathiphyllum wallisii* (D, H) using paper spray analysis. (A–D): the monoisotopic, potassiated molecular ions ([**1,3** +K]⁺) at m/z 683 were isolated and fragmented using CID. The loss of methanol (–32 Da) was found to be the most abundant fragmentation. (E-H): CID fragmentation pattern of the monoisotopic, potassiated molecular ions ([M + K]⁺) of PxB (**2**) at m/z 681. The most prominent fragmentations were found to be the loss of water (–18 Da) as well as the loss of methanol (–32 Da).

Cytotoxic Potential of Phyllobilins

Structurally, phyllobilins bear a remarkable resemblance to heme-derived bilins;[22] whereby PxB, at least structurally, appears to be the bilirubin plant counterpart.[8] The bilins as well as the phyllobilins were long thought to be mere waste products, generated in a detoxification process of heme;[23] this assumption still holds true for the products of the chlorophyll degradation pathway. For the bilins, this paradigm has been disproved; e.g. bilirubin was shown to act as an important physiological antioxidant and to possess cytoprotective potential against various diseases.[24] In addition, dependent on the concentration as well as the state of redox homeostasis in the cell, bilirubin can also act as a cytotoxic agent.[25] This cytotoxicity plays a role in the anti-cancer effects attributed to the heme catabolite, among which anti-tumoral effects on human adenocarcinoma,[26] and apoptosis-inducing activity in colon cancer cells were described.[9]

The growing evidence for physiological activities of the bile pigments fueled the search for relevant properties of phyllobilins. In a first report, Müller et al. were able to demonstrate in vitro antioxidative activities for PleBs isolated from the peels of apples and pears.[27] For the PxBs, we recently reported their potent antioxidative activity in vitro; in addition, PxBs turned out to be rapidly taken up by cells, to be potent ROS scavengers in cells and to possess the ability to protect cells from oxidative stress.[7]

Further bio-relevant effects on cells, however, still remain to be elucidated. In this study, we set out to probe the cytotoxic

EurJOC
European Journal of Organic Chemistry

Full Paper
doi.org/10.1002/ejoc.202000692

Chemistry Europe
European Chemical Societies Publishing

potential of phyllobilins on cancer cells; in a first experiment, we tested the PleB from katsura tree *Cj*-PleB (**1**) and its epimer from plane tree leaves *Po*-PleB (**3**) on two different human cancer cell lines, the highly invasive epithelial breast cancer MDA-MB-231 cell line and the urinary bladder carcinoma T24 cell line. **1** and **3** showed no significant inhibition of cell proliferation over 72 h in the tested concentration range of 1 to 100 μM (Figure 4A).
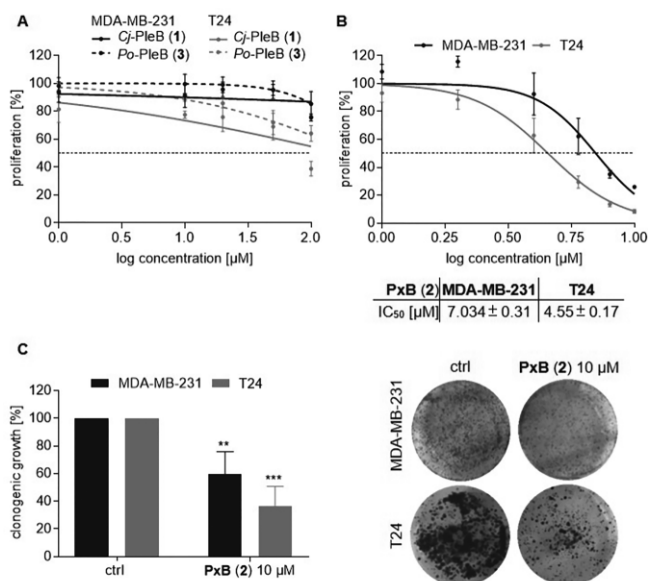
Figure 4. Effect of *Cj*-PleB (**1**) and *Po*-PleB (**3**), and PxB (**2**) on proliferation of T24 and MDA-MB-231 cancer cells. A) Treatment of T24 and MDA-MB-231 cells with **1** and **3** showed no anti-proliferative effect. B) **2** inhibits proliferation of T24 and MDA-MB-231 cells. Cells were treated with compound for 72 h and cell proliferation was assessed by crystal violet staining. C) **2** inhibits colony formation of T24 and MDA-MB-231 cells. PxB (**2**) treated cells were re-seeded and colony formation was assessed by crystal violet assay after one week.

For testing the cytotoxic potential of PxB (**2**), *Cercidiphyllum japonicum* was used as a source for the isolation of **1** and its subsequent oxidation; hence, only *Cj*-PxB (**2**) was used as test reagent and further defined as PxB (**2**), since *Cj*-PxB (**2**) and *Po*-PxB (**2**) are identical compounds due to the unsaturation of the stereocenter at C16 of the PleB (**1** or **3**). In contrast to the PleB precursors (**1** or **3**), **2** exhibited a potent anti-proliferative effect at low micromolar doses in both cell lines with calculated IC$_{50}$ values of 7.0 μM against MDA-MB-231 cells and 4.6 μM against T24 cells (Figure 4B).

Phylloxanthobilin Inhibits Colony Formation

Having established that **2** inhibits the proliferation of two different cancer cell lines, we further investigated this effect by a colony formation assay. This assay assesses the ability of single cells to grow and form colonies after a short time exposure to the compound by a crystal violet staining. The results showed a steep decline of colony formation in comparison to the DMSO vehicle control after brief exposure to 10 μM **2**, indicating **2** to inhibit also long-term survival and proliferation of cancer cells (Figure 4C).

Phylloxanthobilin Induces Apoptosis and a G2/M Cell Cycle Arrest

Furthermore, we assessed the cytotoxic potential of PxB (**2**) by flow cytometry, using a commercial Annexin V/PI staining kit, which allows for the distinction between different types of cell death. FITC conjugated Annexin V targets apoptotic cells and counterstaining with PI identifies cells undergoing early apoptosis (A+/PI-) or late apoptosis (A+/PI+). In contrast, cells with PI positive and Annexin V negative signal are related to a non-apoptotic, necrotic cell death.

The experiment showed that PxB (**2**) induced cell death in a dose-dependent manner with up to overall 30 % dead cells after 24 h, increasing to 45 % after 48 h in T24 cells (Figure 5, A and B). Early and late apoptotic cells, characterized by the
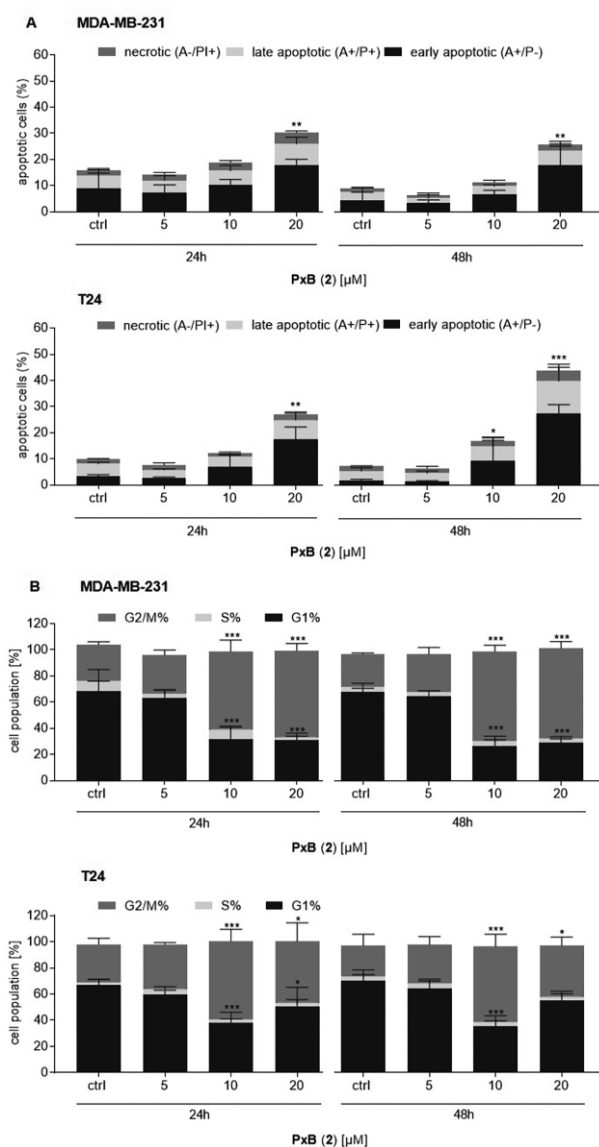

Figure 5. PxB (**2**) induces apoptosis and a G2/M cell cycle arrest in MDA-MB-231 and T24 cells. A) Cells were incubated with **2** for 24 and 48 h, and cell death was analyzed by flow cytometry using Annexin V/PI co-staining. B) Cell cycle distribution of **2** treated MDA-MB-231 and T24 cells was assessed by PI staining and analyzed by flow cytometry, revealing that **2** causes a cell cycle arrest in the G2/M phase.

EurJOC
European Journal of Organic Chemistry

Full Paper
doi.org/10.1002/ejoc.202000692

Chemistry
Europe
European Chemical
Societies Publishing

Annexin V positive/PI negative (A+/PI-) and Annexin V positive/ PI positive (A+/PI+) signal, were increased upon PxB treatment. For necrotic cells, characterized by (A-/PI+), only a slight increase was observed. Taken together, these results demonstrate that **2** is a potent inducer of apoptotic cell death.

We further analyzed the cell death-inducing properties of PxB (**2**) on the cell cycle progression of T24 and MDA-MB-231 cells by PI staining according to the protocol of Nicoletti et al.[28] This method estimates the cellular DNA content by flow cytometry, allows for the quantitative analysis of cells in subG1, G1, S, and G2/M cell cycle phase, and detects cell cycle perturbations (Figure S6). Treatment with 10 µM and 20 µM **2** for 24 h or 48 h resulted in an arrest of cells in the G2/M cell cycle phase (Figure 5, C and D). The proportion of cells in G1 phase decreased significantly, in parallel with an increase of cells in the G2/M phase. In contrast, no effect on the population in the S phase was observed during treatment with **2**. Moreover, a significant increase of cells in the subG1 phase in both cell lines was observed, confirming the results of the Annexin V/PI assay that **2** promotes apoptotic cell death (Figure S7).

Cytotoxicity of PleB Can Be Tuned by Esterification

So far, PleBs have been identified and characterized as approximately 20 different structures, whereby identical PleBs have been isolated from different plant species. All PleBs share the same core structure with four deconjugated pyrrole units. Differences arise from modifications of the rings at four different positions (with the exception of a catabolite from *Arabidopsis thaliana*, which is speculated to result from an incomplete reduction from Chl b to Chl a[29]).

Of particular interest is the esterification of the propionic acid side chain at C12; Oberhuber et al. showed that introducing a methyl ester at the PluB stage by chemical synthesis changed the kinetics of the conversion to PleBs, resulting in increased stability of the esterified PluB.[12b] An esterification of the propionic acid side chain of PBs was also discovered to occur naturally, causing PluBs in banana peels to accumulate and, as a consequence, the peel of ripened bananas to luminesce blue.[30] On the PleB level, esterified compounds were identified in leaves of *Vitis vinifera*[31] and wych elm,[16] and very recently on the PxB level in *Epipremnum aureum*.[32]

In comparison to the PxB, the PleBs as more polar molecules showed no effect on the proliferation of cancer cells. We therefore modified the structure of the PleB by esterification of the propionic acid side chain aiming to decrease its polarity. For our experiments, we used *Cj*-PleB (**1**) as representative compound. We prepared four different esters of the propionic acid side chain with increasing length of the alkyl side chain as described in the experimental section to gradually decrease polarity (Figure 6). Chemical structures were confirmed by HRMS, ESI MS/MS and NMR measurements (Figure S8–S12, Table S3,4).

Indeed, the inhibitory effects on the proliferation of MDA-MB-231 and T24 cells were influenced by esterification, with activities increasing with the chain lengths of the alkyl esters (Figure 7). In MDA-MB-231 cells, the IC_{50} value of the methyl-compared to the ethyl ester showed a decrease with polarity (46.1 µM for the methyl ester (**4**) and 30.9 µM for the ethyl ester (**5**)), and even lower values were observed for the butyl ester (**6**), as well as for the octyl ester (**7**); butyl ester (**6**) exhibited a IC_{50} value of 23.6 µM and octyl ester (**7**) of 16.3 µM. The results for T24 cells showed similar IC_{50} values for **4** and **5** of around 17 µM; the IC_{50} was lower for the **6** (11.0 µM) and as low as 3.4 µM for **7**.

Thus, we reasoned that polarity might be a factor that plays a role in the observed differences in cytotoxic potential between PleBs.

Uptake of PxB (2), PleBs (1, 3), and Esterified PleBs (4–7) by Cancer Cells

A crucial factor for the efficacy of a therapeutic agent is the delivery into the cell, as most of the substances target intracellular constituents. The ability for small drugs to overcome the natural barrier of the cell, the plasma membrane, is mainly determined by the size and lipophilicity of the compound. Whereas lipophilic small molecules can easily enter the cell e.g. through diffusion or active transport, a weak membrane permeability limits the cellular uptake of hydrophilic or larger molecules. Therefore, a common method to improve bioavailability is to alter the lipophilicity of molecules by generating prodrugs.[33]

Although the mechanism of the cellular uptake for phyllobilins remains to be elucidated, the polarity of the different
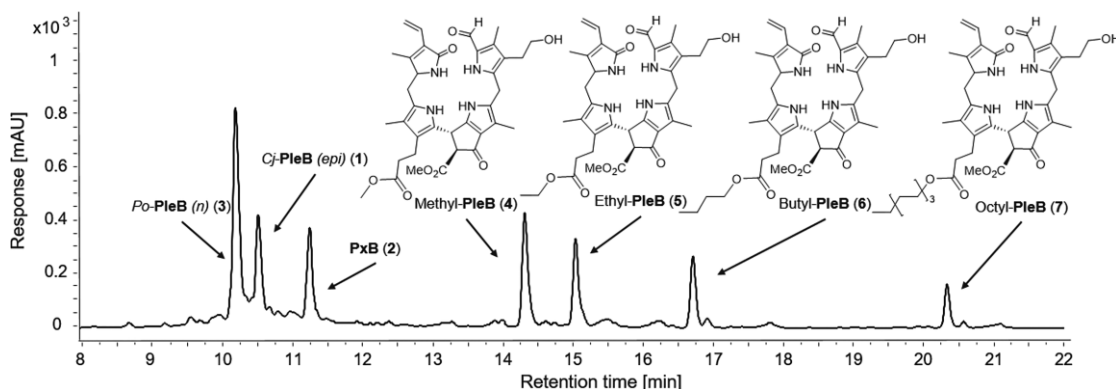

Figure 6. Analytical HPLC trace of a mixture of *Po*-PleB (**3**), *Cj*-PleB (**1**), PxB (**2**) and *Cj*-PleB-esters (**4–7**) (detection at 320 nm), showing a broad polarity range (linear gradient up to 17 min, see Experimental Section).
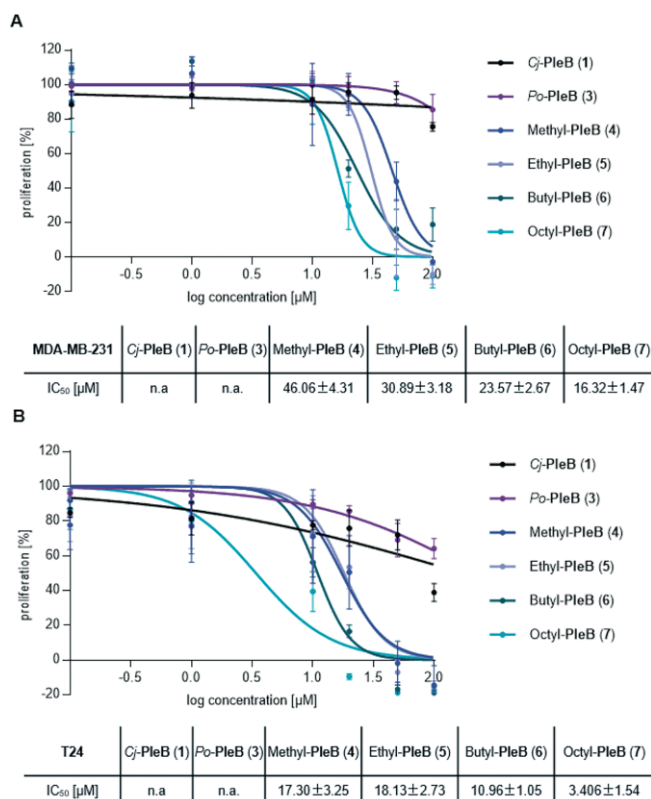
EurJOC
European Journal of Organic Chemistry

Full Paper
doi.org/10.1002/ejoc.202000692

Chemistry Europe
European Chemical
Societies Publishing

Figure 7. Esterification of Cj-PleB (**1**) influences the anti-proliferative activity. Cell proliferation assay of Po-PleB (**3**), Cj-PleB (**1**), PleB-esters (**4–7**) in MDA-MB-231 (A) and T24 (B) cells analyzed by crystal violet staining and corresponding IC$_{50}$ values were calculated.

tetrapyrrolic compounds seems to be a factor influencing the cytotoxicity. We, therefore, investigated the uptake of different PBs by cells, using HPLC to quantify the PB signal from cell lysates. This experiment also aimed at clarifying whether the PleB-esters (**4–7**) act like prodrugs, serving as vehicles of the compounds into the cells. In this case, the esters are cleaved by cellular esterases afterwards, leading to an increase of the effective concentration of PleB (**1**) in the cell compared to the use of the un-esterified compound; it could also be the case, however, that the esterified PleB itself has a cytotoxic activity.

All tested compounds could be found in the lysates of T24 cells, confirming that PBs, in general, can be taken up by cancer cells and are stable under the indicated conditions (Figure S13). In comparison to the PxB (**2**), the Cj-PleB (**1**) and Po-PleB (**3**) were only detected in minute amounts (Figure 8). This indicates the lack of cytotoxicity of the PleB (**1,3**) to correlate with higher polarity and lower intracellular compound concentration.

In contrast, the esterified PleBs (**4–7**) were detected in high concentrations. As expected, the intracellular concentration increased in parallel with apolarity of the compounds, being lowest for the methylated PleB (**4**) and highest for the butylated PleB (**6**). For the most apolar octylated PleB (**7**), however, a decreased intracellular concentration was observed, which might be due to low solubility in medium (Figure 8).

Interestingly, only minute amounts of hydrolyzed "free" PleB (**1**) could be observed in cell lysates when treating cells with the PleB-esters (**4–7**) (Figure S8). These results indicate the anti-
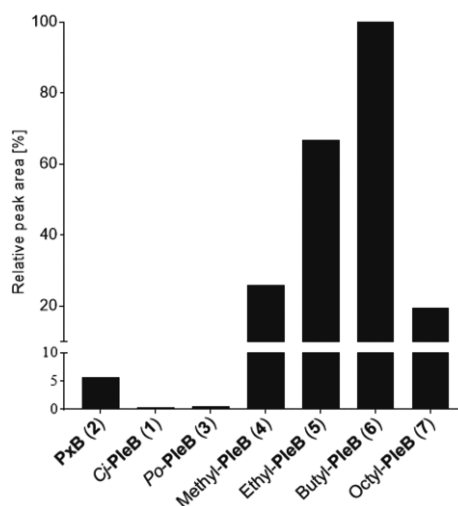
Figure 8. Esterification leads to higher amounts of intracellular compound. Cellular uptake of PxB (**2**), Cj-PleB (**1**), and Po-PleB (**3**) and Cj-PleB-esters (**4–7**) in T24 cells. A discontinuous y axis is shown for better visibility of the (low) uptake of **1** and **3**. Cells were treated with compounds (80 µM) for 5 h, lysed by beat beating, and the supernatant was analyzed by analytical HPLC.

proliferative effects of **4–7** not to depend on the liberation of the "free" PleB (**1**) in the cell. More likely, the esters appear to exhibit cytotoxic activities themselves, which cannot be explained by a prodrug mechanism. The observed reactivity of the PxB (**2**), however, surpasses the activity of **4** and **5**. Although the IC$_{50}$ values of **6**, **7**, and **2** in T24 cells are in a similar low micromolar range, **6** and **7** showed a significantly lower polarity than the PxB **2** (Figure 6) and a higher uptake (Figure 8). Nevertheless, neither polarity nor uptake can account for the difference in potency between PleBs and PxB (**2**). This indicates the structural difference between PleB and PxB, manifested by a double bond, to play a crucial role in inhibiting proliferation of cancer cells.

Whether a PleB-ester acts as a prodrug and the ester gets cleaved by cellular esterases, or the esterified compound itself is the cytotoxic agent, needs yet to be resolved in more detail; our results indicate, however, that only minute amounts of hydrolyzed PleB (**1**) are present in the cells, even 5 h after treatment.

Conclusion

In this study, we identified plane tree as novel source for 3^2-OH-PxB (**2**). This yellow chlorophyll catabolite was shown to be more abundant in Nature than previously thought, as was shown by paper spray MS; we demonstrated the occurrence of PxB (**2**) in leaves of *Spinacia oleracea* and *Spathiphyllum wallisii*, for which only the common 3^2-OH PleB (**1** or **3**) has been reported previously. After all, the discovery of PleBs precedes the discovery of PxBs by 17 years, therefore the studies during that time range did not screen for PxBs. Whether PxBs fulfill biological roles for plants, has yet to be investigated.

Here, we could introduce PxB (**2**) as potent anti-cancer agent in human cells, inhibiting proliferation in the low micromolar range, inducing apoptosis, and causing a G2/M cell cycle arrest.

EurJOC
European Journal of Organic Chemistry

Full Paper
doi.org/10.1002/ejoc.202000692

Chemistry Europe
European Chemical
Societies Publishing

We provide first evidence for anti-cancer activities of PxBs and add another proof that chlorophyll catabolites are more than mere waste products of a degradation pathway.

The discovery of a potent activity for the PxB (**2**), the fact that the cytotoxicity of PleBs (**1,3**) on cancer cells is tunable by a simple modification of the compounds, and the abundance of this family of natural products in the plant kingdom, open the door for further investigations of the anti-tumoral potential of the phyllobilins. Future studies will deal with the mechanism behind the potent killing and apoptosis induction in cancer cells and aim at identifying new sources of PxBs, which hold a large promise to reveal yet to be explored bioactivities.

Experimental Section

General: HPLC grade acetonitrile (ACN), methanol (MeOH), ethanol (EtOH), butanol, octanol, dimethyl sulfoxide (DMSO), hydrochloric acid (HCl), dichloromethane (DCM) and silica gel 60 were obtained from VWR International GmbH (Ismaning, Germany) and ultra-pure water (18 MΩ cm^{-1}) from a Millipore S.A.S. Milli-Q Academic system (18.2 MΩ cm-1, Molsheim, France). Potassium phosphate dibasic (K_2HPO_4), Potassium phosphate monobasic (KH_2PO_4), ammonium acetate (NH$_4$AcO), glass beads (acid washed, 425–600 μm), (benzo-triazol-1-yloxy)tripyrrolidinophosphonium hexafluorophosphate (PyBoP), Triethylamine (Et$_3$N), and [D$_4$]methanol were from Sigma-Aldrich (Taufkirchen, Germany) and SepPak Plus C18 cartridges from Waters Associates (Milford, USA). DMEM medium, penicillin, and streptomycin were from PAN-Biotech (Aidenbach, Germany); fetal calf serum (FCS) was from PAA Laboratories GmbH (Pasching, Austria) and Triton X-100 was from Merck (Darmstadt, Germany). Crystal violet, propidium iodide (PI) and trisodium citrate were purchased from Carl Roth (Karlsruhe, Germany) and sea sand from Fisher Scientific (Waltham, MA, USA).

Human bladder cancer cell line T24 and highly invasive human triple negative breast adenocarcinoma cell line MDA-MB-231 were obtained from the *Deutsche Sammlung von Mikroorgansimen und Zellkulturen* (DSMZ; Braunschweig, Germany) and maintained in DMEM medium supplemented with 10 % fetal calf serum (FCS) and 1 % penicillin/streptomycin. Cells were cultured at 37 °C under 5 % CO_2 atmosphere with constant humidity in 75 cm^3 tissue culture flasks.

Plant Material: Katsura trees (*Cercidiphyllum japonicum*) were located outside of the botanical garden Munich using the tree-finder app https://www.botmuctrees.de/. Senescent leaves were collected in the Maria-Ward-Straße, Munich (48°09′41.0"N 11°29′58.8"E). Senescent leaves of plane tree (*Platanus occidentalis*) were collected from trees in the Feodor-Lynen Straße at the campus Großhadern of the University of Munich (48°06′48.6"N 11°27′56.2"E). Spinach was obtained from a local supermarket and stored in the dark for 3 days to induce Chl breakdown. *Spathiphyllum wallisii* was bought at a local garden center. A senescent leaf was collected directly from the plant.

The identity of the plant material was determined by Prof. Susanne S. Renner (Department of Systematic Botany and Mycology, Faculty of Biology, University of Munich); Voucher specimen of *Platanus occidentalis* (Moser & Karg 2), *Cercidiphyllum japonicum* (Moser & Karg 3), and *Spathiphyllum wallisii* (Moser & Karg 4) have been deposited in the Munich herbarium (acronym M).

Chromatography: i) Analytical HPLC: Agilent 1260 Infinity II LC system with a 1260 Infinity Degasser, a 1260 Series quaternary pump

and 1260 Series diode array detector; Merck LiChrospher® 60 RP-select B (5 μm) LiChroCART® 125–4, protected by a Merck LiChrospher® 100 R$P\bar{1}$8 (5 μm) LiChroCART® 4–4 i.d. pre-column; injection volume: 100 μL (unless stated otherwise). Solvent system: mobile phase A = NH$_4$AcO buffer 10 mM pH 7, B = ACN, flow 0.5 mL/min; Solvent composition: 0–2 min 5 % B, 2–17 min 5 % to 70 % B, 17–20 min 70 % to 100 % B, 20–22 min 100 % B, 22–24 min 100 to 5 % B. Data were processed with OpenLab CDS Data Analysis 2.3.

ii) Semi-preparative HPLC: Gynkotek LC-System with manual sampler, M480 pump, Phenomenex DG-301 online degasser, Gynkotek UVD 640 diode array detector and a Rheodyne injection valve with 5 mL loop; column: Supelco Ascentis® C18, 5 μm, 15 cm × 10 mm, with a Phenomenex pre-column ODS 9 × 16 mm; mobile phase A = NH$_4$AcO buffer 10 mM pH 7, B = MeCN, flow 2.5 mL/min; solvent composition: 0–2 min 12 % B, 2–12 min 12 % to 20 % B, 12–30 min 20 % to 80 % B, 30–40 min 80 % to 100 % B. Data were processed with Gynkosoft 5.50.

Spectroscopy: UV/Vis: Thermo Spectronic Genesys 5 (336001) UV Visible spectrophotometer; λ_{max} in nm (rel. ε). Concentrations of PleB and PleB-esters were calculated using log ε (312 nm) = 4.23,[4] concentrations of PxB were calculated using log ε (426 nm) = 4.51.[3]

Paper spray mass spectrometry: Thermo Scientific Orbitrap XL mass spectrometer. The freshly collected senescent (yellow) leaves were cut into 0.5 cm × 3 cm slices using a razor blade. A freshly cut slice was wrapped into a tapered piece of filter paper and mounted in front of the MS inlet at a distance of 0.5 cm. A high voltage potential of 3.5 kV was applied to the wrapped leaf and MS^n data were recorded within 30 s while 20 μL of methanol were dropped onto the filter paper.

HRMS were measured at the MS facility of the Department of Chemistry, University of Munich. Data were processed with Xcalibur.

NMR spectra were recorded on an Avance III HD 500 MHz NMR spectrometer from Bruker BioSpin equipped with a CryoProbe™ Prodigy broadband probe using CD$_3$OD as solvent. Assignments of ^{13}C signals determined from ^{1}H,^{13}C heteronuclear correlations in HMQC and HMBC spectra. NMR data were analyzed with Mestre Nova 14.1.1.

During all handling steps, the material was protected from light and temperatures above 37 °C were avoided unless stated otherwise.

HPLC Analysis of Plane Tree (*Platanus occidentalis*) PBs: 16 cm^2 of a senescent leaf of plane tree was mixed with sea sand and 2 mL of MeOH in a mortar. The slurry was centrifuged (1000 rpm, 5 min, 4 °C), and a 40 μL aliquot of the supernatant was diluted with 160 μL of phosphate buffer (pH 7.4); a 100 μL aliquot was applied to analytical HPLC. In a co-elution experiment, isolated pure samples *Po*-PleB (**3**) and *Po*-PxB (**2**), respectively, were applied to analytical HPLC. *Cj*-PleB (**1**) and *Cj*-PxB (**2**) were isolated from katsura leaves as described below and were analyzed the same way. In addition, a 1:1 mixture of **1** and **3**, and of **2** from the two different plant sources, respectively, were analyzed by HPLC.

Large Scale Isolation of PleB from Senescent Leaves of Katsura (*Cercidiphyllum japonicum*) and Plane Tree (*Platanus occidentalis*): Senescent leaves of katsura and plane tree were extracted as follows (optimized protocol for plane tree described): 300 g of frozen leaves were ground in a 5 L stainless steel beaker using a Braun hand blender Model MR 5000 and extracted with hot water (1200 mL). The mixture was filtered through a cotton cloth and the residue was again washed with hot water (500 mL). The mixture was cooled to room temperature before extracting twice with 200 mL of DCM. The DCM solution was applied to a silica column (50 mm

EurJOC
European Journal of Organic Chemistry

Full Paper
doi.org/10.1002/ejoc.202000692

Chemistry Europe
European Chemical
Societies Publishing

diameter, 300 mm length, 70 g silica gel 60). The column was washed with DCM, and PBs were eluted with increasing MeOH (DCM/MeOH, 95:5, 80:20, 50:50). The different fractions were analyzed by TLC, PB containing fractions were combined, and the solvent was evaporated. The obtained residue was dissolved in MeOH/potassium phosphate buffer (pH 7.4) and purified by semi-preparative HPLC. Yields were 50 mg (77.6 µmol) of **3** and 10 mg (15.6 µmol) of **2**.

Solid-Phase Synthesis of PxB (2) by Oxidation of *Cj*-PleB (1) and *Po*-PleB (3): 10 mg PleB (**1** or **3**) were dissolved in 5 mL of DCM and 1 mL of MeOH and added to 7 g of silica. The mixture was carefully dried under vacuum and the powder was stirred overnight under a tungsten light bulb. The complete formation of **2** was confirmed by analytical HPLC, the reaction mixture was eluted with EtOH, filtered through a paper filter and the solvent was evaporated on a rotary evaporator. The crude product was purified by semi-preparative HPLC. Fractions containing **2** were pooled and dried by means of a rotary evaporator. The residue was dissolved in ACN/potassium phosphate buffer (pH 2.5) 20:80 and stirred overnight. After SPE (Sep-Pak-C18 cartridge 5 g), pure **2** was eluted with ACN and dried under vacuum. 2 mg (3.1 µmol, 20 %) of **2** were obtained. DMSO stocks were prepared and stored at –20 °C until further use.

Esterification of *Cj*-PleB (1): For synthesis of methyl-PleB (**4**), 4 mg **1** were dissolved in 1 mL of DMSO and 10 µL of MeOH, 2.5 µL of Et$_3$N, and 4.5 mg of PyBoP were added. The mixture was stirred at room temperature overnight. The formation of **4** was confirmed by analytical HPLC. The mixture was purified by semi-preparative HPLC, yielding 1.6 mg (2.4 µmol, 40 %) of **4**.

Syntheses of **5–7** were performed according to the protocol of Li and Kräutler with minor modifications.[5] PyBoP and Et$_3$N were used instead of BOP and TEA. **1** was dissolved in either ethanol, butanol or octanol, followed by addition of the coupling reagents. The formation of the PleB-esters (**5–7**) was confirmed by analytical HPLC. 58 % (1.1 µmol) of ethyl-PleB (**5**), 61 % (1.2 µmol) of butyl-PleB (**6**), and 65 % (1.4 µmol) of octyl-PleB (**7**) were obtained.

Spectroscopic Data: Retention time (t_R) from analytical HPLC.

***Cj*-PleB (1):** t_R = 10.5 min. UV/Vis online spectrum (nm, rel ε): 220 (1.00), 242 (0.8), 314 (0.72) nm. HRMS (ESI): $m/z_{calculated}$ (C$_{35}$H$_{41}$O$_8$N$_4$) = 645.29189 [M + H]$^+$; m/z_{found} = 645.29216 (Δ = 0.4 ppm).

***Cj*-PxB (2):** t_R = 11.3 min. UV/Vis online spectrum (nm, rel ε): 212 (0.94), 246 (0.51), 314 (0.66), 426 (1.00). HRMS (ESI): $m/z_{calculated}$ (C$_{35}$H$_{39}$O$_8$N$_4$) = 643.27624 [M + H]$^+$; m/z_{found} = 643.27679 (Δ = 0.9 ppm).

***Po*-PleB (3):** t_R = 10.2 min. UV/Vis spectrum ($λ_{max}$/nm, log ε): 220 (4.66), 245 (4.28), 310 (4.23) nm (see Figure S1). HRMS (ESI): $m/z_{calculated}$ (C$_{35}$H$_{41}$O$_8$N$_4$) = 645.29189 [M + H]$^+$; m/z_{found} = 645.29245 (Δ = 0.9 ppm).

^{1}H NMR (500 MHz, CD$_3$OD): δ [ppm] = 1.89 (s, H$_3$C17^1), 1.94 (s, H$_3$C13^1), 2.10 (s, H$_3$C7^1), 2.26 (s, H$_3$C2^1), 2.32 (m, H$_2$C12^2), 2.50 (dd, J = 14.5/8.9, H$_A$C15), 2.63 (m, H$_2$C12^1), 2.73 (m, H$_2$C3^1), 2.82 (dd, J = 14.3/5.2, H$_B$C15), 3.47 (m, H$_2$C3^2), 3.74 (s, H$_3$C8^4), 3.85 (m, HC8^2), 3.94 (m, H$_2$C5), 4.06 (m, HC16), 4.91 (s, HC10), 5.31–5.37 (m, H$_A$C18^2), 6.09 (dd, J = 17.7/2.4, H$_B$C18^2), 6.44 (dd, J = 11.7/17.8, HC18^1), 9.36 (s, HC20) (Table S1). ^{13}C NMR (500 MHz, CD$_3$OD): δ [ppm] = 8.06 (2^1), 8.06 (13^1), 8.06 (7^1), 11.92 (17^1), 20.93 (12^1), 20.93 (3^1), 22.65 (5), 27.36 (15), 35.94 (10), 38.52 (12^2), 50.96 (8^4), 59.54 (16), 61.26 (3^2), 111.06 (7), 114.2 (13), 119.59 (3), 117.03 (18^2), 119.59 (12), 123.18 (11), 124.52 (8), 126.04 (18^1), 127.22 (18), 128.11 (1), 133.05 (6), 133.95 (2), 137.09 (4), 155.94 (17), 160.43 (9), 170.31 (8^3), 173.0 (19), 176.23 (20), 180.18 (12^3), 192.75 (8^1) (Table S1).

***Po*-PxB (2):** t_R = 11.3 min. UV/Vis spectrum ($λ_{max}$/nm, log ε): 228 (4.99), 248 (4.51), 310 (4.61), 429 (4.51) nm (see Figure S1). HRMS (ESI): $m/z_{calculated}$ (C$_{35}$H$_{39}$O$_8$N$_4$) = 643.27624 [M + H]$^+$; m/z_{found} = 643.27652 (Δ = 0.4 ppm).

^{1}H NMR (500 MHz, CD$_3$OD): δ [ppm] = 1.98 (s, H$_3$C7^1), 2.12 (s, H$_3$C13^1), 2.16 (s, H$_3$C17^1), 2.19 (s, H$_3$C2^1), 2.37 (m, H$_2$C12^2), 2.64 (m, H$_2$C3^1), 2.70 (m, H$_A$C12^1), 2.79 (m, H$_B$C12^1), 3.59 (m, H$_2$C3^2), 3.78 (s, H$_3$C8^4), 3.85 (m, HC8^2), 3.96 (m, H$_2$C5), 5.01 (HC10), 5.34 (m, H$_A$C18^2), 6.09 (d, J = 17.6, H$_B$C18^2), 6.19 (s, HC15), 6.49 (d, J = 15.0, HC18^1), 9.38 (s, HC20) (Table S2).

***Cj*-methyl-PleB (4):** t_R = 14.3 min. UV/Vis online spectrum (nm, rel ε): 216 (1.00), 242 (0.70), 312 (0.59) nm. HRMS (ESI): $m/z_{calculated}$ (C$_{36}$H$_{43}$O$_8$N$_4$) = 659.30754 [M + H]$^+$; m/z_{found} = 659.30724 (Δ = 0.5 ppm). MS/MS (ESI): m/z (%) = 659.1 (100, [M − H]$^+$); 627.0 (12, [M+H-CH$_4$O]$^+$); 474.2 (2, [M+H- CH$_4$O-ringA]$^+$).

^{1}H NMR (500 MHz, CD$_3$OD): δ [ppm] = 1.85 (s, H$_3$C13^1), 1.91 (s, H$_3$C17^1), 2.09 (s, H$_3$C7^1), 2.22 (s, H$_3$C2^1), 2.25 (m, H$_A$C12^2), 2.38 (m, H$_B$C12^2), 2.53 (m, H$_A$C15), 2.57 (m, H$_2$C3^1), 2.60 (m, H$_2$C12^1), 2.81 (dd, J = 14.6/5.5, H$_B$C15), 3.50 (m, H$_2$C3^2), 3.56 (m, H$_3$12^4), 3.71 (d, J = 3.2, HC8^2), 3.73 (s, H$_3$C8^4), 3.90 (d, J = 6.8, H$_2$C5), 3.99 (m, HC16), 4.82 (s, HC10), 5.31 (dd, J = 11.8/2.4, H$_A$C18^2), 6.05 (dd, J = 17.7/2.4, H$_B$C18^2), 6.40 (m, HC18^1), 9.31 (s, HC20) (Table S3). ^{13}C NMR (500 MHz, CD$_3$OD): δ [ppm] = 8.24 (2^1), 8.67 (7^1), 8.67 (13^1), 11.67 (17^1), 19.82 (12^1), 22.83 (5), 27.55 (3^1), 28.83 (15), 36.56 (10), 35.70 (12^2), 52.00 (8^4), 57.58 (12^4), 61.12 (16), 61.87 (3^2), 68.31 (8^2), 112.29 (7), 114.99 (13), 120.37 (3), 118.51 (18^2), 119.03 (12), 123.97 (14), 125.76 (8), 126.23 (18^1), 128.45 (18), 128.90 (1), 133.84 (6), 134.74 (2), 137.88 (4), 156.29 (17), 160.33 (9), 171.10 (8^3), 174.24 (19), 177.29 (20), 174.69 (12^3), 190.85 (8^1) (Table S3).

***Cj*-ethyl-PleB (5):** t_R = 15.1 min. UV/Vis online spectrum (nm, rel ε): 216 (1.00), 244 (0.71), 312 (0.58) nm. HRMS (ESI): $m/z_{calculated}$ (C$_{37}$H$_{45}$O$_8$N$_4$) = 673.32319 [M + H]$^+$; m/z_{found} = 673.32282 (Δ = 0.5 ppm). MS/MS (ESI): m/z (%) = 673.1 (100, [M + H]$^+$); 504.9 (16, [M+H-C$_2$H$_6$O-ringD]$^+$).

^{1}H NMR (500 MHz, CD$_3$OD): δ [ppm] = 1.14 (t, J = 7.0, H$_3$C12^5), 1.86 (s, H$_3$C13^1), 1.92 (s, H$_3$C17^1), 2.09 (s, H$_3$C7^1), 2.22 (s, H$_3$C2^1), 2.24 (m, H$_A$C12^2), 2.35 (m, H$_B$C12^2), 2.53 (m, H$_A$C15), 2.57 (m, H$_2$C3^1), 2.60 (m, H$_2$C12^1), 2.81 (dd, J = 14.6/5.4, H$_B$C15), 3.51 (m, H$_2$C3^2), 3.57 (q, J = 7.1, H$_2$12^4), 3.71 (d, J = 3.2 HC8^2), 3.73 (s, H$_3$C8^4), 3.90 (d, J = 6.3, H$_2$C5), 4.02 (m, HC16), 4.82 (s, HC10), 5.31 (dd, J = 11.7/2.4, H$_A$C18^2), 6.05 (dd, J = 17.7/2.4, H$_B$C18^2), 6.39 (dd, J = 17.8/11.7, HC18^1), 9.31 (s, HC20) (Table S3). ^{13}C NMR (500 MHz, CD$_3$OD): δ [ppm] = 8.24 (2^1), 8.24 (7^1), 8.67 (13^1), 11.67 (17^1), 17.68 (12^5), 19.82 (12^1), 22.83 (5), 27.12 (3^1), 29.26 (15), 36.56 (10), 36.13 (12^2), 52.00 (8^4), 57.58 (12^4), 60.67 (16), 61.87 (3^2), 68.31 (8^2), 111.84 (7), 114.54 (13), 119.93 (3), 118.50 (18^2), 118.58 (12), 123.52 (14), 125.31 (8), 125.80 (18^1), 128.01 (18), 128.45 (1), 133.39 (6), 134.29 (2), 137.43 (4), 155.84 (17), 159.43 (9), 170.65 (8^3), 173.79 (19), 174.24 (12^3), 177.28 (20), 190.85 (8^1) (Table S3).

***Cj*-butyl-PleB (6):** t_R = 16.7 min. UV/Vis online spectrum (nm, rel ε): 216 (1.00), 242 (0.71), 312 (0.57) nm. HRMS (ESI): $m/z_{calculated}$ (C$_{39}$H$_{49}$O$_8$N$_4$) = 701.35449 [M + H]$^+$; m/z_{found} = 701.35422 (Δ = 0.4 ppm). MS/MS (ESI): m/z (%) = 701.2 (100, [M + H]$^+$); 627.4 (8, [M+H-C$_4$H$_{10}$O]$^+$); 504.6 (21, [M+H-C$_4$H$_{10}$O-ringD]$^+$).

^{1}H NMR (500 MHz, CD$_3$OD): δ [ppm] = 0.87 (t, J = 7.4 H$_3$C12^7), 1.3 (m, H$_2$C12^6), 1.52 (m, H$_2$C12^5), 1.86 (s, H$_3$C13^1), 1.91 (s, H$_3$C17^1), 2.09 (s, H$_3$C7^1), 2.22 (s, H$_3$C2^1), 2.25 (m, H$_A$C12^2), 2.36 (m, H$_B$C12^2), 2.53 (m, H$_A$C15), 2.58 (m, H$_2$C3^1), 2.60 (m, H$_2$C12^1), 2.77 –2. 85 (m, H$_B$C15), 3.51 (m, H$_2$C3^2), 3.71 (d, J = 1.9 HC8^2), 3.73 (s, H$_3$C8^4), 3.90 (d, J = 6.1, H$_2$C5), 3.96 (m, HC16), 3.97 (m, H$_2$12^4), 4.82 (s, HC10), 5.31 (dd, J = 11.7/2.4, H$_A$C18^2), 6.05 (dd, J = 17.7/2.4, H$_B$C18^2), 6.39

EurJOC
European Journal of Organic Chemistry

Full Paper
doi.org/10.1002/ejoc.202000692

Chemistry Europe
European Chemical Societies Publishing

(dd, J = 17.8/11.7, HC18^1), 9.31 (s, HC20) (Table S4). ^{13}C NMR (500 MHz, CD$_3$OD): δ [ppm] = 8.24 (2^1), 8.24 (7^1), 8.67 (13^1), 11.67 (17^1), 12.35 (12^7), 17.50 (12^6), 19.82 (12^1), 22.83 (5), 27.12 (3^1), 29.26 (15), 30.37 (12^5), 36.56 (10), 36.13 (12^2), 52.00 (8^4), 61.12 (16), 61.87 (3^2), 63.84 (12^4), 112.29 (7), 114.99 (13), 118.51 (18^2), 119.03 (12), 120.37 (3), 123.97 (14), 125.76 (8), 126.23 (18^1), 128.45 (18), 128.90 (1), 133.84 (6), 134.74 (2), 137.88 (4), 156.29 (17), 159.88 (9), 171.10 (8^3), 174.24 (19), 174.69 (12^3), 177.29 (20) (Table S4).

***Cj*-octyl-PleB (7):** t_R = 20.4 min. UV/Vis online spectrum (nm, rel ε): 216 (1.00), 242 (0.70), 310 (0.56) nm. MS/MS (ESI): $m/z_{calculated}$ (C$_{43}$H$_{57}$O$_8$N$_4$) = 757.41709 [M + H]$^+$; m/z_{found} = 757.41669 (Δ = 0.5 ppm). MS/MS (ESI): m/z (%) = 757.1 (100, [M + H]$^+$); 725.2 (6, [M+H-CH$_4$O]$^+$); 504.8 (18, [M+H-C$_8$H$_{18}$O-ringD]$^+$).

^{1}H NMR (500 MHz, CD$_3$OD): δ [ppm] = 0.85 (m, H$_3$C12^{11}), 1.18–1.61 (m, H$_2$C12$^{7–10}$), 1.46–1.61 (m, H$_2$C12^5, H$_2$C12^6), 1.86 (s, H$_3$C13^1), 1.91 (s, H$_3$C17^1), 2.09 (s, H$_3$C7^1), 2.22 (s, H$_3$C2^1), 2.27 (m, H$_A$C12^2), 2.33 (m, H$_B$C12^2), 2.53 (m, H$_A$C15), 2.57 (m, H$_2$C3^1), 2.60 (m, H$_2$C12^1), 2.81 (dd, J = 14.6/5.4 H$_B$C15), 3.51 (m, H$_2$C3^2), 3.71 (d, J = 3.3 HC8^2), 3.73 (s, H$_3$C8^4), 3.90 (d, J = 5.7, H$_2$C5), 3.97 (m, HC16), 3.97 (m, H$_2$12^4), 4.82 (s, HC10), 5.31 (dd, J = 11.7/2.4, H$_A$C18^2), 6.05 (dd, J = 17.8/2.4, H$_B$C18^2), 6.39 (dd, J = 17.8/11.6, HC18^1), 9.31 (s, HC20) (Table S4). ^{13}C NMR (500 MHz, CD$_3$OD): δ [ppm] = 8.24 (2^1), 8.67 (7^1), 8.67 (13^1), 11.67 (17^1), 13.82 (12^{11}), 14.68 (12^{10}), 20.25 (12^1), 21.97 (12^9), 22.83 (5), 25.40 (12^8), 27.55 (3^1), 28.83 (12^6), 29.26 (15), 29.69 (12^7), 31.84 (12^5), 36.56 (10), 36.13 (12^2), 52.00 (8^4), 60.67 (16), 61.87 (3^2), 64.87 (12^4), 68.31 (8^2), 111.85 (7), 114.54 (13), 118.51 (18^2), 118.58 (12), 119.93 (3), 123.52 (14), 125.31 (8), 126.66 (18^1), 128.01 (18), 128.45 (1), 133.39 (6), 134.29 (2), 137.43 (4), 155.84 (17), 159.43 (9), 170.65 (8^3), 173.79 (19), 174.24 (12^3), 177.29 (20) (Table S4).

Cell Proliferation Assay: Proliferation of PB treated T24 and MDA-MB-231 cells was determined by a crystal violet staining. 4×10^3 (MDA-MB-231) or 2.5×10^3 (T24) cells were seeded in 96 well plates and grown for 24 h. Cells were incubated with indicated concentrations of compounds for 72 h, followed by washing with PBS + and staining with 0.5 % crystal violet solution for 10 min. After washing the cells with water and drying overnight, crystal violet was redissolved with trisodium citrate solution, and absorption at 550 nm was measured with a SpectraFluor Plus plate reader (Tecan, Crailsheim, Germany). The number of viable cells was calculated by subtracting the average of the day 0 control values and normalizing to the corresponding DMSO control.

Clonogenic Assay: T24 and MDA-MB-231 cells were seeded at 3×10^5 cells/well in a 6 well plate and allowed to attach for one day, before incubating with PxB (**2**) (10 μM) and DMSO vehicle control for 24 h. Cells were harvested and re-seeded at 5000 cells/well for MDA-MB-231 and 3000 cells/well for T24 cells in 6 well plates in triplicates. After one week, cells were washed with PBS+, stained with 0.5 % crystal violet solution for 10 min and again washed with water. The plate was dried overnight and pictures of the colonies were captured with a digital camera (Canon DS126181). After the addition of trisodium citrate solution, the absorption was measured at 550 nm with a SpectraFluor Plus plate reader (Tecan, Crailsheim, Germany). The clonogenic growth of treated cells was normalized to the corresponding DMSO control.

Annexin V/PI Staining Assay: To quantify *Cj*-PxB (**2**) induced cell death, a co-staining with FITC conjugated AnnexinV (AnnV) and propidium iodide (PI) was performed with an AnnexinV/PI staining kit (Thermo Fisher Scientific, Waltham, MA, USA) according to the manufacturer's instructions. In brief, 3×10^4 cells were cultured in 24 well plates for 24 h before incubating with indicated concentrations of **2** for 24 or 48 h. Cells were harvested, washed with PBS, and incubated with FITC conjugated AnnV in binding buffer for 10 min. After washing with binding buffer, PI solution was added and cells were immediately analyzed by a BD FACS Canto™ II cytometer. PI and AnnV negative cells were identified as living cells, PI negative and AnnV positive as early apoptotic cells, PI positive and AnnV positive as late apoptotic, and PI positive and AnnV negative as necrotic cells. Data were processed with FlowJo 7.6 software.

Cell Cycle Analysis Assay: The cell cycle distribution of T24 and MDA-MB-231 cells was determined by propidium iodide staining and flow cytometry according to the protocol of Nicoletti et al.[28] Briefly, 3×10^4 cells were seeded and allowed to attach for one day. Next, cells were treated with **2** (5, 10, 20 μM), and DMSO as a vehicle control and incubated for 24 or 48 h. Subsequently, cells were detached, washed with PBS, and stained with fluochrome solution (50 μg/mL PI in a solution of 0.1 % sodium citrate (w/v) and 0.1 % Triton X-100 (v/v) in deionized water) for 30 min at 4 °C in the dark. Cell cycle was analyzed using a BD FACS Canto™ II and data were evaluated using FlowJo 7.6 software.

Cell Uptake Assay: The uptake of PBs was determined by analytical HPLC analysis. 1.5×10^6 T24 cells were seeded in 60 mm dishes and incubated for one day. Next, cells were treated with *Cj*-PleB (**1**), *Po*-PleB (**3**), PxB (**2**), and PleB-esters (**4–7**) (80 μM) for 5 h. After washing twice with ice-cold PBS, cells were scraped off in 500 μL of PBS and cell suspension was centrifuged at 13000 rpm for 5 min at 4 °C. The supernatant was discarded and the cell pellet was again washed with PBS. Cells were lysed by bead beating and proteins were precipitated with 120 μL of ACN/PBS (20:80) for 1 h on ice. Lysates were centrifuged again and a 50 μL aliquot of the supernatant was analyzed by HPLC. The peak areas of the different compounds were normalized to the peak area of the butylated ester, which was set to 100 %.

Statistical Analysis: Results represent the mean of at least three independent experiments (means ± standard deviation) performed in at least three replicates unless stated otherwise. Statistical significance was carried out by two-way analysis of variance with post hoc analysis using Dunnett's multiple comparison test; all statistical analyses were processed with GraphPad Prism 7.05.

Acknowledgments

[1] a) B. Kräutler, *Chem. Soc. Rev.*, **2014**, 43, 6227-6238; b) B. Kräutler, B. Jaun, K. Bortlik, M. Schellenberg, P. Matile, *Angew. Chem. Int. Ed. Engl.* **1991**, 30, 1315–1318; *Angew. Chem.* **1991**, 103, 1354.

[2] C. Curty, N. Engel, *Phytochemistry* **1996**, 42, 1531–1536.

[3] S. Moser, M. Ulrich, T. Müller, B. Kräutler, *Photochem. Photobiol. Sci.* **2008**, 7, 1577–1581.

[4] C. Vergeiner, M. Ulrich, C. Li, X. Liu, T. Müller, B. Kräutler, *Chem. Eur. J.* **2015**, 21, 136–149.

[5] C. J. Li, K. Wurst, S. Jockusch, K. Gruber, M. Podewitz, K. R. Liedl, B. Kräutler, *Angew. Chem. Int. Ed.* **2016**, 55, 15760–15765; *Angew. Chem.* **2016**, 128, 15992.

[6] S. Moser, B. Kräutler, *Isr. J. Chem.* **2019**, *59*, 420–431.

[7] C. A. Karg, P. Wang, A. M. Vollmar, S. Moser, *Phytomedicine* **2019**, *60*, 152969.

[8] C. Karg, C. Schilling, L. Allmendinger, S. Moser, *J. Porphyrins Phthalocyanines* **2019**, *23*, 881–888.

[9] P. Keshavan, S. J. Schwemberger, D. L. H. Smith, G. F. Abcock, S. D. Zucker, *Int. J. Cancer* **2004**, *112*, 433–445.

[10] M. Ulrich, S. Moser, T. Müller, B. Kräutler, *Chem. Eur. J.* **2011**, *17*, 2330–2334.

[11] K. L. Wüthrich, L. Bovet, P. E. Hunziker, I. S. Donnison, S. Hörtensteiner, *Plant J.* **2000**, *21*, 189–198 .

[12] a) B. Kräutler, *Angew. Chem. Int. Ed.* **2016**, *55*, 4882–4907; *Angew. Chem.* **2016**, *128*, 4964; b) M. Oberhuber, J. Berghold, K. Breuker, S. Hörtensteiner, B. Kräutler, *Proc. Natl. Acad. Sci. USA* **2003**, *100*, 6910–6915.

[13] D. Wakana, H. Kato, T. Momose, N. Sasaki, Y. Ozeki, Y. Goda, *Tetrahedron Lett.* **2014**, *55*, 2982–2985.

[14] M. Scherl, T. Müller, B. Kräutler, *Chem. Biodiversity* **2012**, *9*, 2605–2617.

[15] T. Erhart, C. Mittelberger, C. Vergeiner, G. Scherzer, B. Holzner, P. Robatscher, M. Oberhuber, B. Kräutler, *Chem. Biodiversity* **2016**, *13*, 1441–1453.

[16] M. Scherl, T. Müller, C. Kreutz, R. G. Huber, E. Zass, K. R. Liedl, B. Kräutler, *Chem. Eur. J.* **2016**, *22*, 9498–9503.

[17] B. Kuai, J. Chen, S. Hörtensteiner, *J. Exp. Bot.* **2017**, *69*, 751–767.

[18] J. Liu, H. Wang, N. E. Manicke, J.-M. Lin, R. G. Cooks, Z. Ouyang, *Anal. Chem.* **2010**, *82*, 2463–2471.

[19] J. Liu, H. Wang, R. G. Cooks, Z. Ouyang, *Anal. Chem.* **2011**, *83*, 7608–7613.

[20] B. Christ, M. Hauenstein, S. Hörtensteiner, *Plant J.* **2016**, *88*, 505–518.

[21] T. Müller, S. Vergeiner, B. Kräutler, *Int. J. Mass Spectrom.* **2014**, *365–366*, 48–55.

[22] A. Gossauer, *The Chemistry of Linear Oligopyrroles and Bile Pigments* (Ed.: H. Falk), Springer, Wien **1989**. XII, 621 pp., ISBN 3-211-82112-0. **1990**, 102 (3), 345–346. **1990**, *102*, 345–346.

[23] J. Y. Takemoto, C.-W. T. Chang, D. Chen, G. Hinton, *Isr. J. Chem.* **2019**, *59*, 378–386.

[24] S. Gazzin, L. Vitek, J. Watchko, S. M. Shapiro, C. Tiribelli, *Trends Mol. Med.* **2016**, *22*, 758–768.

[25] J. Kapitulnik, *Mol. Pharmacol.* **2004**, *66*, 773–779.

[26] P. Rao, R. Suzuki, S. Mizobuchi, T. Yamaguchi, S. Sasaguri, *Biochem. Biophys. Res. Commun.* **2006**, *342*, 1279–1283.

[27] T. Müller, M. Ulrich, K. H. Ongania, B. Krautler, *Angew. Chem. Int. Ed.* **2007**, *46*, 8699–8702; *Angew. Chem.* **2007**, *119*, 8854.

[28] a) I. Nicoletti, G. Migliorati, M. C. Pagliacci, F. Grignani, C. Riccardi, *J. Immunol. Methods* **1991**, *139*, 271–279; b) C. Riccardi, I. Nicoletti, *Nat. Protoc.* **2006**, *1*, 1458–1461.

[29] I. Süssenbacher, C. Kreutz, B. Christ, S. Hörtensteiner, B. Kräutler, *Chem. Eur. J.* **2015**, *21*, 11664–11670.

[30] S. Moser, T. Müller, M.-O. Ebert, S. Jockusch, N. J. Turro, B. Kräutler, *Angew. Chem. Int. Ed.* **2008**, *47*, 8954–8957; *Angew. Chem.* **2008**, *120*, 9087.

[31] T. Erhart, C. Mittelberger, X. Liu, M. Podewitz, C. Li, G. Scherzer, G. Stoll, J. Valls, P. Robatscher, K. R. Liedl, M. Oberhuber, B. Kräutler, *Chem. Eur. J.* **2018**, *24*, 17268–17279.

[32] M. Roca, A. Pérez-Gálvez, *J. Nat. Prod.* **2020**, *83*, 873–880.

[33] R. Zhang, X. Qin, F. Kong, P. Chen, G. Pan, *Drug Delivery* **2019**, *26*, 328–342.

Supporting Information

Phylloxanthobilins are Abundant Linear Tetrapyrroles from Chlorophyll Breakdown with Activities Against Cancer Cells

Cornelia A. Karg, Pengyu Wang, Florian Kluibenschedl, Thomas Müller, Lars Allmendinger, Angelika M. Vollmar, Simone Moser*

Content   S1

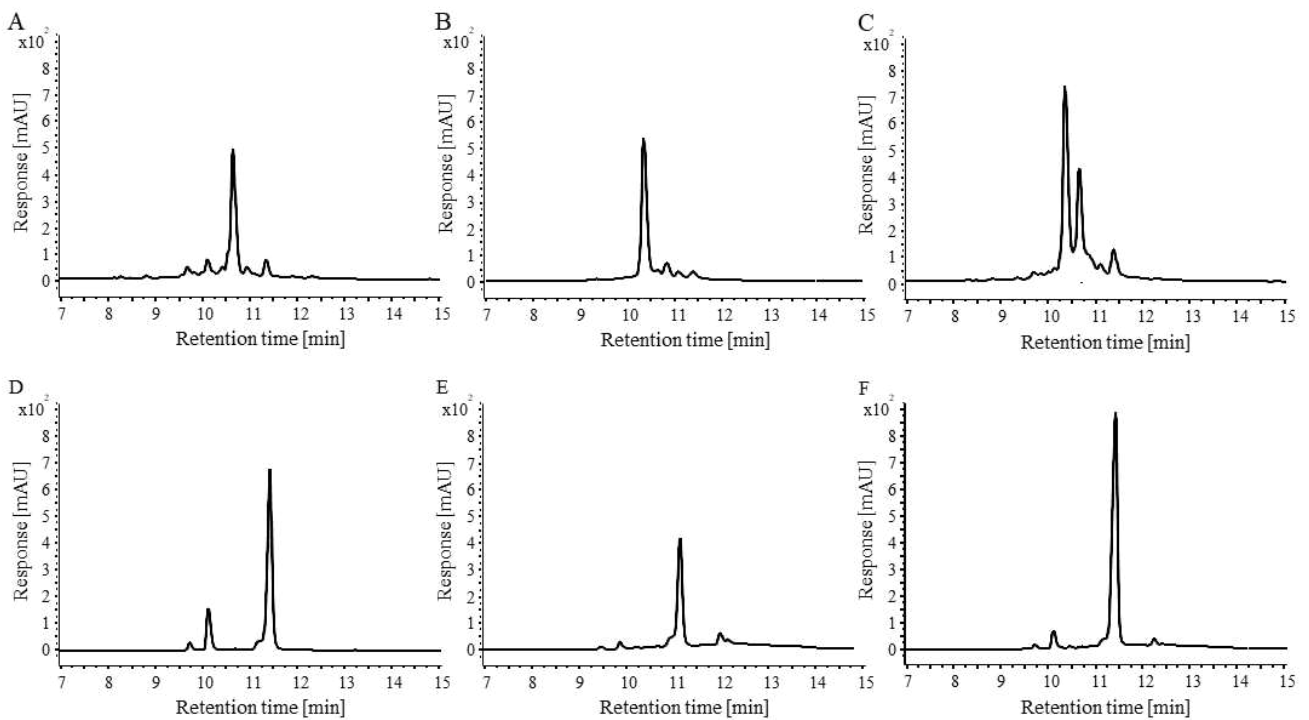**Figure S1**. UV Vis spectra of PBs. *Po*-**PleB** (**3**) (A) and *Po*-**PxB** (**2**) (B) detected in a senescent leaf of Plane tree (see main text Figure 1).

Figure S2. Co-elution experiments with isolated *Cj*-**PleB** (**1**) (A), *Po*-**PleB** (**3**) (B), a mixture of *Cj*-**PleB** (**1**) and *Po*-**PleB** (**3**) (C), *Cj*-**PxB** (**2**) (D), *Po*-**PxB** (**2**) (E) and a mixture of *Cj*-**PxB** (**2**) and *Po*-**PxB** (**2**) (F). (Detection at 320 nm). Shoulders result from epimerization at the 8^2 position, which has been reported previously.[1]
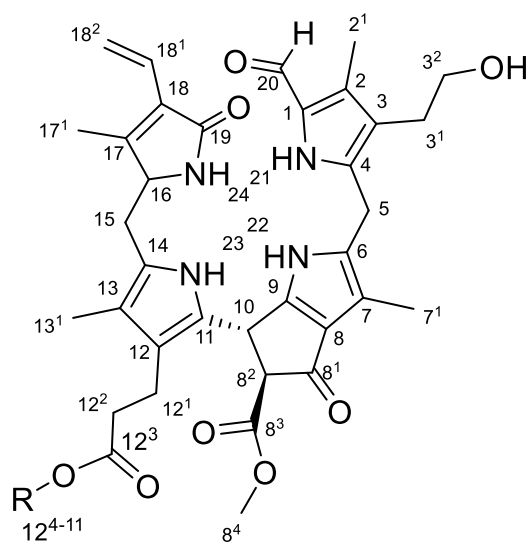
Figure S3. Atom-numbering for PBs as described previously.[2]
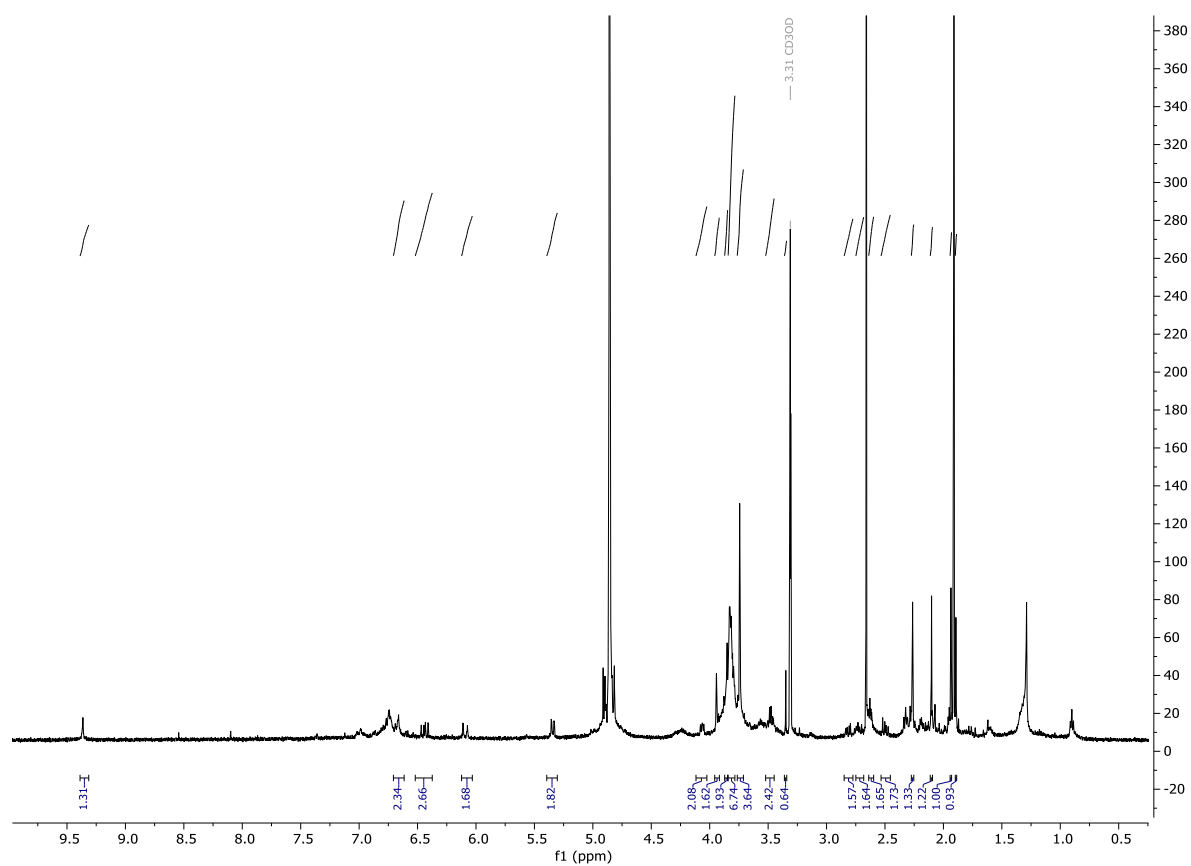
Figure S4. ^{1}H NMR spectrum of isolated *Po*-**PleB** (**3**) in d_4-methanol.
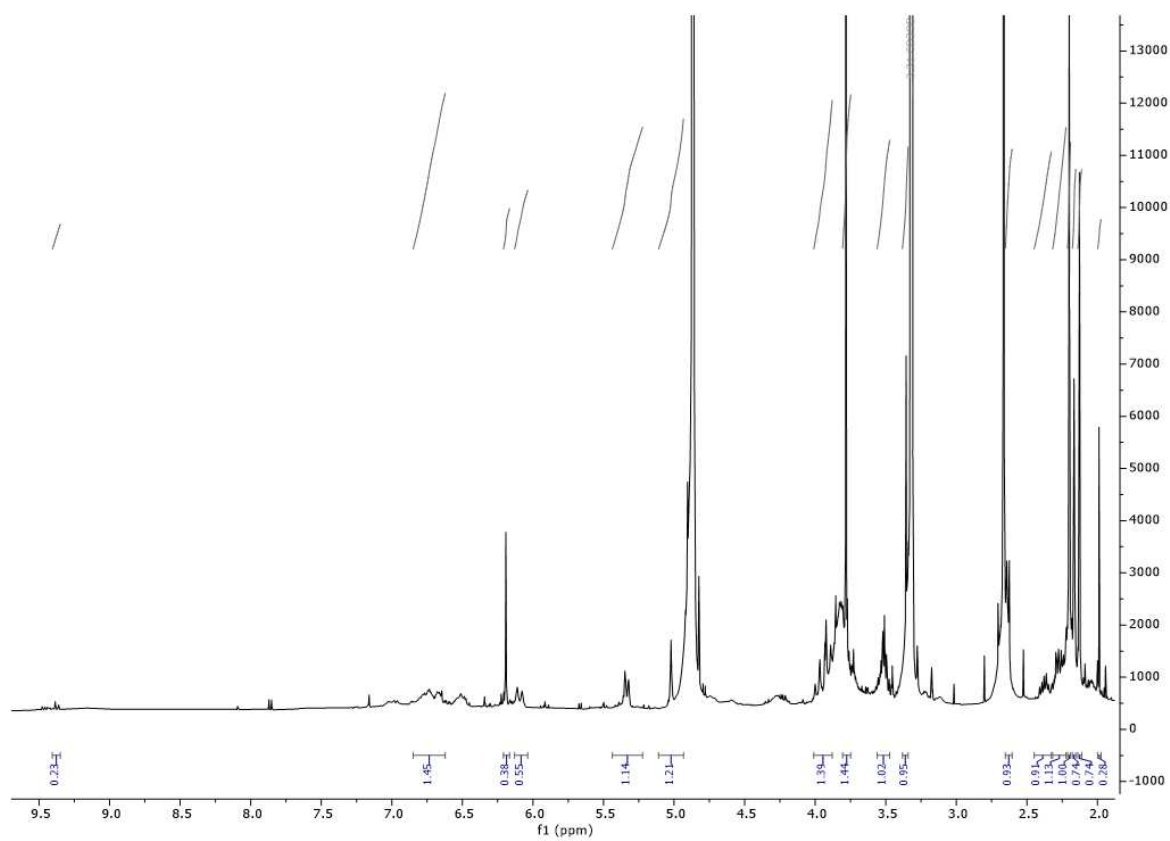
Figure S5. ^{1}H NMR spectrum of isolated *Po*-**PxB** (**2**) in d_4-methanol.

Table S1. ^{1}H and ^{13}C NMR data of *Po*-**PleB** (**3**) (500 MHz, CD$_3$OD) and published ^{1}H NMR data of *Sw*-PleB-58 (500 MHz, CD$_3$OD).[3]

	δ^{1}H/J (*Po*-PleB (3))	δ^{13}C (*Po*-PleB (3))	δ^{1}H/J (*Sw*-PleB-58) from reference [1]
C1		128.11	
C2		133.95	
H$_3$C2^1	2.26, s	8.06	2.28, s
C3		119.59	
H$_2$C3^1	2.73, m	20.93	2.71, m
H$_2$C3^2	3.47, m	61.26	3.46-3.53, m
C4		137.09	
H$_2$C5	3.94, m	22.65	3.96, s
C6		133.05	
C7		111.06	
H$_3$C7^1	2.10, s	8.06	2.11, s
C8		124.52	
C8^1		192.75	
HC8^2	3.85, m		
C8^3		170.31	
H$_3$C8^4	3.74, s	50.96	3.76, s
C9		160.43	
HC10	4.91, s	35.94	
C11		123.18	
C12		119.59	
H$_2$C12^1	2.63, m	20.93	2.61, m
H$_2$C12^2	2.32, m	38.52	2.28-2.40, m
C12^3		180.18	
C13		114.20	
H$_3$C13^1	1.94, s	8.06	1.96, s
C14			
H$_A$C15	2.50, dd, J = 14.5/8.9	27.36	2.51, dd, J = 8.9/14.4
H$_B$C15	2.82, dd, J = 14.3/5.2		2.75-2.85, m
HC16	4.06, m	59.54	4.06-4.10, m
C17		155.94	
H$_3$C17^1	1.89, s	11.92	1.90, s
C18		127.22	
HC18^1	6.44, dd, J = 11.7/17.8	126.04	6.46, dd, J = 11.6/17.7
H$_A$C18^2	5.31-5.37, m	117.03	5.36, dd, J = 1.6/11.5
H$_B$C18^2	6.09, dd, J = 17.7/2.4		6.11, dd, J = 1.7/17.7
C19		173.00	
HC20	9.36, s	176.23	9.38, s

Table S2. ^{1}H NMR data of *Po*-**PxB** (**2**) (500 MHz, CD[3]OD) and published ^{1}H and ^{13}C NMR data of *Cj*-**PxB**-2 (500 MHz, CD[3]OD).[4]

	δ[1]H/J *(Po-PxB (2))*	δ[1]H/J *(Cj-PxB-2)* from reference [2]	δ^{13}C *(Cj-PxB-2)* from reference [2]
C1			129.6
C2			
H[3]C2[1]	2.19, s	2.23, s	9.01
C3			120.7
H[2]C3[1]	2.64, m	2.63, m	28.0
H[2]C3[2]	3.59, m	3.48, m	62.6
C4			138.4
H[2]C5	3.96, s	3.96, s	23.6
C6			134.9
C7			112.2
H[3]C7[1]	1.98, s	2.13, s	9.3
C8			125.8
C8[1]			
HC8[2]	3.85, m		67.3
C8[3]			171.1
H[3]C8[4]	3.78, s	3.77, s	52.7
C9			159.9
HC10	5.01, s	5.05, s	37.1
C11			131.6
C12			124.1
H[A]C12[1] H[B]C12[1]	2.70, m 2.79, m	2.71, m 2.79, m	22.0
H[2]C12[2]	2.37, m	2.35, m	40.0
C12[3]			182.0
C13			102.6
H[3]C13[1]	2.12, s	2.15, s	9.5
C14			125.5
HC15	6.19, s	6.21, m	102.6
C16			143.1
C17			131.4
H[3]C17[1]	2.16, s	2.20, s	9.5
C18			125.0
HC18[1]	6.49, d *J* = 15.0	6.55, m	129.3
H[A]C18[2] H[B]C18[2]	5.34, m 6.09, d *J* = 17.6	5.35, dd, *J* = 2/11.5 6.11, d broad, *J* = 17.5	118.1
C19			
HC20	9.38, s		

Figure S6. Cell cycle analysis of T24 and MDA-MB-231 cells using FlowJo 7.6 software. Representative sample plot of cell cycle analysis cells treated with 20 µM of **PxB** (**2**) for 24 and 48 hours (G1 phase = green, S phase = yellow, G2/M phase = blue).
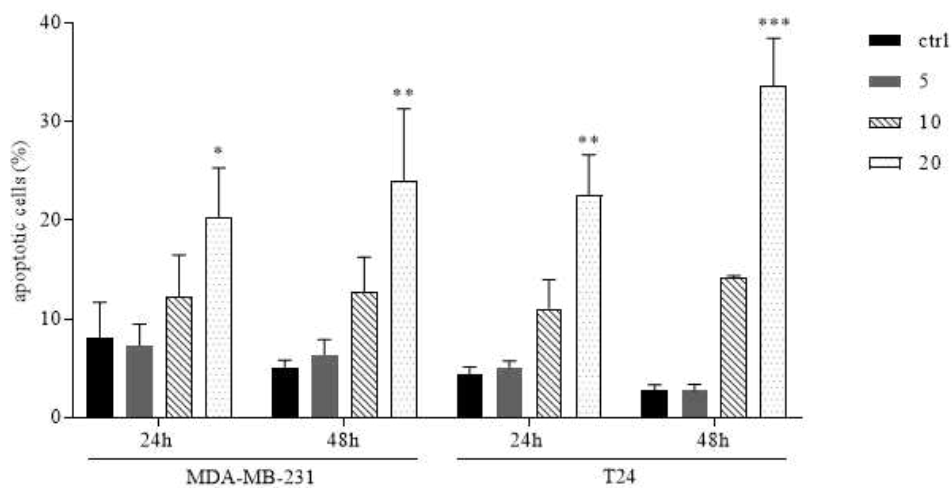
Figure S7. Flow cytometry analysis of apoptotic cells using propidium iodide. Cells were incubated with vehicle control or 5, 10 and 20 µM of **PxB** (**2**) for 24 and 48 h, harvested, permeabilized and stained with propidium iodide. Apoptotic cells were defined as percentage of cells in the subG1 cell cycle phase.
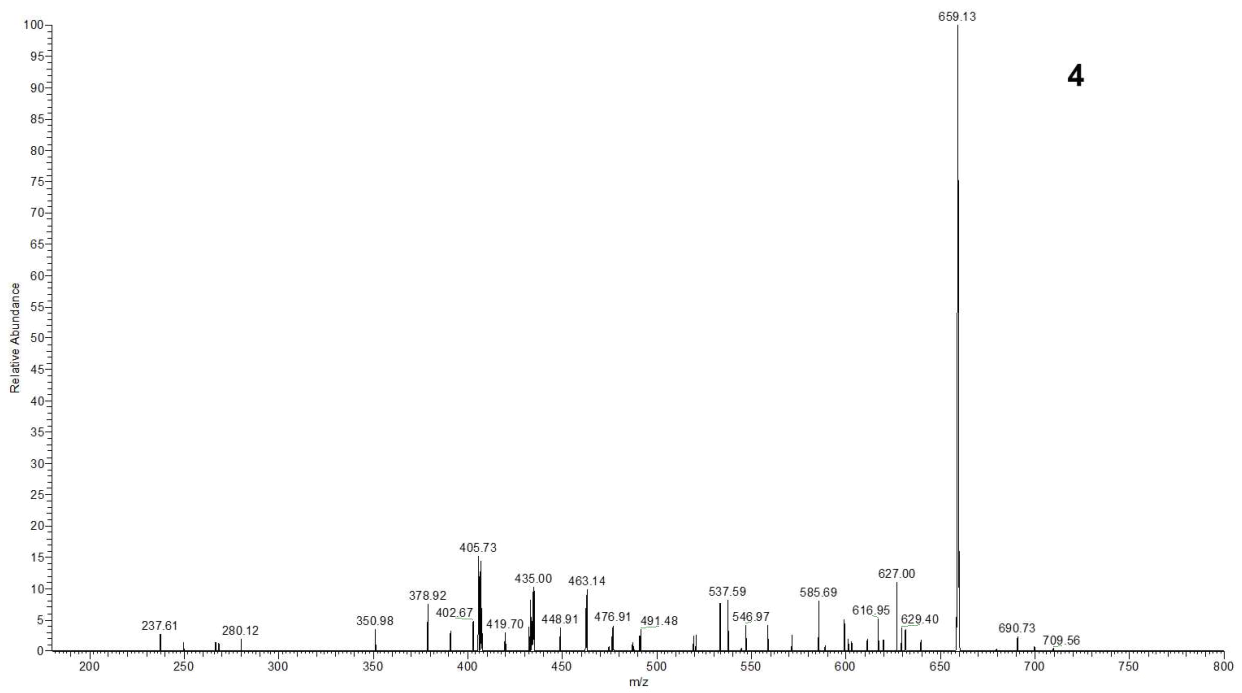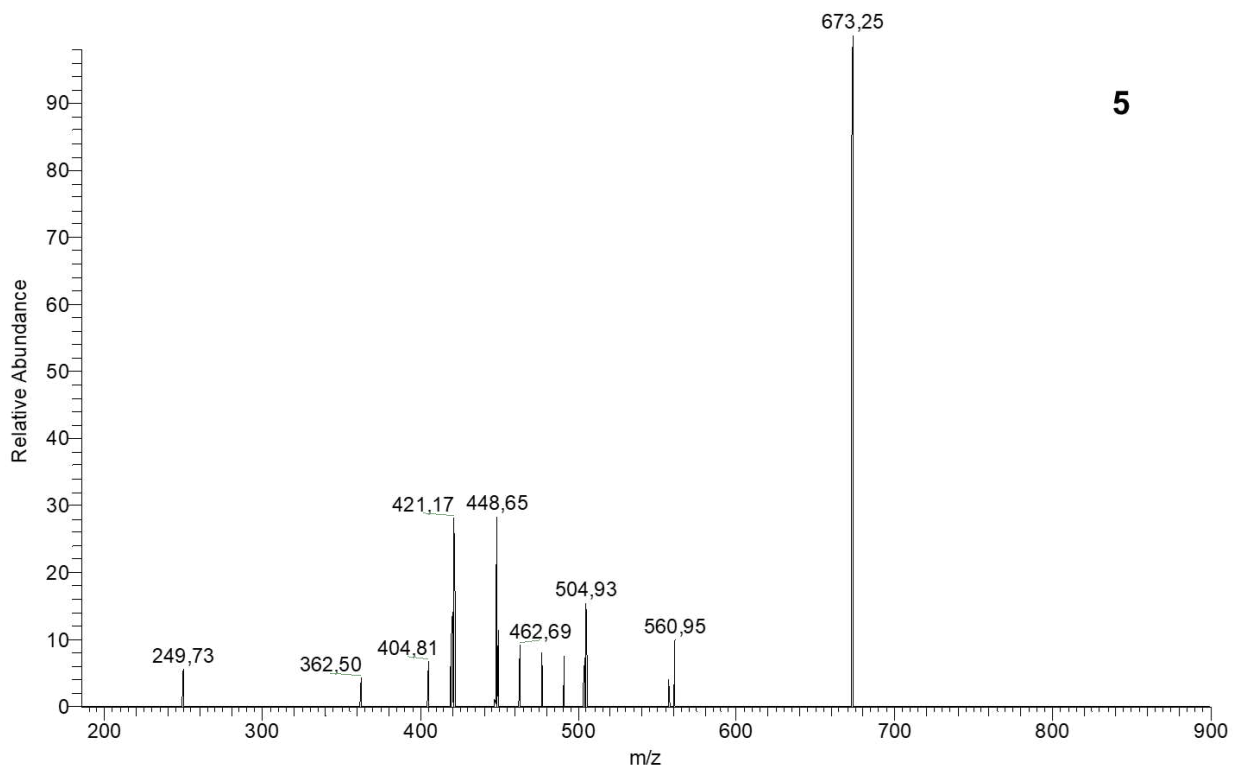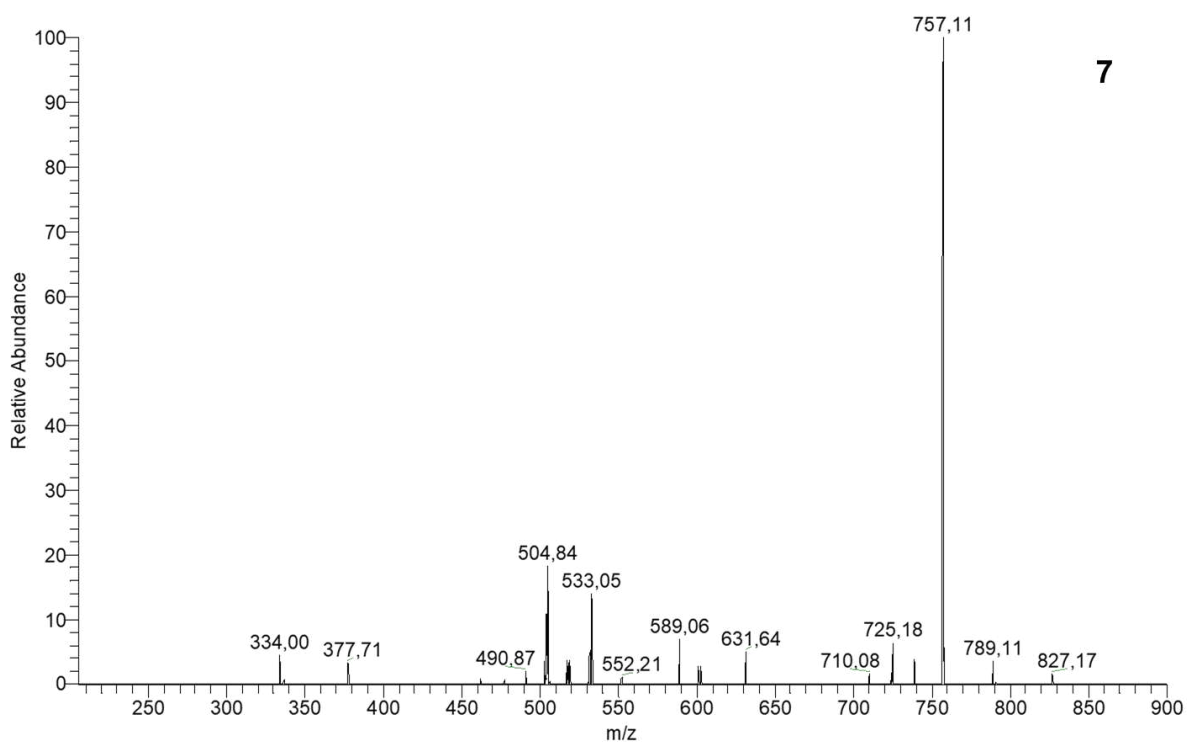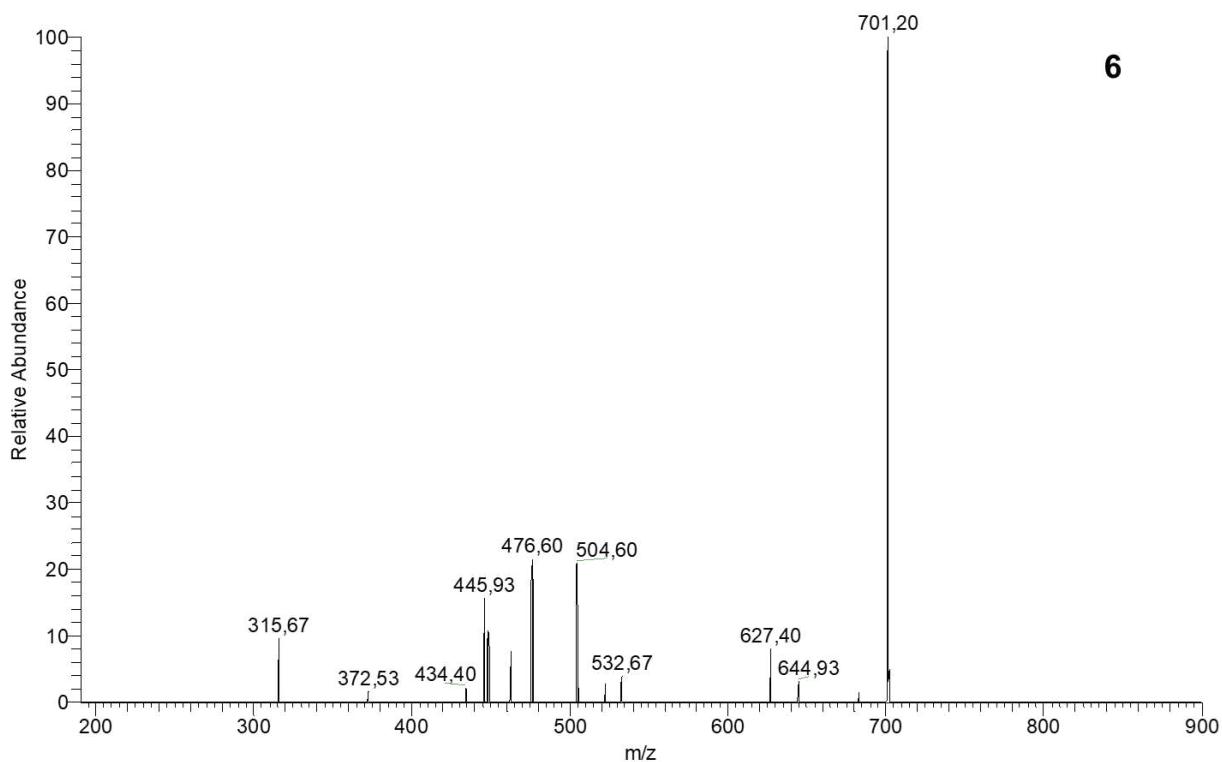
Figure S8. MS/MS (ESI) spectra of the *Cj*-PleB esters **4-7** (*Cj*-methylester **4**, *Cj*-ethylester **5**, *Cj*-butylester **6**, *Cj*-octylester **7**)
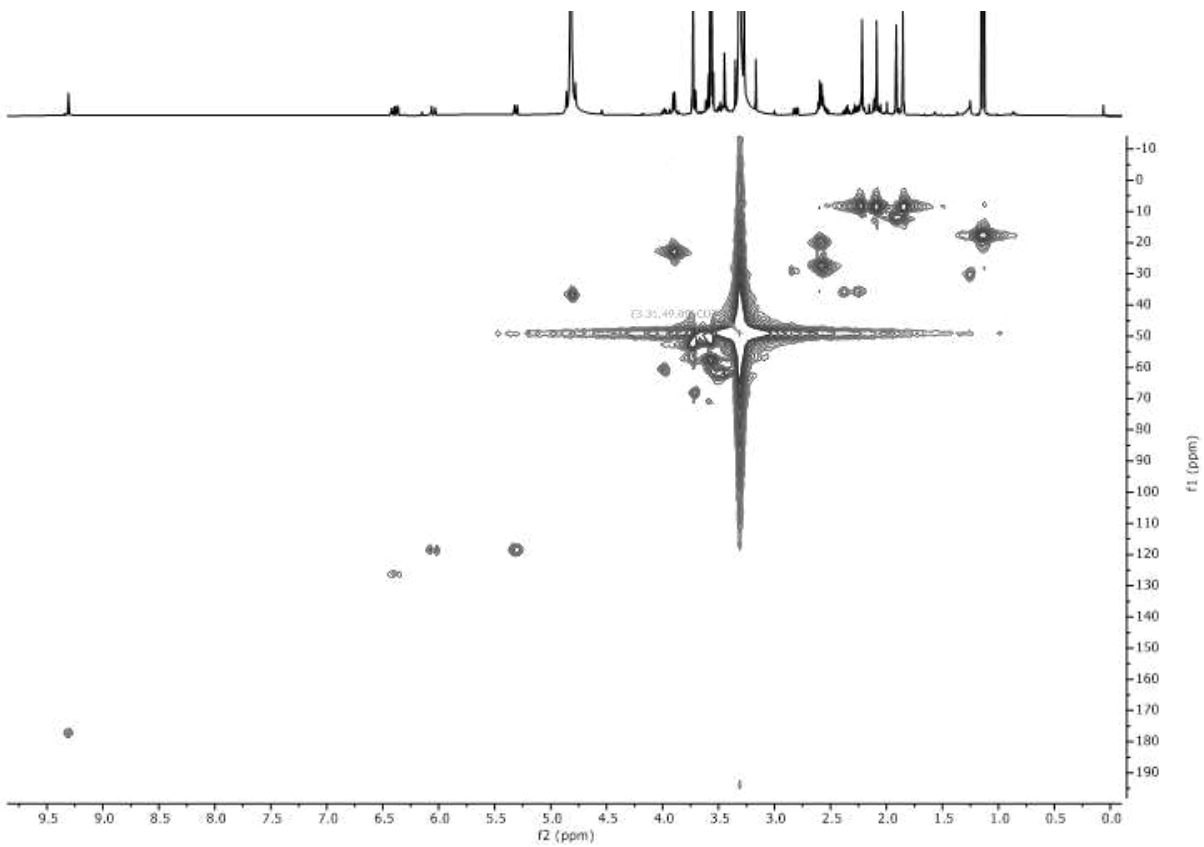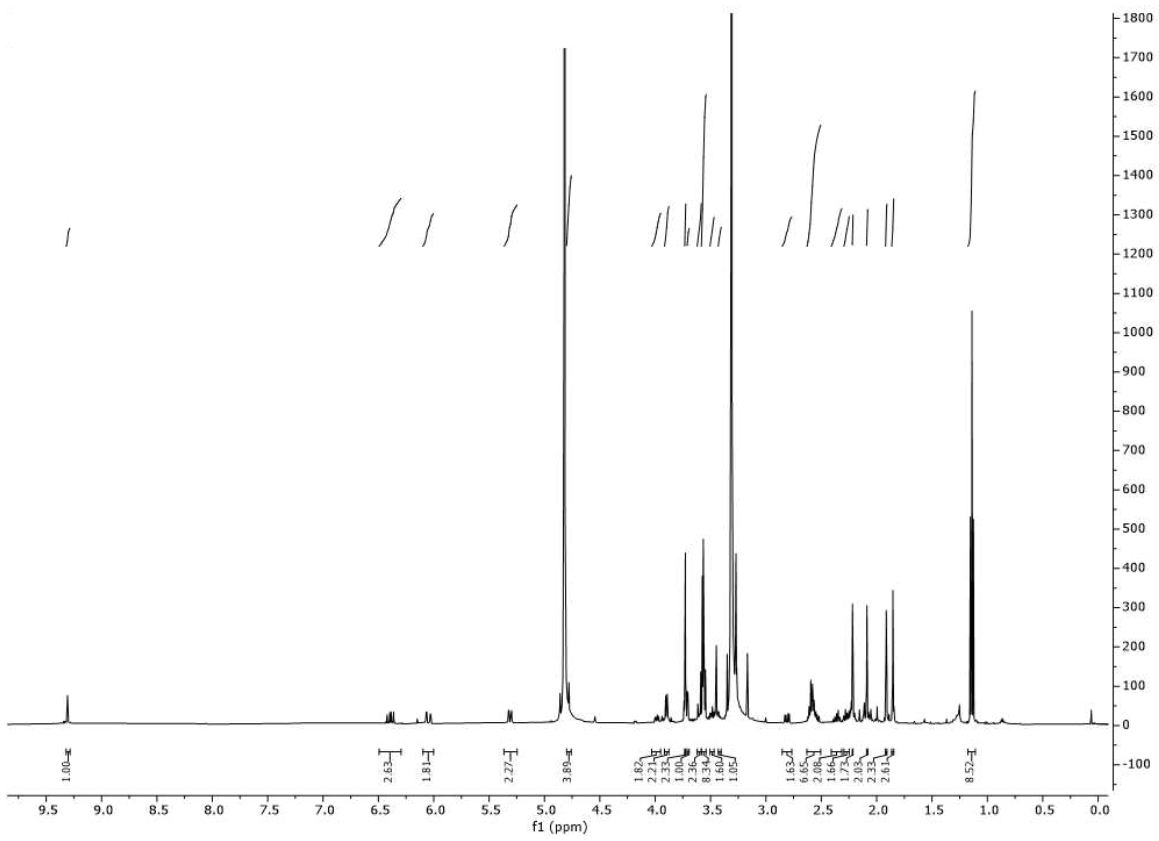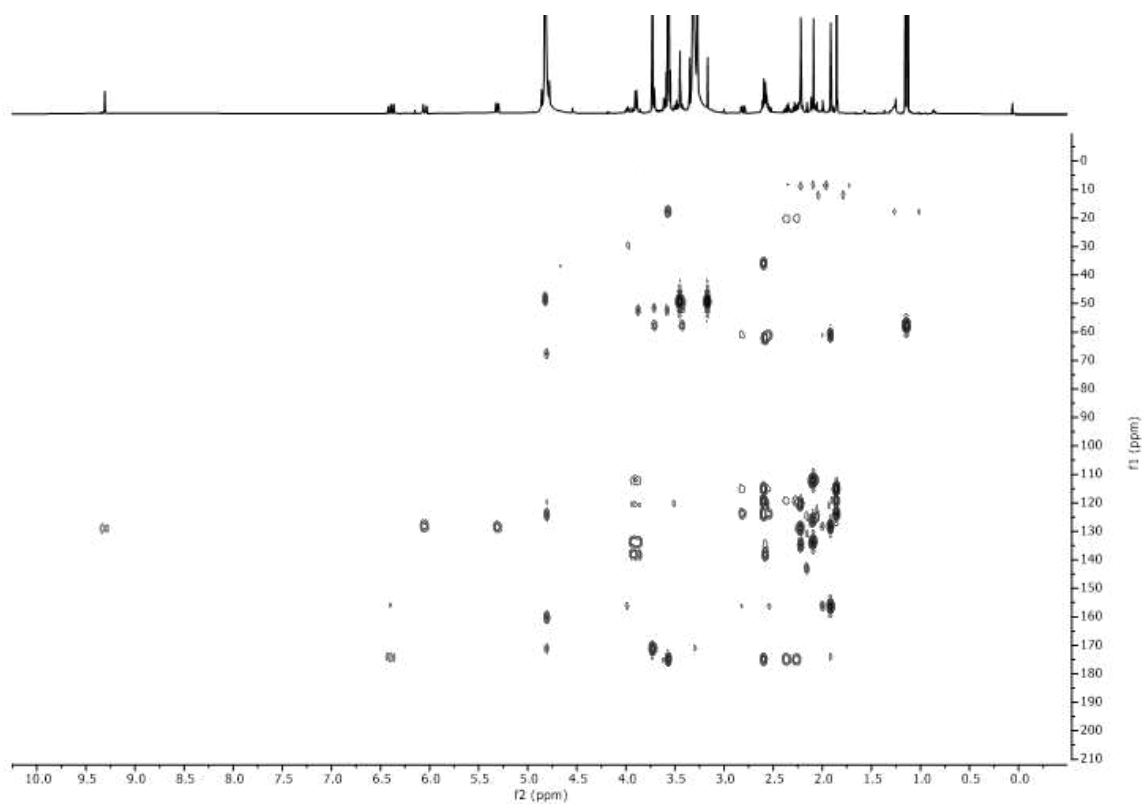
Figure S9. ^{1}H NMR and ^{1}H,^{13}C heteronuclear HMQC and HMBC spectra of synthesized *Cj*-methyl-**PleB** (**4**) in d_4-methanol.
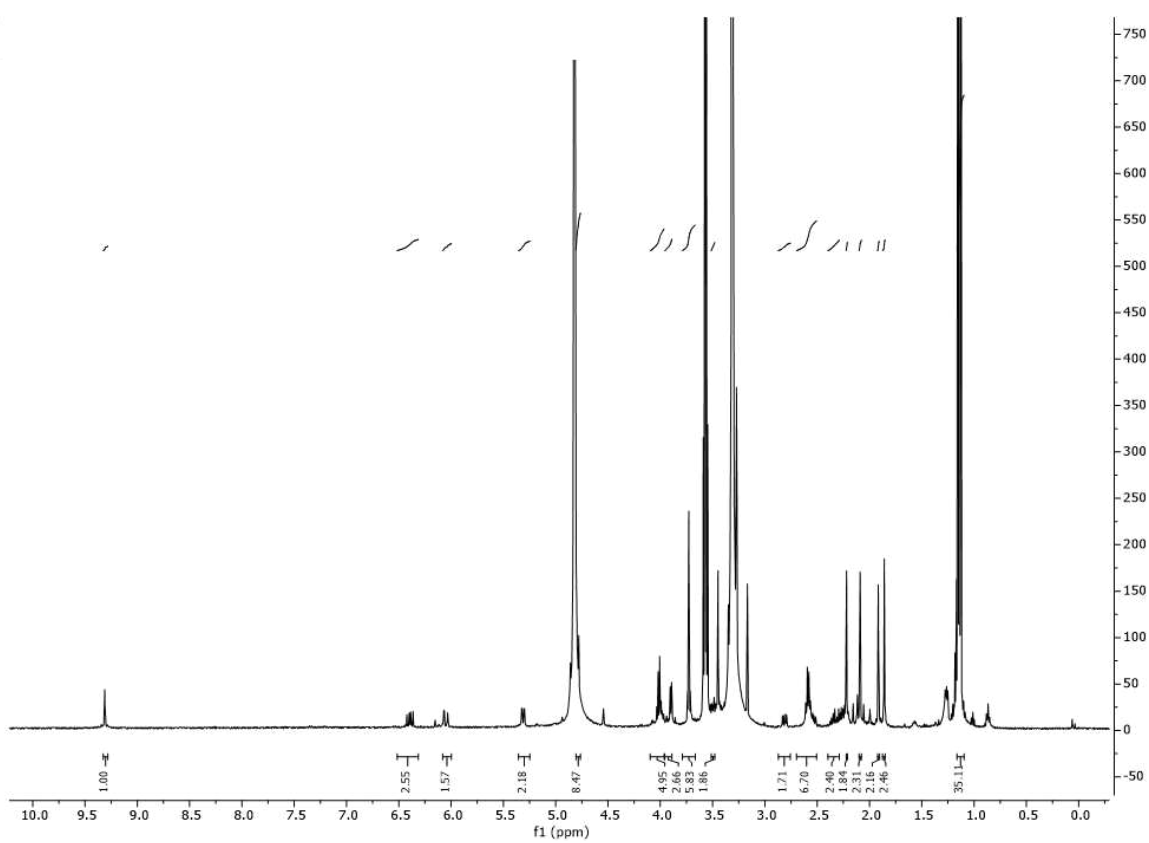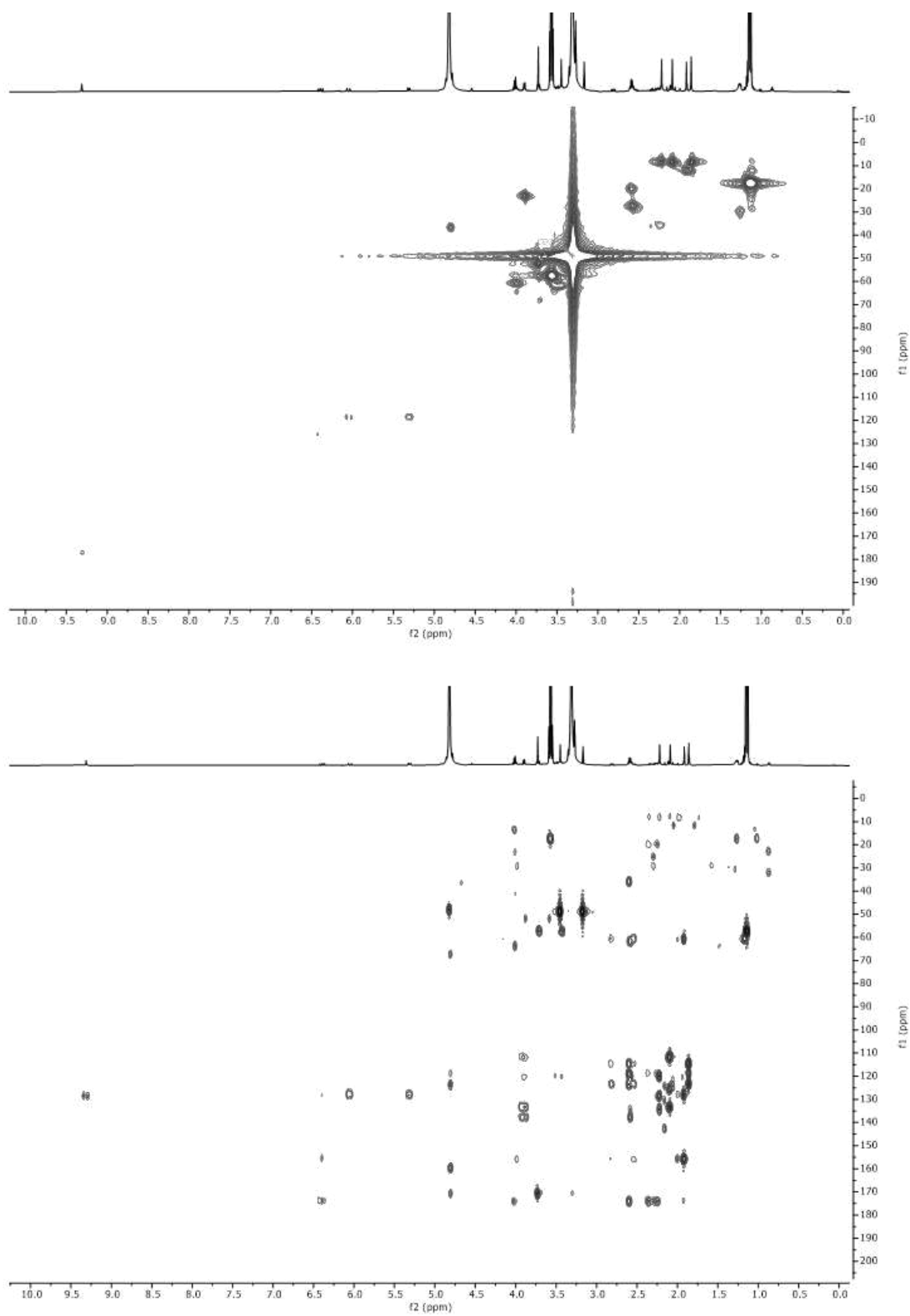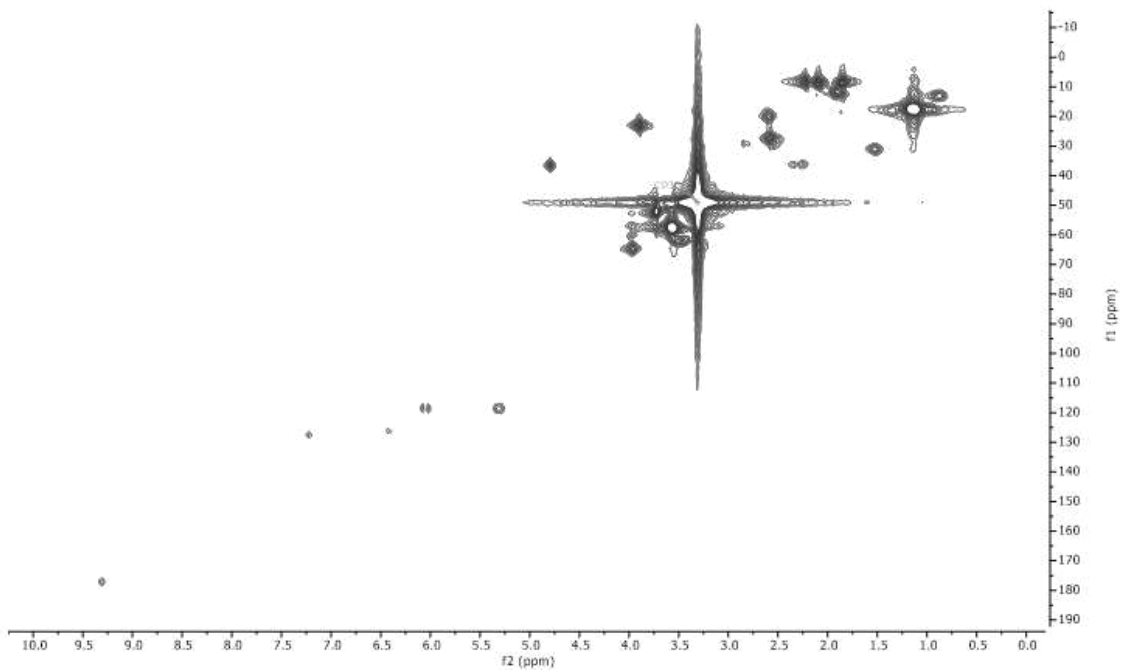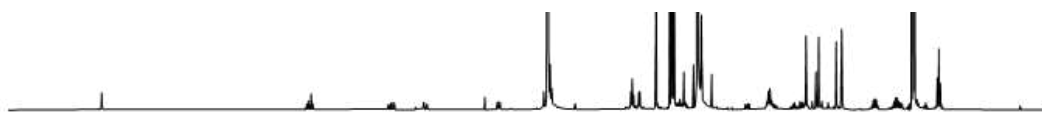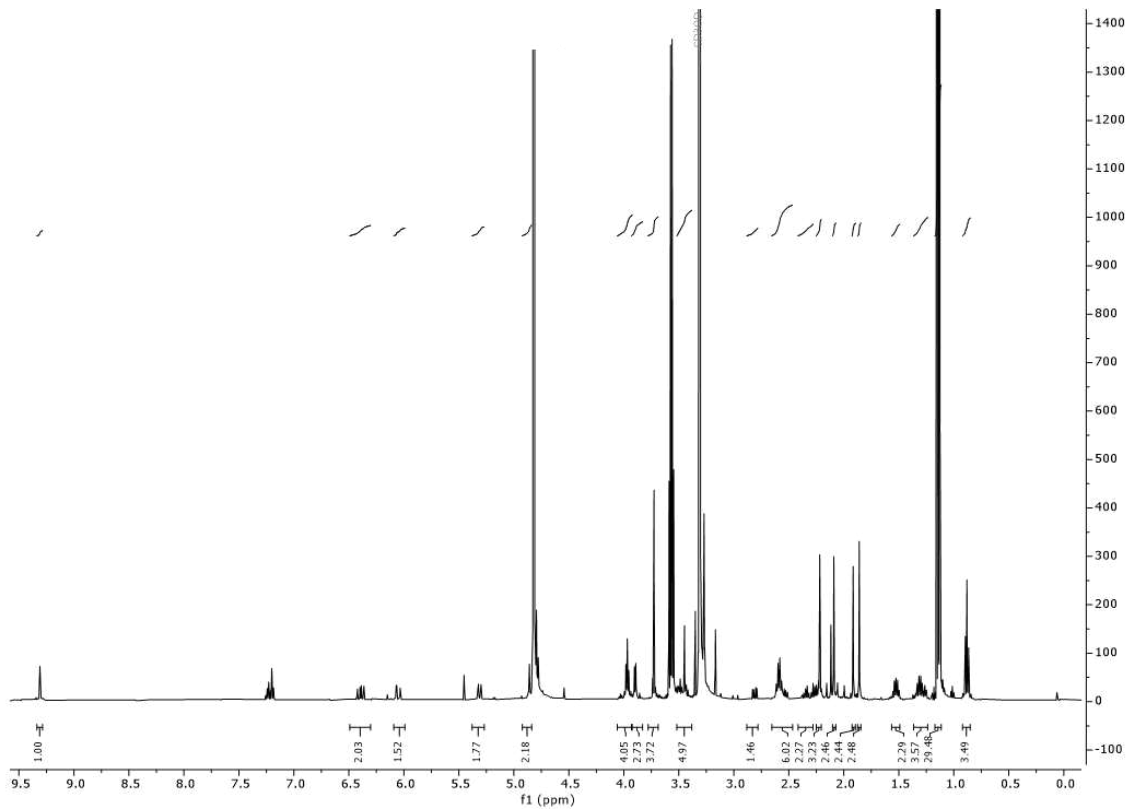
Figure S10. ^{1}H NMR and ^{1}H,^{13}C heteronuclear HMQC and HMBC spectra of synthesized *Cj*-ethyl-**PleB** (**5**) in *d*4-methanol.
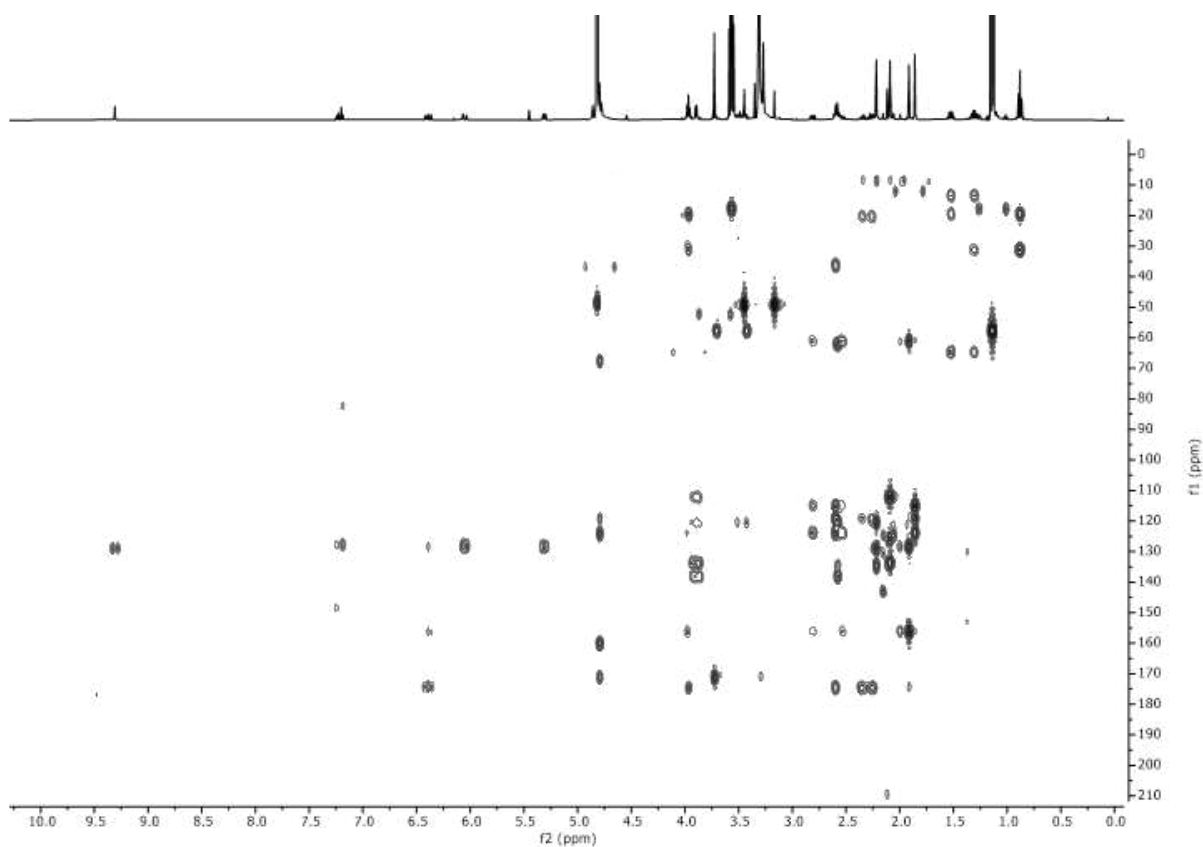
Figure S11. ^{1}H NMR and ^{1}H,^{13}C heteronuclear HMQC and HMBC spectra of synthesized *Cj*-butyl-**PleB** (**6**) in *d*$_4$-methanol.
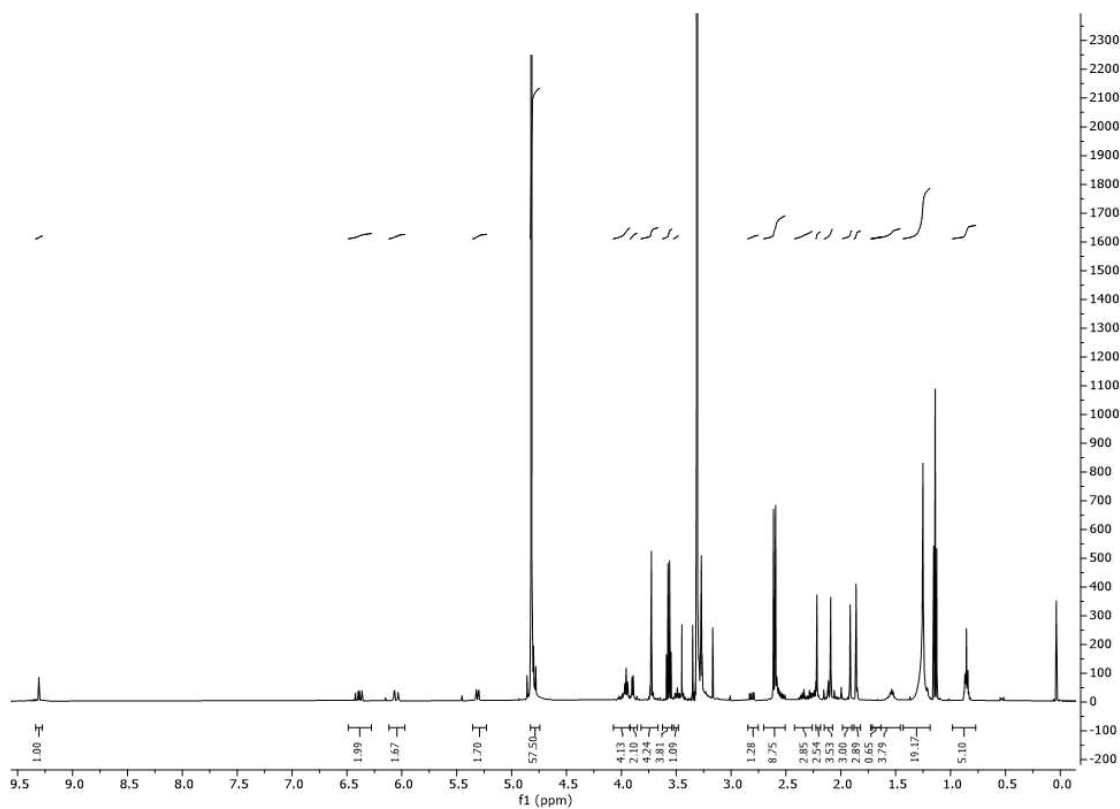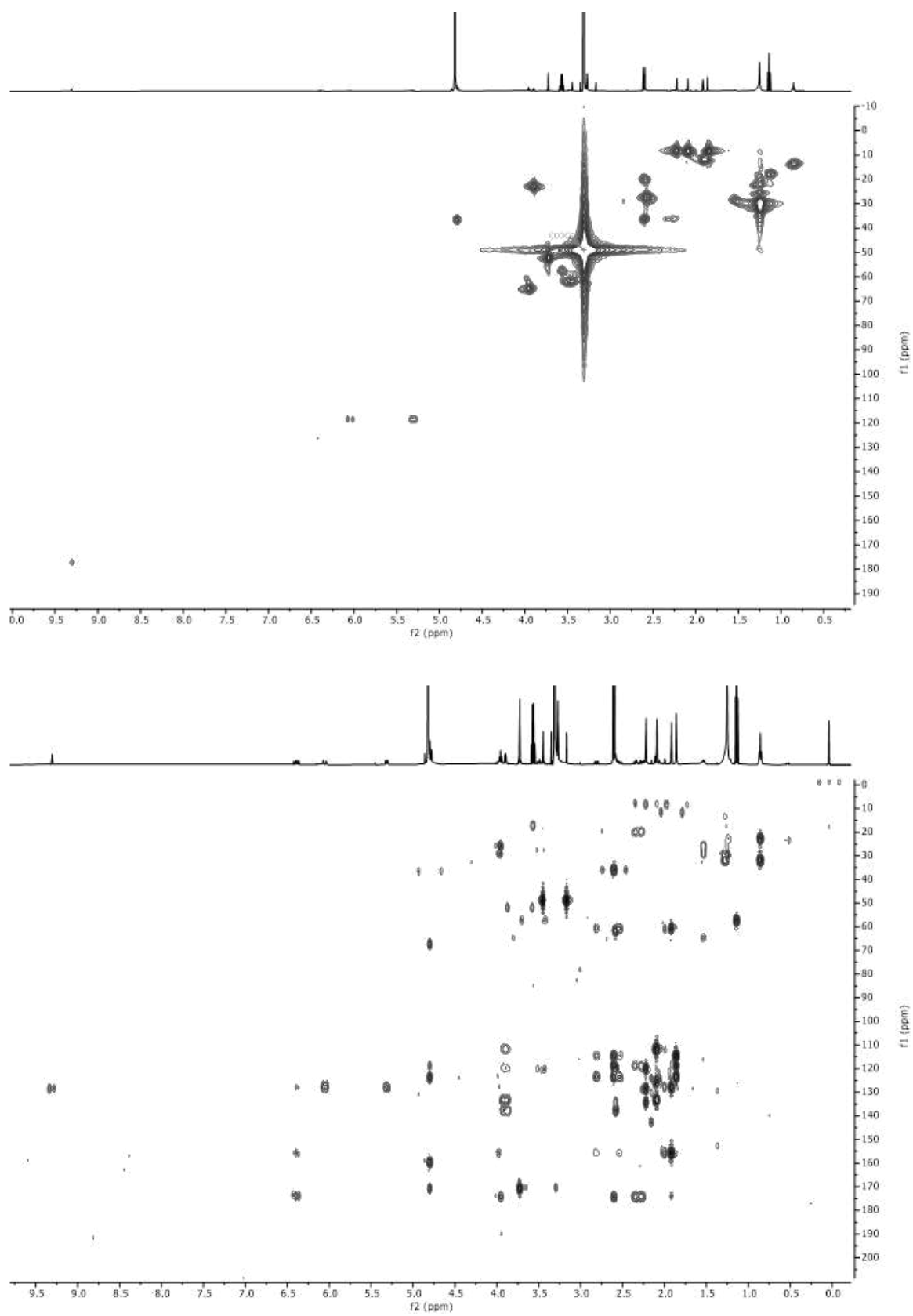
Figure S12. ^{1}H NMR and ^{1}H,^{13}C heteronuclear HMQC and HMBC spectra of synthesized *Cj*-octyl-**PleB** (**7**) in d_4-methanol.

Table S3. ^{1}H and ^{13}C NMR data of *Cj*-methyl- and *Cj*-ethyl-**PleB** (**4, 5**) (500 MHz, CD₃OD).

	δ[1]H/J (*Cj*-methyl-PleB (4))	δ^{13}C (*Cj*-methyl-PleB (4))		δ[1]H/J (*Cj*-ethyl-PleB (5))	δ^{13}C (*Cj*-ethyl-PleB (5))
C1		128.90	C1		128.45
C2		134.74	C2		134.29
H₃C2¹	2.22, s	8.24	H₃C2¹	2.22, s	8.24
C3		120.37	C3		119.93
H₂C3¹	2.57, m	27.55	H₂C3¹	2.57, m	27.12
H₂C3²	3.50, m	61.87	H₂C3²	3.51, m	61.87
C4		137.88	C4		137.43
H₂C5	3.90, d *J* = 6.8	22.83	H₂C5	3.90, d *J* = 6.3	22.83
C6		133.84	C6		133.39
C7		112.29	C7		111.84
H₃C7¹	2.09, s	8.67	H₃C7¹	2.09, s	8.24
C8		125.76	C8		125.31
C8¹		190.85	C8¹		190.85
HC8²	3.71, d *J* = 3.2	68.31	HC8²	3.71, d *J* = 3.2	68.31
C8³		171.10	C8³		170.65
H₃C8⁴	3.73, s	52.00	H₃C8⁴	3.73, s	52.00
C9		160.33	C9		159.43
HC10	4.82, s	36.56	HC10	4.82, s	36.56
C11			C11		
C12		119.03	C12		118.58
H₂C12¹	2.60, m	19.82	H₂C12¹	2.60, m	19.82
H_AC12² H_BC12²	2.25, m 2.38, m	35.70	H_AC12² H_BC12²	2.24, m 2.35, m	36.13
C12³		174.69	C12³		174.24
H₃C12⁴	3.56, m	57.58	H₂C12⁴	3.57, q *J* = 7.1	57.58
			H₃C12⁵	1.14, t *J* = 7.0	17.68
C13		114.99	C13		114.54
H₃C13¹	1.85, s	8.67	H₃C13¹	1.86, s	8.67
C14		123.97	C14		123.52
H_AC15 H_BC15	2.53, m 2.81, dd *J* = 14.6/5.5	28.83	H_AC15 H_BC15	2.53, m 2.81, dd *J* = 14.6/5.4	29.26
HC16	3.99, m	61.12	HC16	4.02, m	60.67
C17		156.29	C17		155.84
H₃C17¹	1.91, s	11.67	H₃C17¹	1.92, s	11.67
C18		128.45	C18		128.01
HC18¹	6.40, m	126.23	HC18¹	6.39, dd *J* = 17.8/11.7	125.80
H_AC18² H_BC18²	5.31, dd *J* = 11.8/2.4 6.05, dd *J* = 17.7/2.4	118.51	H_AC18² H_BC18²	5.31, dd *J* =11.7/2.4 6.05, dd *J* = 17.7/2.4	118.50
C19		174.24	C19		173.79
HC20	9.31, s	177.29	HC20	9.31, s	177.28

Table S4. ^{1}H and ^{13}C NMR data of *Cj*-butyl- and *Cj*-octyl-**PleB** (**6, 7**) (500 MHz, CD$_3$OD).

	δ^{1}H/J (*Cj*-butyl-PleB (6))	δ^{13}C (*Cj*-butyl-PleB (6))		δ^{1}H/J (*Cj*-octyl-PleB (7))	δ^{13}C (*Cj*-octyl-PleB (7))
C1		128.90	C1		128.45
C2		134.74	C2		134.29
H$_3$C2^1	2.22, s	8.24	H$_3$C2^1	2.22, s	8.24
C3		120.37	C3		119.93
H$_2$C3^1	2.58, m	27.12	H$_2$C3^1	2.57, m	27.55
H$_2$C3^2	3.51, m	61.87	H$_2$C3^2	3.51, m	61.87
C4		137.88	C4		137.43
H$_2$C5	3.90, d J = 6.1	22.83	H$_2$C5	3.90, d J = 5.7	22.83
C6		133.84	C6		133.39
C7		112.29	C7		111.85
H$_3$C7^1	2.09, s	8.24	H$_3$C7^1	2.09, s	8.67
C8		125.76	C8		125.31
C8^1		-	C8^1		-
HC8^2	3.71, d J = 1.9	-	HC8^2	3.71, d J = 3.3	68.31
C8^3		171.10	C8^3		170.65
H$_3$C8^4	3.73, s	52.00	H$_3$C8^4	3.73, s	52.00
C9		159.88	C9		159.43
HC10	4.82, s	36.56	HC10	4.82, s	36.56
C11			C11		
C12		119.03	C12		118.58
H$_2$C12^1	2.60, m	19.82	H$_2$C12^1	2.60, m	20.25
H$_A$C12^2 H$_B$C12^2	2.25, m 2.36, m	36.13	H$_A$C12^2 H$_B$C12^2	2.27, m 2.33, m	36.13
C12^3		174.69	C12^3		174.24
H$_2$C12^4	3.97, m	63.84	H$_2$C12^4	3.97, t	64.87
H$_2$C12^5	1.52, m	30.37	H$_2$C12^5 H$_2$C12^6	1.46-1.61, m	31.84 28.83
H$_2$C12^6	1.30, m	17.50	H$_2$C12^7 H$_2$C12^8 H$_2$C12^9 H$_2$C12^{10}	1.18-1.35, m	29.69 25.40 21.97 14.68
H$_3$C12^7	0.88, t J = 7.4	12.35	H$_3$C12^{11}	0.85, m	13.82
C13		114.99	C13		114.54
H$_3$C13^1	1.86, s	8.67	H$_3$C13^1	1.86, s	8.67
C14		123.97	C14		123.52
H$_A$C15 H$_B$C15	2.53, m 2.77-2.85, m	29.26	H$_A$C15 H$_B$C15	2.53, m 2.81, dd J =14.6/5.4	29.26
HC16	3.96, m	61.12	HC16	3.97, m	60.67
C17		156.29	C17		155.84
H$_3$C17^1	1.91, s	11.67	H$_3$C17^1	1.91, s	11.67
C18		128.45	C18		128.01
HC18^1	6.39, dd J = 17.8/11.7	126.23	HC18^1	6.39, dd J = 17.8/11.6	126.66
H$_A$C18^2 H$_B$C18^2	5.31, dd J =11.7/2.4 6.05, dd J = 17.7/2.4	118.51	H$_A$C18^2 H$_B$C18^2	5.31, dd J =11.7/2.4 6.05, dd J = 17.8/2.4	118.51
C19		174.24	C19		173.79
HC20	9.31, s	177.29	HC20	9.31, s	177.29

Figure S13. Analytical HPLC traces of cell lysates of T24 cells treated with **PxB** (**2**), *Cj*-**PleB** (**1**), *Po*-**PleB** (**3**), *Cj*-**PleB** esters (**4-7**) (80 µM) for 5 h.

References:

[1]   S. Moser, G. Scherzer, B. Kräutler, *Chemistry & Biodiversity* **2017**, *14*, e1700368.
[2]   B. Kräutler, *Chem. Soc. Rev.*, **2014**, 43(17), 6227-6238.
[3]   B. Kräutler, S. Banala, S. Moser, C. Vergeiner, T. Muller, C. Lutz, A. Holzinger, *FEBS letters* **2010**, *584*, 4215-4221.
[4]   S. Moser, M. Ulrich, T. Müller, B. Kräutler, *Photochem. Photobiol. Sci.* **2008**, *7*, 1577-1581.

COMMUNICATION

Tetrapyrrolic pigments are actin-targeting compounds

Cornelia A. Karg,[a] Shuaijun Wang,[a] Nader Danaf,[b] Ryan Pemberton,[c] Denzil Bernard,[c] Maibritt Kretschmer,[a] Sabine Schneider,[d] Themistoklis Zisis,[a] Angelika M. Vollmar,[a] Don C. Lamb,[b] Stefan Zahler[a] and Simone Moser*[a]

[a]   C.A. Karg, Dr. S. Wang, M. Kretschmer, Dr. T. Zisis, Prof. Dr. A. M. Vollmar, Prof. Dr. Stefan Zahler, Dr. S. Moser
        Pharmaceutical Biology
        Department of Pharmacy
        Ludwig-Maximilians University of Munich
        Butenandtstraße 5-13, 81377 Munich, Germany
        E-mail: simone.moser@cup.uni-muenchen.de
[b]   N. Danaf, Prof. Dr. D. C. Lamb
        Center for Nanoscience (CeNS) and Nanosystems Initiative Munich (NIM),
        Department of Chemistry
        Ludwig-Maximilians University of Munich
        Butenandtstraße 5-13, 81377 Munich, Germany
[c]   Dr. D. Bernard, Dr. R. Pemberton
        Atomwise Inc,
        717 Market Street, Suite 800, San Francisco, CA, 94103, USA
[d]   Dr. S. Schneider
        Department of Chemistry
        Ludwig-Maximilians University Munich
        Butenandtstrasse 5-13, 81377 Munich, Germany

        Supporting information for this article is given via a link at the end of the document

Abstract: Chlorophyll and heme are among the 'pigments of life', tetrapyrrolic structures, without which life on Earth would not be possible. Their catabolites, the phyllobilins and the bilins, respectively, share not only structural features, but also a similar story: Long considered waste products of detoxification processes, important bioactivities for both classes have now been demonstrated. For phyllobilins, however, research on physiological roles is sparse. Here, we introduce actin, the major component of the cytoskeleton, as the first biological target of phyllobilins and as a novel target of bilins. We demonstrate the inhibition of actin dynamics *in vitro* and effects on actin and related processes in cancer cells. A direct interaction with G-actin was shown by *in silico* studies and confirmed by affinity chromatography. Our data open a new chapter in bioactivities of tetrapyrroles, especially for phyllobilins, for which they hint towards interesting therapeutic applications.

Tetrapyrrolic pigments are among the most important natural products on Earth. Some of these pigments are part of essential processes in living organisms, which brought them the name 'pigments of life'.[1] Among those, the green pigment chlorophyll (Chl) and the red blood pigment heme play important roles in several biological processes.[2] When released from their binding proteins, both substances are toxic and need to be degraded.[3] The resulting degradation products are the bilins from the breakdown of heme and the phyllobilins, formed during Chl catabolism.

Bilins are primarily known as the metabolic products of heme catabolism in mammals, but can also be found in lower vertebrates, plants, algae, and bacteria. During heme degradation, heme oxygenase catalyzes the oxygenolytic opening of the macrocycle at one of the four methene bridges furnishing the linear tetrapyrrole biliverdin (BV) (Scheme 1). In the mammalian liver, BV is reduced to BR by biliverdin reductase A.

Originally, bilins were assumed to be waste products of a catabolism pathway, however, extensive literature exists reporting beneficial activities of BR and BV, e.g. as strong endogenous antioxidants.[4] Moreover, studies demonstrated protective capabilities against a variety of pathological conditions including cardiac injuries, gastrointestinal inflammations, or neurodegenerative diseases.[5]

Phyllobilins (PBs) are the degradation products of the green plant pigment Chl and are generated in senescent leaves during autumn as well as in ripening fruit and vegetables.[6] PBs were first suspected to be 'only' products of a detoxification process, similar to the bilins. The corresponding breakdown process turned out to be much more complex than degradation of its structural analogue heme, but similarly involving an enzymatic opening of the macrocycle; in the case of Chl degradation, catalyzed by pheophorbide a oxygenase.[7] In a strictly controlled process, non-colored chlorophyll catabolites, the phylloleucobilins (PleBs), are generated and accumulate in the vacuoles of the plant cell.[6, 8] In addition, oxidation products of the PleB, so called phyllochromobilins, could be identified: a yellow chlorophyll catabolite, phylloxanthobilin (PxB) and a pink chlorophyll catabolite, phylloroseobilin (PrB).[9] In contrast to the enzymatic reduction of BV, the mechanism of the formation of PxB and PrB in plants is not yet elucidated; recent studies, however, suggest an enzymatic 'oxidative activity' that effectively transforms PleBs to PxBs.[10]

The late stage chlorophyll catabolites PxB and PrB share a remarkable structural similarity with BR and BV.[6] PxB resembles the final heme degradation product BR featuring a double bond at C15, whereas PrB, the oxidation product of PxB, represents the analogue of BV due to an extended conjugated π-system. Structural differences become evident in the 1-formyl moiety at ring A and the additional ring E section of the PBs (Scheme 1).

COMMUNICATION
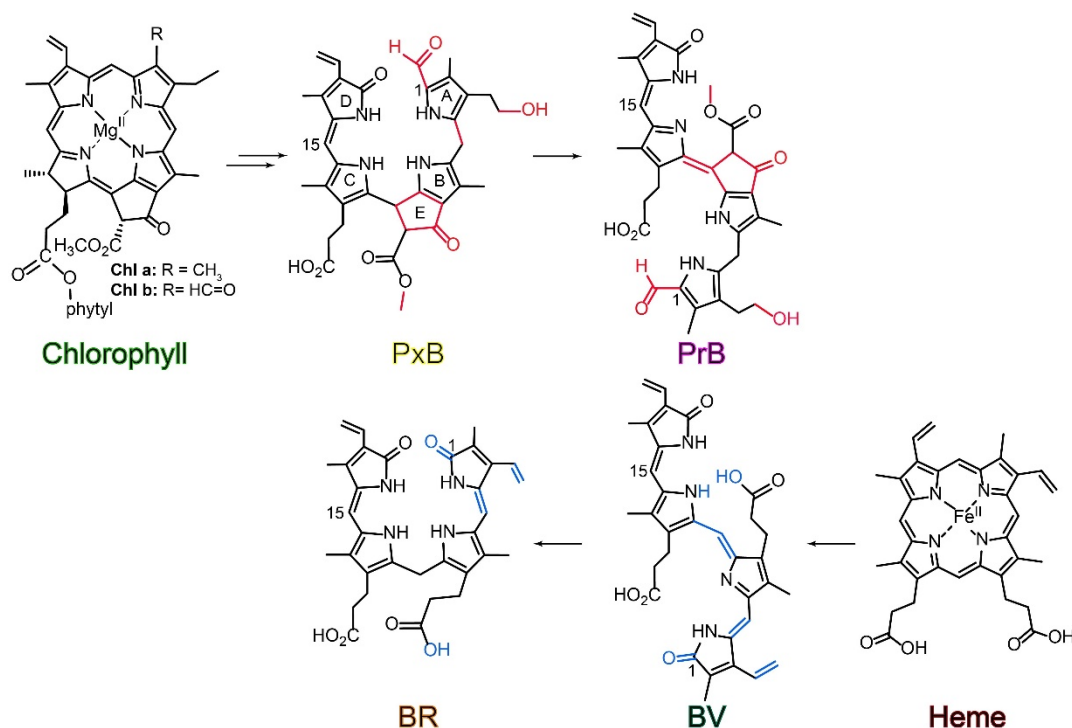
Scheme 1. Structural outline for comparison of heme degradation resulting in bilins, bilirubin (BR) and biliverdin (BV), and late steps of chlorophyll catabolism revealing the phyllobilins phylloxanthobilin (PxB) and phylloroseobilin (PrB). Structural differences between metabolites of the heme and Chl catabolism are highlighted in color.

PBs were found to possess very interesting chemical properties and possible bioactivities have already been suggested.[6, 11] First indications were provided by Müller *et al* in 2007, demonstrating that PleBs in peels of apples and pears possess strong antioxidative activities.[12] In the meanwhile, antioxidative properties as well as anti-inflammatory activities could be revealed also for PxBs.[13] Furthermore, PxBs were shown to be taken up by cells and possess promising anti-cancer activities [14] In comparison to the bilins, however, investigations of the physiological roles of PBs still lag behind.

Bilins and PBs are ubiquitous tetrapyrrolic structures and the relevance of identifying their targets has become more evident by recent research.[15] In general, identification of direct protein interactions is crucial for elucidating detailed mechanisms and mode of action(s) of natural products. Currently, therapeutically relevant targets for both classes of tetrapyrroles are sparse. In the case of PBs, no human target has yet been identified.

Actin is one of the most abundant proteins in eukaryotic cells and plays an essential role in many cellular processes, such as cell motility, control of cell shape, cell division, and intracellular transport.[16] All these processes largely depend on the dynamics of actin filaments, i.e., polymerization and depolymerization. Malfunctions of the actin cytoskeleton can lead to the development of different diseases,[17] targeting actin or actin binding proteins could therefore provide an interesting option for therapeutic approaches.

We demonstrate here that PxB and PrB as well as the bilins BR and BV possess inhibitory effects on *in vitro* actin dynamics and actin-dependent functions in cells. Furthermore, *in silico* docking studies of all four compounds show the potential for direct binding to G-actin, which was supported by affinity chromatography and compe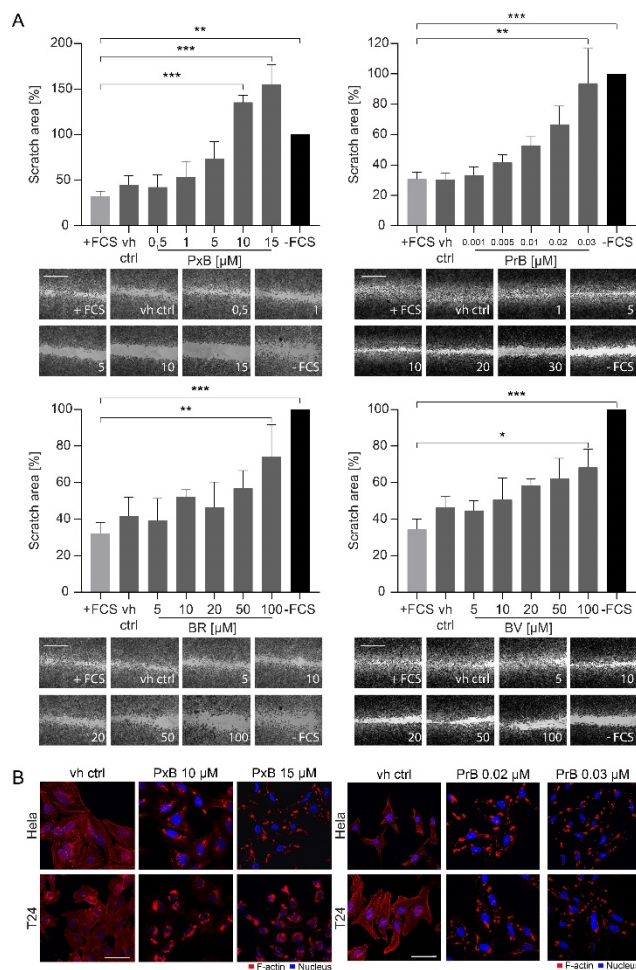tition pull down experiments. Moreover, we identified influences of PBs and bilins on cellular functions related to the actin cytoskeleton.

We tested the bilins BR and BV, which are commercially available, and PxB and PrB, which were prepared by partial synthesis as described in the Supporting Information. Identities were confirmed by HPLC, UV-Vis, HR-MS, and ^{1}H-NMR (Figure S1). We examined the influence of the tetrapyrroles on cell migration using a scratch wound-healing assay in two different human cancer cell lines, T24 and Hela cells. The scratch assay revealed all tested tetrapyrroles to affect cell migration to a different extent without altering cell viability (Figure 1A, Figure S2, S3). The PrB appeared to be the most potent compound, which significantly inhibited cell migration even at low nanomolar doses. BR and BV affected cell migration only at high micromolar doses; both showed a significant effect at 100 µM in T24 cells.

The actin cytoskeleton is a key player in many cellular processes including cell migration.[18] Next, we investigated the effects of the four anti-migratory compounds on the actin cytoskeleton in cells. T24 and Hela cells were treated with PxB, PrB, BR, and BV for 4 hours before the cells were fixed and F-actin stained by a phalloidin rhodamine dye.

In cells treated with low micromolar concentrations of PxB and low nanomolar concentrations of PrB, actin agglomerated close to the nucleus, and, in comparison to the control, actin filaments were clearly disorganized (Figure 1B). In contrast, incubating cells with BV and BR in concentrations up to 100 µM revealed no effect on the organization of actin filaments (Figure S4).

Having established that the tested compounds had an effect on actin and actin-dependent processes in cells, their influence on assembly and disassembly of actin was investigated by different *in vitro* approaches. Using pyrene labeled actin, we assessed the polymerization and depolymerization processes by monitoring the

COMMUNICATION

Figure 1. Effects of PBs and bilins on cell migration and F-actin morphology. A) Cell migration of T24 cells treated with PxB, PrB, BR, BV, and vehicle control (vh ctrl) was analyzed by a scratch wound-healing assay. Treatment with cell medium with FCS served as a negative control and medium without FCS as a positive control. (Upper panels) The bar plots indicate the relative scratch gap normalized to the control without FCS given as mean±SEM of three independent experiments performed in triplicates, (one-way ANOVA followed by Dunnett's multiple comparison test, *P < 0.05, **P < 0.01, ***P < 0.001. (Lower panels) Representative images from the wound healing assay collected 16-24 h after generating the scratch are shown. Scale bar: 1 mm. B) Images of immunofluorescence stained Hela and T24 cells treated with PxB and PrB for 4 h. Nuclei were stained with Hoechst (shown in blue) and F-actin with rhodamine-phalloidin (shown in red). Scale bar: 50 µm. Representative images taken from three independent experiments are shown.

change in pyrene fluorescence intensities upon addition of PxB, PrB, BR, and BV. All four compounds showed an inhibition of actin polymerization compared to the vehicle control. A decelerated polymerization process and a lower plateau of fluorescence intensity was observed in response to PBs and bilins (Figure 2A). Again, PBs were active at lower concentrations than bilins, with PrB affecting polymerization *in vitro* at the low micromolar range. Furthermore, we investigated the influence of the tetrapyrroles on F-actin depolymerization. All four tetrapyrroles showed an increased depolymerization rate compared to the control sample. Comparing the effects with the actin depolymerizer latrunculin B (LatB)[19] measured at 10 µM, PrB (measured at 50 µM), and PxB and BV (measured at 100 µM) all showed enhanced depolymerization rates. BR showed only a slight effect on the rate of depolymerization at a high concentration of 1000 µM (Figure 2B). Using TIRF microscopy, we additionally investigated the

effects of the linear tetrapyrroles on actin nucleation, the initial step of the actin polymerization process.[20] Nucleation was found to be significantly inhibited by both, PBs and bilins (Figure 3).
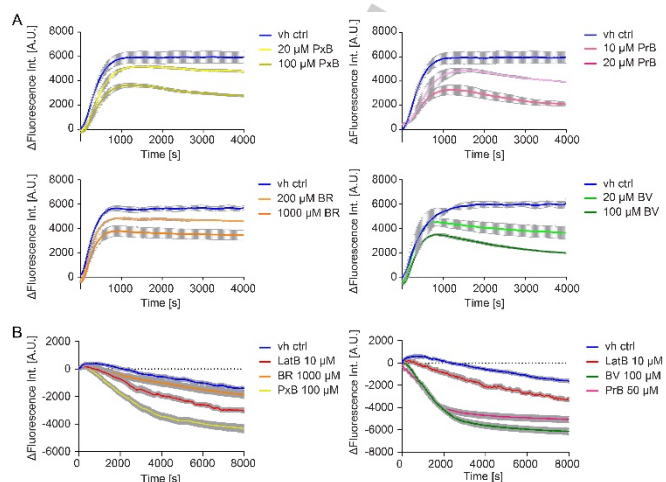
Figure 2. Inhibition of *in vitro* actin dynamics by PBs and bilins. A) Polymerization of pyrene labeled G-actin incubated with PxB, PrB, BR, BV, and the vehicle control (vh ctrl). Data are presented as mean±SEM of three independent experiments performed in duplicates (SEM depicted in grey). B) After allowing the actin to polymerize for 1 h, the depolymerization of pyrene labeled actin was monitored upon addition of PBs, bilins, LatB, and a vehicle control (vh ctrl). Data represent mean±SEM of three independent experiments performed in triplicates (SEM depicted in grey).
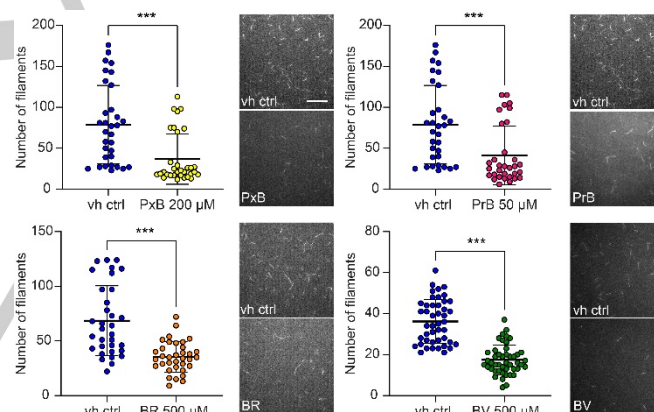

Figure 3. Inhibition of actin nucleation. TIRF assay of Atto488 labeled G-actin incubated with PxB, PrB, BR, BV, and a vehicle control (vh ctrl). The number of actin nuclei present in each frame (calculated from the number of filaments) are presented as a scatter plot. Same control cells are shown for PrB and PxB as experiments were performed simultaneously. Average of nuclei±SEM (left panel, two-tailed unpaired Student's t-test, *** P< 0.001). Representative images with corresponding vehicle control measurements are shown in the right panel.

In order to investigate whether the observed effects are caused by a direct interaction with G-actin, we used affinity chromatography with G-actin immobilized on sepharose beads. The amount of compounds bound to G-actin beads was analyzed by analytical HPLC and compared with agarose beads, which were used as a negative control for non-specific binding to beads. Upon elution, a significantly higher amount of all compounds released from G-actin beads was observed in contrast to agarose beads (Figure 4A).

Next, we used *in silico* studies to investigate the potential interaction of the tetrapyrroles with G-actin. Docking of the compounds to the binding site of kabiramideC (KabC), a known

actin binder,[21] indicated several different binding orientations for each molecule. Interestingly, among the different conformations generated for each ligand, a common binding mode shared by all four compounds placed a pyrrolin-2-one ring into a hydrophobic pocket present in G-actin (Figure 4B, C) lined with residues Y133, I136, V139, Y169, and F375 (Figure S5). Upon polymerization of G-actin, this binding side is normally occupied by the D-loop of the next actin monomer in the actin filament and is generally targeted by natural products such as macrolides that promote actin depolymerization.[22] The N-vinylformamide moiety in the critical tail region of KabC also interacts with the same hydrophobic pocket and the lack of specific hydrogen bonds or polar interactions permits the placement of both 17-methyl-18-vinyl-17-pyrrolin-19-one (ring D) as well as 2-methyl-3-vinyl-2-pyrrolin-1-one (ring A) (BR and BV) in the same pocket (for numbering, see Scheme 1). Due to the presence of a number of polar atoms on these compounds, further refinement of docked models should consider both intramolecular and solvent interactions.

Confirmation of the predicted binding site was carried out by a competitive pull-down approach using G-actin beads and the actin binding protein profilin, which is known to interact with the common binding site of actin binding proteins and small molecules such as KabC.[23] The amount of profilin bound to G-actin was quantified with and without pre-treatment with the compounds and showed a significant decrease of profilin binding for PxB and PrB compared to the vehicle control. These results indicate that PBs are likely to occupy the same binding pocket of G-actin and therefore prevent profilin binding. In contrast, incubation with bilins resulted in a minor reduction of profilin binding (Figure 4D, Figure S6).

The four tested tetrapyrroles, albeit being structurally related, vary greatly in their physico-chemical properties such as solubility, polarity, and fluorescence behavior. To characterize the binding affinity of each compound to G-actin and to determine the dissociation constants (K_d), different biophysical techniques were applied including fluorescence quenching, microscale thermophoresis (MST), and isothermal calorimetry (ITC) (Figure 4E, Figure S7-10).

The interaction of PxB with G-actin was studied by MST, which monitors the thermophoretic movement of Atto647 labeled G-actin with increasing concentrations of PxB and revealed a K_d of 65.2 µM (50.6 to 79.8). The binding strength of PrB was determined by fluorescence titration spectroscopy and measuring the quenching of Atto647 labeled G-actin by adding PrB. A K_d of 1.9 µM (1.5 to 2.5) was determined. Quenching of Atto647 labeled G-actin was also observed during titration with BR. However, saturation of the quenching could not be achieved due to the low solubility of BR. Therefore, a K_d value could not be determined, but appears to be in the µM range. For BV, a K_d of 80.1 µM (67.2 to 93) was obtained using ITC. In summary, PxB, PrB, and BV all exhibited binding affinities to G-actin in the low micromolar range, in accordance with the results from biological assays, with the PrB possessing the strongest interaction with G-actin.

BR has been shown to play important cytoprotective roles at physiological concentrations. However, increased concentrations of albumin-bound or unconjugated BR are known to cause hyperbilirubinemia. Several factors such as concentration,

conjugation status, or redox state and target location in cells seem to play important roles.[24] Therefore, it is questionable whether the herein reported effects of bilins on actin dynamics and actin functions at this high concentration range are of physiological relevance. For PBs, however, which affect actin and related functions at lower concentrations, we provide the basis for elucidating further effects on cellular functions and the underlying mode of actions in more detail. This is of special interest for PrB, the most potent candidate, where no bioactivities have yet been reported. Previous studies have already shown that PxB is a promising anti-cancer reagent, inhibiting the proliferation of cancer cells and inducing apoptosis.[14b] Furthermore, it was shown that a G2/M-cell cycle arrest is induced at concentrations lower than 20 µM. Since the actin cytoskeleton plays an important role in cell division, future studies will investigate the role of actin binding and agglomeration of actin filaments on the progression of the cell cycle.

There are many arguments against the assumption that the breakdown of the 'pigments of life' is only a detoxification process. Questions concerning the roles of the degradation products, however, still remain puzzling. Many organisms such as bacteria, plants, or animals produce natural substances with actin-binding properties[25] and accumulating research suggests that these substances play possible roles in host-defense mechanisms.[26] Interestingly, PBs were recently associated with plant defense against pathogen attack.[27]

PBs and bilins are a class of ubiquitous natural products; both have previously been shown to possess multiple physiologically relevant properties. In this study, by introducing the first human target for PBs and a novel target for bilins, we go one step further in unravelling the question behind the degradation of two of the most important pigments on Earth. In particular for PBs, this study opens the door for interesting therapeutic applications of this for long overlooked class of tetrapyrroles.
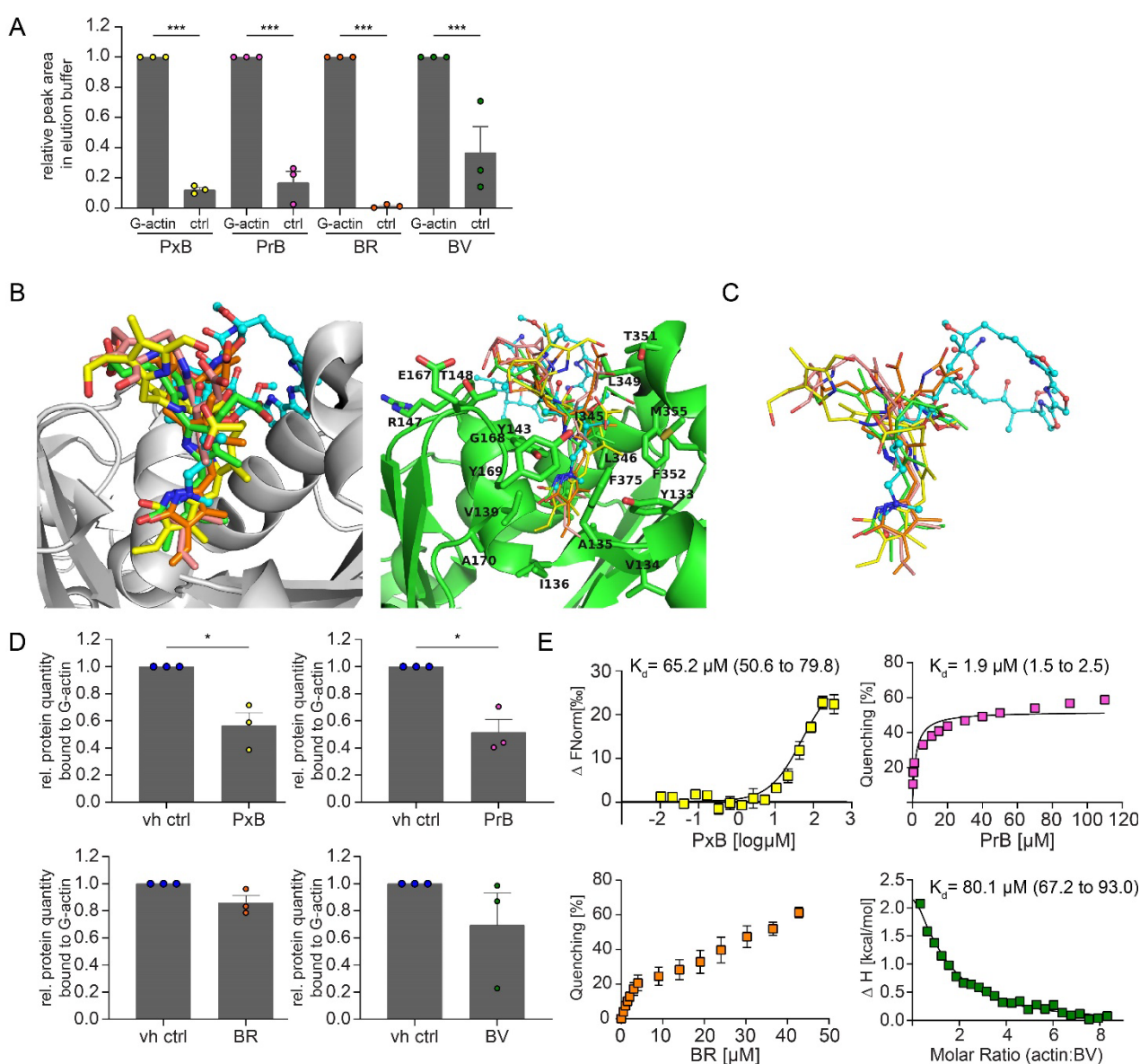
Figure 4. Characterization of *in vitro* binding of PBs and bilins to G-actin. A) G-actin binding assay was performed with G-actin attached to sepharose beads. G-actin or agarose beads (ctrl) were incubated with compounds at 50 µM concentration for 1h before the mixture was centrifuged and washed. Compounds were eluted from beads and the eluate was analyzed by analytical HPLC. Results represent the relative peak area and mean±SEM of three independent experiments. The significance was investigated using a one-way ANOVA followed by Dunnett's multiple comparison test, *** P< 0.001. B) Predicted binding mode of PBs and bilins (carbon atoms shown for PxB in yellow; PrB in pink; BV in green; BR in orange) docked onto actin (grey or green ribbon) (PDB code: 4K41). The residues of actin involved in binding are labeled and shown as sticks. KabC is depicted using a ball and stick model (cyan). C) Overlay of docked conformers of PxB in yellow, PrB in pink, BV in green, BR in orange and KabC in cyan (PDB code:4K41) showing the pyrrolin-2-one (ring D) occupying the same regions as the KabC N-vinylformamide. D) Competitive G-actin binding assay of compounds in combination with the actin binding protein profilin. G-actin beads were incubated with PBs or bilins at 50 µM concentration for 1 h prior to addition of profilin (0.667 µM). Beads were centrifuged and the solubilised pellet fraction was analyzed using SDS-PAGE. The amount of profilin was quantified and normalized to the vehicle control (vh ctrl). Data represent mean±SEM of three independent experiments. The significance was tested using a two-tailed unpaired Student's t-test with Welch's correction, * P< 0.05. E) Determination of K_d values using MST for PxB (protein concentration = 71.4 nM), fluorescence quenching for PrB and BR (protein concentration = 200 nM), and ITC for BV (protein concentration = 50 µM). A K_d for BR was not calculated because of the poor fit to the binding model. Results for PxB, PrB, and BR represent mean±SEM of three independent experiments. K_d values are expressed as mean values (68 % CI).

[1]   A. R. Battersby, *Nat. Prod. Rep* **2001**, *17*, 507-526.
[2]   S. Granick, in *Evolving Genes and Proteins* (Eds.: V. Bryson, H. J. Vogel), Academic Press, **1965**, pp. 67-88.
[3]   aK. Apel, H. Hirt, *Annu. Rev. Plant Biol.* **2004**, *55*, 373-399; bS. Kumar, U. Bandyopadhyay, *Toxicol. Lett.* **2005**, *157*, 175-188.
[4]   R. Stocker, *Antioxid. Redox Signal.* **2004**, *6*, 841-849.
[5]   aF. H. Bach, *FASEB J* **2005**, *19*, 1216-1219; bS. Gazzin, L. Vitek, J. Watchko, S. M. Shapiro, C. Tiribelli, *Trends Mol* **2016**, *22*, 758-768.
[6]   B. Kräutler, *Angew. Chem. Int. Ed.* **2016**, *55*, 4882-4907.
[7]   S. Hörtensteiner, F. Vicentini, P. Matile, *The New Phytologist* **1995**, *129*, 237-246.

[8]   S. Hörtensteiner, M. Hauenstein, B. Kräutler, in *Advances in Botanical Research, Vol. 90* (Ed.: B. Grimm), Academic Press, **2019**, pp. 213-271.
[9]   aM. Ulrich, S. Moser, T. Müller, B. Kräutler, *Chem. Eur. J.* **2011**, *17*, 2330-2334; bS. Moser, M. Ulrich, T. Müller, B. Krautler, *Photochem. Photobiol. Sci.* **2008**, *7*, 1577-1581.
[10]   C. Vergeiner, M. Ulrich, C. Li, X. Liu, T. Müller, B. Kräutler, *Chem. Eur. J.* **2015**, *21*, 136-149.
[11]   aS. Banala, S. Moser, T. Müller, C. Kreutz, A. Holzinger, C. Lütz, B. Kräutler, *Angew. Chem. Int. Ed.* **2010**, *49*, 5174-5177; bI. Süssenbacher, S. Hörtensteiner, B. Kräutler, *Angew. Chem. Int. Ed.* **2015**, *54*, 13777-13781.

[12] T. Müller, M. Ulrich, K. H. Ongania, B. Kräutler, *Angew. Chem. Int. Ed.* **2007**, *46*, 8699-8702.

[13] aC. A. Karg, C. Doppler, C. Schilling, F. Jakobs, M. C. S. Dal Colle, N. Frey, D. Bernhard, A. M. Vollmar, S. Moser, *Food Chem.* **2021**, *359*, 129906; bC. A. Karg, C. M. Schilling, L. Allmendinger, S. Moser, *J. Porphyr. Phthalocyanines* **2019**, *23*, 881-888; cC. A. Karg, P. Wang, A. M. Vollmar, S. Moser, *Phytomedicine* **2019**, *60*, 152969.

[14] aP. Wang, C. A. Karg, N. Frey, J. Frädrich, A. M. Vollmar, S. Moser, *Arch Pharm (Weinheim)* **2021**, *in press*; bC. A. Karg, P. Wang, F. Kluibenschedl, T. Müller, L. Allmendinger, A. M. Vollmar, S. Moser, *Eur. J. Org. Chem.* **2020**, *2020*, 4499-4509.

[15] A. Rosa, V. E. Pye, C. Graham, L. Muir, J. Seow, K. W. Ng, N. J. Cook, C. Rees-Spear, E. Parker, M. S. dos Santos, C. Rosadas, A. Susana, H. Rhys, A. Nans, L. Masino, C. Roustan, E. Christodoulou, R. Ulferts, A. G. Wrobel, C.-E. Short, M. Fertleman, R. W. Sanders, J. Heaney, M. Spyer, S. Kjær, A. Riddell, M. H. Malim, R. Beale, J. I. MacRae, G. P. Taylor, E. Nastouli, M. J. van Gils, P. B. Rosenthal, M. Pizzato, M. O. McClure, R. S. Tedder, G. Kassiotis, L. E. McCoy, K. J. Doores, P. Cherepanov, *Sci. Adv* **2021**, *22*, 7.

[16] T. D. Pollard, J. A. Cooper, *Science (New York, N.Y.)* **2009**, *326*, 1208-1212.

[17] D. Kunze, B. Rüstow, *European journal of clinical chemistry and clinical biochemistry : journal of the Forum of European Clinical Chemistry Societies* **1993**, *31*, 477-489.

[18] X. Trepat, Z. Chen, K. Jacobson, in *Comprehensive Physiology, Vol. 2*, **2012**, pp. 2369-2392.

[19] M. May, T. Wang, M. Müller, H. Genth, *Toxins* **2013**, *5*, 106-119.

[20] R. Dominguez, *Crit. Rev. Biochem. Mol. Biol.* **2009**, *44*, 351-366.

[21] J. Tanaka, Y. Yan, J. Choi, J. Bai, V. Klenchin, I. Rayment, G. Marriott, *Proc Natl Acad Sci U S A* **2003**, *100*, 13851-13856.

[22] S. Wang, F. A. Gegenfurtner, A. H. Crevenna, C. Ziegenhain, Z. Kliesmete, W. Enard, R. Müller, A. M. Vollmar, S. Schneider, S. Zahler, *J. Nat. Prod.* **2019**, *82*, 1961-1970.

[23] R. Dominguez, in *Actin-Monomer-Binding Proteins* (Ed.: P. Lappalainen), Springer New York, New York, NY, **2007**, pp. 107-115.

[24] J. Kapitulnik, *Mol. Pharmacol.* **2004**, *66*, 773-779.

[25] R. Ueoka, A. R. Uria, S. Reiter, T. Mori, P. Karbaum, E. E. Peters, E. J. N. Helfrich, B. I. Morinaka, M. Gugger, H. Takeyama, S. Matsunaga, J. Piel, *Nat. Chem. Biol.* **2015**, *11*, 705-712.

[26] G. Lackner, E. E. Peters, E. J. N. Helfrich, J. Piel, *Proc Natl Acad Sci U S A* **2017**, *114*, E347-E356.

[27] S. Moser, T. Erhart, S. Neuhauser, B. Kräutler, *J. Agric. Food Chem* **2020**, *68*, 7132-7142.

Entry for the Table of Contents
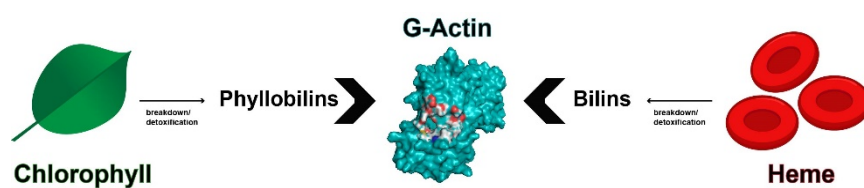
The physiological role of the degradation products of chlorophyll and heme, exogenous phyllobilins and endogenous bilins, respectively, remained an unsolved mystery for decades. We describe the influence of these tetrapyrroles on the actin cytoskeleton and introduce G-actin as the first human target protein for phyllobilins and a novel target for bilins. This study opens up a completely new perspective of the importance of these ubiquitous natural products.

Institute and/or researcher Twitter usernames: PhylloLab

Tetrapyrrolic pigments are actin-targeting compounds

Cornelia A. Karg,[a] Shuaijun Wang,[a] Nader Danaf,[b] Ryan Pemberton,[c] Denzil Bernard,[c] Maibritt Kretschmer,[a] Sabine Schneider,[d] Themistoklis Zisis,[a] Angelika M. Vollmar,[a] Don C. Lamb,[b] Stefan Zahler[a] and Simone Moser*[a]

[a]   C.A. Karg, Dr. S. Wang, M. Kretschmer, Dr. T. Zisis, Prof. Dr. A. M. Vollmar, Prof. Dr. Stefan Zahler, Dr. S. Moser
       Pharmaceutical Biology
       Department of Pharmacy
       Ludwig-Maximilians University of Munich
       Butenandtstraße 5-13, 81377 Munich, Germany
       E-mail: simone.moser@cup.uni-muenchen.de
[b]   N. Danaf, Prof. Dr. D. C. Lamb
       Center for Nanoscience (CeNS) and Nanosystems Initiative Munich (NIM),
       Department of Chemistry
       Ludwig-Maximilians University of Munich
       Butenandtstraße 5-13, 81377 Munich, Germany
[c]   Dr. D. Bernard, Dr. R. Pemberton
       Atomwise Inc,
       717 Market Street, Suite 800, San Francisco, CA, 94103, USA
[d]   Dr. S. Schneider
       Department of Chemistry
       Ludwig-Maximilians University Munich
       Butenandtstrasse 5-13, 81377 Munich, Germany

Supplementary Information

Table of contents

1. Material and Methods

1.1 General

Chemicals and Materials

Acetic acid (AcOH), HPLC grade acetonitrile (ACN), dichloromethane (DCM), dimethylsulfoxide (DMSO), hydrochloric acid (HCl), HPLC grade methanol (MeOH), sodium hydroxide (NaOH), and silica gel 60 were obtained from VWR (Ismaning, Germany) and ultra-pure water ($18 M\Omega.cm^{-1}$) from a Millipore S.A.S. Milli-Q Academic system ($18,2$ MΩ cm-1, Molsheim, France). Adenosine 5′-triphosphate (ATP), ammonium acetate (NH_4AcO), bovine serum albumin (BSA), calcium chloride ($CaCl_2$), catalase, d_6-DMSO, ethylene glycol-bis(2-aminoethylether)-N,N,N′,N′-tetraacetic acid (EGTA), D-glucose, glucose oxidase from Aspergillus Niger, Hoechst 33342, imidazole, methylcellulose, β-mercaptoethanol, potassium phosphate dibasic (K_2HPO_4), potassium phosphate monobasic (KH_2PO_4), rhodamine-phalloidin, Tris-HCl, pyronin Y, pyridine, zink acetate ($Zn(AcO)_2$), and 96 well black polystyrene half-area microplates were purchased from Sigma-Aldrich (Taufkirchen, Germany). SepPak Plus C18 cartridges were obtained from Waters Associates (Milford, USA). DMEM medium was purchased from PAN-Biotech (Aidenbach, Germany); fetal calf serum (FCS) from PAA Laboratories (Pasching, Austria), and Triton X-100, (3-(4,5-dimethylthiazol-2-yl)-2,5-diphenyl tetrazolium bromide) (MTT reagent) and FluorSave® reagent mounting medium were obtained from Merck (Darmstadt, Germany). Magnesium chloride ($MgCl_2$) and glycerol were purchased from AppliChem (Darmstadt, Germany). Dithiothreithol (DTT) was purchased from SERVA Electrophoresis (Heidelberg, Germany). Crystal violet, potassium chloride (KCl), and sodium dodecyl sulfate (SDS) were purchased from Carl Roth (Karlsruhe, Germany). Paraformaldehyde (PFA) was obtained from Thermo Fisher Scientific (Waltham, USA). Coomassie Brilliant Blue R-250 staining solution was purchased from Bio-Rad (Munich, Germany). Bilirubin and biliverdin from Cayman chemicals were purchased from biomol (Hamburg, Germany).

Cell culture

The human bladder cancer cell line T24 and the cervical cancer cell line Hela were obtained from the *Deutsche Sammlung von Mikroorgansimen und Zellkulturen* (DSMZ; Braunschweig, Germany) and maintained in DMEM medium supplemented with 10% fetal calf serum (FCS). Cells were cultured at 37°C under 5% CO_2 atmosphere with constant humidity.

Plant Material

Senescent leaves of the Katsura tree (*Cercidiphyllum japonicum*) were collected in the Maria-Ward-Straße, Munich (48°09'41.0"N 11°29'58.8"E). Prof. Susanne S. Renner (Department of Systematic Botany and Mycology, Faculty of Biology, University of Munich) determined the identity of the plant material; the voucher specimen of *Cercidiphyllum japonicum (*Moser & Karg 3) has been deposited in the Munich herbarium (acronym M).

Chromatography

i) Analytical HPLC: An Agilent 1260 Infinity II LC system was used with a 1260 Infinity Degasser, a 1260 Series quaternary pump and 1260 Series diode array detector; Merck LiChrospher® 100 RP-18 (5 µm) LiChroCART® 125-4, protected by a Merck LiChrospher® 100 RP-18 (5 µm) LiChroCART® 4-4 i.d. pre-column; injection volume: 100 µL (unless stated otherwise). Solvent system: mobile phase A = NH_4AcO buffer 10 mM pH 7, B = ACN, flow 0.5 mL/min; Solvent composition: 0-2 min 5% B, 2-17 min 5% to 100% B, 17-20 min 100% B, 20-22 min 100% to 5% B. Solvent system for bilirubin detection: mobile phase A = 0.1% formic acid, B = ACN, flow 0.5 mL/min; Solvent composition: 0-2 min 40% B, 2-10 min 40% to 75% B, 10-18 min 75% to 95% B, 18-28 min 95% B, 28-35 min 95% to 40% B. Data were processed with OpenLab CDS Data Analysis 2.3.

ii) Semi-preparative HPLC: Büchi Pure C-830 with prep HPLC pump 300 bar, fraction collector, and prep sample injection valve. Gynkotek LC-System with manual sampler, M480 pump, Phenomenex DG-301 online degasser, Gynkotek UVD 640 diode array detector and a Rheodyne injection valve with 5 mL loop. Column: Supelco Ascentis® C18, 5 µm, 15 cm x 10 mm, with a Phenomenex pre-column ODS 9 x 16 mm; mobile phase A = NH_4AcO buffer 10 mM pH 7, B = MeCN, flow 2.5 mL/min; solvent composition: 0-2 min 12% B, 2-12 min 12% to 20% B, 12-30 min 20% to 80% B, 30-40 min 80% to 100% B. Data were processed with Gynkosoft 5.50 or Büchi Pure software 1.5.

Spectroscopy

UV-Vis: Thermo Spectronic Genesys 5 (336001) UV-Visible spectrophotometer. Concentrations of PxB were calculated using log ε (426 nm) = 4.51[1], concentrations of PrB were calculated using log ε (523 nm) = 4.56[2].

HR-MS were measured at the MS facility of the Department of Chemistry, University of Munich. Data were processed using Xcalibur. NMR spectra were recorded on an Avance III HD 500 MHz NMR spectrometer from Bruker BioSpin equipped with a CryoProbe™ Prodigy broadband probe holder. NMR data were analyzed with Mestre Nova.

Compounds

During all handling steps, the material was protected from light and temperatures above 37 °C were avoided, if not stated otherwise.

Bilirubin and biliverdin were dissolved immediately before use in 0.2 N NaOH or 0.1 N NaOH for cell assays, respectively, or in DMSO for all *in vitro* assays to a final stock concentration of 10 mM or 20 mM and further diluted as indicated.

PxB was synthesized from its precursor PleB, which was isolated from senescent leaves of Katsura tree according to the published protocol with minor modifications [2-3]. Briefly, 500 g of senescent leaves of *Cercidiphyllum japonicum* were extracted by hot water extraction with 1.5 L of boiling water. The aqueous mixture was extracted twice with 1:1 volumes of DCM. The organic phases were combined

and the solvent was evaporated. The dry residue was dissolved in 20 mL of DCM, 10 g silica were added and the solvent was carefully evaporated under vacuum. The silica was transferred into a beaker and illuminated under a tungsten light bulb overnight while stirring. The oxidation of PleB to PxB was controlled by analytical HPLC. After eluting the mixture with MeOH and filtering it through a paper filter, PxB and the remaining PleB were isolated by semi-preparative HPLC. The purity of PxB was confirmed by analytical HPLC. Pure PxB was dried, diluted with 5 mL of ACN/potassium phosphate buffer (pH 2.5) 20/80 and stirred overnight in the dark. The solution was first applied to a Sep-Pak-C18 column (5g), PxB was eluted with ACN and solvent was evaporated before dissolving the product in DMSO and storing it at -20°C until further use. Yields were typically in the range of 5 to 10 mg of pure PxB.

PrB was synthesized from PxB according to the protocol of Li et al with modifications[3]. 27 mg of PxB (42.06 µmol) was dissolved in 15 mL DMF, and 39.67 mg of $Zn(AcO)_2$ (216.21 µmole, 5.1 eq) and 3 mL of pyridine were added. The mixture was stirred overnight under air and in the dark until the dark yellow solution turned dark blue. After 20 h, the mixture was diluted with 50 mL of water and extracted three times with 50 mL of DCM each. DCM was evaporated before 30 mL of ACN, 30 mL of PBS (pH 4.7) and 50% (v/v) AcOH were added until a pH value of 2.5 was reached. While the solution was stirred for 1 h, the colour changed from dark blue to dark red. Next, the mixture was extracted with equal volumes of DCM. The solvent was again evaporated, the residue was dissolved in MeOH/potassium phosphate buffer (pH 7) 20/80 and applied to a Sep-Pak-C18 cartridge (5g). PrB was eluted with MeOH and the purity was confirmed by analytical HPLC. The methanolic solution was dried and pure PrB was diluted with 5 mL of ACN/potassium phosphate buffer (pH 2.5) 20/80 and stirred overnight in the dark. The solution was applied to a Sep-Pak-C18 cartridge (5g), PrB was eluted with ACN and solvent was evaporated before dissolving the obtained PrB with DMSO. Yields were typically in the range of 90 to 93%.

Spectroscopic data

PxB. UV/Vis online spectrum (nm, rel λ): 212 (1.00), 244 (0.58), 312 (0.70), 424 (0.94) nm. HR-ESI-MS: $m/z_{calculated}$ ($C_{35}H_{39}O_8N_4$) = 643.27624 $[M+H]^+$; m/z_{found} = 643.27652 (Δ = 0.28 ppm).

^{1}H-NMR (500 MHz, d_6-DMSO): δ [ppm] = 2.03 (s, H_3C7^1); 2.06 (s, H_3C13^1); 2.15 (s, H_3C17^1); 2.17 (s, H_3C2^1); 2.20 (m, H_AC12^2); 2.36 (m, H_BC12^2); 2.46 (m, H_2C3^1); 2.54 (m, H_2C12^1); 3.34 (m, H_2C3^2); 3.66 (s, H_3C8^5); 3.77 (m, H_2C5); 3.86 (m, $HC8^2$); 4.80 (m, HC10); 5.31 (m, H_AC18^2); 6.06 (s, HC15); 6.20 (m, H_BC18^2); 6.57 (ddd, J = 11.4/17.6, $HC18^1$), 9.46 (s, HC20), 10.07 (s, HN24).

PrB. UV/Vis online spectrum (nm, rel λ): 208 (0.59), 314 (0.72), 524 (1.00) nm. HR-ESI-MS: $m/z_{calculated}$ ($C_{35}H_{37}O_8N_4$) = 641.26059 $[M+H]^+$; m/z_{found} = 641.26129 (Δ = 0.7 ppm).

^{1}H-NMR (500 MHz, d_6-DMSO): δ [ppm] = 2.09 (s, H_3C13^1), 2.12 (s, H_3C7^1), 2.19 (s, H_3C2^1), 2.20 (s, H_3C17^1), 2.15 (m, H_2C12^2), 2.53 (m, H_2C3^1), 3.07 (s, H_2C12^1), 3.61 (s, H_3C8^5), 4.11 (d, J = 4.0, H_2C5), 5.04 (s, $HC8^2$), 5.49 (dd, J = 2.38/11.58, H_AC18^2), 6.30 (dd, J =2.4/17.59, H_BC18^2), 6.15 (s, HC15), 6.65 (dd, J = 11.59/17.64, $HC18^1$), 9.51 (s, HC20), 10.00 (s, HN24).

1.2 Immunofluorescence staining

T24 or Hela cells (2×10^4 cells/well) were seeded in 8-well ibiTreat µ-slides (ibidi GmbH, Gräfelfing, Germany) and allowed to adhere overnight. Cells were treated with the indicated concentrations of compounds or vehicle controls and incubated for 4 h at 37°C. Afterwards, cells were washed twice with PBS+ (PBS including Ca^{2+}, Mg^{2+}), fixed with 4% (v/v) paraformaldehyde in PBS for 10 min and permeabilized with 0.2% (v/v) Triton X-100 in PBS for 10 min. Antibody solution containing rhodamine-phalloidin (1:400) to stain F-actin and Hoechst 33342 (1:50) to label nuclei in 1% bovine serum albumin (BSA) in PBS was added and incubated for 60 min. Cells were finally washed three times with PBS for 10 min and covered with FluorSave™ reagent mounting medium and glass coverslips. Images were collected with a Leica SP8 confocal laser scanning using Leica LAS X software and analyzed with ImageJ 1.45s.

1.3 Wound-healing assay

Cell migration was analyzed in a wound healing assay. T24 and Hela cells were seeded into 96 well plates (3×10^4 cells/well) and allowed to adhere until a cell density of 100% confluence was reached (for experiments with PxB and BR, plates were coated with 0.001% collagen G in PBS). The monolayers were wounded in a 96-well format with a custom made tool, washed with PBS+ and treated with the indicated concentrations of compounds or vehicle controls prepared in DMEM medium with FCS. DMEM medium without FCS served as a negative control and DMEM medium with serum as positive control. Cells were allowed to migrate until first contacts of cells in the positive control were observed (16-24 h). Next, medium was discarded; cells were washed with PBS+, stained with 0.5% crystal violet solution for 10 min and washed with water. After drying overnight, images were taken on a Leica DMi1 microscope and a Leica MC120 HD camera with a 4x phase contrast objective (Leica Microsystems, Wetzlar, Germany) and the uncovered area was analyzed using a custom-written program in Matlab R2017a. Migration was quantified as the percentage of the uncovered area normalized to the negative control, which was set to 100%.

1.4 MTT assay

Cell viability was determined using an MTT assay in parallel to the migration assay to exclude cytotoxic effects of the different compounds at the applied concentrations. As described above, 3×10^4 T24 or Hela cells were seeded in 96 well plates. After incubating overnight, cells were treated with the indicated concentrations of compounds or vehicle controls and incubated in parallel to the scratch assay. 2 h before the end of stimulation time of the scratch assay, 10 µL of MTT reagent (3-(4,5-dimethylthiazol-2-yl)-2,5-diphenyltetrazolium bromide) were added to each well and cells were incubated for 1 h at 37°C. Next, 190 µL of DMSO was added and the cells were again incubated for 1 h at room temperature while shaking and protected from light before absorbance was measured at 550 nm using a Tecan SpectraFluor plus microplate reader. Results were normalized to the vehicle control, which was set to 100%.

1.5 Actin polymerization and depolymerization assay

The actin polymerization or depolymerisation assays were performed by using pyrene labeled actin (10%), F-Actin BufferKit and PolyMix (10×stock), purchased from Hypermol (Bielefeld, Germany), according to the manufacturer's instructions. Briefly, pyrene labeled actin (10%) was diluted with H_2O to a concentration of 1mg/mL (24 µM) or 1.1mg/mL (26 µM) stock solution and subsequently centrifuged at 55,000xg and 4 °C for 60 min to remove any aggregates from freeze-drying.

Polymerization:
For the polymerization assay, a 1mg/mL (24 µM) pyrene actin stock solution was prepared. Actin polymerization solution consisting of 20 µL of H_2O, 10 µL of 10 mM $MgCl_2$, 5 µL of F-actin buffer (100 mM Imidazole-Cl pH 7.4, 10 mM ATP), as well as 5 µL of either DMSO or the respective compound, was prepared in a 96-well black polystyrene half-area microplate. 10 µL/well of pyrene labeled actin was added and pyrene fluorescence was immediately monitored every 20 s over 1 h with a Tecan Infinite® 200 PRO fluorescence plate reader at 360 nm excitation and 400 nm emission wavelength. Baseline fluorescnece intensities were substracted from total fluorescence values.

Depolymerization:
For depolymerization, pyrene labeled F-actin was obtained by incubating pyrene labeled actin (1.1 mg/ml, 26 µM) in 10× PolyMix buffer (1 M KCl, 0.1 M imidazole pH 7.4, 10 mM ATP, 20 mM $MgCl_2$) at room temperature for 1 h. This yields a 24 µM pyrene labled F-actin stock solution. Before use, F-actin was diluted 1:1 with 1× PolyMix buffer, resulting in a 12 µM sample solution. Depolymerization solution (consisting of 25 µL of 1× PolyMix buffer and 5 µL of either DMSO or compound) was added into a 96-well black polystyrene half-area microplate immediately before rapid addition of 20 µL of pyrene labeled F-actin (12 µM). Depolymerization was monitored by measuring pyrene fluorescence every 20 s over 2 h with a Tecan Infinite® 200 PRO fluorescence plate reader at 360 nm excitation and 400 nm emission wavelength. Initial fluorescnece values of each condition were substracted from total fluorescence values.

1.6 TIRF assay

The TIRF (Total Internal Reflection Fluorescence) microscopy assay was performed according to published protocols with minor modifications.[4] Flow cells (containing 15-20 µL of fluid) were made as a sandwich of a cover slip (22 × 22 mm), two parafilm strips forming an approximately 5 mm wide channel and a glass slide (76 × 26 mm).
For TIRF microscopy, flow-cell chambers were used with the cover slip down, facing the objective lens, and slide up. Solutions were loaded directly into the chamber via capillary action.
Labeled actin was prepared by mixing Atto488-actin and actin 1:1 (v/v) from rabbit skeletal muscle (Hypermol, Bielefeld, Germany). α-actinin from turkey gizzard smooth muscle (Hypermol, Bielefeld, Germany) was prepared by adding ultrapure water to obtain a 1 mg/mL stock solution and used as tethering protein.

Flow cell chambers were freshly passivated by incubation with 25 µL of 1% (w/v) BSA in PBS for 10 min. 25 µL of α-actinin (0.1 mg/mL) were then applied for 5 min. In the meantime, Mg-ATP-actin (5 µM) was prepared. Labeled actin (10 µM) was incubated 1:1 with 1/10 volume of 10 × Mg-exchange buffer (2 mM EGTA, 400 µM $MgCl_2$) and 1:8 with G-buffer (2 mM Tris-HCl, pH 8.0, 0.2 mM $CaCl_2$, 0.5 mM DTT, 0.2 mM ATP, final pH 7.8) on ice for 5 min to exchange Ca-ATP-actin for Mg-ATP-actin. Actin polymerization was triggered by a 1:1 mixing of Mg-ATP-actin (5 µM) with 2 × TIRF buffer (100 mM KCl, 2 mM $MgCl_2$, 2 mM EGTA, 30 mM imidazole, 30 mM D-glucose, 40 µg/mL catalase, 400 µg/mL glucose oxidase, 1% methylcellulose, 2% β-mercaptoethanol, final pH 7.4) containing the indicated concentrations of compounds. 30 µL of polymerizing actin was immediately loaded into the flow-cell chamber and placed on the TIRF microscope (Leica Microsystems, Wetzlar, Germany). The number of actin nuclei present in each frame (calculated from the number of filaments) was analyzed by using custom-written programs in Matlab R2017a.

1.7   Computational methods

Docking experiments were performed to evaluate the binding of the phyllobilins (PxB and PrB) and the bilins (BR and BV) to actin. The actin structure (PDB ID 4k41) in complex with Kabiramide C (KabC) was prepped in Molsoft's ICM version 3.9.1 KabC.1.[5] KabC bound to actin was removed from the structure and receptor maps were generated for docking studies encompassing the KabC binding site. Docking of each ligand was performed with the evaluation of multiple conformations for each ligand.

1.8   G-actin binding assay

The G-actin binding assay was performed using the 'Actin-Toolkit G-Actin Binding' (Hypermol, Bielefeld, Germany), in which G-actin is coupled to SepharoseTM as G-actin beads.

To investigate the binding of the compounds to G-actin, supernatants of the G-actin binding assay were analyzed for the respective compounds by HPLC. Agarose beads served as negative control. According to the manufacturer's instructions, G-actin beads and agarose beads were prepared in MonoMix buffer (Hypermol, Bielefeld, Germany) and 50 µL each were incubated with the different compounds (50 µM) for 1 h at room temperature under agitation in G-actin buffer (20 mM Tris-HCl, 0.2 mM ATP, 0.2 mM $CaCl_2$, pH 7.9). After incubation, samples were spun at 6,000×g for 4 min and supernatants were collected. The pellets were washed (3~4 times) and washing buffer was collected. After washing, the pellets were incubated with elution buffer (50% ACN, for BR 0.1 N NaOH) for 30 min under agitation and the samples were again centrifuged. The collected elution buffer was analyzed by HPLC. Peak areas of different compounds were analyzed using OpenLab CDS 2.3 software (for PxB detection at 420 nm, for PrB at 520 nm, for BR at 450 nm, and for BV at 320 nm) and peak areas of agarose beads were normalized to values with G-actin beads, which were defined as 1.0.

For further investigating the binding of PxB, PrB, BR, and BV to G-actin in competition with the actin binding protein profilin, G-actin beads and profilin (Hypermol, Bielefeld, Germany) were prepared

according to the manufacturer's instructions. G-actin beads were pre-treated with compounds (50 µM) or vehicle control for 1 h at room temperature under agitation. Then profilin (0.667 µM) was added and incubated for 1 h at room temperature under agitation. Samples were spun at 6,000×g for 4 min and 40 µL of supernatant was prepared for an SDS-sample by adding 10 µL of 5x SDS buffer (3.125 M Tris-HCl pH 6.8, 50% glycerol, 5% SDS, 2% DTT, 0.025% pyronin Y, H_2O). The pellet was washed, boiled for 2 min at 95°C to release profilin from the beads, and mixed with 25 µL of 1xSDS-sample buffer. Both the supernatant and pellet were analyzed by sodium dodecyl sulfate polyacrylamide gel electrophoresis (SDS-PAGE) in electrophoresis buffer (100 V, 21 min then 200 V, 55 min) using a 18% polyacrylamide gel. Gels were stained for 30 min in Coomassie blue solution, washed with water and destained in destaining solution overnight (10% glacial acetic acid, 30% methanol, and 60% distilled water). Images of the gels were captured using a ChemiDoc Imaging System (Bio-Rad Laboratories GmbH). The amount of each protein was quantified by using Image Lab 6.0 Software and normalized to the vehicle control, which was defined as 1.0.

1.9   Determination of K_d values by fluorescence quenching

To characterize the interaction between G-actin and PrB or G-actin and BR, fluorescence measurements were conducted on an FLS 1000 Fluorimeter (Edinburgh Instruments). The emission spectra were recorded using a 450 W continuous wave Xenon lamp. Fluorescence spectra of Atto647 labeled G-actin (Hypermol, Bielefeld, Germany; 200 nM) alone and upon titration with PrB or BR were measured at an excitation wavelength of 635 nm using an excitation and emission band width of 2 nm in a quartz cuvette (Hellma Analytics, Müllheim, Germany). The spectra were measured in 1 nm steps between 640 and 700 nm with 0.5 and 2s dwell time for PrB and BR, respectively, on a photon multiplier tube (PMT 900 detector, Hamamatsu). Fluorescence intensities at the emission maximum of 669 nm were normalized to the initial fluorescence of labeled actin and the quenching activity in % was plotted against the concentration of PrB/BR. To determine the dissociation constant (K_d) of PrB, three independent experiments were performed and a one-site-specific binding model was applied for curve fitting using GraphPad Prism 9.1.1.

1.10   Microscale thermophoresis (MST)

For determination of the dissociation constant of PxB binding to G-actin, microscale thermophoresis measurements were conducted using Atto647 labeled G-actin from Hypermol (Bielefeld, Germany). Briefly, 16 1:1 dilutions of the ligand PxB were prepared in G-actin buffer yielding final concentrations from 10 nM to 345 µM. Each ligand dilution was mixed with one volume of labeled protein (final concentration of 71.4 µM). The samples were loaded into Monolith NT.115 Capillaries and MST was measured using a Monolith NT.115 instrument (NanoTemper Technologies) at an ambient temperature of 25°C. Data of three independently pipetted measurements were analyzed using the signal from an MST-on time of 5 s and the K_d was calculated by MO.Affinity Analysis software version 2.3 (NanoTemper Technologies).

1.11 Isothermal calorimetry (ITC)

ITC measurements were performed in order to determine the dissociation constant (K_d) of the interaction of G-actin and BV using a MicroCal PEAQ-ITC (Malvern Instruments, Malvern, UK). Rabbit skeletal muscle alpha actin (Hypermol, Bielefeld, Germany) was diluted, centrifuged for 15 min at 4°C and purified by size exclusion chromatography on a Cytiva ÄktaGo system, equipped with a Superdex 200 increase 10/300 column, equilibrated with 20 mM Tris-HCl, 150 mM NaCl, 0.4m M ATP, pH 8.2. Two sequential ITC measurements with 12 injections of a 1 mM solution of BV in the same sample cell with purified G-actin protein solution (50 µM) were performed. After finishing the experiment, a control experiment with buffer in buffer injections was performed keeping all the parameters same. Data sets of both titrations were merged using MicroCal Concat ITC software and merged data were analysed and the K_d was calculated assuming a 1/1 binding model using MicroCal PEAQ-ITC Analysis Software (v121).

1.12 Statistical analysis

Results represent the mean of at least three independent experiments (means ± SEM) performed in at least three replicates, unless stated otherwise. Statistical significance was carried out by two-way analysis of variance with post hoc analysis using Dunnett's multiple comparison test or an unpaired t-test with Welch's correction; all statistical analyses were processed with GraphPad Prism 9.1.1.
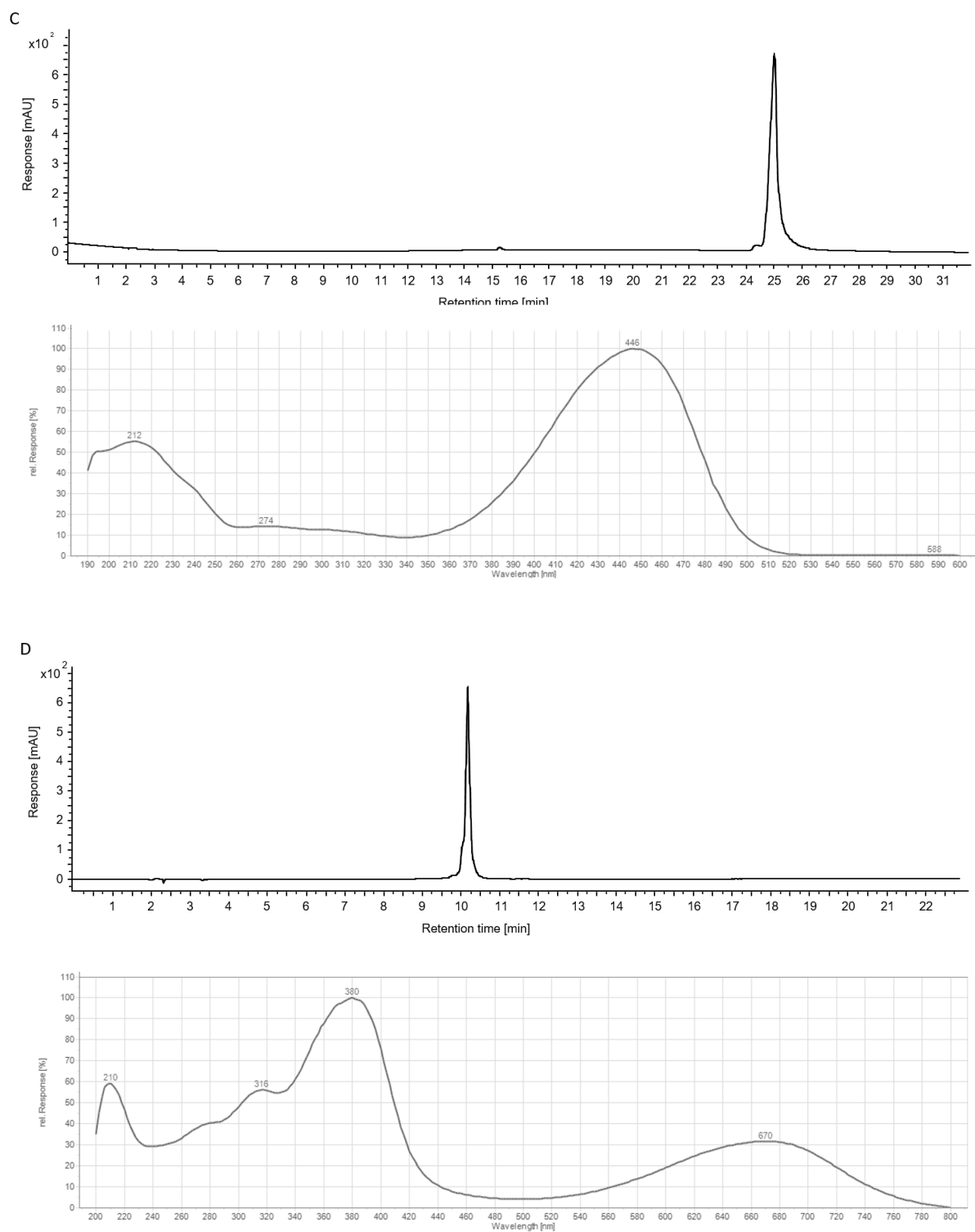
2. Supplementary Figures

A

B
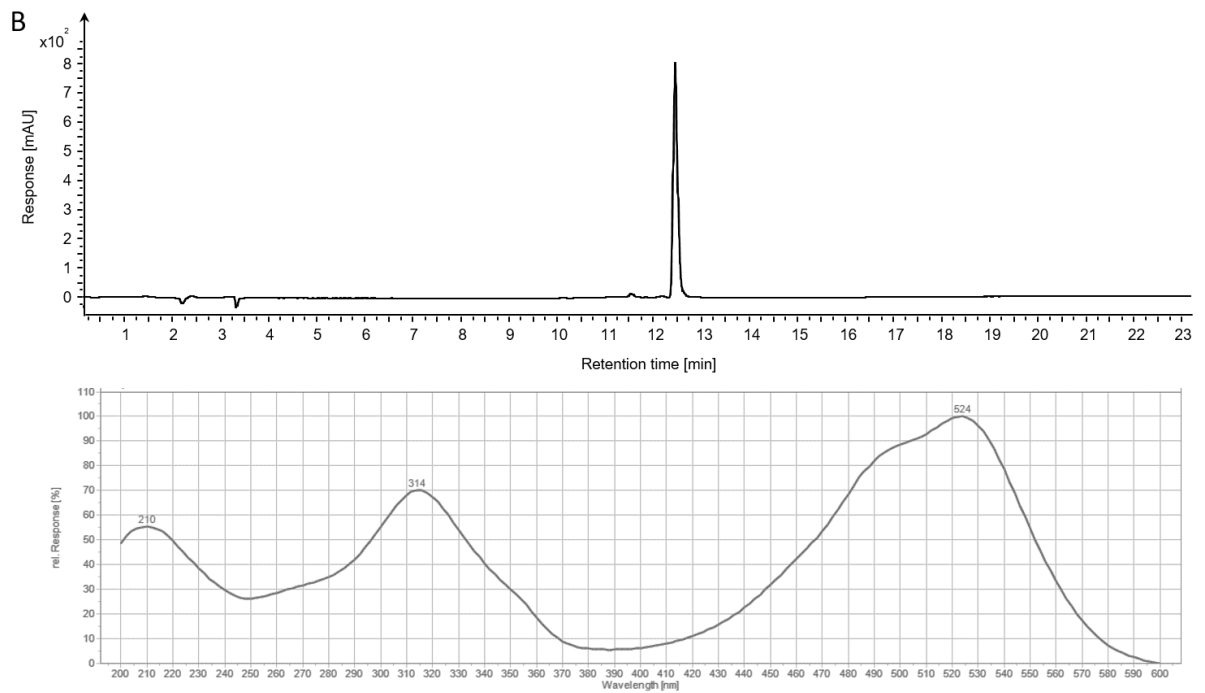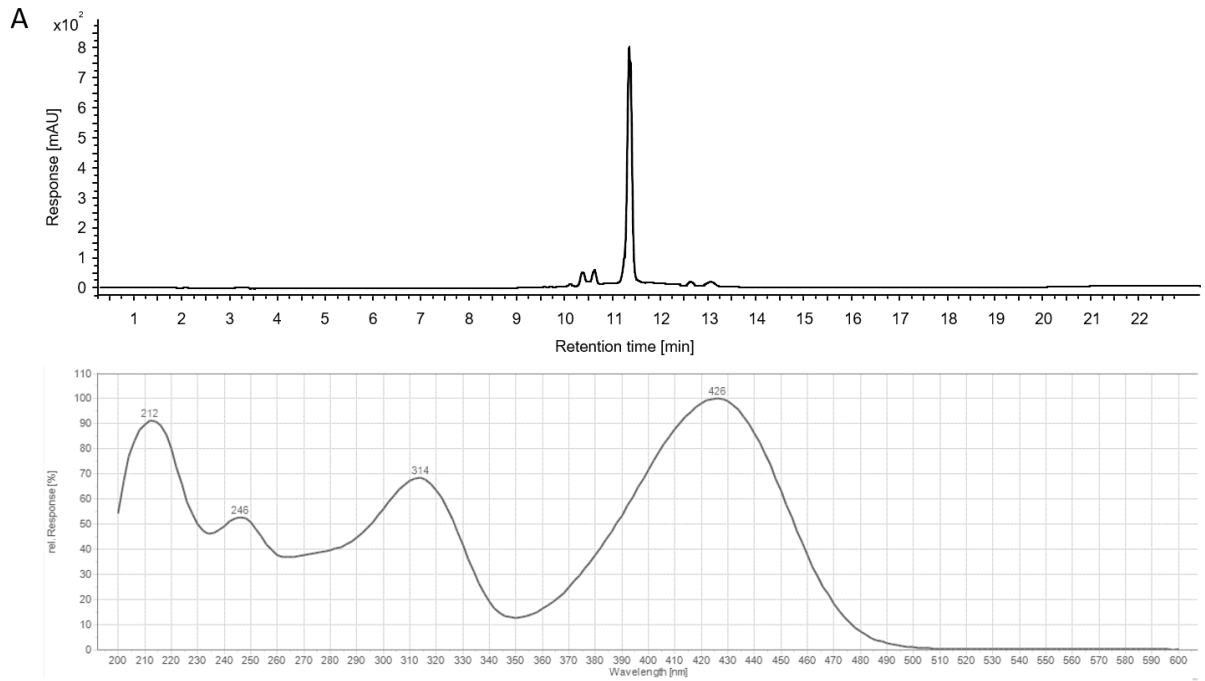
Figure S1. Characterization of tetrapyrroles. HPLC analysis (upper panels) and UV-Vis online spectra (lower panels) of isolated/synthesized PxB (A) and PrB (B), and commercial BR (C) and BV (D). For the HPLC analysis, detection was performed at 320 nm for PxB, PrB and BV and at 450 nm for BR.
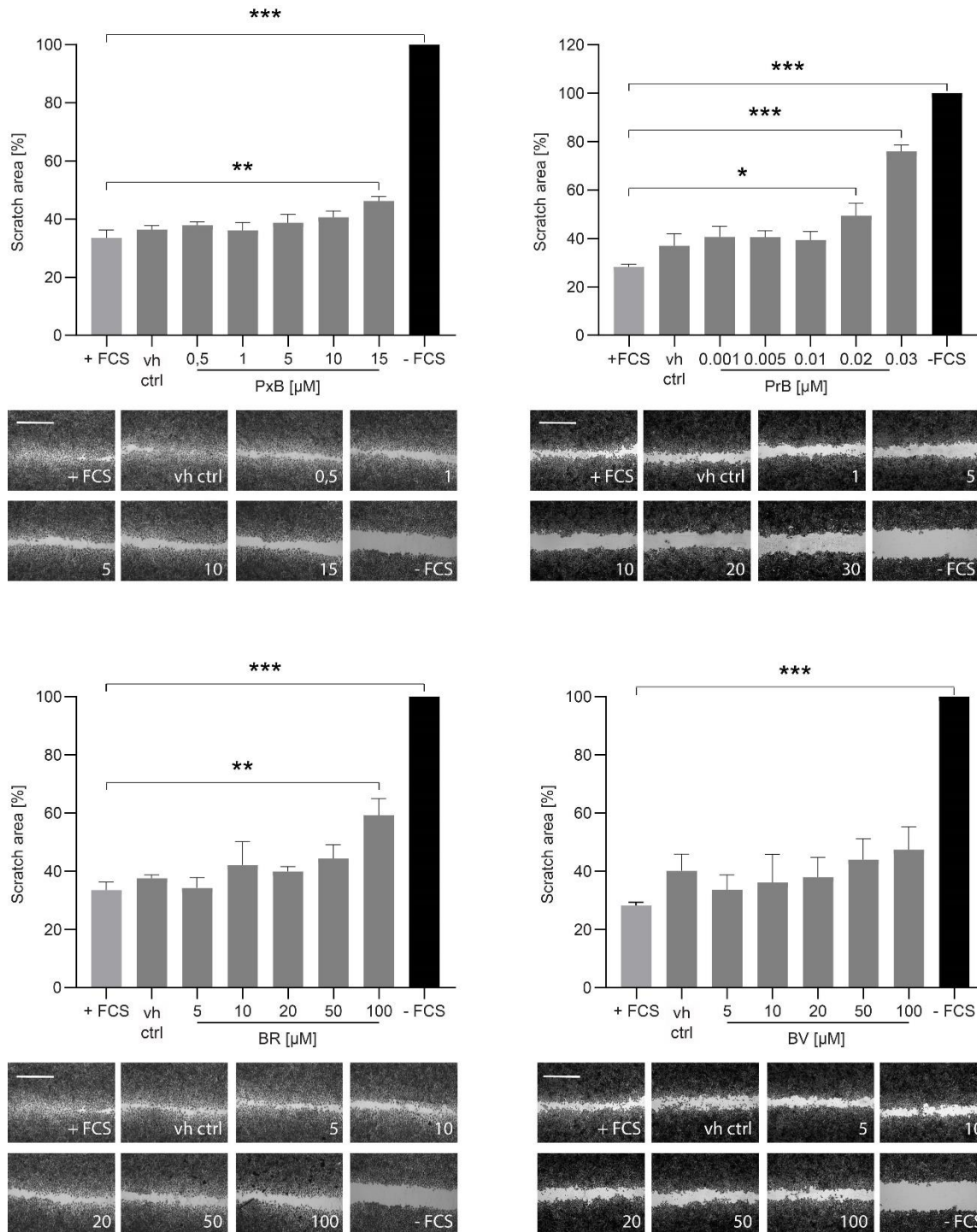
Figure S2. Impact of tetrapyrroles in wound healing assays. Cell migration of Hela cells treated with increasing concentrations of PxB, PrB, BR, BV, and vehicle control (vh ctrl) analyzed by a scratch wound-healing assay. Treatment with cell medium containing FCS served as a negative control and medium without FCS as a positive control. (Upper panels) Bar graphs showing the relative scratch gap normalized to the control without FCS. The bars present the mean±SEM of three independent experiments performed in triplicates at 37°C. (The significance was analyzed using a one-way ANOVA followed by Dunnett's multiple comparison test, *P < 0.05, **P < 0.01, **P < 0.001). (Lower panels) Representative images for the scratch analysis collected 16-24 hrs after generating the scratch are shown. Scale bar: 1 mm.
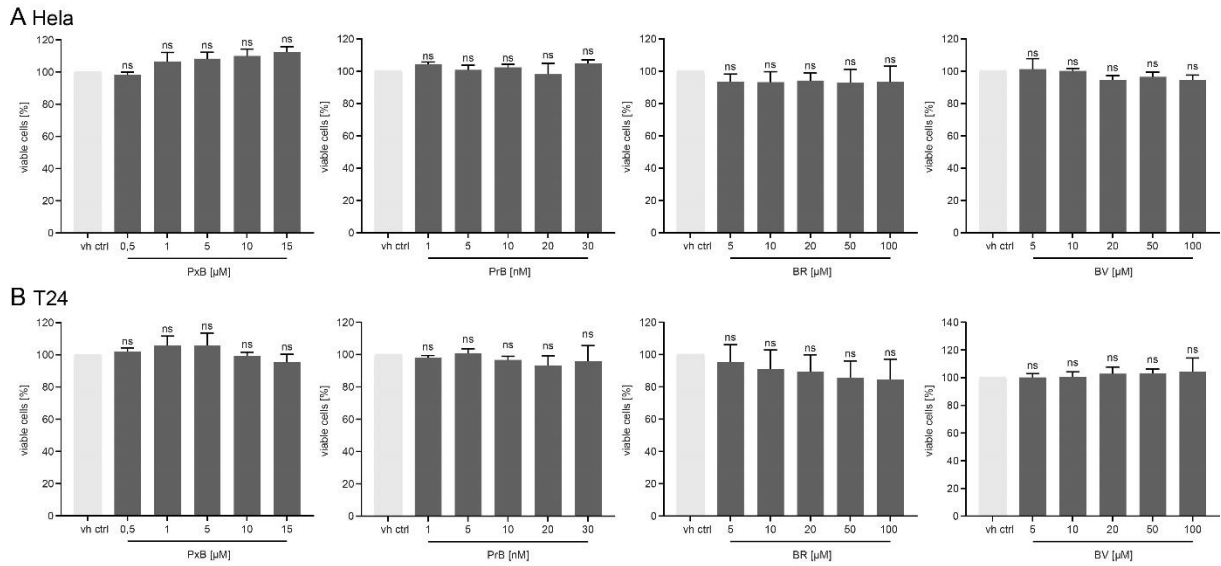
Figure S3. Influence of tetrapyrroles on cell viability. Cell viability assay of Hela (A) and T24 (B) cells treated with indicated concentrations of phyllobilins and bilins analyzed by a MTT assay. The percentage of viable cells were normalized to the vehicle control (vh ctrl). Bars show the mean±SEM of three independent experiments performed in triplicates. Significance was calculated using a one-way ANOVA followed by Dunnett's multiple comparison test, ns = not significant.
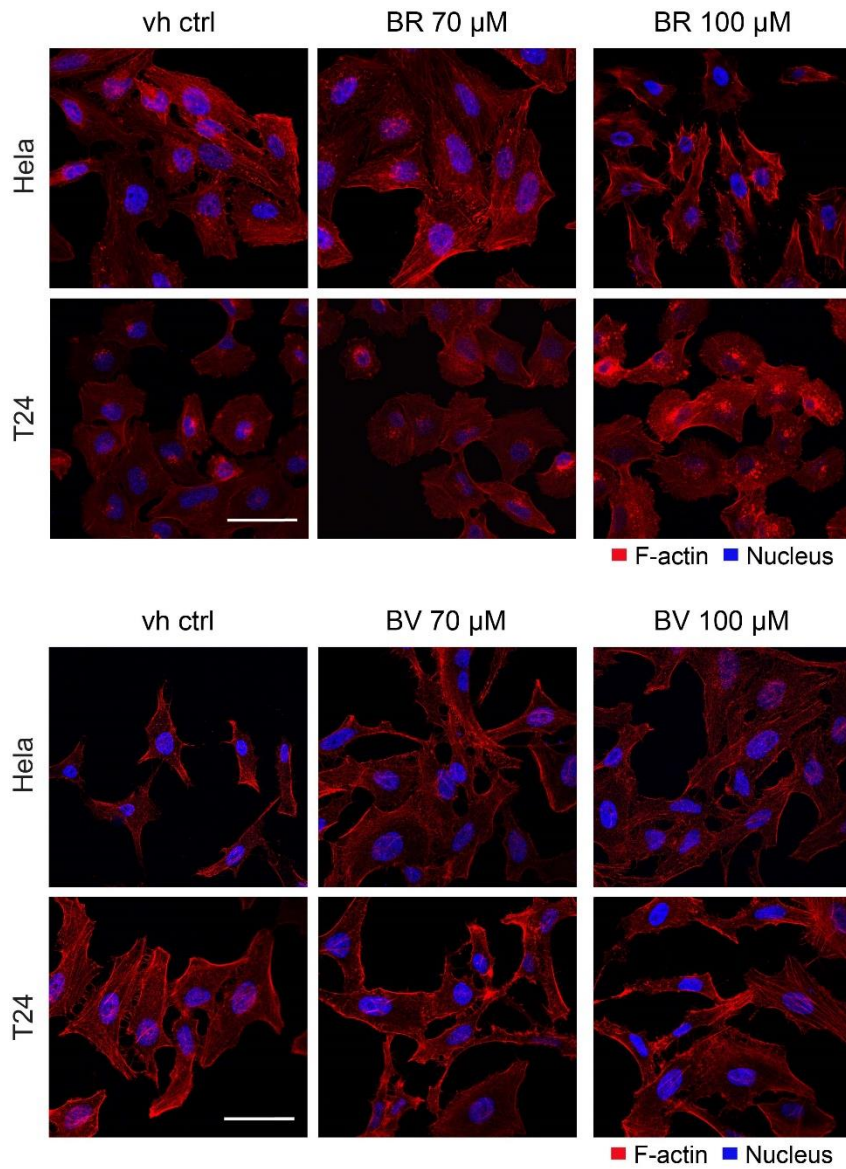
Figure S4. Influence of tetrapyrroles on the cellular cytoskeleton. Immunofluorescence staining of Hela and T24 cells treated with the indicated concentrations of BR and BV for 4 h. Nuclei were stained with Hoechst (shown in blue) and F-actin with rhodamine-phalloidin (shown in red). Scale bar: 50 μm. Representative images of three independent experiments are shown.
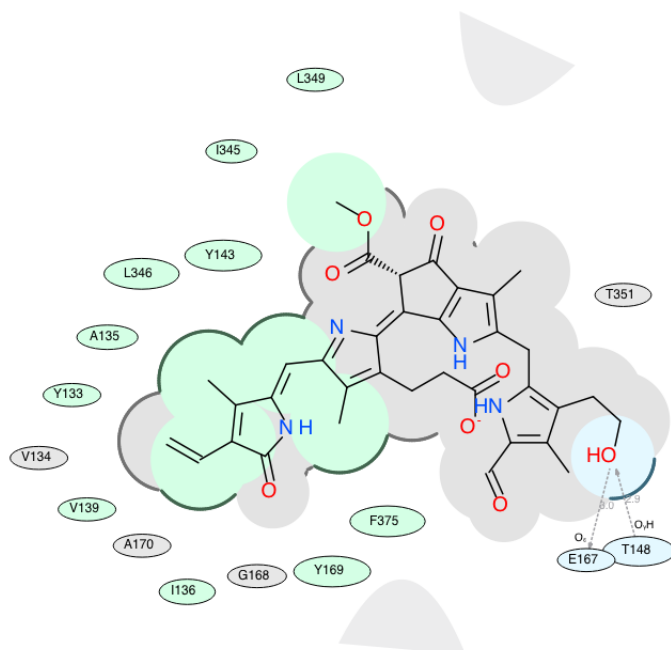
Figure S5: 2D ligand interaction map from the docking analysis of PrB binding to G-actin. The structure of PrB with hydrophobic regions shaded in green, hydrogen bond acceptors shaded in blue, and hydrogen bonds are shown as dashed arrows. The accessible surface areas are illustrated by grey parabolas and as broken thick lines around the ligand. Residues in van der Waals contact are coloured grey and the size of residue ellipse indicates the strength of the contact.
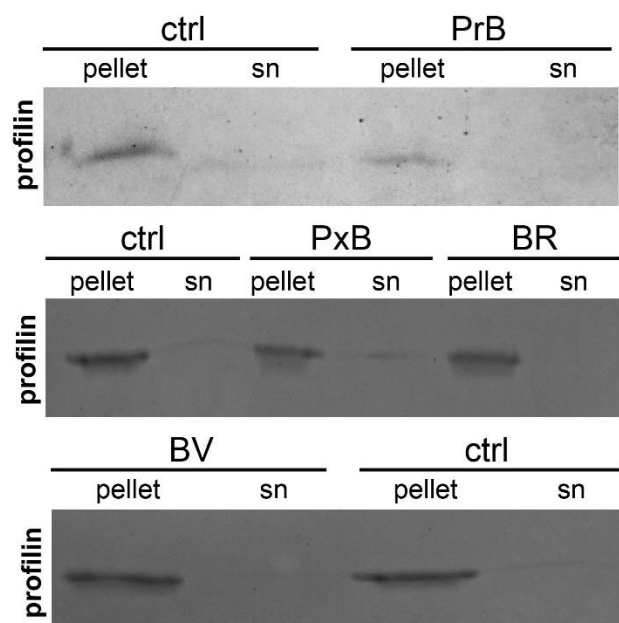
Figure S6. Competitive G-actin binding assay with compounds and profilin. G-actin beads were pre-treated with compounds or a vehicle control for 1h before profilin was added. Beads were centrifuged, the supernatant (sn) was collected and the beads thoroughly washed. Only profilin that was bound to G-actin was co-precipitated in the pellet. Pellets were solubilised by boiling to release the bound profilin. Samples were analysed by SDS- PAGE followed by a Coomassie staining. The shown data are representative gels taken from three independent experiments.
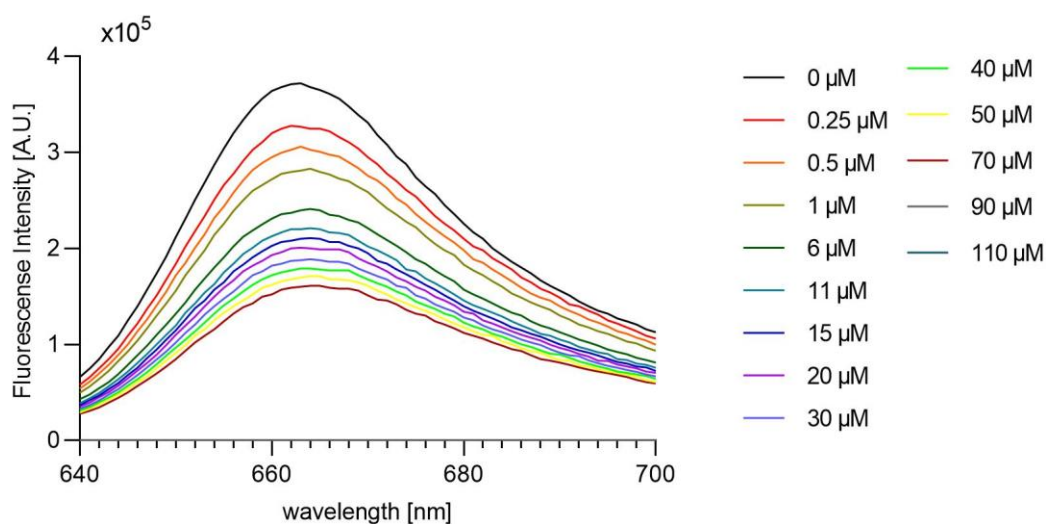

Figure S7. Fluorescence titration experiments of PrB with G-actin. Fluorescence spectra (Ex. 635 nm; Em. 640-700 nm) were recorded while titrating with increasing concentrations of PrB (0.25 µM – 110 µM) to a solution of Atto647 labeled G-actin (0.2 µM) in G-actin buffer. Three independent experiments were performed and spectra taken from one representative experiment are shown.
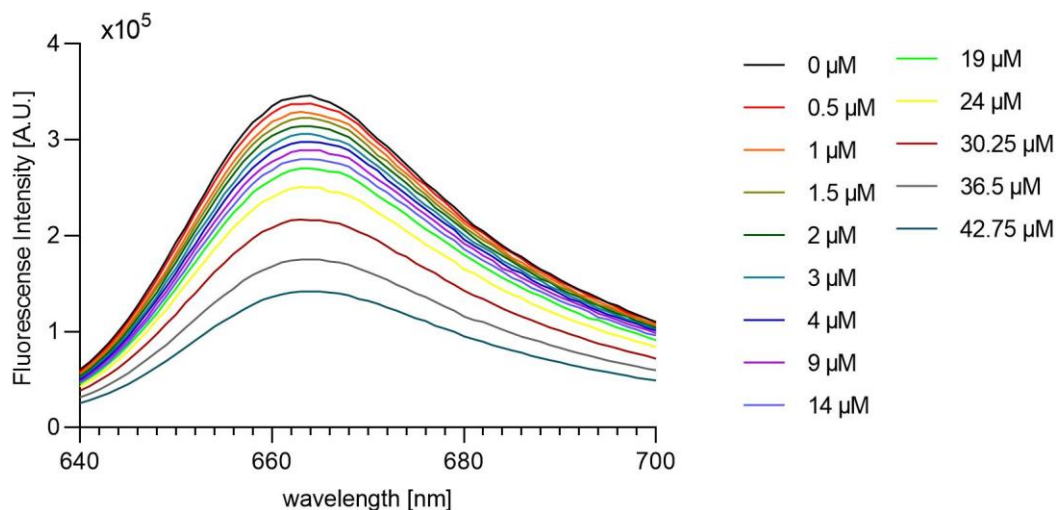
Figure S8. Fluorescence titration experiments of BR with G-actin. Fluorescence spectra (Ex. 635 nm; Em. 640-700 nm) were recorded while titrating with increasing concentrations of BR (0.5 µM – 42.75 µM) to a solution of Atto647 labeled G-actin (0.2 µM) in G-actin buffer. Three independent experiments were performed and spectra taken from one representative experiment are shown.
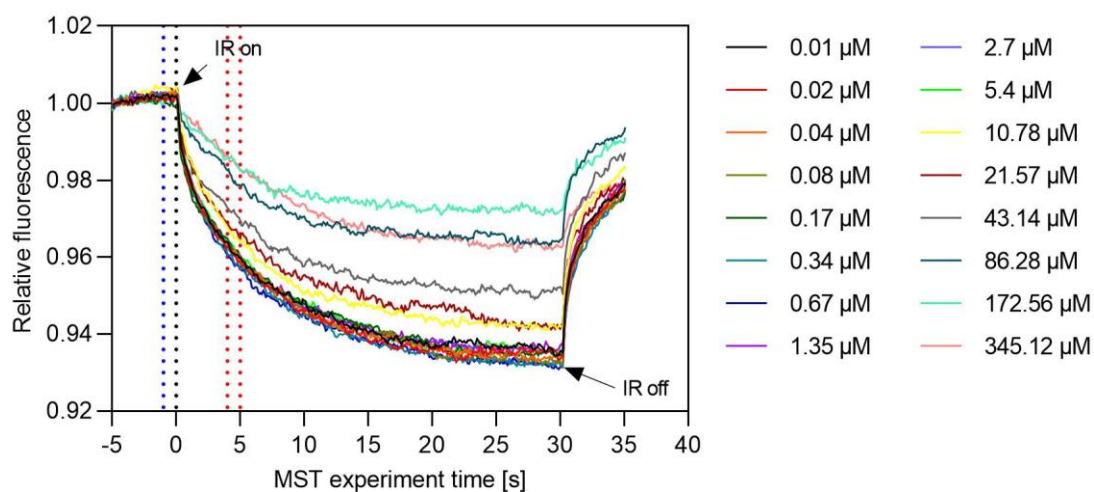

Figure S9. MST interaction analysis of PxB and Atto647 labeled G-actin. MST measurements were carried out with labeled G-actin protein solution (71.4 nM) and increasing concentrations of ligand PxB (0.01 µM to 345.12 µM) in G-actin buffer. MST traces presented are representative traces taken from one of three independent experiments.
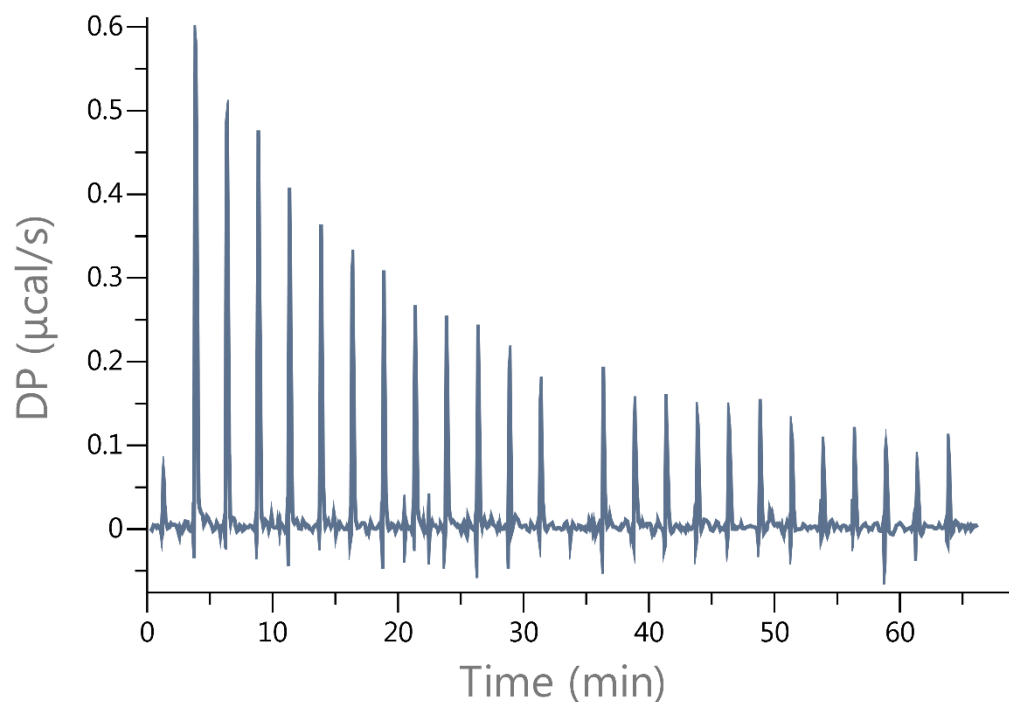
Figure S10. Direct binding of BV to G-actin analyzed by ITC. ITC trace of two subsequent titrations of a 1 mM solution of ligand BV into the same sample cell with purified G-actin protein solution (50 µM).

3. References

[1] S. Moser, M. Ulrich, T. Müller, B. Kräutler, *Photochemical & photobiological sciences* **2008**, *7*, 1577-1581.

[2] C. Li, M. Ulrich, X. Liu, K. Wurst, T. Müller, B. Kräutler, *Chemical Science* **2014**, *5*, 3388-3395.

[3] C. A. Karg, P. Wang, F. Kluibenschedl, T. Müller, L. Allmendinger, A. M. Vollmar, S. Moser, *European Journal of Organic Chemistry* **2020**, *2020*, 4499-4509.

[4] aD. Breitsprecher, A. K. Kiesewetter, J. Linkner, J. Faix, in *Chemotaxis: Methods and Protocols* (Eds.: T. Jin, D. Hereld), Humana Press, Totowa, NJ, **2009**, pp. 401-415; bL. K. Doolittle, M. K. Rosen, S. B. Padrick, in *Adhesion Protein Protocols* (Ed.: A. S. Coutts), Humana Press, Totowa, NJ, **2013**, pp. 273-293.

[5] R. Abagyan, M. Totrov, D. Kuznetsov, *Journal of Computational Chemistry* **1994**, *15*, 488-506.